

**Development of Cancer-Stem-Cell Targeting Pan-Aldehyde Dehydrogenase Inhibitors as
an Adjunct to Chemotherapy in the Treatment of Ovarian Cancer**

by

Brandt C. Huddle

A dissertation submitted in partial fulfillment
of the requirements for the degree of
Doctor of Philosophy
(Medicinal Chemistry)
in the University of Michigan
2018

Doctoral Committee:

Research Professor Scott D. Larsen, Co-Chair
Professor Nouri Neamati, Co-Chair
Professor Ronald J. Buckanovich, University of Pittsburgh
Professor Henry I. Mosberg

Brandt C. Huddle

bchuddle@umich.edu

ORCID iD: 0000-0002-3653-2573

Acknowledgements

I would like to thank my advisor, Dr. Scott Larsen, for sharing his knowledge of and passion for medicinal chemistry. He has been a role model both as a scientist and as a manager who cultivates mutual respect with his students and employees.

The work in this document would not be possible without the substantial efforts of our collaborators in the Buckanovich, Hurley, Neamati, and Sun labs. I would like to especially thank Ed Grimley for stepping up in the past year to drive the cancer biology forward in this project. Funding for this project was provided internally by Rackham and the Center for Discovery of New Medicines (CDNM) and externally by the National Cancer Institute (NCI-NIH).

I thank Dr. Mosberg, Mike Wilson, Kim Hutchings, and Walajapet Rajeswaran for their assistance and advice over the years.

Thanks to friends Tony Nastase, Jeff Zwicker, Allie Sowa, Max Stefan, Helen Waldschmidt, Aaron Bender, Aubrie Harland, Larisa Yeomans, Scott Barraza, Janice Sindac, Dylan Kahl, Lindsey Drake, Sarah Burris, Nick Ragazzone, Jeremy O'Brien, Julie Boulanger, DeAnna Mylander, and Mike Gilbert for occasionally managing not to talk about work at the bar.

Thanks to Erin Gallagher, for supporting me, offering advice, and putting up with me after a frustrating day at work.

Finally, thanks to my family for their emotional (and financial) support throughout my 21 years of school.

Table of Contents

Acknowledgements	ii
List of Figures.....	vi
List of Tables	viii
List of Schemes.....	ix
Abstract.....	x
Chapter 1 Introduction and Background.....	1
1.1 Ovarian Cancer: Current Treatments and Prognosis	1
1.2 The Cancer Stem Cell Hypothesis	3
1.3 Markers for CSCs in Ovarian Cancer	4
1.4 Function of CD133 in CSCs	7
1.5 Function of ALDH in CSCs.....	8
1.6 Possible Connections Between ALDH and CD133 in CSCs.....	10
1.7 Validation of ALDH1A as a Target in Ovarian Cancer Stem Cells	11
1.8 Rationale for Isoform Selective ALDH Inhibitors.....	12
1.9 Structural Basis for ALDH Isoform Selectivity.....	16
1.10 Review of ALDH Inhibitors	17
1.11 Conclusions.....	21
Chapter 2 : Synthesis and Characterization of 673A Analogs	22
2.1 Characterization of 673A	22
2.3. SAR of 673A Analogs.....	24
2.4. 673A SAR Conclusions	35
2.5. Development of a 673A Affinity Probe	36
2.6. Synthesis of 673A Analogs	38
2.7. Experimental Procedures.....	44
Chapter 3 Development of 1st Generation Pyrazolopyrimidinone Aldehyde Dehydrogenase Inhibitors	71
3.1. Characterization of Lead Compound CM39	71

3.2.	Crystal Structure of ALDH1A1 complexed with CM39	72
3.3.	Optimization of Pyrazole Substituents	74
3.4.	Crystal Structure of ALDH1A1 Complexed with Compound 258083	81
3.5.	Homology Models to Explain Isoform Selectivity	83
3.6.	Confirming Activity in Live Cells	85
3.7.	Evaluation of Synergy with Cisplatin	86
3.8.	Evaluation of In Vivo Metabolic Stability	89
3.9.	Efficacy of 258085 in Xenograft Studies	90
3.10.	Conclusions	91
3.11.	Synthesis of CM39 Analogs	93
3.12.	Experimental Procedures	95
Chapter 4	Development of 2nd Generation CM39 Analogs.....	140
4.1.	Rationale.....	140
4.2.	Optimization of Thioether Linker	141
4.3.	Exploring Alternative Heterocyclic Cores	148
4.4.	Conformational Restriction of the Thioether	149
4.5.	Optimization of the Benzyl Pendant	152
4.6.	Exploring Polar <i>p</i> -Phenyl Substituents	158
4.7.	Combining Optimal Thiol and Pyrazole Substituents.....	162
4.8.	Analysis of Pharmacokinetic Data for the CM39 Series.....	166
4.9.	Conclusions	170
4.10.	Chemistry.....	173
4.11.	Experimentals	183
Chapter 5	Future Directions and Conclusions.....	238
5.1.	New and Proposed CM39 Analogs with Improved Property Forecast Index	238
5.2.	Attempted Development of Proteolysis Targeting Chimeras (PROTACS) and Future Directions	242
5.3.	Selective Inhibitors Based on ALDH1A2 Crystal Structure 6B5H	244

5.4. Future Evaluation of Analogs and Project Conclusion	247
5.5. Chemistry	248
5.6. Experimental Procedures.....	251
Bibliography	266

List of Figures

Figure 1.1: Mechanism of Aldehyde Dehydrogenase (Morgan et al. ⁴¹).....	9
Figure 1.2: Effect of ALDH1A Knockdown on Ovarian Cancer Cell Lines.....	12
Figure 1.3: ALDEFLUOR Assay	12
Figure 1.4 Effect of 1A1/1A2 Knockdown on 1A3 Expression.....	15
Figure 1.5 ALDH1A Expression in Ovarian Cancer Cell Lines	15
Figure 1.6: Active Site Homology of ALDH1A family and ALDH2	17
Figure 1.7: Structure of Selected Literature ALDH Inhibitors	18
Figure 1.8: DEAB is a Slow Substrate of ALDH	20
Figure 2.1: 673A Depletes CSCs and Sensitizes Patient Derived Tumors to Carboplatin.....	23
Figure 2.2: Ortho Substituents Destabilize the Hypothesized Quinoid Tautomer.....	25
Figure 2.3: Crystal Structure of 673B Bound in ALDH1A1 Active Site Overlaid with ALDH2 (PDB: 5L13).....	28
Figure 2.4: Structure of 673A Affinity Probe 264441	37
Figure 3.1: Biochemical and Cellular ALDH Inhibition by CM39	71
Figure 3.2 Structure of ALDH1A1 N121S with CM39 (2.10 Å, PDB 5TEI)	73
Figure 3.3 Isoform Selectivity of Compound 258081	81
Figure 3.4 258083-1A1 Crystal Structure.....	82
Figure 3.5 1A2 and 1A3 Homology Models Provide Rationale for 1A1 Selectivity of CM39 ...	83
Figure 3.6 Homology Model Docking of 258085	84
Figure 3.7 Pan-ALDH1A Inhibitors Engage ALDH in Cells and Deplete Cells Bearing Putative CSC Marker CD133.....	86
Figure 3.8 Compounds 258082, 258083, and 258085 Synergistically Enhance the Effect of Cisplatin on Ovarian Cancer Cell Lines and Patient Derived Spheroids.....	88
Figure 3.9 258085 Reduces OVSAHO Xenograft Tumor Volume as a Single Agent.....	90
Figure 4.1 Crystal Structures of ALDH1A1 Bound to 258083 and 262548	146
Figure 4.2 Energy Minimized Conformationally Restricted Analogs	152
Figure 4.3 The 1A1 Crystal Structure of 262548 Indicates Potential to Engage Polar Side Chains of W178 and T129	155
Figure 4.4 Features of Active Site Adjacent to Ortho Position of N-Phenyl in 262548-1A1 Crystal Structure	159
Figure 4.5 Homology Model Docking to Rationalize 1A3 Selectivity of Nitrile 246202.....	161
Figure 4.6 In Vivo Metabolites Identified for 263052.....	164
Figure 4.7 Overlay 258083 and 262548 From Their Respective 1A1 Crystal Structures	166

Figure 4.8 Analysis of Correlation Between cLogP, MLM stability, and In Vivo Exposure and Stability.....	170
Figure 5.1 Overlay of ALDH Inhibitors in ALDH1A1 Active Site.	239
Figure 5.2 Proposed Thiol Substituents	242
Figure 5.3 257723-Linalidomide Chimeras and Proposed 673A-Linalidomide Chimera.....	244
Figure 5.4 Overlay of 1A1 and 1A2 Crystal Structure	246

List of Tables

Table 2.1 Commercial SAR of DEAB Analogs	29
Table 2.2 Characterization of Novel Analogs of 673A	30
Table 2.3 Characterization of Alternative Electrophile Analogs.....	33
Table 2.4 Characterization of Alternative Core Analogs.....	34
Table 3.1 Characterization of N-1 Pyrazole Substituents	76
Table 3.2 Characterization of N-2 Pyrazole Substituents	77
Table 3.3 Characterization of N-phenyl Modifications	79
Table 3.4 In Vivo Exposure Following IP Injection in Mice.	89
Table 4.1 Optimization of the Thioether Linker	141
Table 4.2 Characterization of Alternative Heterocyclic Core Analogs	148
Table 4.3 Characterization of Conformationally Restricted Analogs.....	149
Table 4.4 Characterization of Benzyl Pendant Modifications	153
Table 4.5 Characterization of <i>p</i> -Phenyl Substituted Analogs.....	158
Table 4.6 Characterization of Optimized Compounds	162
Table 4.7 Pharmacokinetic Characterization of Selected Compounds.....	167
Table 5.1 Characterization of Non-Aromatic Thiol Substituents	241
Table 5.2 C-3 Substituted Pyrazole Analogs	247

List of Schemes

Scheme 2.1: Synthesis of Compounds 223960, 223903-223906 ^a	38
Scheme 2.2: Synthesis of Analogs 223940 ^a	39
Scheme 2.3: Synthesis of 224258, 223908, 224260, 224262 ^a	40
Scheme 2.4: Synthesis of 22151, 223902, 224259, and 232721 ^a	41
Scheme 2.5: Synthesis of 224256 ^a	41
Scheme 2.6: Synthesis of 224257 ^a	42
Scheme 2.7: Synthesis of 232200, 232483, 232662, and 232720 ^a	42
Scheme 2.8: Synthesis of Affinity Probe 264441 ^a	43
Scheme 3.1 Synthesis of Pyrazole substituted analogs (Table 3.1, Table 3.2). ^a	93
Scheme 3.2 Synthesis of N-Phenyl Modifications (Table 3.3) ^a	94
Scheme 4.1 Synthesis of Modified Linker Analogs ^a	174
Scheme 4.2: Synthesis of Branched Alkyl Analogs ^a	175
Scheme 4.3: Synthesis of De-aza Analogs 258469-70 ^a	176
Scheme 4.4: Synthesis of Analog 259010 ^a	177
Scheme 4.5: Synthesis of Conformationally Restricted Analogs ^a	179
Scheme 4.6: Synthesis of Para-substituted N-Phenyl Analogs ^a	180
Scheme 4.7: Synthesis of Homologated Para-substituted N-Phenyl Analogs ^a	181
Scheme 4.8: Synthesis of N-2 Pyrazole Substituted Analogs ^a	182
Scheme 5.1 Synthesis of Non-Aromatic Thiol Substituents ^a	248
Scheme 5.2 Synthesis of 257723-Linalidomide Degraders ^a	249
Scheme 5.3 Synthesis of C-3 Substituted Analogs ^a	250

Abstract

Aldehyde Dehydrogenase (ALDH) activity is commonly used as a marker to identify cancer stem-like cells. The three ALDH1A isoforms have all been individually implicated in cancer stem-like cells and in chemoresistance; however, which isoform is preferentially expressed varies considerably between various cell lines and tumors. An inhibitor of these three isoforms could provide a useful broad-spectrum tool to study ALDH1A biology in any of these cells and could potentially be used as a therapeutic. The redundant expression and function of the ALDH1A isoforms also suggests that cells could develop resistance to a single isoform selective inhibitor by simply expressing an alternate isoform. Lead compound **673A**, a pan ALDH1A inhibitor, selectively depleted cancer stem cells and reversed chemosensitivity in vivo. Based on this compelling activity we set out to optimize **673A** and another HTS hit **CM39** for ALDH1A potency and selectivity, cellular potency, and pharmacokinetic properties. Although progress in the development of **673A**-based inhibitors has been limited, an affinity probe has been synthesized to uncover new targets of the potentially promiscuous compound and to search for protein-protein interactions involving ALDH. Our campaign to optimize **CM39** with ALDH1A1 afforded first-in-class pan-inhibitors of ALDH1A1, 1A2, and 1A3 with excellent selectivity over ALDH2. We have developed compounds with up to 1000-fold improvement in inhibition of specific ALDH isoforms and 5-10 fold improved solubility and metabolic stability. Exemplary compounds exhibited potent cellular inhibition of ALDH, depleted the CD133⁺ putative cancer stem cell population, and were highly synergistic with cisplatin in patient derived ovarian cancer spheroids. We have also developed the most potent, selective ALDH1A3 inhibitor to date and

have begun to define the structural features determining selectivity between the three ALDH1A isoforms.

Chapter 1 Introduction and Background

1.1 Ovarian Cancer: Current Treatments and Prognosis

In 2018, more than 22,000 U.S. women will be diagnosed with ovarian cancer and more than 14,000 will succumb to the disease, making it the 5th most deadly cancer in women.

Although ovarian cancer diagnosed at the local stage (Stage 1) has a 5-year survival rate of over 90%, 3 in 5 women are diagnosed after the cancer has spread to distant sites in the abdomen. In these cases, the 5-year survival rate is 29%. Unfortunately, there are no early symptoms or reliable tests to detect ovarian cancer in the early stages. The most common symptoms of bloating, pain in the back or abdomen, feeling full quickly, or bladder problems are attributable to disease dissemination.

90% of ovarian cancers are epithelial in origin. High grade serous carcinoma, the most common and most aggressive ovarian cancer subtype, is now thought to originate in the serous epithelium of the fallopian tubes in many cases before migrating to the ovaries, where the first observable tumor will eventually form. The first line therapy for the majority of epithelial ovarian cancer (EOC) cases is surgical debulking of the primary tumor at which point the cancer is staged and the histological subtype is determined.¹

In addition to surgery, platinum- and taxane-based chemotherapeutics are used to treat the residual disease.²⁻³ Approximately 70% of EOC patients are initially responsive to chemotherapeutics; however, most relapse and ultimately become unresponsive to further chemotherapy.⁴ Platinum resistance may be mediated by: 1) reduced expression of copper

transporters which promote active transport of platinum drugs into the cell, 2) increased expression of copper efflux transporters or ATP-Binding Cassette transporters both of which can efflux platinum, 3) increased production of glutathione (GSH) and increased expression of GSH-S-transferases to promote formation of platinum-thiol adducts, 4) increased activity of DNA repair mechanisms, and 5) suppression of DNA-damage sensing apoptotic pathways.⁵

There have been few breakthroughs in ovarian cancer treatment since the approval of taxane-based chemotherapeutics in the 1990s. Two new therapeutic strategies, targeting vascular endothelial growth factor (VEGFR) and poly(ADP-ribose) polymerase (PARP), have recently been FDA approved for treatment of ovarian cancer.

The VEGFR targeting monoclonal antibody Bevacizumab inhibits tumor angiogenesis, and normalizes existing vasculature, which improves the efficacy of traditional chemotherapeutics. Bevacizumab is generally better tolerated than traditional chemotherapeutics. Unfortunately, Bevacizumab provides very modest improvements in overall survival and progression-free survival in EOC patients.⁶

The genes involved in homologous recombination, the repair of DNA double strand breaks, are mutated or epigenetically silenced in about 50% of high grade serous ovarian cancers. Tumors with these deficiencies tend to be more sensitive to DNA damaging chemotherapeutics such as the platinum drugs, because they are unable to repair the drug induced DNA damage.⁵ Mutation or silencing of the BRCA1/2 genes specifically is present in up to 30% of high grade serous ovarian tumors and diminishes homologous recombination activity. Inhibiting alternative DNA repair mechanisms is selectively toxic to homologous recombination deficient cancers. The enzymes PARP1-3 bind single strand DNA breaks and synthesize negatively charged poly(ADP-ribose) polymers, recruiting DNA repair enzymes. PARP inhibition in combination

with homologous recombination deficiency leads to an accumulation of DNA strand breaks and prevents mitosis. Three approved PARP inhibitors, Olaparib, Rucaparib and Niraparib, show compelling efficacy in homologous repair deficient high grade serous ovarian cancer. As a maintenance therapy, Niraparib improves progression free survival from 5.5 to 21 months in BRCA-mutation-positive cancers. In homologous recombination deficient tumors without BRCA mutations progression free survival was improved from 3.8 to 12.9 months. More modest, but still significant, improvements in progression-free survival were also observed in homologous repair competent tumors.⁷⁻⁹ Despite these promising results, PARP inhibitors have yet to demonstrate an improvement in overall survival and work best only in a minority of ovarian cancer patients. Therefore, new treatments to address ovarian cancer are still needed.

1.2 The Cancer Stem Cell Hypothesis

Similar to healthy tissue where distinct cell types serve different functions, tumors contain distinct subpopulations of cells with a multitude of observable phenotypic differences. The 2001 review by Reya et al. was perhaps the first to formalize the cancer stem cell (CSC) hypothesis to explain the heterogeneous populations of cells within a tumor.¹⁰ The central tenants of the CSC hypothesis are: 1) the oncogenic mutations which lead to tumor formation occur in stem cells, and therefore stem cells are the origin of tumors; and 2) tumors contain a heterogeneous population of cells, and a stem-like subpopulation of cells are necessary to drive tumor progression and maintain heterogeneity.¹⁰⁻¹¹ The alternative hypothesis, the stochastic model of tumor heterogeneity, asserts that all of the heterogeneous cell types are able to replicate and can produce other cell types through random “stochastic” events. In this model, chemoresistance is acquired through natural selection of chemoresistant cells.¹⁰ Recent evidence

suggests a combination of the two models is most likely correct. Mutations in differentiated cells may reverse epigenetic suppression of stem-ness genes, allowing de-differentiation¹²

As a consequence of CSCs being vital to maintaining tumor heterogeneity, CSCs are uniquely able to repopulate a tumor following insult with chemotherapy. Eradication of CSCs is therefore vital to sustain a response following treatment. Unfortunately, chemotherapeutics which target rapidly dividing cells have less effect on CSCs which are relatively quiescent. Additionally, CSCs may harbor enhanced DNA repair mechanisms or express efflux transporters or enzymes capable of inactivating chemotherapeutics.^{11, 13}

The high initial response rate, subsequent relapse, and eventual development of chemoresistance can be explained by the CSC hypothesis; chemotherapy initially is able to kill the bulk of the tumor comprised of non stem-like cells, but chemoresistant CSCs are able to repopulate the tumor and eventually confer newly acquired or existing chemoresistance traits to their progeny.

While, historically, facile assays measuring bulk cytotoxicity have been employed to assess the efficacy of potential new cancer therapeutics in vitro and in vivo, more sophisticated measurement techniques which can assess the phenotype of individual cells such as flow cytometry and high content imaging are needed to specifically probe the impact of therapeutics on CSCs.

1.3 Markers for CSCs in Ovarian Cancer

Given that a tenant of the CSC hypothesis is that CSCs originate from somatic stem cells, it follows that the markers used to identify somatic stem cells may also be useful in identifying CSCs. CSC markers relevant to ovarian cancer have been reviewed in depth elsewhere. Briefly, surface glycoproteins (CD24, CD44, CD117, CD133, and epithelial cell adhesion molecule), cell

surface antigens (LY6A), GPCRs (LGR5), catalytic enzymes (aldehyde dehydrogenase (ALDH)), and ATP-binding cassette transporter proteins (ABCG2) all have potential utility in identifying ovarian CSCs.¹⁴⁻¹⁵ CSC markers are typically validated by separating cells with and without the marker by flow cytometry and assessing the tumorigenicity of the two separate populations by engrafting a defined number of cells in immunocompromised mice.¹⁶ Increased tumorigenicity for a particular sub-population is taken as evidence of stemness. A practical limitation of this method is that it biases studies towards marker populations which can withstand the considerable manipulation associated with flow cytometric separation and engraftment without significant changes in marker expression, rather than the most biologically relevant marker populations. Additionally, an immunocompromised mouse presents a different tumor environment than an immunocompetent patient, and therefore such models may select for markers which are not biologically relevant in patients.¹⁶ Validating putative cancer stem cell markers in humanized mouse models may eventually provide a more conclusive assessment of their biological relevance.¹⁷

In 2011, Silva et al. assessed several potential CSC markers in a number of epithelial ovarian tumors, primary peritoneal tumors, and ovarian cancer cell lines.¹⁸ They found a small population (0.25% to 9%) of ALDH^{Bright} (high ALDH activity as determined by ALDEFLUOR) cells in every sample, consistent with a common assertion that CSCs should be relatively rare. While cisplatin affected a dose dependent decrease in the total viable cell count in the SKOV3 ovarian cancer cell line, the relative percentage of ALDH^{Bright} cells *increased* with higher concentrations of cisplatin, suggesting that either cisplatin induces ALDH expression or ALDH identifies a chemoresistant subpopulation. Brief cisplatin treatment of FACS (fluorescence-activated cell sorting) purified ALDH^{Dim} (low ALDH activity as determined by ALDEFLUOR)

and ALDH^{Bright} cell populations revealed a greater number of viable cells with high ALDH activity immediately following treatment and a faster recovery following treatment cessation. ALDH^{Bright} SKOV3 and Hey1 cells were substantially more tumorigenic than ALDH^{Dim} cells. Engraftment of 1000 ALDH^{Bright} primary human tumor cells resulted in tumor growth in 2 of 9 mice while 50,000 ALDH^{Dim} cells did not generate any tumors in 9 attempts. In light of previous work demonstrating a highly tumorigenic population of ALDH^{Bright}/CD133⁺ cells in hepatocellular carcinoma, this rare population of cells purified from primary human ovarian tumor cells was assessed for tumorigenicity.¹⁹ Interestingly, between 11 and 500 ALDH^{Bright}/CD133⁺ cells were able to initiate tumors in 4 of 9 cases while cells with only one marker were unable to initiate tumors following injection of the same number of cells. Furthermore, ALDH^{Dim}/CD133⁻ cells were unable to initiate tumors in 9 trials following injection of 50,000 cells. To assess the clinical relevance of the ALDH^{Bright}/CD133⁺, 56 patient tumors were scored for ALDH and CD133 positivity. For the 18 patients with tumors bearing cells with both ALDH^{Bright} and CD133⁺ cells, the overall survival at 10 years was approximately 10%. For the remaining patients with tumors without one or both markers, overall survival ranged from 40-60% at 10 years. Many of the key findings from the Silva et al. study were corroborated in the near simultaneous disclosure by Kryczek et al.²⁰

In a follow up study, single cell techniques were used to demonstrate an ovarian CSC hierarchy. ALDH^{Bright}/CD133⁺ cells can self-renew or produce progeny without one or both putative CSC markers. ALDH^{Dim}/CD133⁺ and ALDH^{Bright}/CD133⁻ were capable of self-renewal or differentiation into ALDH^{Dim}/CD133⁻ cells. ALDH^{Dim}/CD133⁻ cells did not produce any progeny bearing either putative CSC marker. Interestingly out of over 1000 observed cell divisions, only one case of a stochastic event in which a ALDH^{Bright}/CD133⁻ primary ovarian

tumor cell produced an ALDH^{Bright}/CD133⁺ daughter cell was noted. Bone morphogenetic protein 2 (BMP-2) is more highly expressed in the differentiated ALDH^{Dim}/CD133⁺, ALDH^{Bright}/CD133⁻, or ALDH^{Dim}/CD133⁻ cells, but not ALDH^{Bright}/CD133⁺ cells. This cytokine signaling molecule produced primarily in ALDH^{Dim}/CD133⁻ appears to mediate a feedback loop regulating relative cell populations by stimulating proliferation of putative CSCs (ALDH^{Bright}/CD133⁺) and inhibiting growth of differentiated (ALDH^{Dim}/CD133⁻) cells.²¹

1.4 Function of CD133 in CSCs

CD133, also known as prominin-1, is a surface glycoprotein with an N-terminal extracellular domain, 5 transmembrane domains, 8 sites of glycosylation, and a c-terminal intracellular tail with multiple tyrosine residues known to be phosphorylated by Src kinase. Although countless studies have correlated CSC properties and the function of various cellular pathways with CD133 expression, compelling evidence of a specific role of CD133 in CSCs has remained elusive.²²⁻²³ Liu et al. demonstrated that binding of the Src SH2 regulatory domain to the phosphorylated intracellular tail of CD133 activates Src kinase, promoting phosphorylation of focal adhesion kinase and eventually leading to activation of oncogenic pathways promoting survival, migration, and metastases.^{22, 24} In glioma, interaction between the phosphorylated tail of CD133 and p85 similarly leads to activation of the oncogenic Akt pathway. Weng et al. discovered direct interaction between CD133 and epidermal growth factor receptor (EGFR) which may lead to ligand-independent activation of the receptor which may also activate the Akt pathway. They also demonstrated that CD133⁺ overexpression increased the resistance of pancreatic cancer cell lines to chemotherapeutics, but sensitized cells to the EGFR inhibitor gefitinib.²⁵ In hepatocellular carcinoma, expression of CD133 correlated with increased autophagy and knockdown of CD133 reduced viability in low glucose media. These results

suggest CD133 may help CSCs evade death in nutrient poor conditions by increasing nutrient uptake via autophagy.²⁶ CD133⁺ knockdown in hepatocellular carcinoma reduced cellular glutathione levels, decreasing resistance against reactive oxygen species (ROS) and chemotherapy. Pharmacological depletion of intracellular glutathione with sulfasalazine similarly increased the efficacy of chemotherapy in vitro and in vivo.²⁷ Although none have been disclosed thus far, specific inhibitors of the protein-protein interactions between CD133 and Src, p85, and EGFR would have great value as biological probes to elucidate the specific roles of CD133.

1.5 Function of ALDH in CSCs

The ALDH superfamily of enzymes is primarily responsible for the NAD(P)⁺-dependent oxidation of endogenous and exogenous aldehydes into the corresponding carboxylates. The detailed mechanism is illustrated in Figure 1.1. They also possess NAD(P)⁺ independent esterase activity.²⁸ Both ALDH1A1 (1A1) and ALDH1A3 (1A3) have been extensively linked to stem-like characteristics in a number of malignancies.²⁹⁻³⁰ Additionally knockdown or inhibition of 1A1 increases chemosensitivity in a number of cancers.³¹⁻³⁷ ALDH1A2 (1A2) and 1A3 show a high degree of sequence homology with 1A1 and have also been implicated in chemoresistance.³⁸⁻³⁹ The ability of 1A1 and ALDH3A1 (3A1) to promote chemoresistance to cyclophosphamide is well understood; the two isoenzymes are able to oxidize an aldehyde on an intermediate (aldophosphamide) in the bioactivation of cyclophosphamide, preventing formation of the active phosphoramidate mustard.⁴⁰ The role of ALDH in chemoresistance to other chemotherapeutics and in CSCs is not well understood.

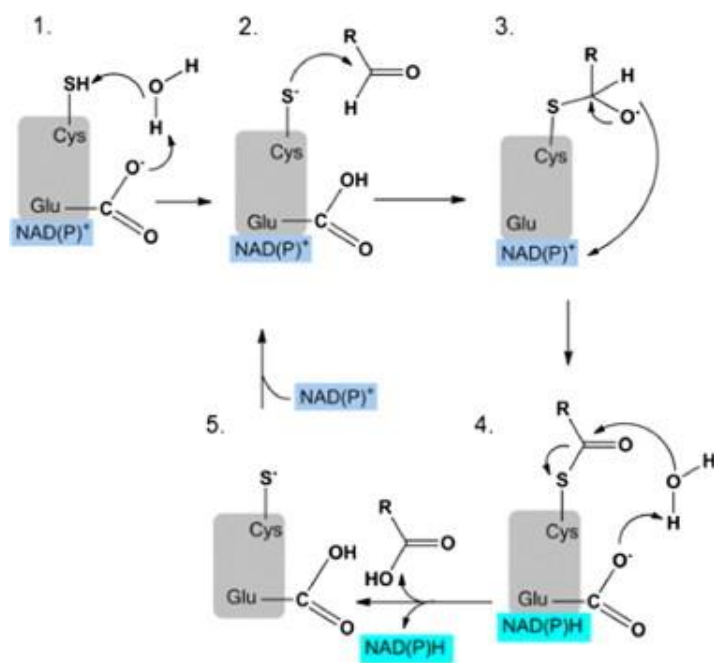


Figure 1.1: Mechanism of Aldehyde Dehydrogenase (Morgan et al.⁴¹)

1) Water mediates deprotonation of catalytic Cys302 by Glu268. 2) Nucleophilic attack of substrate aldehyde by cysteine anion. 3) NAD(P)⁺ abstracts hydride from the tetrahedral intermediate. 4) The resulting thioester is hydrolyzed by water and NAD(P)H is ejected, regenerating the enzyme to accept a new substrate and cofactor molecule. 5) Another molecule of NAD(P)⁺ enters the cofactor binding site.

Lipid peroxidation is a common source of endogenous aldehydes. Cellular metabolic processes, primarily in the mitochondria, can release “free radicals” and peroxides (e.g. superoxide radical (O₂⁻), hydrogen peroxide). These short lived reactive intermediates form lipid peroxides which eventually can break down to lipid aldehydes such as malonaldehyde, hexanal, 4-hydroxynonal, and acrolein. These reactive electrophiles can form adducts with glutathione, proteins and DNA. Many tumors exhibit increased levels of reactive oxygen species compared to healthy tissue, which can lead to detectable DNA damage such as the mutagenic oxidation of guanosine (8-Oxo-2'-deoxyguanosine). Antitumor agents, including cisplatin,

promote lipid peroxidation leading to further oxidative stress. Given that ALDH is able to neutralize the aldehyde end-products of lipid peroxidation, the elevated ALDH activity in CSCs may function to confer resistance against oxidative stress.⁴²

The three ALDH1A isoforms, along with ALDH8A1, also participate in cellular signaling by oxidizing retinaldehyde into all-trans retinoic acid (ATRA).²⁸ The retinoic acid signaling function of ALDH may also be relevant in CSCs. In many healthy stem cell types and in leukemia, ATRA can promote differentiation of stem cells by binding to Retinoic Acid Receptors (RAR) in the nucleus and enhancing expression of genes responsible for loss of stem cell markers, differentiation, and morphological changes. ATRA is an effective therapeutic for acute promyelocytic leukemia, demonstrating that depletion of the cancer stem cell pool by inducing differentiation can reduce tumor cell propagation. Unfortunately, in many solid tumors, epigenetic modification prevents expression of RAR β . In this context, combination of ATRA with emerging epigenetic modifiers may restore the ability of ATRA to promote differentiation. In solid tumors retinoic acid can also activate transcription of oncogenic pathways PDK-1/Akt, c-MYC, and cyclin D1.⁴³⁻⁴⁴

In contrast to CD133⁺, ALDH is a classical “druggable” protein possessing a well-defined enzyme active site; many small molecule inhibitors of ALDH have been disclosed which will be discussed below.

1.6 Possible Connections Between ALDH and CD133 in CSCs

Although any direct mechanistic link between expression of CD133 and ALDH in CSCs is unclear, they are involved in many similar pathways which may explain their role in the hierarchy of CSCs proposed by Choi et al. First, CD133 is able to activate proliferation-

inducing and anti-apoptotic Akt pathway through interaction with p85 and EGFR. Retinoic acid, produced by ALDH, can stimulate expression of Akt genes by binding to the nuclear hormone receptors PPAR β and δ .⁴⁵ Importantly Akt activation is associated with the pro-metastatic epithelial-to-mesenchymal transition in ovarian cancer.⁴⁶⁻⁴⁷ Furthermore, ovarian cancer cells bearing the hallmarks of the mesenchymal phenotype exhibit increased resistance to platinum-based chemotherapy.⁴⁸ Second, knockdown of CD133 diminished the ability of hepatocellular carcinoma cells to survive in nutrient starved environments.²⁶ ALDH may likewise be linked to the acquisition of nutrients; Kang et al. demonstrated that inhibition or knockdown of ALDH significantly diminishes the ability of non-small-cell lung carcinoma cells to produce ATP.⁴⁹ They propose these cells depend directly on the ALDH mediated production of NAD(P)H to power the electron transport chain, but do not address the abundant source of aldehydes required for such a hypothesis. Finally, CD133⁺ promotes resistance to ROS, and ALDH is a scavenger of reactive oxygen species.

As noted above, BMP2 appears regulate ALDH+CD133+ CSC self-renewal. Interestingly, BMP-2 can activate Akt, similarly to CD133 and ALDH.⁵⁰⁻⁵² The role of BMP-2 in maintaining cell population homeostasis in ovarian cancer deserves further study.

1.7 Validation of ALDH1A as a Target in Ovarian Cancer Stem Cells

To assess whether inhibition of ALDH might influence the CD133⁺ cell population in ovarian cancer cell lines the Buckanovich lab performed knockdown experiments of various ALDH isoforms. As shown in Figure 1.2 siRNA knockdown indicated targeting 1A1, 1A2, and 1A3 could deplete of CD133⁺ A2780 ovarian cancer cells and furthermore, the effects of

knocking down multiple isoforms were additive. These results were confirmed in the additional ovarian cancer cell lines PEO-4 and Kuramochi.

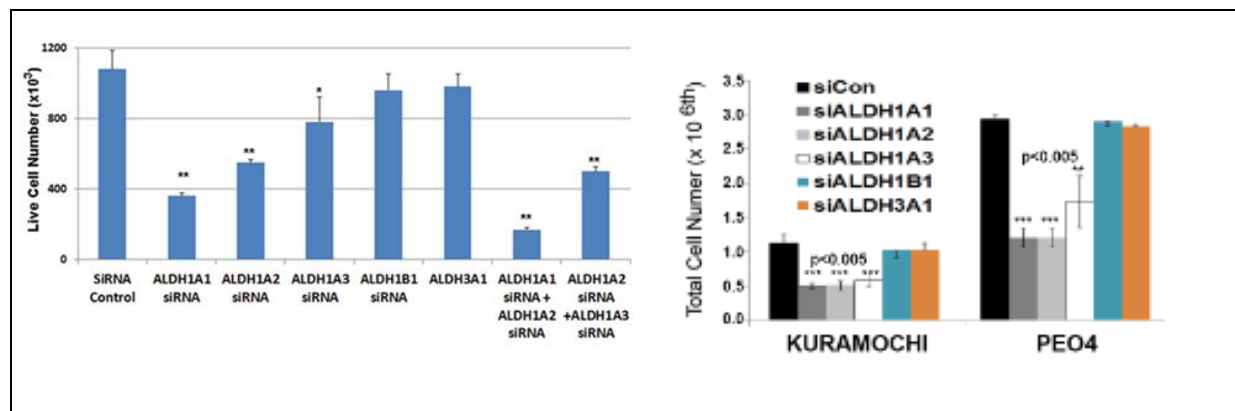
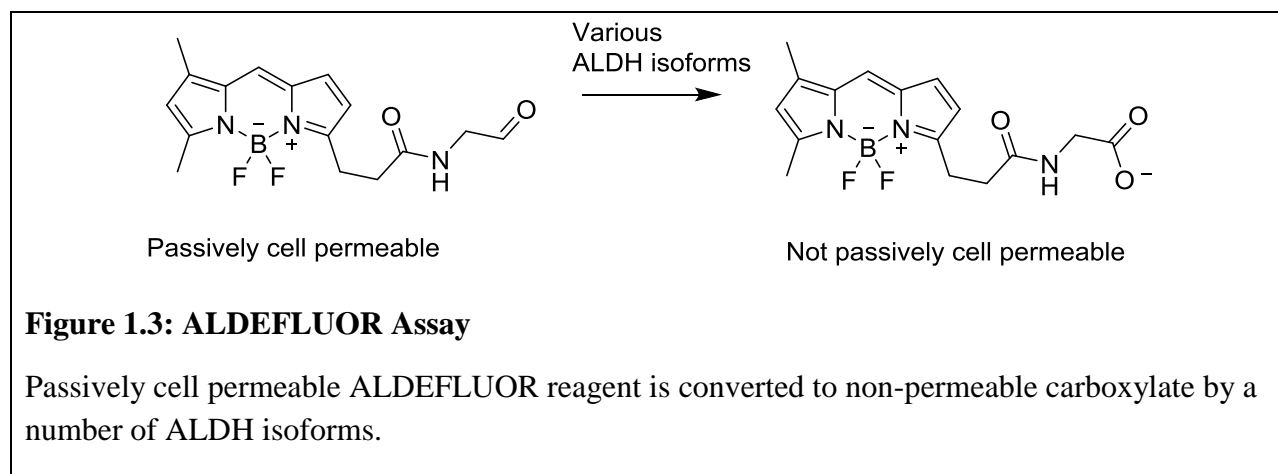


Figure 1.2: Effect of ALDH1A Knockdown on Ovarian Cancer Cell Lines.

(Left) Average live cell numbers following transfection of FACS purified CD133⁺ A2780 cells with the specified siRNAs. *p<0.05, **p<0.01 vs control. (Right) Average live cell numbers following transfection of FACS purified CD133⁺ Kuramochi and PEO4 cells with the specified siRNAs.

1.8 Rationale for Isoform Selective ALDH Inhibitors



Currently, ALDEFLUOR is the standard assay for determining ALDH activity in cells.

As shown in Figure 1.3, the assay relies on accumulation of the cell impermeable BODIPY-

carboxylate following oxidation of the ALDEFLUOR reagent aldehyde by ALDH. A PGP inhibitor is included in the assay to prevent active transport of either species. A serious limitation of the ALDEFLUOR assay is that the reagent is a substrate for many ALDH isoforms, making it impossible to attribute the ALDEFLUOR activity in cells to a specific ALDH isoform.⁵³⁻⁵⁴ A further complication is the lack of published Michaelis-Menten kinetic parameters for the ALDEFLUOR reagent with respect to the various ALDH isoforms. (Obtaining this information may be difficult due to the potential for interference between the highly fluorescent ALDEFLUOR reagent and the typical readout of NAD(P)H absorbance used in ALDH assays.) Given that there is a 250-fold discrepancy in K_m for the very simple substrate acetaldehyde between 1A1 and ALDH2, it is conceivable that expression of ALDH isoforms for which ALDEFLUOR is a poor substrate are currently going undetected by this methodology.^{53, 55} Additionally, expression of an isoform which rapidly turns over ALDEFLUOR may obfuscate subtle changes in expression of other isoforms.

A platform to rapidly elucidate the ALDH isoforms responsible for ALDEFLUOR activity would facilitate discovery of the underlying mechanisms of ALDHs function in CSCs. Such a platform might consist of a panel of isoform specific ALDEFLUOR-like substrate probes, or a panel of isoform selective inhibitors. A panel of isoform specific ALDEFLUOR probes with different absorbance/emission spectra might one day enable simultaneous tracking of multiple isoforms.^{53, 56} It is unclear whether modified ALDEFLUOR analogs, likely with higher molecular weight and more steric crowding of the aldehyde to affect isoform selectivity, would maintain the favorable cell permeability properties which are vital to the function of the assay. In the case of isoform selective inhibitors, looking for a decrease in ALDEFLUOR signal following compound administration would implicate that isoform in the ALDEFLUOR activity.

Isoform selective inhibitors would, of course, have the added advantage of enabling rapid assessment of the effect of inhibiting a particular isoform in various cellular assays, which is currently often achieved using siRNA techniques.

Given the strong evidence for the role of the ALDH1A family in CSCs, we have pursued isoform selective inhibitors of the ALDH1A subfamily. Given the homology and overlapping substrate specificity of the ALDH1A family, the Buckanovich Lab evaluated whether cells could compensate by increasing 1A3 expression in response to selective inhibition of 1A1 or 1A2. As shown in Figure 1.4 1A1 or 1A2 knockdown increased expression of 1A3 by 4 to 6 fold. Analysis of mRNA levels for the ALDH1A isoforms in ovarian cancer cell lines uncovered variation in which isoform was preferentially expressed (Figure 1.5). In light of this, we reasoned that in contrast to isoform selective inhibitors, the pan-ALDH1A inhibitors could overcome compensatory expression of other isoforms in response to ALDH inhibition, and also might have efficacy in a wider array of cell lines and tumors with different ALDH1A expression profiles. For proof-of-concept studies we desired pan-ALDH1A inhibitors with good selectivity over other isoforms; however, for the reasons mentioned above, single isoform selective inhibitors could also provide valuable information.

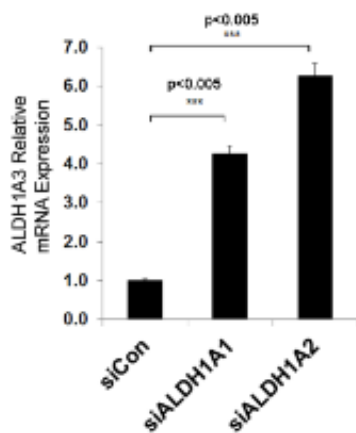


Figure 1.4 Effect of 1A1/1A2 Knockdown on 1A3 Expression

mRNA expression of ALDH1A3 following treatment of PEO4 cells with the specified siRNAs. (Unpublished work, courtesy Buckanovich Lab)

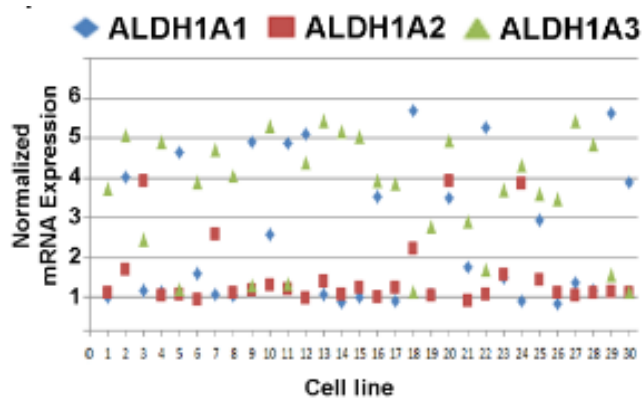


Figure 1.5 ALDH1A Expression in Ovarian Cancer Cell Lines

Analysis of Cancer Cell Line Encyclopedia ALDH1A expression data for ovarian cancer cell lines. (Unpublished work, courtesy Buckanovich Lab)

In addition to desiring selective inhibitors to provide the most unambiguous results in studies probing the function of ALDH1A, from a therapeutic standpoint, ALDH2 deficiency or inhibition causes adverse reactions to alcohol, may promote liver fibrosis, and reduces the

efficacy of nitroglycerin.⁵⁷⁻⁵⁹ Additionally, there is evidence that ALDH2 may mitigate ischemia-induced cardiac and cerebrovascular damage.⁶⁰ Therefore, we felt that selectivity over the closely related ALDH2 was desirable in our ALDH1A probes.

1.9 Structural Basis for ALDH Isoform Selectivity

The members of the ALDH1A family possess ~70% sequence homology. ALDH2 and ALDH1B1 are also closely related, with 66% and 62% homology respectively.²⁸ As shown in Figure 1.6, the main difference between the ALDH1A1 and 1A2-1A3 active sites is an asparagine (N475) in 1A2, 1A3 at the residue corresponding to G458 in ALDH1A1. According to the crystal structure of 1A2 (PDB: 6B5H) the conformation of the peptide backbone changes to accommodate the N475 without reducing the size of the mouth of the active site. The homology model of ALDH1A3 suggests the asparagine is reducing the size of the active site mouth. More subtle differences between the ALDH1A isoforms will be discussed in subsequent chapters. ALDH2 presents a significantly narrower passage to the catalytic cysteine due to M125; the corresponding residue in ALDH1A is glycine. Based on the similar active sites of ALDH1A and the much narrower active site in ALDH2 we reasoned that pan-ALDH1A inhibitors with selectivity over ALDH2 were possible.

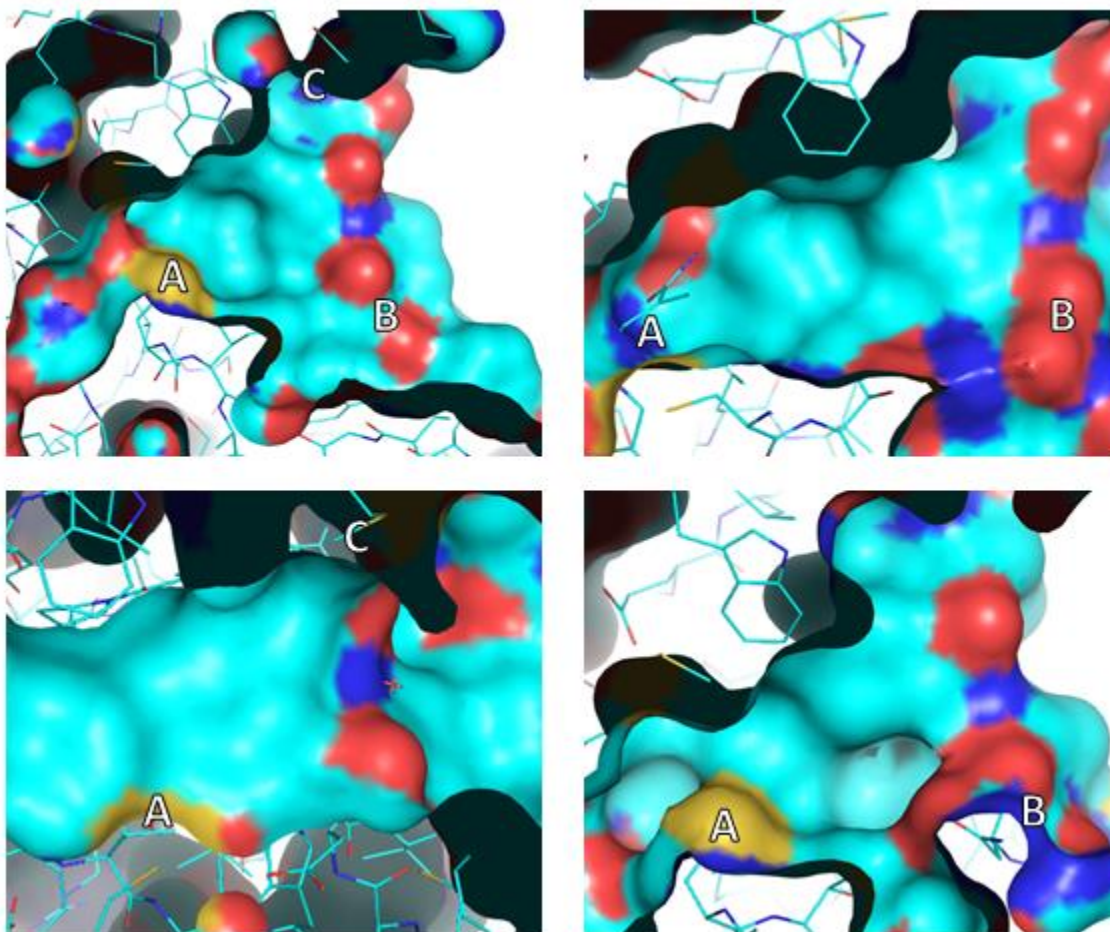


Figure 1.6: Active Site Homology of ALDH1A family and ALDH2

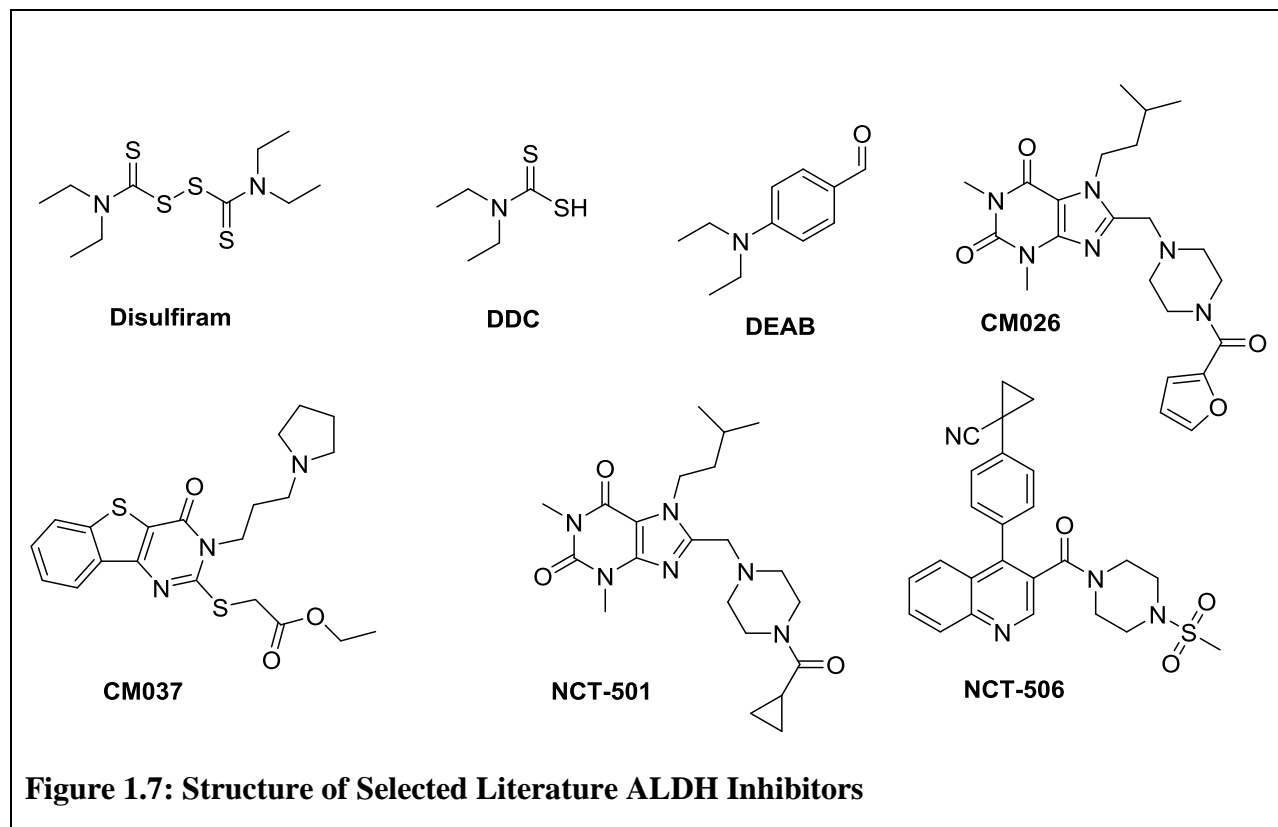
Clockwise from top left: ALDH1A1 (PDB: 5TEI), ALDH1A2 (PDB: 6B5H), ALDH1A3 (Homology model courtesy Dr. Bikash Debnath), ALDH2 (PDB: 5L13). A) Catalytic cysteine, B) Residue corresponding to Gly458 in ALDH1A1 is Asn in 1A2 and 1A3, C) Met125 in ALDH2 reduces the size of the active site mouth.

1.10 Review of ALDH Inhibitors

The 2012 comprehensive review by Koppaka et al. named 15 distinct chemotypes of ALDH inhibitors.²⁸ Eight of these inhibitor classes inhibit ALDH through covalent modification of the

catalytic cysteine, which is conserved throughout all 19 members of the ALDH superfamily.

Key compounds from the review are addressed here (See Figure 1.7 for structures).



Disulfiram, perhaps the most well-known ALDH inhibitor, is an FDA approved treatment for alcoholism. Disulfiram is rapidly and extensively metabolized into a number of covalent ALDH inhibitors with varied isoform selectivity which are responsible for its activity in vivo.

Disulfiram promotes aversion to alcohol consumption by altering the metabolism of ethanol.

Ethanol is metabolized to acetic acid in two steps. In the first step, alcohol dehydrogenase converts ethanol to acetaldehyde, the metabolite responsible for many symptoms associated with hangover.⁶¹ Subsequently ALDH (predominately ALDH2) metabolizes acetaldehyde to acetic acid. Thus, in the presence of the ALDH2 inhibitor Disulfiram, even moderate alcohol

consumption causes the rapid onset of unpleasant symptoms including tachycardia, palpitations, hypotension, headache, and nausea.⁵⁷ A mutant variant of ALDH2 with reduced ability to metabolize acetaldehyde is also responsible for an adverse reaction to alcohol consumption known as Asian Flush in approximately 1/3 of East Asians.⁶²

Interestingly, Disulfiram, or its metabolite diethyldithiocarbamic acid (DDC), has demonstrated efficacy in the treatment of cancer in vitro and in vivo.⁶³⁻⁶⁴ This effect is not entirely ALDH mediated; it is attributed, at least in part, to the stable complex of DDC and copper, which can inhibit the p97 protein degradation by binding to the NPL4 protein.⁶⁴ Nevertheless, disulfiram demonstrates that relatively broad spectrum ALDH inhibitors are clinically tolerable.

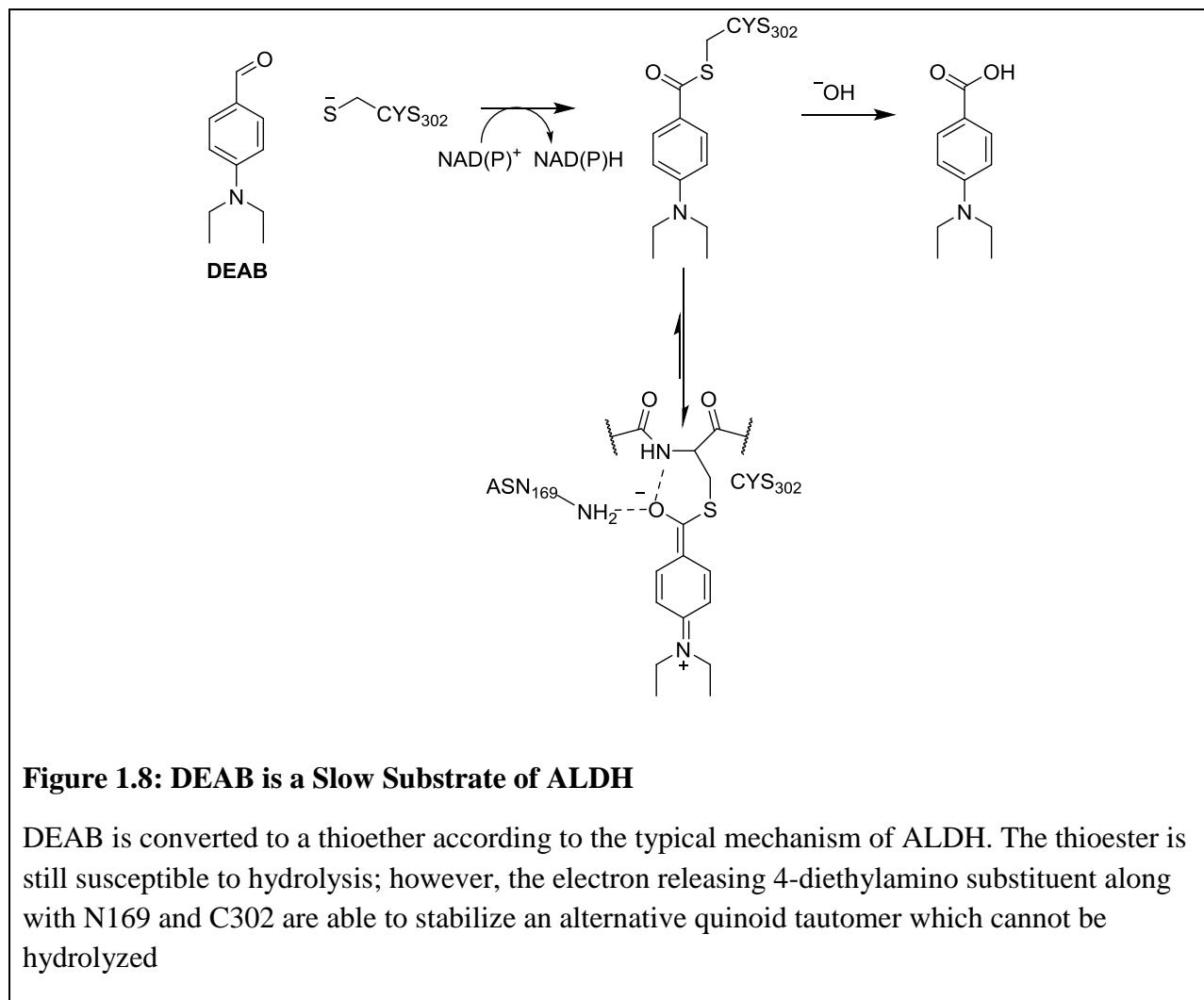


Figure 1.8: DEAB is a Slow Substrate of ALDH

DEAB is converted to a thioether according to the typical mechanism of ALDH. The thioester is still susceptible to hydrolysis; however, the electron releasing 4-diethylamino substituent along with N169 and C302 are able to stabilize an alternative quinoid tautomer which cannot be hydrolyzed

One of most widely studied ALDH inhibitors and the standard positive control in ALDEFUOR assays, 4-diethylaminobenzaldehyde (DEAB), inhibits at least 6 isoforms of ALDH with an IC₅₀ <15 μM and is a substrate of at least 5 isoforms, including 1A1. The diethylamino substituent of DEAB retards turnover of the aldehyde as shown in Figure 1.8.⁴¹ DEAB suffers from poor cellular activity, requiring concentrations of ~100 μM to induce chemosensitization of CSCs.⁶⁵

In recent years, there has been significant progress in the development of more drug-like ALDH inhibitors. A fruitful HTS campaign for 1A1 inhibitors disclosed by the Hurley lab resulted in the discovery of 19 novel 1A1 inhibitors from 12 distinct chemotypes.⁶⁶ Encouragingly, follow up studies of 2 chemotypes from this series, **CM026** and **CM037**, demonstrated that potent, selective inhibition of 1A1 was possible.⁶⁷

The Maloney lab further developed the **CM026** chemotype resulting in **NCT-501**, a 40nM 1A1 selective inhibitor.⁶⁸ A recent effort from the same group to improve cell permeability by scaffold hopping resulted in **NCT-506** a 7nM 1A1 selective inhibitor with potent ALDEFLUOR activity and good exposure following oral administration. Importantly, this compound potentiated the effect of paclitaxel in a paclitaxel resistant 1A1 high cell line.⁶⁹

1.11 Conclusions

There is a notable absence of pan-ALDH1A selective inhibitors with selectivity over ALDH2. Given the significant evidence supporting the role of the ALDH1A isoforms in chemoresistance and CSC biology, this is a critical unmet need. Additionally, there have been no systematic studies attempting to elucidate the structural motifs which impart selectivity between 1A1, 1A2 and 1A3. In following chapters, I document my efforts to develop metabolically stable pan-ALDH1A selective inhibitors based on two chemotypes. As a result of our rigorous assessment of inhibition against the three ALDH1A isoforms, we have also made significant inroads in development of selective dual 1A2-1A3 inhibitors and 1A3 selective inhibitors to compliment the 1A1 selective inhibitors already in the literature.

Chapter 2 : Synthesis and Characterization of 673A Analogs

2.1 Characterization of 673A

Prior to my involvement, a survey of commercial analogs of DEAB in search of compounds with improved cellular potency resulted in the discovery of the promising compound **673A** (Table 2.1). The Buckanovich lab has extensively characterized the effects of this compound for a forthcoming publication. As shown in Figure 2.1, **673A** durably inhibits ALDEFLUOR, albeit at a relatively high concentration (25 μ M). Although ALDEFLUOR positivity is widely considered a marker of stem-ness, the decrease in ALDEFLUOR signal indicates target engagement, but does not indicate an actual reduction in the number of ALDH⁺ cells. Gratifyingly, **673A** also reduced the CD133⁺ cell population. FACS purification of ALDH^{Bright/Dim} and CD133^{+/-} cells showed enhanced toxicity of the compound against the ALDH^{Bright} and CD133⁺ populations. This suggests that **673A** is selectively toxic to the two stem cell pools, rather than promoting a loss of markers. In contrast DEAB had little effect on any cell population, and cisplatin spared CD133⁺ cells. **673A** also demonstrated synergy with chemotherapy in vitro, and enhanced the efficacy of cisplatin against cell line xenografts and platinum resistant patient derived xenografts in vivo. There is significant evidence to suggest that **673A** mediates programmed cell death by necroptosis, an alternative cell death pathway to apoptosis: 1) Cells killed by **673A** do not stain positive for Annexin-5, a marker of apoptosis, 2) **673A** treatment increases intracellular calcium, a marker and mediator of necroptosis, 3) pre-

treatment with the calcium chelator BAPTA rescues cells from **673A** toxicity 4) **673A** treated cells show a swollen morphology consistent with necroptosis, 5) HMBG1 undergoes a nuclear to cytoplasmic shift, 6) appropriate phosphorylation changes are seen in necroptosis associated proteins Drp-1 and PGAM5, and 7) **673A** induced cell death can be partially rescued with the MLKL inhibitor necrosulfonamide. It has been speculated that induction of necroptosis may be a viable strategy to treat tumors with apoptosis resistant cells.⁷⁰

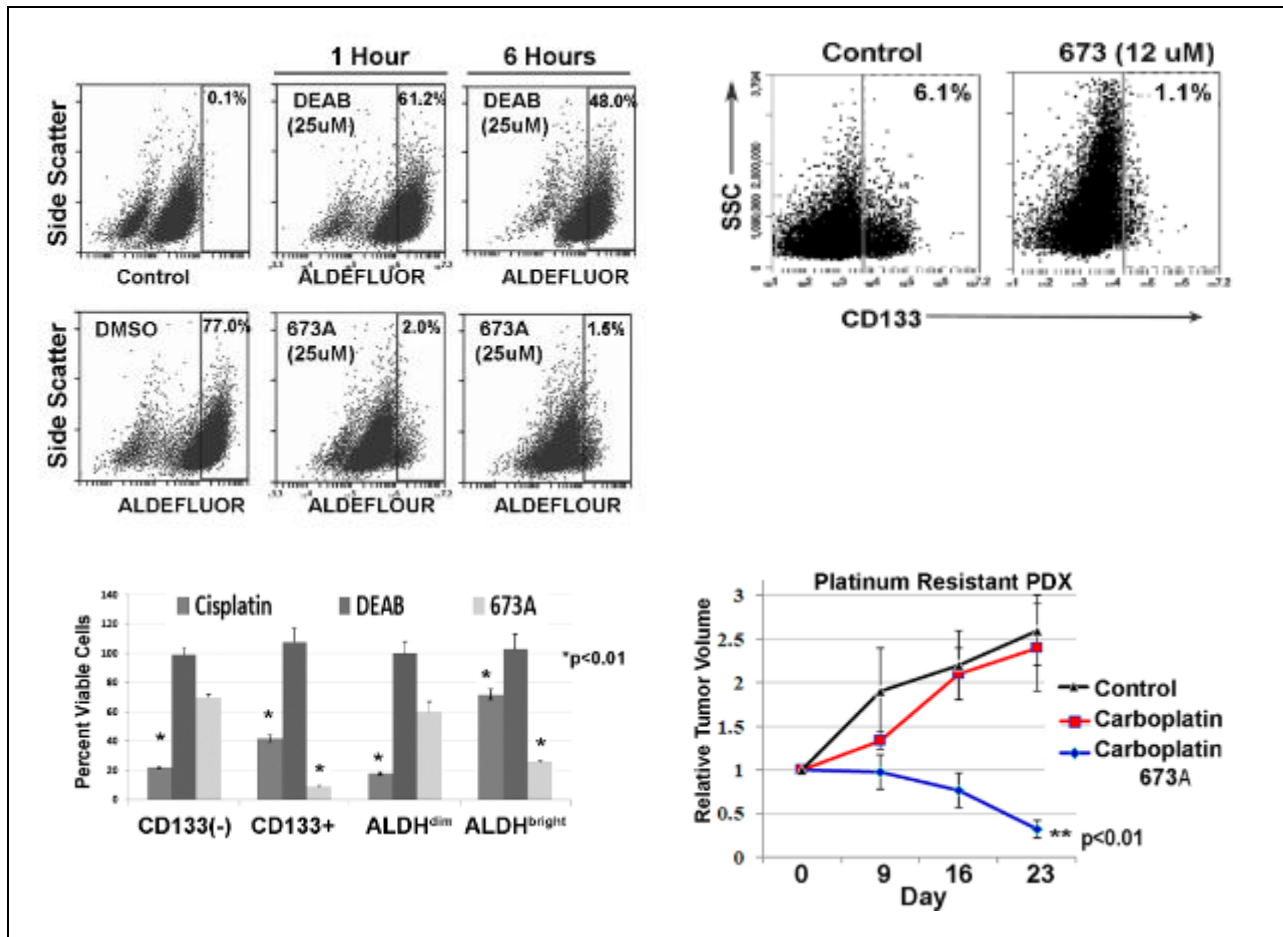


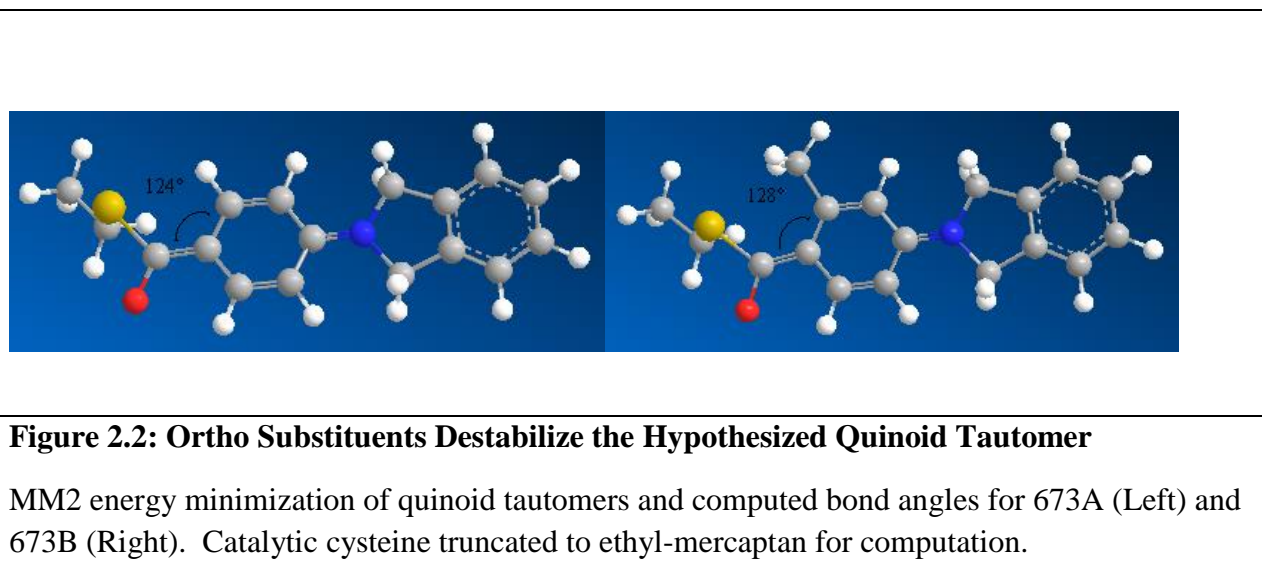
Figure 2.1: 673A Depletes CSCs and Sensitizes Patient Derived Tumors to Carboplatin

(Top Left) **673A** depletion of ALDEFLUOR in PEO1 cells at 1 and 6 hours is superior to DEAB at 25 μ M, (Top Right) **673A** depletes A2780 CD133⁺ cells, (Bottom Left) In FACS purified cells (ALDH^{Bright/Dim} in SKOV3 and CD133^{+/-} in A2780), **673A** preferentially depletes ALDH^{Bright} and CD133⁺ in contrast to Cisplatin which spares ALDH^{Bright} cells, (Bottom Right) **673A** reverses chemoresistance in a platinum-resistant patient derived xenograft model. (Unpublished work, courtesy of Buckanovich Lab)

2.3. SAR of 673A Analogs

With this compelling cellular data in hand, we set out to further optimize the **673A** scaffold primarily to address the low metabolic stability and relatively poor cellular potency. Biochemical, crystallographic, and cellular data are unpublished work, courtesy of the Hurley and Buckanovich labs. General experimental protocols for these assays are included in Chapter 3. Prior to adding the assay substrate, the ability of ALDH to catalyze oxidation of the inhibitors was assessed. We began our SAR campaign employing 1A1 as our representative ALDH1A family member and using ALDH2 as our indicator of selectivity given that selectivity over ALDH2 was desirable as discussed in Chapter 1.8. Although the crystal structure of analog **673B**, an ortho-methyl analog of **673A**, bound to ALDH1A1 did not indicate covalent interaction with the catalytic cysteine (Figure 2.3), **673A** and **673B** were both slow substrates for 1A1 and 1A2, leading us to believe they engage the catalytic cysteine with a mechanism similar to **DEAB**. We felt the covalent interaction was likely the primary contributor to the activity, given the low molecular weight and simple architecture of **673A**. We reasoned that deriving significant affinity from a covalent interaction with a cysteine found in every ALDH isoform would make it difficult to achieve selectivity. Additionally, there are few aldehydes found in clinical candidates or approved drugs, likely due to metabolic instability and concerns about their reactivity. We therefore set out to expand the **673A** scaffold to engage more features in the ALDH1A active site, reasoning that increasing non-covalent interactions would eventually enable us to use more accepted electrophilic warheads or eliminate the warhead altogether. The ability of ALDH to slowly oxidize the inhibitors complicates analysis of SAR trends. Paradoxically, improving the non-covalent affinity for the enzyme can conceivably promote turnover by increasing the residence time of the aldehyde in the active site, effectively lowering the Michaelis-Menten parameter K_M .

Attempts to add substituents ortho to the aldehyde were poorly tolerated by 1A1 and ALDH2 (**673B**, **6702972**, **206560**, **215121**)(Table 2.1). Being symmetrical, **673A** would have more possible approaches to the catalytic cysteine, perhaps enhancing the on-rate relative to **673B**, which may only be able to bind in the orientation depicted in Figure 2.3. Additionally, the tetrahedral intermediate formed upon addition of the catalytic cysteine is likely destabilized by steric crowding. The quinoid tautomer which is hypothesized to stabilize the thioester **DEAB**-ALDH complex (see Figure 1.8) is likely especially sensitive to steric crowding as it requires the cysteine sulfur, oxyanion, and phenyl moieties to be co-planar. The ortho-group is predicted to clash with Cys302 distorting the ideal 120° bond geometry for sp^2 carbons as depicted in Figure 2.2.⁷¹



The ortho-OMe analog **6702972** was 2-fold less potent than **673B**. Electronically, the OMe should further stabilize the quinoid through resonance; however, it seems that the steric bulk counteracts the electronic effects. The OBn (**206560**) and 2,5-dimethyl substituents **232721** completely abolished activity. The loss of activity between the sterically similar methyl

of **673B** and chloro of **215121** suggests that electron withdrawing substituents are additionally disfavorable. Electron withdrawing substituents may inhibit hydride abstraction, stalling the catalytic cycle at the reversible addition of the catalytic cysteine into the aldehyde.⁴¹ The diminished formation of the stable thioester may reduce the residence time of the inhibitor in the active site.

The meta-chloro analog **215123** was also substantially less potent than **673A**. Interestingly, the meta-methoxy analog **223960** was 2-fold more potent against 1A1 (0.1 μM) and 68-fold more potent against ALDH2 (0.025 μM). **223960** exhibited far better MLM stability than **673A**, perhaps due to steric blocking of the metabolically labile isoindoline.

We predicted that clash with the ALDH2 specific residue Phe292 (Figure 2.3) would cause translation of the isoindoline towards the cleft in ALDH1A which is occluded by Met125 of ALDH2. This translation should bring large meta substituents into close proximity with Met125, preventing ALDH2 binding to provide our desired selectivity profile. Surprisingly, extending to the benzyloxy **223903** and substituted benzyloxy **223905-223906** analogs diminished ALDH potency overall but maintained the ALDH2 selectivity observed for **223960**. The benzyloxy analogs were substrates of 1A1 but not ALDH2, suggesting that more effective stabilization of the quinoid tautomer in ALDH2 may explain the observed selectivity; however, a meta substituent is not capable of stabilizing the quinoid tautomer through resonant electron donation. Alkoxy substituents exhibit inductive electron withdrawing character, albeit weaker than for chloro substituents (Hammett Values: $\sigma_{\text{Meta}} = +0.37$ and $+0.12$ for $-\text{Cl}$ and $-\text{OMe}$, respectively).⁷² Therefore, from an electronic standpoint, the alkoxy substituents are predicted to be detrimental to stabilization of the quinoid tautomer, suggesting that the increased affinity is best explained by direct interaction of the alkoxy with the active site. Interestingly, the alkyl-

branched analog **223904** restored 1A1 potency and modest selectivity against ALDH2; however, it was still inferior to **673A** in both aspects. Based on an overlay of the 1A1-**673B** crystal structure with ALDH2, we expected that branching at this position would improve selectivity against ALDH2.

Appending a benzyloxy substituent at the 4-position on the isoindoline (**223940**) resulted in a 4-fold decrease in 1A1 potency relative to **673A** but a complete loss of inhibition of ALDH2. According to the **673B** crystal structure, substituents at the 5 position were expected to project into solvent. Surprisingly, 5-hydroxy analog **224258** exhibited no inhibition of ALDH. 5-Benzyloxy analog was only 2-fold less potent than **673A** against 1A1 but inactive against ALDH2. 2-Cl benzyloxy analog **224260** was inactive against 1A1, while 2-OMe benzyloxy analog **224262** weakly inhibited 1A1. The surprisingly tight SAR for substituents at the 5-position suggests an alternative binding mode in which the 5-benzyloxy substituent is not projecting into solvent.

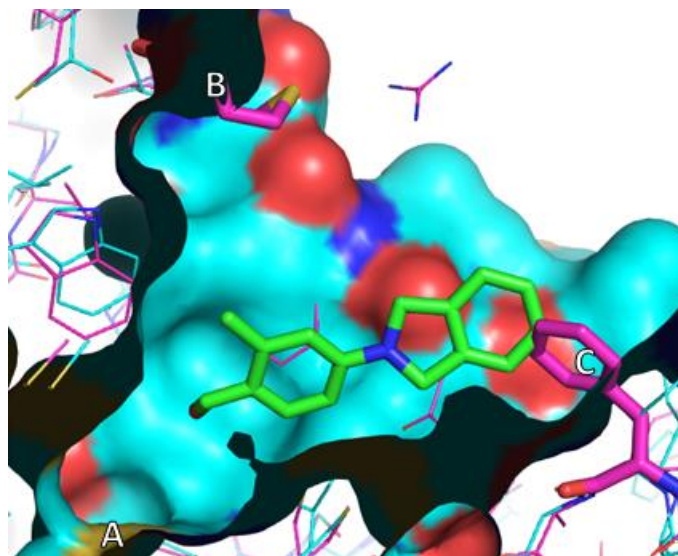
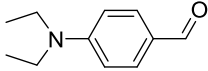
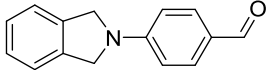
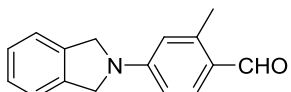
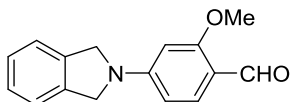
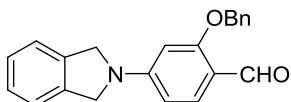


Figure 2.3: Crystal Structure of 673B Bound in ALDH1A1 Active Site Overlaid with ALDH2 (PDB: 5L13)

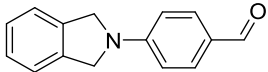
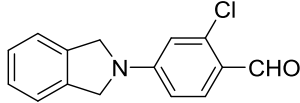
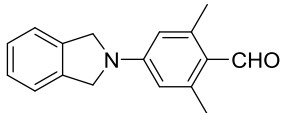
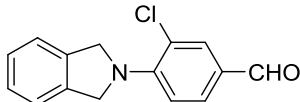
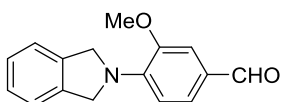
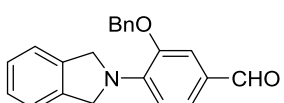
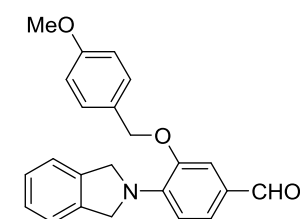
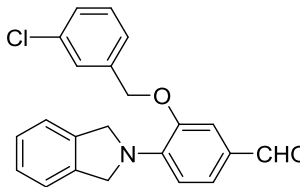
(A) Catalytic Cys302, (B) ALDH2 Specific Met125 (C) ALDH2 Specific Phe292. (Unpublished work, courtesy Hurley Lab)

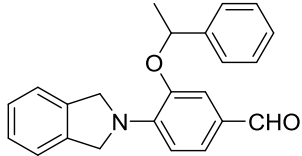
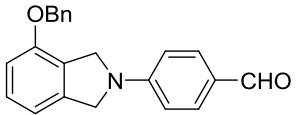
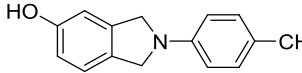
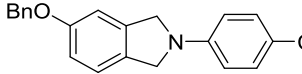
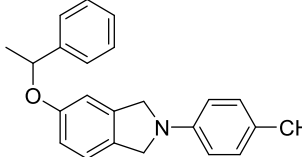
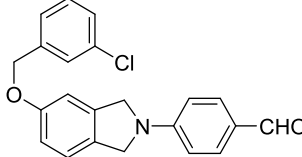
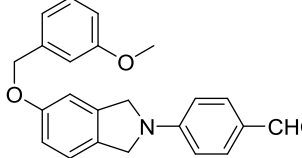
Table 2.1 Commercial SAR of DEAB Analogs

	Cmpd	ALDH IC ₅₀ (μ M)		FACS Purified SKOV3 CC ₅₀ (μ M)	
		1A1	2	CD133 ⁻	CD133 ⁺
	DEAB	0.057*	0.16	400	180
	673A	0.22*	1.7*	55	4
	673B	1.3*	>20	80	6
	6702972	2.2*	>10	30	9
	206560^a	~10	~10	160	30

IC₅₀ values are N=1 performed in triplicate, CC₅₀ values are N=1. *Denotes compound is a slow substrate. ^aSynthesized by Ron Sorenson. FACS = Fluorescence Activated Cell Sorting

Table 2.2 Characterization of Novel Analogs of 673A

	Cmpd.	ALDH IC ₅₀ (μ M)		Inhibition at 50 μ M in A2780 Cells		MLM Stability (% remaining at 5 min)
		1A1	2	Total	CD133 ⁺	
	673A	0.22*	1.7*	72%	90%	17%
	215121^b	>10*	>10	61%	71%	38%
	232721	>10	N.D.	31%	13%	
	215123^b	14	5.2	35%	45%	
	223960	0.104*	0.025*	40%	47%	87%
	223903	1.5*	0.27	0%	0%	
	223905	2.8*	0.69			
	223906	3.6*	0.26			

	223904	0.36*	0.61	41%	25%
	223940	0.86*	>10*	50%	50%
	224258	~10*	~10*		70%
	223908	0.5*	>10*		36%
	223941	1.8*	>10*		
	224260	>10*	>10*		77%
	224262	3	>10		
<p>IC₅₀ values are N=1 performed in triplicate, CC₅₀ values are N=1. *Denotes compound is a slow substrate. ^bSynthesized by Dr. Scott Barraza. MLM = Mouse liver microsomes</p>					

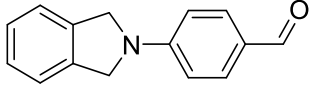
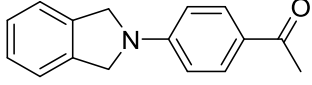
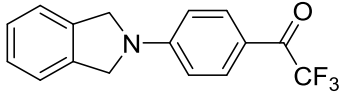
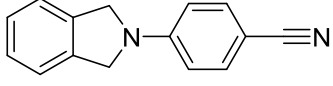
Since the alkoxy scan did not afford a compelling avenue to improve ALDH inhibition, we briefly surveyed electrophiles to replace the aldehyde as shown in Table 2.3. As mentioned previously, aldehydes are undesirable in drug development, and the slow substrate nature of this series complicates interpretation of the SAR trends. Unfortunately the ketone and nitrile

analogs (**22151**, **224259**) were inactive against ALDH. Tuning the electronic properties of the aryl nitrile to enhance electrophilicity towards the catalytic cysteine might restore activity.⁷³

The trifluoroacetyl analog **223902** was weakly active against 1A1 and ALDH2. The results were consistent with our hypothesis that the aldehyde contributed significantly to the ALDH1A1 activity.

Cell data for the early SAR (Table 2.1) was obtained using FACS purified CD133^{+/-} cells in the SKOV3 cell line. Only 0.33% of cells in this line are CD133⁺.¹⁸ Due to the resource intensive nature of FACS purified cell assays, especially when observing rare cell populations, further cellular SAR was conducted in the A2780 cell line. Because 10% of cells in this line are CD133⁺, it is possible to simultaneously quantify total cell kill and CD133⁺ cell kill in the same assay. Compound **673A** at 50 μ M was able to selectively deplete the CD133⁺ population by 90% in this cell line, with modest selectivity over the total cell population. Unfortunately for the novel analogs in the series, there was very little correlation between enzymatic ALDH activity and the cytotoxicity against CD133⁺ cells. Notably, only the compounds with 1A1 and ALDH2 IC₅₀s equal or greater than 10 μ M (**206560**, **215121**, **224258**, and **224260**) were able to deplete CD133⁺ cells by greater than 50% at 50 μ M. The reasonably potent ALDH1A1 inhibitors (**223904**, **223940**, **223960**) exhibited little to no selectivity for CD133⁺ cells vs. the total cell population. There also wasn't any correlation between ALDH2 inhibition and bulk or CD133⁺ cytotoxicity.

Table 2.3 Characterization of Alternative Electrophile Analogs

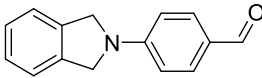
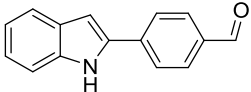
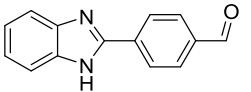
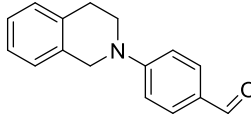
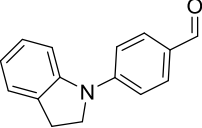
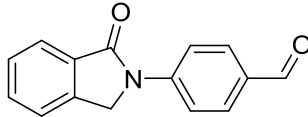
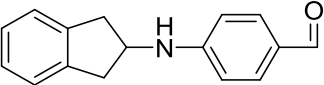
	Compound	ALDH IC ₅₀ (μM)	
		1A1	2
	673A	0.22	1.7
	22151	>10	>10
	223902	3.5	6.1
	224259	>10	>10

IC₅₀ values are N=1 performed in triplicate.

We predicted that the isoindoline moiety was unstable to oxidative metabolism at the sp³ carbons. Consistent with the mechanism of covalent inhibition proposed for DEAB, analogs without a nitrogen para to the aldehyde were rendered excellent ALDH substrates (**224256-224257**)(Table 2.4). Tetrahydroisoquinoline and indoline analogs **232200** and **232720** were also excellent ALDH substrates. The transition from tetrahedral to trigonal planar for the amine in **232200** upon donating its lone pair into the phenyl may introduce additional ring strain in the tetrahydroquinoline core, destabilizing the quinoid resonance form. In the case of **232720**, conjugation of the amine lone pair with the aromatic system of the indoline would reduce the contribution of the quinoid tautomer. Amide **232483** was a weak inhibitor and slow substrate of ALDH1A1. Resonance of the amide in **232483** would likewise occupy the amine lone pair and reduce its electron donating character. The rapid turnover of **232662** suggests that the electron

releasing character of the two alkyl substituents is important to stabilize the positively charged amine in the quinoid resonance form.

Table 2.4 Characterization of Alternative Core Analogs

	Compound	ALDH IC ₅₀ (μM)	
		1A1	2
	673A	0.22*	1.7*
	224256	Substrate	Substrate
	224257	Substrate	Substrate
	232200	Substrate	Substrate
	232720	Substrate	Substrate
	232483	6.1*	Substrate
	232662	Substrate	Substrate

IC₅₀ values are N=1 performed in triplicate. *Denotes compound is a slow substrate.

2.4. 673A SAR Conclusions

There was no obvious correlation between CD133⁺ toxicity and 1A1 potency. It is probable, given the structural simplicity and reactivity of **673A**, that it inhibits proteins other than ALDH at the relatively high concentrations required for efficacy in cells. Increasing the structural complexity of the compound, especially adding steric bulk near the aldehyde, may reduce the ability of the series to access cysteines but likely reduces the number of non-specific targets of **673A** and limits cytotoxicity mediated through off target mechanisms. A search of the PubChem database for HTS assays in which **673A** was active returned only 3 validated hits for enzymatic targets, the SUMO specific proteases SENP6, SENP7, and SENP8. Other members of this class have been proposed as targets in prostate cancer and it is reasonable to expect that **673A** could inhibit enzymes bearing catalytic cysteine such as the SENP family.⁷⁴ **673A** was also submitted for a broad safety profile (Eurofins SafetyScreen44) and bound or inhibited 5 of 44 targets (monoamine oxidase-A, androgen receptor, norepinephrine transporter, COX1, and COX2) by more than 50% at 10 μ M. Of these proteins, androgen receptor⁷⁵, COX1⁷⁶, and COX2⁷⁷ have been proposed as targets in ovarian cancer while monoamine oxidase-A⁷⁸⁻⁷⁹ has been proposed as a target in prostate cancer and is expressed in the ovary. Out of a panel of 102 kinases implicated in cancer (Eurofins Kinase Profiler, Broad Oncology Panel), **673A** inhibited c-Kit(V560G) and DNA-PKc by > 50% at 30 μ M. While c-Kit has a possible, but controversial, role in ovarian cancer⁸⁰⁻⁸², DNA-PKc is involved in a non-homologous repair mechanism for DNA double strand breaks critical in homologous recombination deficient ovarian tumors.⁸³

An activity based probe proteomics approach performed in the Cravatt lab verified cellular target engagement of 1A1 for **673A** and indicated **673A** bound near the catalytic cysteine of four additional proteins, FNBL1L, IDI1, MSRB2, and S100A3.⁸⁴

The inability to significantly improve 1A1 inhibition by expanding the scaffold, and the inability to replace the undesirable aldehyde and isoindoline moieties encouraged us to pursue more attractive leads for further therapeutic development, which will be discussed in the following chapters.

2.5. Development of a 673A Affinity Probe

Although the semi-covalent aldehyde warhead of **673A** was undesirable for developing a therapeutic, we reasoned that the slow off-rate typical of semi-covalent inhibitors would be a useful feature in an affinity probe. Our objectives in performing pulldown experiments were: 1) to identify targets for **673A** other than ALDH, such as those mentioned above, and 2) to search for new protein-protein interactions involving ALDH, which might link the enzyme to known necroptosis pathways. Differentiating protein-protein interactions from direct binding of **673A** can be achieved by established methods.⁸⁵ Currently, the only proteins known to interact directly with 1A1 are P300/CBP-associated factor (PCAF) and sirtuin 2(SIRT2). PCAF can inactivate 1A1 by acetylating K353 in the cofactor binding site. SIRT2 can re-activate 1A1 by deacetylating K353. The acetylation status of 1A1 is controlled, at least in part, by the oncogenic NOTCH pathway through its effect on SIRT2 activity.⁸⁶

Based on the **673B**-1A1 crystal structure, I designed the biotinylated affinity probe **264441** (Figure 2.4) such that the linker-biotin portion of the molecule would project into solvent. Although this fairly high molecular weight probe was not necessarily expected to retain the cell permeability of **673A**, it showed comparable ALDEFLUOR activity. As a result, we can treat live cells, rather than lysate, with the probe to obtain more biologically relevant binding

partners for ALDH. Cell lysis conditions which preserve relatively strong protein-protein interactions have been reported.⁸⁷

The Buckanovich Lab has successfully pulled down 1A3 in two ovarian cancer cell lines, validating the probe. In depth proteomic studies to determine additional targets of **673A** and binding partners of ALDH are underway.

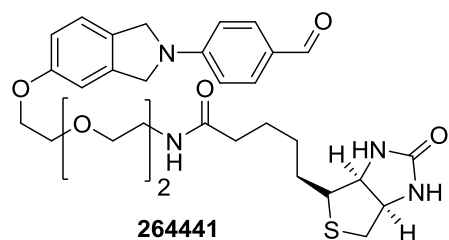
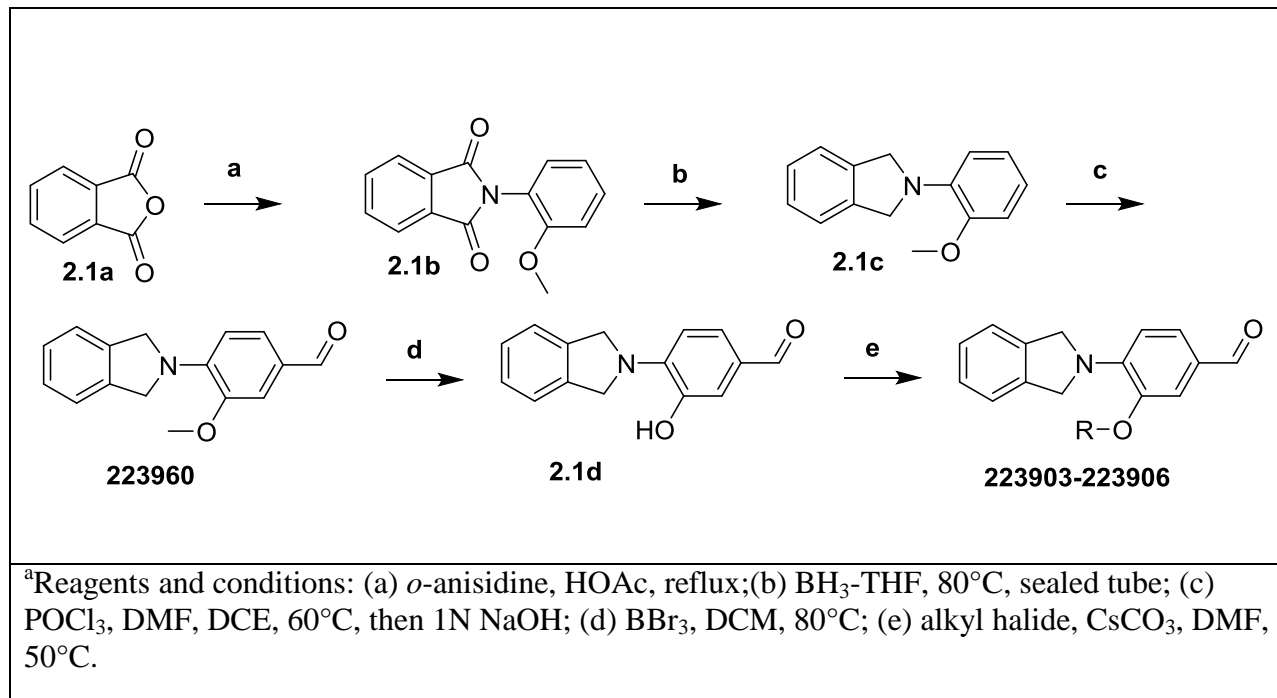


Figure 2.4: Structure of 673A Affinity Probe 264441

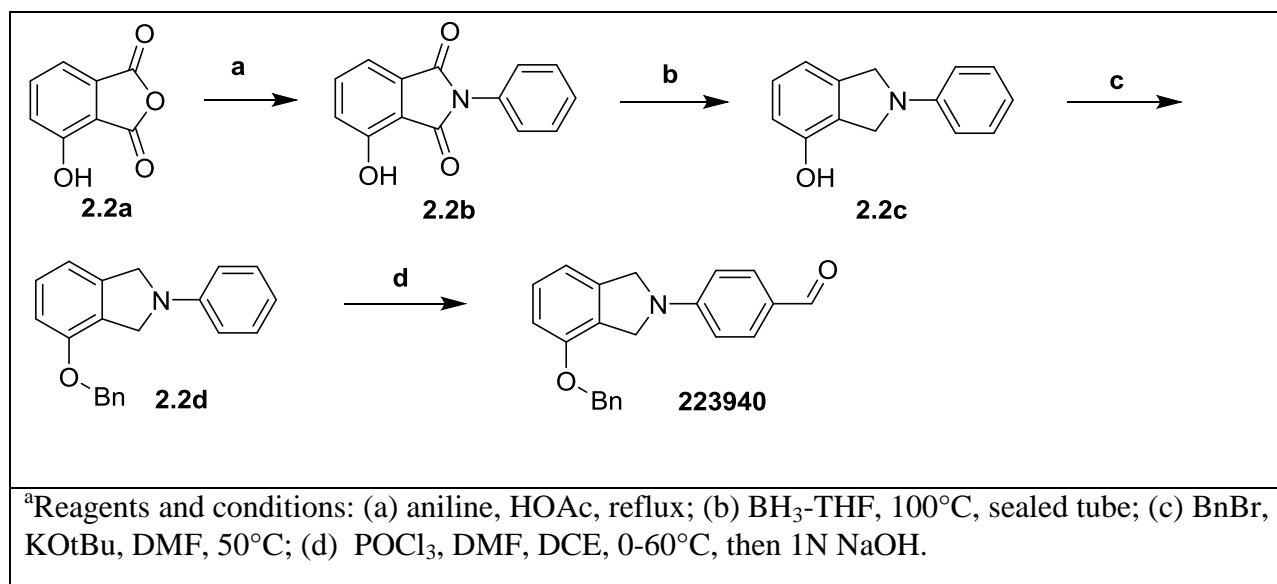
2.6. Synthesis of 673A Analogs

Scheme 2.1: Synthesis of Compounds 223960, 223903-223906^a



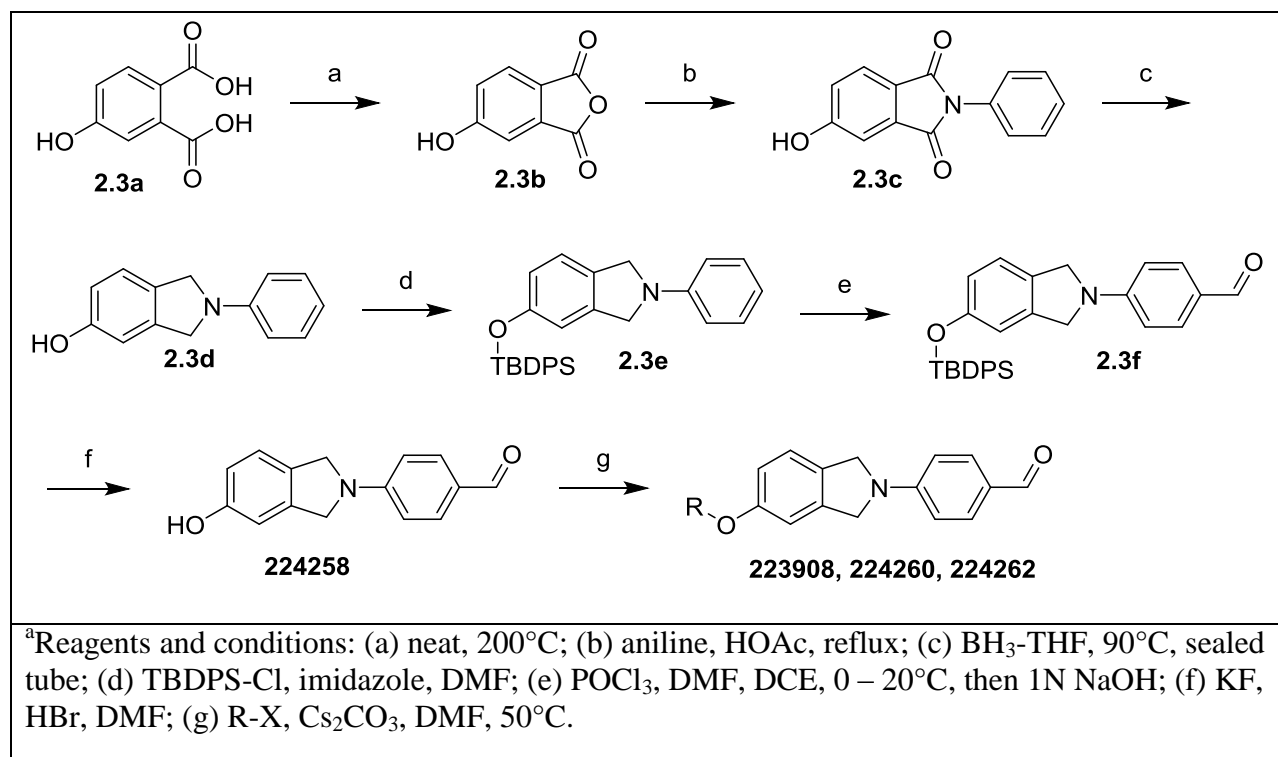
As shown in Scheme 2.1, synthesis of compounds **223960**, and **223903-223906** began with the condensation of phthalic anhydride **2.1a** and *o*-anisidine in refluxing acetic acid followed by BH₃-THF reduction to afford the isoindoline **2.1c**. Vilsmeier-Haack formylation provided aldehyde **223960**. Deprotection of the phenol by BBr₃ yielded intermediate **2.1d** which was subsequently alkylated to generate compounds **223903-223906**.

Scheme 2.2: Synthesis of Analogs 223940^a



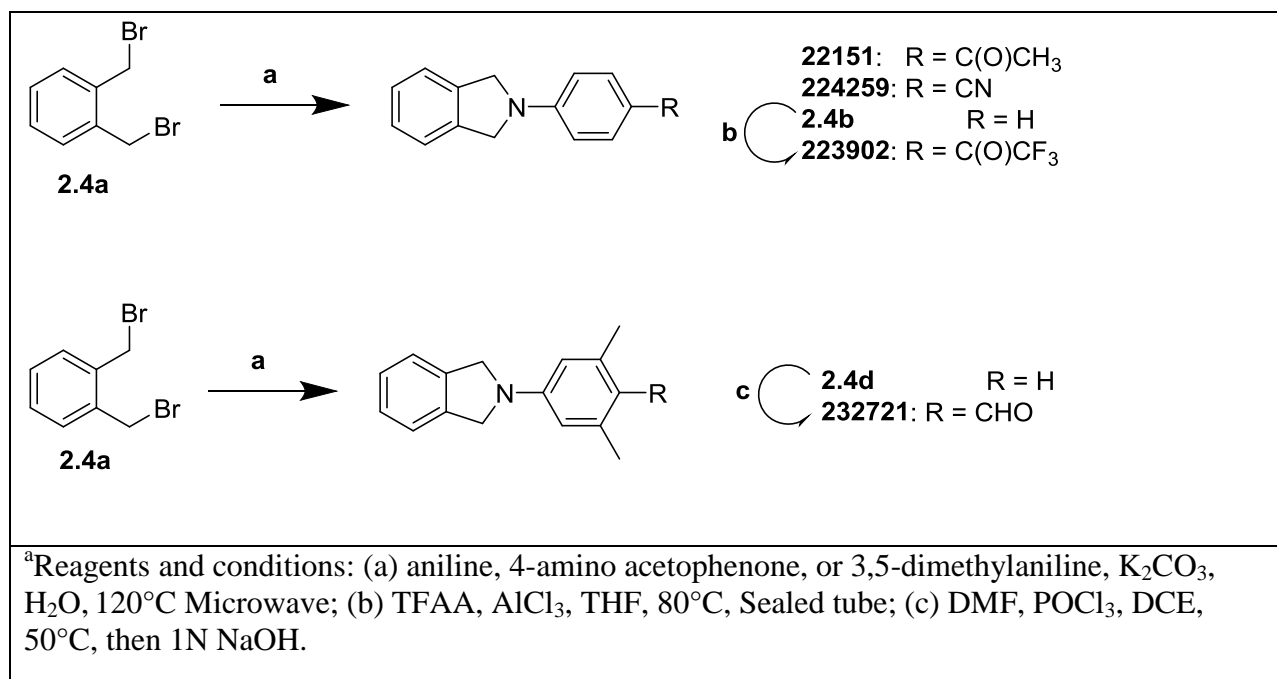
Synthesis of **223940** began with condensation of the commercially available **2.2a** with aniline in refluxing acetic acid and subsequent reduction with BH₃-THF to afford the isoindoline **2.2c** as shown in Scheme 2.2. Installation of the benzyl pendent followed by Vilsmeier-Haack formylation yielded **223940**.

Scheme 2.3: Synthesis of 224258, 223908, 224260, 224262^a



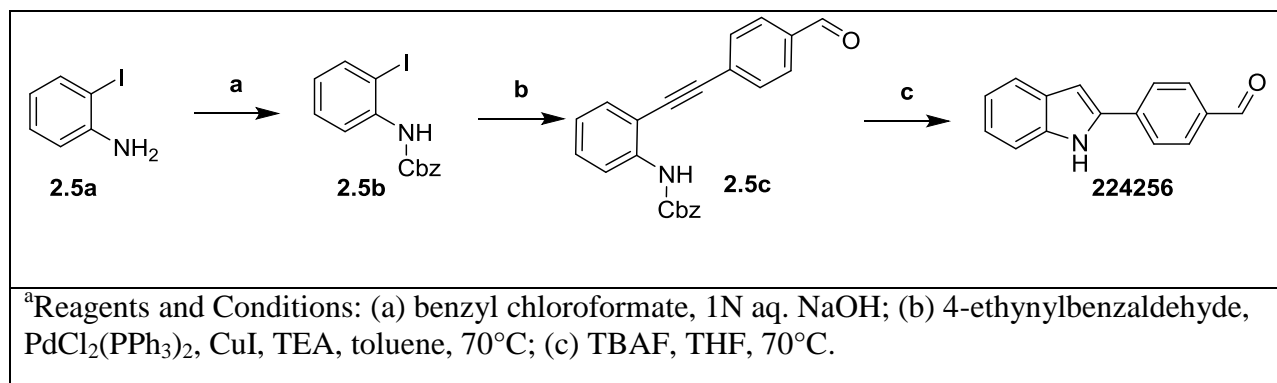
As shown in Scheme 2.3, synthesis of **224258** began with the thermal dehydration of commercially available 4-hydroxyphthalic acid **2.3a** to afford the anhydride **2.3b**.⁸⁸ Treatment of the anhydride with aniline in refluxing acetic acid provided imide **2.3c**; subsequent reduction with BH₃-THF yielded isoindoline **2.3d**. Attempts to directly formylate **2.3d** directly resulted in an inseparable emulsion upon basic hydrolysis of the iminium intermediate, likely due to the very poor solubility of **224258** in most solvents. TBDPS protection of the phenol facilitated Vilsmeier-Haack formylation. **2.3f** was easily purified by recrystallization and removal of the TBDPS group was achieved by in situ generation of hydrofluoric acid; pure **224258** precipitated from the reaction mixture upon addition of water.⁸⁹ Alkylation with the appropriate alkyl halides afforded **223908**, **224260**, and **224262**.

Scheme 2.4: Synthesis of 22151, 223902, 224259, and 232721^a



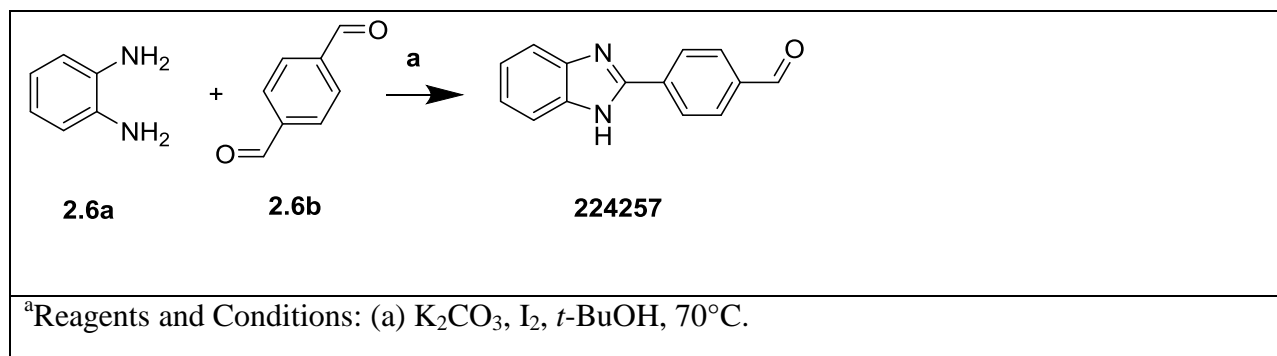
Synthesis of analogs **22151**, **223902**, **224259**, and **232721** began with the microwave-assisted ring-forming bis-alkylation of the appropriate aniline with α,α' -dibromo-*o*-xylene (Scheme 2.4).⁹⁰ Aluminum trichloride mediated Friedel-Crafts acylation of **2.4b** with TFAA afforded **223902**. Vilsmeier-Haack formylation of **2.4d** gave **232721**.

Scheme 2.5: Synthesis of 224256^a



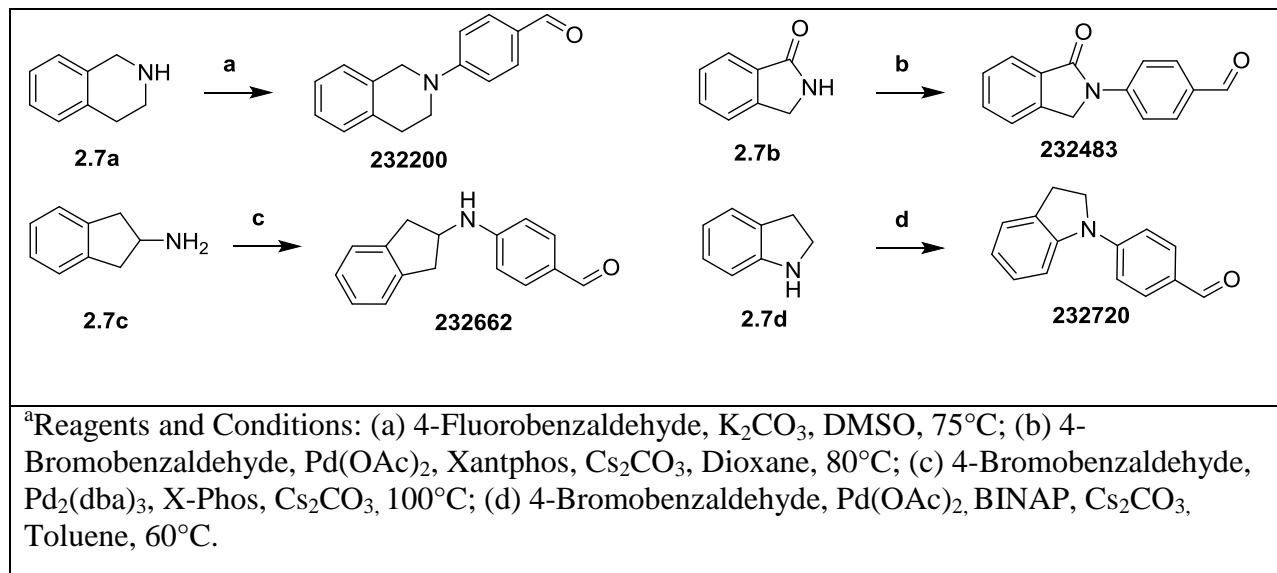
As shown in Scheme 2.5, synthesis of **224256** began with Cbz protection of 2-iodoaniline **2.5a**, followed by Sonogashira cross coupling with 4-ethynylbenzaldehyde to yield compound **2.5c**. TBAF mediated cyclization afforded **224256**.⁹¹

Scheme 2.6: Synthesis of 224257^a



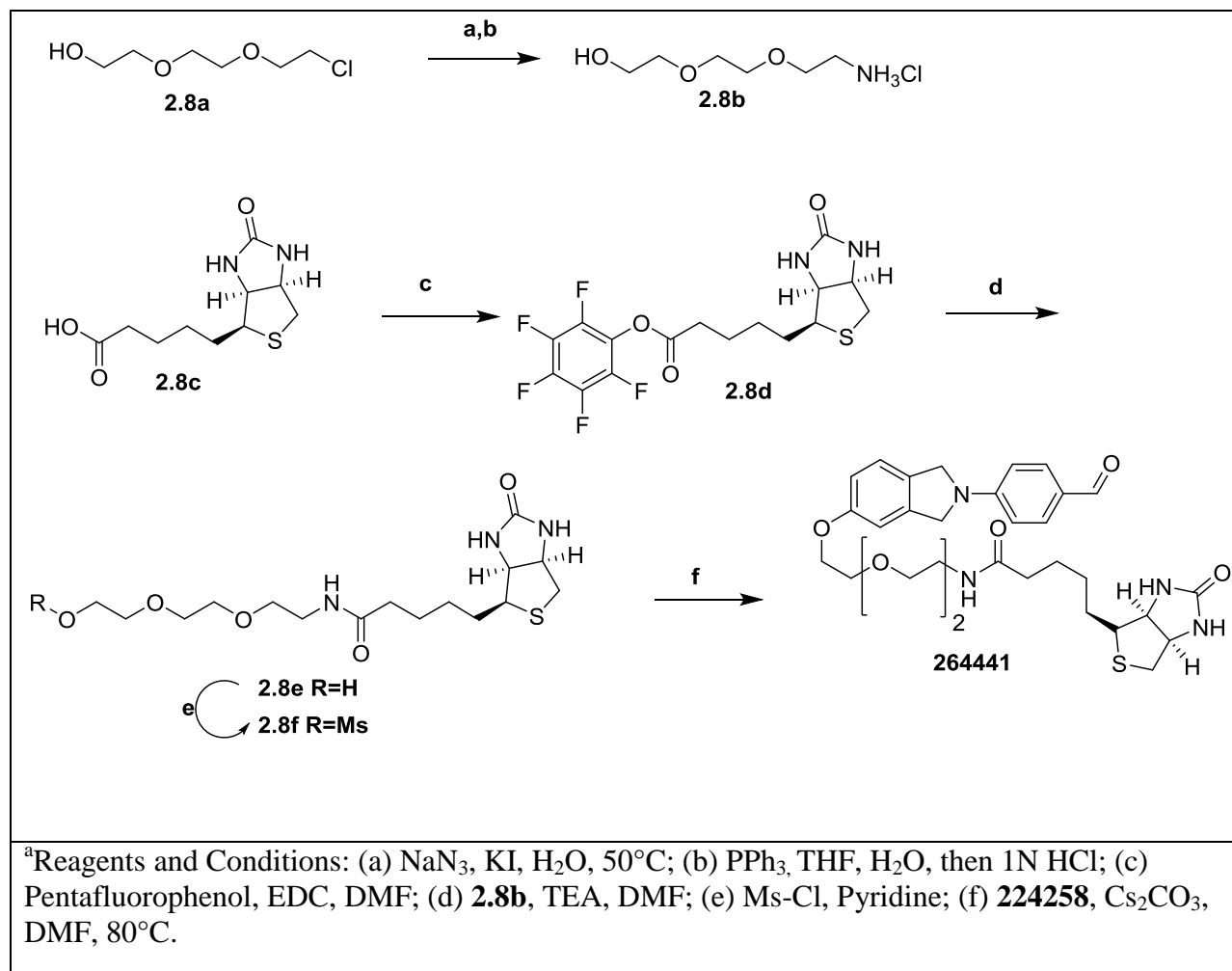
As shown in Scheme 2.6, benzimidazole **224257** was synthesized by iodine mediated oxidative cyclization between 1,2-diaminobenzene **2.6a**, and terephthalaldehyde **2.6b**.

Scheme 2.7: Synthesis of 232200, 232483, 232662, and 232720^a



232200 was synthesized according to Scheme 2.7 by S_NAr of 4-fluorobenzaldehyde with tetrahydroisoquinoline. **232483**, **232662**, and **232720** were synthesized by Buchwald-Hartwig coupling of 4-bromobenzaldehyde with the appropriate nucleophiles **2.7b-d** (Scheme 2.7).

Scheme 2.8: Synthesis of Affinity Probe 264441^a

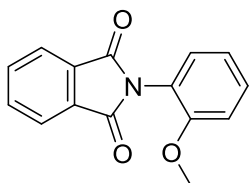


As shown in Scheme 2.8, synthesis of **264441** began by KI mediated displacement of chloride **2.8a** with sodium azide followed by PPh₃ reduction to afford **2.8b**. Biotin (**2.8c**) was activated for amide coupling by generating the pentafluorophenol ester with EDC. The aqueous workup necessitated by standard one-step amide coupling procedures was complicated by the

tendency of **2.8e** to partition into water. Following acylation of amine **2.8b** with ester **2.8d**, the crude reaction mixture could be concentrated and immediately purified by flash chromatography to afford **2.8e**. Mesylation in pyridine followed by displacement with phenol **224258** afforded probe **264441**.

2.7. Experimental Procedures

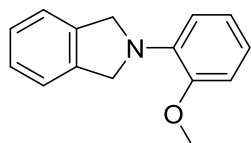
All reagents were used in the condition received from commercial sources. ^1H NMR and ^{13}C NMR were taken in CDCl_3 or $\text{DMSO}-d_6$ at room temperature on Varian Inova 400 or 500 MHz instruments. Reported chemical shifts are expressed in parts per million (ppm) on the δ scale from an internal standard of tetramethylsilane (0 ppm). Mass spectrometry data were obtained on either an Agilent TOF or Agilent Q-TOF. An Agilent 1100 series HPLC with an Agilent Zorbax Eclipse Plus-C18 column was used to determine purity of biologically tested compounds. All tested compounds were determined to be >95% pure using a 6 minute gradient of 10-90% acetonitrile in water followed by a 2 minute hold at 90% acetonitrile with detection at 254 nm. Flash chromatographic purifications were performed using a Teledyne ISCO Combiflash RF with Redisep Gold RF columns.



2-(2-methoxyphenyl)isoindoline-1,3-dione (2.1b)

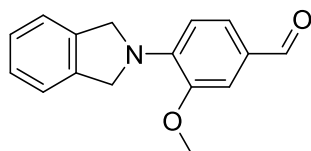
Phthalic anhydride (**2.1a**) (5 g, 33.8 mmol) and *o*-anisidine (4.57 mL, 40.5 mmol) were added to 50 mL of glacial acetic acid. After refluxing for 12 h the solution was cooled and added to 100

mL of distilled water. Collection of the precipitate by vacuum filtration yielded the titled compound as a tan powder (8.24 g, 96%). ^1H NMR (500 MHz, CDCl_3) δ 7.95 (m, 2H), δ 7.78 (m, 2H), δ 7.45 (m, 1H), δ 7.27 (m, 1H), δ 7.08 (m, 1H) δ 7.05 (m, 1H), δ 3.8(s, 3H).



2-(2-methoxyphenyl)isoindoline (2.1c)

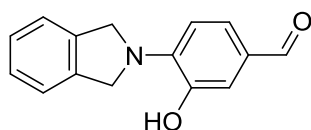
2.1b (2.5 g, 10 mmol) was dissolved in anhydrous THF in an oven dried pressure tube. While stirring the solution, 1M BH_3 in THF (40 mL) was added dropwise. The headspace of the pressure tube was purged with Ar and the sealed tube was heated to 80°C for 12 h. The reaction was quenched by slow addition of distilled water. The mixture was diluted with EtOAc and washed 2x with saturated aq. NH_4Cl , once with saturated aq. NaHCO_3 , and once with brine. The organic layer was dried over Na_2SO_4 and concentrated yielding a yellow oil which was purified by flash chromatography (10-20% EtOAc in Hexanes) to afford the titled compound as a colorless oil (1.4 g, 62%). ^1H NMR (500 MHz, CDCl_3) δ 7.28 (m, 4H), δ 6.94 (m, 2H), δ 6.84 (m, 2H), δ 4.76 (s, 4H), δ 3.87 (s, 3H).



4-(isoindolin-2-yl)-3-methoxybenzaldehyde (223960)

The Vilsmeier-Haack reagent was formed by cooling 4 mL DCE and DMF (4.12 ml, 53.3 mmol) to -10°C in a dry RBF under N_2 . POCl_3 (3.31 ml, 35.5 mmol) was added slowly by syringe while

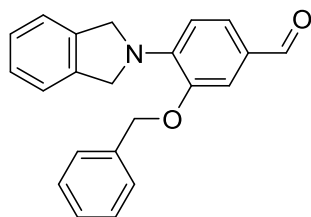
stirring the mixture. After 1 h **2.1c** (4 g, 17.76 mmol), a free flowing oil, was added and the total volume of the mixture was brought to 25mL with DCE forming a viscous suspension. The reaction was warmed to RT then heated to 50°C overnight. A yellow precipitate formed, which was collected by vacuum filtration and washed with EtOAc. The Vilsmeier adduct was hydrolyzed by adding the solid to a separatory funnel along with EtOAc and 10% aq. NaOH and shaking vigorously until all of the solid dissolved in the organic layer. The aqueous layer was back extracted with EtOAc and the combined organic layers were washed with brine, dried with sodium sulfate and concentrated, yielding 3g crude orange crystalline solid. The crude was recrystallized from hot ethanol yielding the titled compound as orange crystalline sheets (2.5 g, 9.87 mmol, 55.6 % yield). MS (ESI): m/z 254.2 $[M+H]^+$ 1H NMR (500 MHz, $CDCl_3$) δ 9.74 (s, 1H), δ 7.42 (d, 1H), δ 7.39 (s, 1H), δ 7.32 (m, 4H), δ 6.70 (d, 1H), δ 5.00 (s, 4H), δ 3.92 (s, 3H). ^{13}C NMR (126 MHz, $CDCl_3$) δ 190.13, 148.68, 143.90, 137.12, 128.26, 127.26, 126.76, 122.19, 112.91, 109.99, 56.56, 55.96.



3-hydroxy-4-(isoindolin-2-yl)benzaldehyde (2.1d)

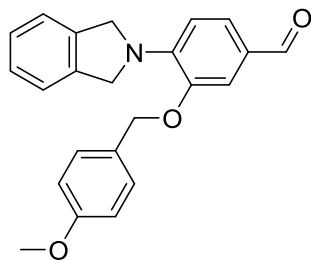
To a dry pressure tube **223960** (500 mg, 1.97 mmol) was added and dissolved in DCM. The pressure tube was purged with N_2 and cooled to 78 °C. 1M BBr_3 in DCM (7.9 mL, 7.9 mmol) was added dropwise over 5 minutes. The pressure tube was sealed and heated to 80°C overnight. The reaction was quenched by dropwise addition of aqueous $NaHCO_3$ at 0°C with vigorous stirring. The mixture was diluted with EtOAc, and vacuum filtered through celite. The organic layer was washed with brine, dried over Na_2SO_4 , and concentrated yielding a dark brown crude

product. Further purification by flash chromatography (5-25% EtOAc in Hexanes) yielded the titled compound as a yellow solid (100 mg, 20%). ^1H NMR (500 MHz, $\text{DMSO-}d_6$) δ 9.67 (brs, 1H), δ 9.62 (s, 1H), δ 7.37 (m, 1H), δ 7.29 (m, 4H), δ 7.21 (s, 1H), δ 6.73 (d, 1H), δ 4.94 (m, 4H).



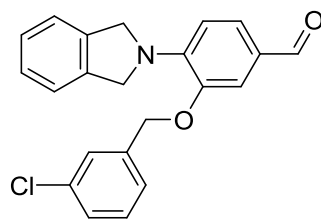
3-(benzyloxy)-4-(isoindolin-2-yl)benzaldehyde (223903)

2.1d (15 mg, .063 mmol) dissolved in 1mL anhydrous DMF was added to a dry pressure tube charged with Cs_2CO_3 (61.3 mg, .188 mmol). Benzyl bromide (9.3 μL , .078 mmol) was added and the mixture was stirred overnight under N_2 at 50°C . Upon addition of water, a precipitate formed. The mixture was centrifuged and the solvent decanted. The crude material was further purified by flash chromatography (10-25% EtOAc in Hexanes) yielding the titled compound as an off white solid (3.8 mg, 18%) ESIMS: 330.2 $[\text{M}+\text{H}]^+$ ^1H NMR (500 MHz, CDCl_3) δ 9.73 (s, 1H), δ 7.48 (d, 2H), δ 7.47 (s, 1H), δ 7.44 (m, 2H), δ 7.43 (m, 1H), 7.37 (t, 1H), δ 7.26 (m, 4H), δ 6.73 (d, 1H), δ 5.14 (s, 2H), δ 4.98 (s, 4H) ^{13}C NMR (125 MHz, CDCl_3) δ 190.02, δ 147.62, δ 144.10, δ 137.02, δ 136.46, δ 128.66, δ 128.24, δ 127.86, δ 122.18, δ 113.19, δ 111.71, δ 109.98, δ 71.66, δ 56.69.



4-(isoindolin-2-yl)-3-((4-methoxybenzyl)oxy)benzaldehyde (223905)

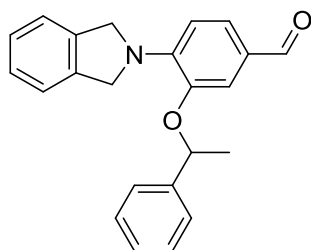
2.1d (15 mg, .06 mmol) dissolved in 1mL anhydrous DMF was added to a dry pressure tube charged with Cs₂CO₃ (61.3 mg, 0.19 mmol). 1-(bromomethyl)-4-methoxybenzene (11 μL, .08 mmol) was added and the mixture was stirred overnight under N₂ at 50°C. Upon addition of water, a precipitate formed. The mixture was centrifuged and the solvent decanted. The crude material was further purified by flash chromatography (10-25% EtOAc in Hexanes) yielding the titled compound as an off white solid (12 mg, 53%). ESIMS: 360.2 [M + H]⁺ ¹HNMR (500 MHz, CDCl₃), δ 9.73 (s, 1H), δ 7.44 (td, 2H), δ 7.33 (t, 1H), δ 7.25 (m, 4H), δ 7.03 (td, 2H), δ 6.91 (d, 1H), δ 6.71 (d, 1H), δ 5.11 (s, 2H), δ 4.99 (s, 4H), δ 3.83 (s, 3H); ¹³CNMR (125 MHz, CDCl₃) δ 190.00, δ 159.85, δ 147.56, δ 144.06, δ 138.04, δ 137.01, δ 129.71, δ 128.22, δ 127.24, δ 126.70, δ 122.17, δ 119.96, δ 113.71, δ 113.21, δ 71.52, δ 56.70, δ 55.27.



3-((3-chlorobenzyl)oxy)-4-(isoindolin-2-yl)benzaldehyde (223906)

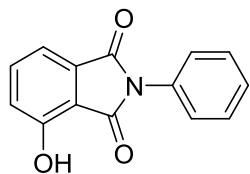
2.1d (15 mg, .063 mmol) dissolved in 1mL anhydrous DMF was added to a dry pressure tube charged with Cs₂CO₃ (61.3 mg, .188 mmol). 1-(bromomethyl)-3-chlorobenzene (10 μL, .078

mmol) was added and the mixture was stirred overnight under N₂ at 50°C. Upon addition of water, a precipitate formed. The mixture was centrifuged and the solvent decanted. The crude material was further purified by flash chromatography (10-25% EtOAc in Hexanes) yielding the titled compound as an off white solid (2.2 mg, 10%). ESIMS: 364.2 [M + H]⁺ ¹HNMR (500 MHz, CDCl₃) δ 9.74 (s, 1H), 7.50 (s, 1H), 7.46 (dd, 2H), 7.35 (m, 3H), 7.26 (m, 4H), 6.74 (d, 1H), 5.12 (s, 2H), 5.00 (s, 4H); ¹³CNMR (125 MHz, CDCl₃) δ 192.12, 147.47, 144.17, 138.66, 137.06, 134.76, 130.14, 128.52, 127.97, 127.47, 126.83, 125.89, 122.36, 113.46, 71.01, 56.90.



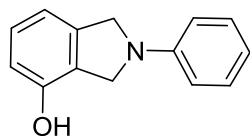
4-(isoindolin-2-yl)-3-(1-phenylethoxy)benzaldehyde (223904)

2.1d (15 mg, .063 mmol) dissolved in 1mL anhydrous DMF was added to a dry pressure tube charged with Cs₂CO₃ (61.3 mg, .188 mmol). (1-bromoethyl)benzene (10.7 μL, .078 mmol) was added and the mixture was stirred overnight under N₂ at 50°C. Upon addition of water, a precipitate formed. The mixture was centrifuged and the solvent decanted. The crude product was further purified by recrystallization in boiled ethanol, yielding the titled compound as orange crystals (10 mg, 47%). ESIMS: 366.2 [M + H]⁺ ¹HNMR (500 MHz, CDCl₃) δ 9.62 (s, 1H), 7.45 (d, 2H), 7.33 (m, 9H), 6.70 (d, 1H), 5.46 (q, 1H), 5.09 (q, 4H), 1.76 (d, 3H); ¹³CNMR (125 MHz, CDCl₃) δ 189.94, 146.50, 144.17, 142.32, 137.16, 128.77, 127.77, 127.33, 127.28, 126.69, 125.77, 122.23, 113.35, 112.90, 77.22, 56.76, 24.00.



4-hydroxy-2-phenylisoindoline-1,3-dione (2.2b)

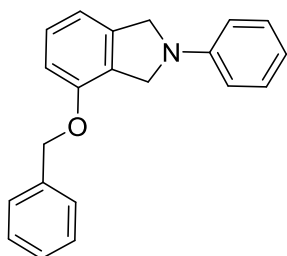
Aniline (334 μ l, 3.66 mmol) and 4-hydroxyisobenzofuran-1,3-dione (**2.2a**) (500 mg, 3.05 mmol) were refluxed in 50mL HOAc overnight. The next day the product was precipitated by pouring the mixture into 100mL cold water. The solid was filtered and washed with additional water to yield the titled compound as a tan powder (570mg, 2.383 mmol, 78 % yield). $^1\text{H NMR}$ (500 MHz, CDCl_3) δ 7.80 (s, 1H), 7.65 (t, $J = 7.8$ Hz, 1H), 7.54 - 7.46 (m, 2H), 7.45 - 7.37 (m, 3H), 7.23 (d, $J = 8.4$ Hz, 1H).



2-phenylisoindolin-4-ol (2.2c)

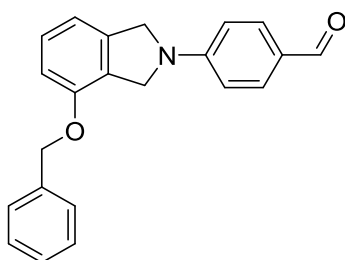
1M BH_3 -THF (10.400 mL, 10.40 mmol) was added slowly to a pressure tube at 0°C charged with 4-hydroxy-2-phenylisoindoline-1,3-dione (**2.2b**) (620mg, 2.59 mmol) under a stream of nitrogen. The tube was stirred at room temperature for 1 h then sealed and heated to 100°C overnight. The tube was cooled to 0°C and quenched by slow addition of sat. aq. NH_4Cl and extracted 2x with EtOAc. The combined organics were washed with brine, dried over sodium

sulfate and concentrated. The isoindolinone was poorly soluble in DCM so the crude residue was taken up in DCM and filtered to yield the titled compound in the filtrate as an off white solid. (250 mg, 1.183 mmol, 45.5 % yield). $^1\text{H NMR}$ (500 MHz, CDCl_3) δ 7.37 - 7.29 (m, 2H), 7.17 (t, $J = 7.7$ Hz, 1H), 6.92 (d, $J = 7.5$ Hz, 1H), 6.78 (t, $J = 7.3$ Hz, 1H), 6.72 - 6.66 (m, 3H), 4.64 (q, $J = 3.1$ Hz, 4H).



4-(benzyloxy)-2-phenylisoindoline (2.2d)

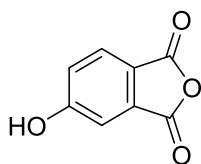
Benzyl bromide (0.113 ml, 0.947 mmol) was added to a flask was charged with **2.2c** (100mg, 0.473 mmol), KOtBu (159 mg, 1.420 mmol) and 1mL DMF. The reaction was heated to 50°C for 4 hours. The mixture was diluted with EtOAc and washed 3x with water and 1x with brine. The organic portion was dried over MgSO_4 and concentrated to yield an oily brown crude residue which was purified by flash (10-25% EtOAc in Hexanes) to yield the titled compound as a pink crystalline solid. (73mg, 0.242 mmol, 51.2 % yield) $^1\text{H NMR}$ (400 MHz, CDCl_3) δ 7.33 - 7.08 (m, 7H), 7.05 (t, $J = 8.1$ Hz, 1H), 6.75 (d, $J = 7.7$ Hz, 1H), 6.64 - 6.53 (m, 2H), 6.49 (d, $J = 8.2$ Hz, 2H), 4.91 (s, 2H), 4.44 (d, $J = 12.2$ Hz, 4H).



4-(4-(benzyloxy)isoindolin-2-yl)benzaldehyde (223940)

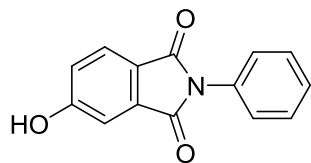
To a flask at 0°C charged with 0.25 mL DCE and DMF (0.027 ml, 0.348 mmol) was added POCl₃ (0.022 ml, 0.232 mmol). The solution was stirred for an hour at which point **2.2d** (35mg, 0.116 mmol) dissolved in 0.75 mL DCE was added by syringe. The solution was stirred at 60°C for two hours at which point the mixture was diluted with ethyl acetate and 10% aq. NaOH to hydrolyze the Vilsmeier adduct. The organic portion was subsequently washed with brine, dried over sodium sulfate, and concentrated. The crude product was purified by flash (10-25% EtOAc in Hex) to yield the titled compound as a yellow solid. (20mg, 0.061 mmol, 52.3 % yield)

ESIMS: 330.1 [M+H]⁺ ¹H NMR (500 MHz, CDCl₃) δ 9.76 (s, 1H), 7.79 (d, J = 8.4 Hz, 2H), 7.48 - 7.40 (m, 4H), 7.40 - 7.35 (m, 1H), 7.28 (t, J = 8.0 Hz, 1H), 6.95 (d, J = 7.5 Hz, 1H), 6.86 (d, J = 8.1 Hz, 1H), 6.69 (d, J = 8.4 Hz, 2H), 5.14 (s, 2H), 4.76 - 4.60 (m, 4H). ¹³C NMR (126 MHz, CDCl₃) δ 190.37, 153.93, 151.40, 138.58, 136.66, 132.23, 129.30, 128.66, 128.15, 127.40, 125.52, 125.31, 114.97, 111.24, 110.16, 69.95, 54.17, 51.86.



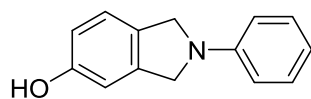
5-Hydroxyisobenzofuran-1,3-dione (2.3b)

4-hydroxyphthalic acid (**2.3a**) (10g, 54.9 mmol) was added to a 100mL pressure tube. A septum was fitted on the tube and punctured with a nitrogen inlet and outlet needle to drive off water as the reaction proceeded. The reaction was heated to 200°C overnight and the titled compound was obtained as a white solid upon cooling (8.81 g, 53.7 mmol, quantitative yield). ¹H NMR (500 MHz, DMSO-*d*₆) δ 11.42 (s, 1H), 7.91 (d, 1H), 7.30 (d, 1H), 7.27 (s, 1H).



5-Hydroxy-2-phenylisoindoline-1,3-dione (2.3c)

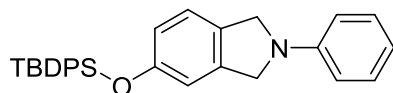
2.3b (8.81 g, 53.7 mmol) was added to a flask along with 100 mL of glacial acetic acid. Aniline (5.88 ml, 64.4 mmol) was added, and the flask was fitted with a condenser and refluxed for 4 h. The acetic acid was removed in vacuo and the residue was taken up in ethyl acetate and washed 3x with sat. aq. NaHCO₃ and 1x with brine. The organic portion was dried over sodium sulfate and concentrated. The orange-red crude solid was taken up in boiling ethanol and upon cooling the titled compound recrystallized as a light orange solid (11.37 g, 47.5 mmol, 89 % yield). ¹H NMR (500 MHz, DMSO-*d*₆) δ 11.00 (s, 1H), 7.78 (d, 1H) 7.50 (m, 2H), 7.41 (m, 2H), 7.40 (s, 1H), 7.19 (m, 2H).



2-Phenylisoindolin-5-ol (2.3d)

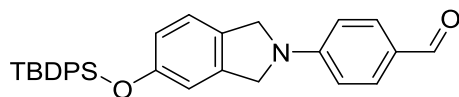
A pressure tube under a stream of nitrogen was charged with **2.3c** (3.99 g, 16.67 mmol). The tube was cooled in an ice-brine bath and 1M BH₃.THF (50ml, 50.0 mmol) over 15 minutes by syringe. The mixture was stirred in the cooling bath until for (~30 min) then warmed to room temperature. The tube was capped and heated to 90 °C overnight (high heat is essential to good conversion). After 24 hours the initially reddish brown solution had turned pale yellow and the reaction was complete by HPLC. The mixture was poured into an oversized flask and cooled to 0°C before careful addition of sat. aq. NH₄Cl. The mixture was extracted with ethyl acetate and

the organic portion washed 2x with water and 1x with brine. The organic portion was dried over sodium sulfate and concentrated to yield the titled compound as an off white powder (3.45 g, 16.33 mmol, 98 % yield). ¹H NMR (500 MHz, Chloroform-*d*) δ 7.31 (d, *J* = 8.3 Hz, 2H), 7.20 (d, *J* = 8.1 Hz, 1H), 6.83 (s, 1H), 6.80 – 6.72 (m, 2H), 6.68 (d, *J* = 9.0 Hz, 2H), 4.59 (d, *J* = 10.5 Hz, 4H).



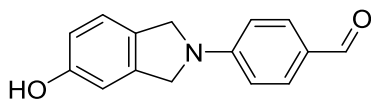
5-((tert-butyldiphenylsilyl)oxy)-2-phenylisoindoline (2.3e)

A flask was charged imidazole (2.095 g, 30.8 mmol), (**2.3d**) (2.6 g, 12.31 mmol) and 25mL DMF. Following this TBDPS-Cl (3.48 ml, 13.54 mmol) was added dropwise by syringe. A slight warming over the course of addition was observed. The flask was stirred overnight at room temp at which point the reaction was complete by TLC. The contents of the flask were poured over 125 mL water and stirred for 20 min. The white precipitate was collected by vacuum filtration and dried in vacuo yielding 6.1g of the crude which was homogenous by TLC but cannot be detected on reverse phase (sticks on column). The crude was recrystallized by dissolving in ~450 mL hot ethanol and allowing to gradually cooling yielding the titled compound as a white crystalline solid (5 g, 11.12 mmol, 90 % yield). Taken forward without further purification.



4-(5-((tert-butyldiphenylsilyl)oxy)isoindolin-2-yl)benzaldehyde (2.3f)

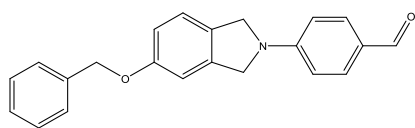
To a flask at 0°C charged with DMF (2.97 ml, 38.4 mmol) in 10mL DCE was added POCl₃ (2.86 ml, 30.7 mmol). The mixture was stirred at 0°C for 5 minutes then allowed to warm to RT for 10 minutes. Another flask was charged with **2.3e** (6.9 g, 15.34 mmol) and 30mL of DCE and cooled to 0°C. The contents of the first flask were transferred to the second flask by cannula and the flask was stirred overnight at RT. At this point the mixture was green with yellow precipitate. The reaction was quenched by cooling the flask back to 0°C and adding 10% aq. NaOH solution until the color changed from green to red. The flask was removed from the cooling bath and stirred for 1 h. The mixture was extracted 2x with ethyl acetate. The organic portions were combined, washed with brine and dried over sodium sulfate. Following removal of the solvent 7.3g of rust red crude material was recovered. The crude was taken up in hot ethanol and the titled compound crystallized out as a golden crystalline solid upon cooling (5.88 g, 12.31 mmol, 80 % yield). ¹H NMR (500 MHz, CDCl₃) δ 9.76 (s, 1H), 7.77 (d, J = 8.4 Hz, 2H), 7.73 (d, J = 7.0 Hz, 4H), 7.45 (t, J = 7.5 Hz, 2H), 7.39 (t, J = 7.1 Hz, 4H), 7.05 (d, J = 8.8 Hz, 1H), 6.77 - 6.68 (m, 2H), 6.62 (d, J = 8.5 Hz, 2H), 4.58 (d, J = 27.9 Hz, 4H), 1.12 (s, 9H).



4-(5-hydroxyisoindolin-2-yl)benzaldehyde (224258)

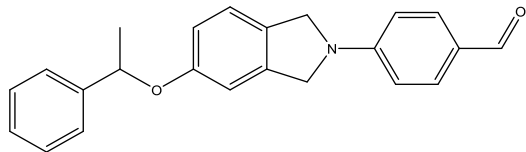
2.3e (2.48 g, 5.19 mmol) and potassium fluoride (0.603 g, 10.38 mmol) were added to a flask along with 25mL of DMF yielding an orange solution. To this was added 48% aq. HBr (0.583 ml, 5.19 mmol) dropwise. With each addition the solution darkened then gradually returned to the light orange color at which point the next portion was added. After addition over about fifteen minutes the flask was allowed to stir for another 15 at which point the solution was orange with a green hue. The SM was consumed by TLC and the mixture was poured over

100mL cold water and stirred for five minutes yielding a fine yellow silty precipitate which was collected by vacuum filtration using a FINE frit. The precipitate was washed with 30mL water and 30 mL diethyl ether before drying under high vacuum (1g, 4.18 mmol, 80 % yield). ESIMS: m/z 240.1 $[M+H]^+$ 1H NMR (500 MHz, DMSO- d_6) δ 9.69 (s, 1H), 9.63 (s, 1H), 7.38 (m, 2H), 7.32 (d, 1H), 7.29 (m, 2H), 7.22 (s, 1H), 6.74 (d, 1H), 4.95 (s, 4H). ^{13}C NMR (126 MHz, DMSO- d_6) δ 190.44, 157.48, 151.78, 138.47, 132.25, 127.15, 125.40, 123.88, 115.22, 111.86, 109.72, 53.93, 53.35.



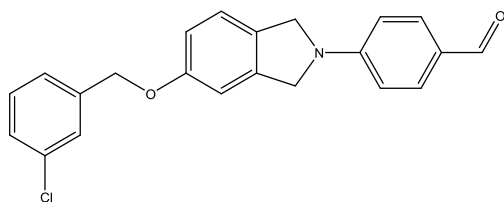
4-(5-(benzyloxy)isoindolin-2-yl)benzaldehyde (223908)

224258 (20 mg, .084 mmol) was dissolved in 2 mL anhydrous DMF and transferred to a dry flask charged with KO t Bu (14 mg, 1.25 mmol) under N $_2$. Benzyl bromide (10.9 μ L, .092 mmol) was diluted in 1 mL anhydrous DMF and added dropwise to the flask and the mixture was stirred for 3 h. The mixture was diluted in EtOAc and washed with water and brine. After concentration, the crude material was further purified by flash chromatography (10-25% EtOAc in Hexanes). In order to achieve >95% purity it was necessary to recrystallize the product in boiled ethanol yielding the titled compound as yellow needles (3.2 mg, 11.6%). ESIMS: 330.1 $[M+H]^+$ 1H NMR (500 MHz, CDCl $_3$) δ 9.78 (s, 1H), 7.81 (d, 2H), 7.44 (d, 2H), 7.40 (td, 2H), 7.34 (tt, 1H), 7.25 (d, 1H), 6.97 (m, 1H), 6.96 (s, 1H), 6.69 (d, 2H), 5.10 (s, 2H), 4.72 (s, 2H), 4.69 (s, 2H); ^{13}C NMR (125 MHz, CDCl $_3$) δ 190.40, 158.77, 151.43, 138.11, 136.76, 132.29, 128.94, 128.65, 128.06, 127.43, 125.62, 123.46, 114.85, 111.22, 108.94, 70.34, 53.94.



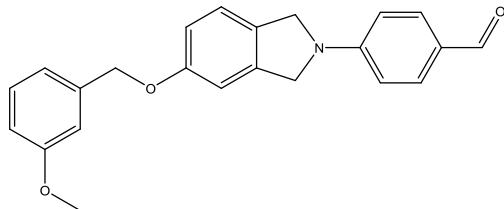
4-(5-(1-phenylethoxy)isoindolin-2-yl)benzaldehyde (223941)

Prepared according to the procedure for **223908**. Yellow crystalline solid. (14mg, 0.041 mmol, 32.5 % yield). ESIMS: 344.1 [M+H]⁺ ¹H NMR (500 MHz, CDCl₃) δ 9.75 (s, 1H), 7.78 (d, *J* = 8.8 Hz, 2H), 7.42 – 7.32 (m, 4H), 7.30 – 7.24 (m, 1H), 7.15 (d, *J* = 8.2 Hz, 1H), 6.87 – 6.80 (m, 2H), 6.64 (d, *J* = 8.5 Hz, 2H), 5.32 (q, *J* = 6.5 Hz, 1H), 4.61 (s, 4H), 1.66 (d, *J* = 6.4 Hz, 3H). ¹³C NMR (126 MHz, CDCl₃) δ 190.38, 157.92, 151.40, 142.94, 137.89, 132.24, 128.69, 128.61, 127.56, 125.51(2 carbons), 123.28, 115.82, 111.16, 110.04, 76.38, 53.87, 53.24, 24.54



4-(5-((3-chlorobenzyl)oxy)isoindolin-2-yl)benzaldehyde (224260)

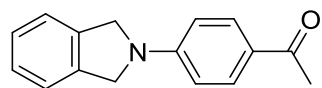
Prepared according to the procedure for **223908**. (12mg, 0.033 mmol, 16.44 % yield) M+H 364.1 ¹H NMR (500 MHz, CDCl₃) δ 9.78 (d, *J* = 1.0 Hz, 1H), 7.86 - 7.75 (m, 2H), 7.46 (s, 1H), 7.36 - 7.29 (m, 3H), 7.28 - 7.24 (m, 1H), 7.02 - 6.89 (m, 2H), 6.69 (d, *J* = 8.4 Hz, 2H), 5.07 (s, 2H), 4.70 (d, *J* = 11.0 Hz, 4H). ¹³C NMR (126 MHz, CDCl₃) δ 190.38, 158.45, 151.39, 138.86, 138.20, 134.58, 132.26, 129.91, 129.25, 128.18, 127.36, 125.65, 125.27, 123.53, 114.78, 111.22, 108.96, 69.46, 53.90, 53.27.



4-(5-((3-methoxybenzyl)oxy)isoindolin-2-yl)benzaldehyde (224261)

Prepared according to the procedure for **223908** (15mg, 0.042 mmol, 20.80 % yield). ESIMS:

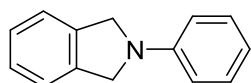
360.2 [M+H]⁺ ¹H NMR (500 MHz, CDCl₃) δ 9.76 (s, 1H), 7.82 – 7.76 (m, 2H), 7.32 (t, *J* = 7.8 Hz, 1H), 7.28 – 7.21 (m, 1H), 7.02 (d, *J* = 7.7 Hz, 1H), 7.00 (d, *J* = 1.8 Hz, 1H), 6.95 (d, *J* = 8.7 Hz, 2H), 6.88 (dd, *J* = 8.3, 2.6 Hz, 1H), 6.69 – 6.62 (m, 2H), 5.07 (s, 2H), 4.66 (dd, *J* = 10.3, 2.4 Hz, 5H), 3.83 (s, 2H). ¹³C NMR (126 MHz, CDCl₃) δ 190.38, 159.87, 158.71, 151.41, 138.40, 138.09, 132.26, 129.70, 128.94, 125.59, 123.44, 119.54, 114.85, 113.41, 112.95, 111.21, 108.92, 70.17, 55.26, 53.90, 53.27.



1-(4-(isoindolin-2-yl)phenyl)ethanone (22151)

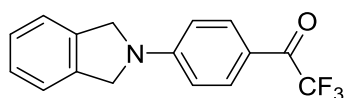
2.4a (98 mg, .37 mmol), 4-aminoacetophenone (50 mg, .37 mmol) and K₂CO₃ (51 mg, .37 mmol) were added to a microwave reaction vessel along with 2 mL distilled water and a magnetic stirrer. The vessel was sealed and heated to 120°C for 20 minutes on a Biotage Initiator microwave reactor. An orange-red solid formed during the reaction which was washed

with water and cold hexanes. The crude was further purified by recrystallization from hot methanol, followed by recrystallization from hot ethanol, yielding the titled compound as red crystals (30 mg, 34%). ESI MS: 238.1[M + H]⁺ ¹HNMR (500 MHz, CDCl₃) δ 7.95 (d, 2H), 7.36 (d, 2H), 7.34 (d, 2H), 6.65 (d, 2H), 4.74 (s, 4H), 2.53 (s, 3H); ¹³CNMR (125 MHz, CDCl₃) δ 195.60, 150.49, 137.06, 130.96, 127.68, 125.90, 122.81, 110.87, 53.87, 26.20.



2-phenylisoindoline (2.4b)

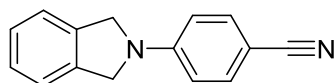
2.4a (213 mg, .805 mmol), aniline (70 μL, .805 mmol), and K₂CO₃ (111 mg, .805 mmol) were added to a microwave reaction vessel along with 2 mL distilled water and a magnetic stirrer. The vessel was sealed and heated to 120°C for 20 minutes on a Biotage Initiator microwave reactor. A red solid formed during the reaction which was washed with water and cold hexanes yielding the titled compound as a red solid (130 mg, 82%). ¹HNMR (400 MHz, CDCl₃) δ 7.34 (m, 7H), 6.92 (m, 2H), 4.76 (s, 4H).



2,2,2-trifluoro-1-(4-(isoindolin-2-yl)phenyl)ethanone (223902)

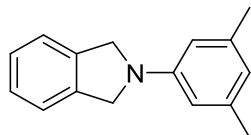
A dry pressure tube was charged with AlCl₃ (1.3 mg, .01 mmol) purged with N₂ and cooled to 0°C at which point 1 mL of dry THF was added. **2.4b** (20 mg, .102 mmol) was dissolved in 2 mL dry THF and added via syringe to the pressure tube. TFAA (58 μL, .41 mmol) was added dropwise by syringe while stirring. The pressure tube was sealed and the reaction was heated to 80°C with stirring under N₂ for 3 h. The mixture was diluted with EtOAc and washed with

saturated aq. NaHCO₃ and brine. The organic layer was dried over Na₂SO₄ and the solvent removed by rotary evaporation yielding orange crude material. The crude was first purified by flash chromatography (30-60% DCM in Hexanes) and then recrystallized twice in boiled ethanol yielding the titled compound as faintly yellow needles (10 mg, 33%). ESIMS: 292.0 [M + H]⁺ ¹H NMR (500 MHz, CDCl₃) δ 8.04 (d, 2H), 7.38 (m, 2H), 7.36 (m, 2H), 6.70 (d, 2H), 4.79 (s, 4H); ¹³C NMR (125 MHz, CDCl₃) δ 151.82, 136.29, 132.91, 127.82, 122.72, 118.02, 116.28, 111.32, 53.81; ¹⁹F NMR δ -70.33.



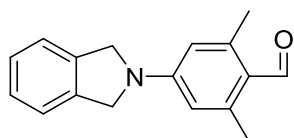
4-(isoindolin-2-yl)benzonitrile (224259)

2.4a (112 mg, 0.423 mmol), 4-aminobenzonitrile (50mg, 0.423 mmol), and K₂CO₃ (58.5 mg, 0.423 mmol) were added to a 2mL microwave tube along with 1mL of water. The tube was sealed and irradiated for 20 minutes at 120°C with 15 sec of prestirring. The solids were filtered from the reaction and washed with additional water and hexanes yielding a red solid. The solid was taken up in ethyl acetate and filtered. The filtrate was concentrated and taken up in boiling ethanol. The titled compound recrystallized as a yellow solid upon cooling (22mg, 0.095 mmol, 22.42 % yield) ESIMS: 221.1[M+H]⁺ ¹H NMR (500 MHz, CDCl₃) δ 7.54 (d, *J* = 8.31 Hz, 2H), 7.29 - 7.39 (m, 4H), 6.64 (d, *J* = 7.83 Hz, 2H), 4.70 (s, 4H) ¹³C NMR (126 MHz, CDCl₃) δ 149.5, 136.6, 133.7, 127.6, 122.7, 120.7, 111.5, 97.9, 53.6



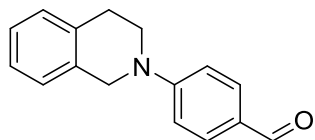
2-(3,5-dimethylphenyl)isoindoline (2.4d)

3,5-dimethylaniline (249 μ l, 2 mmol), **2.4a** (528 mg, 2.000 mmol), and K_2CO_3 (829 mg, 6.00 mmol) were added to a pressure tube along with 2mL of water. The tube was sealed and heated to 120°C for 1 h then left at RT overnight. The solid was filtered, and washed with water before discarding the filtrate. The solid was then taken up in DCM, filtered to remove a fine precipitate and the filtrate was concentrated. The crude solid was taken up in acetone and the titled compound precipitated as a white solid upon addition of methanol (365mg, 1.634 mmol, 82 % yield). Taken forward without further characterization.



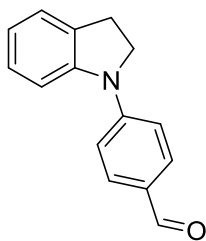
4-(isoindolin-2-yl)-2,6-dimethylbenzaldehyde (232721)

To a dry flask charged with 2-(3,5-dimethylphenyl)isoindoline (360mg, 1.612 mmol) in 5mL DCE was added a solution of DMF (374 μ l, 4.84 mmol) and $POCl_3$ (376 μ l, 4.03 mmol) in 5mL DCE which had been pre stirred at RT for 15 min. The mixture was heated to 50°C for 1 h at which point the reaction appeared complete by HPLC. The reaction was quenched by addition of 10% NaOH and then extracted with EtOAc. The organic portion was dried over sodium sulfate and the crude red residue was taken up in boiling ethanol. The titled compound recrystallized as an orange solid up cooling (90mg, 0.358 mmol, 22.21 % yield). ESIMS: 252.1 $[M+H]^+$ 1H NMR (400 MHz, $CDCl_3$) δ 10.38 (s, 1H), 7.41 - 7.28 (m, 4H), 6.31 (s, 2H), 4.72 (s, 4H), 2.64 (s, 6H). ^{13}C NMR (101 MHz, $CDCl_3$) δ 190.61 (d, $J = 10.8$ Hz), 149.93, 144.55, 136.83, 127.55, 122.75, 112.28, 112.07, 53.57, 21.59 (d, $J = 15.7$ Hz).



4-(3,4-dihydroisoquinolin-2(1H)-yl)benzaldehyde (232200)

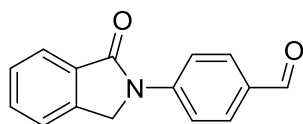
4-fluorobenzaldehyde (0.216 ml, 2.014 mmol) was dissolved in 2.5mL anhydrous DMSO in a dry pressure vessel. To this was added K_2CO_3 (418 mg, 3.02 mmol) and 1,2,3,4-tetrahydroisoquinoline (0.278 ml, 2.216 mmol). The headspace of the tube was purged with argon and the tube was capped. The mixture was heated to 75°C overnight. To the resultant mixture was added 20mL of water. The mixture was extracted with EtOAc. The organic portion was washed 2x with brine and then dried over sodium sulfate and concentrated yielding a yellow oil. The crude was purified by flash (0-25% EtOAc in Hexanes) yielding the titled compound as a yellow solid (195mg, 0.822 mmol, 40.8 % yield). ESIMS: 238.1 $[M+H]^+$ 1H NMR (500 MHz, $CDCl_3$) δ 9.78 (s, 1H), 7.72 - 7.84 (m, $J = 8.80$ Hz, 2H), 7.18 - 7.26 (m, 4H), 6.90 - 6.97 (m, $J = 8.80$ Hz, 2H), 4.57 (s, 2H), 3.70 (t, $J = 5.87$ Hz, 2H), 3.02 (t, $J = 5.87$ Hz, 2H) ^{13}C NMR (126 MHz, $CDCl_3$) δ 190.3, 154.0, 135.0, 133.5, 132.0, 128.1, 126.9, 126.5, 126.5, 126.1, 112.1, 48.8, 44.6, 29.0



4-(indolin-1-yl)benzaldehyde (232720)

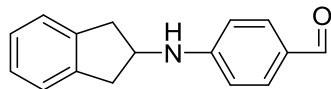
4-bromobenzaldehyde (311 mg, 1.678 mmol), indoline (189 μ l, 1.678 mmol), BINAP (115 mg, 0.185 mmol), $PdOAc_2$ (37.7 mg, 0.168 mmol) and Cs_2CO_3 (820 mg, 2.52 mmol) were added to 4mL degassed toluene and heated to 60°C for 2 h. The mixture was diluted with EtOAc and washed with water and brine. The organic portion was dried over sodium sulfate and

concentrated. Purification by flash (EA in Hex) yielded the titled compound as a brown oil (160mg, 0.717 mmol, 42.7 % yield). ^1H NMR (400 MHz, CDCl_3) δ 9.84 (s, 1H), 7.89 - 7.79 (m, 2H), 7.34 (d, $J = 8.0$ Hz, 1H), 7.31 - 7.26 (m, 2H), 7.23 (d, $J = 7.4$ Hz, 1H), 7.16 (d, $J = 7.8$ Hz, 1H), 6.89 (t, $J = 7.4$ Hz, 1H), 4.05 (t, $J = 8.3$ Hz, 2H), 3.18 (t, $J = 8.3$ Hz, 2H). ^{13}C NMR (101 MHz, CDCl_3) δ 190.38, 149.02, 144.72, 132.27, 131.74, 128.41, 127.09, 125.53, 121.00, 115.32, 110.35, 51.88, 28.02.



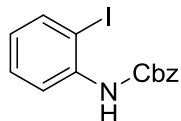
4-(1-oxoisindolin-2-yl)benzaldehyde (232483)

Cs_2CO_3 (734 mg, 2.253 mmol), PdOAc_2 (8.43 mg, 0.038 mmol), Xantphos (43.5 mg, 0.075 mmol), 4-bromobenzaldehyde (139 mg, 0.751 mmol), isoindolin-1-one (100mg, 0.751 mmol), were added to a flask equipped with a stir bar. The flask was vacuum purged and backfilled with argon. 10mL of rigorously degassed anhydrous dioxane was transferred to the reagent flask by syringe. The flask was stirred at 80°C for 1 hour at which point TLC indicated a clean and complete conversion of the starting materials to a new spot. The reaction was filtered through celite and the filter cake washed with EtOAc. The filtrate was concentrated in vacuo and the residue taken up in EtOAc, washed twice with brine and the organic portion dried over sodium sulfate. The solvent was removed yielding a white solid crude. The residue was taken up in hot ethanol and the titled compound recrystallized upon cooling (150mg, 0.632 mmol, 84 % yield). ESIMS: 238.0 $[\text{M}+\text{H}]^+$ ^1H NMR (500 MHz, CDCl_3) δ 9.99 (s, 1H), 8.13 (d, $J = 8.80$ Hz, 2H), 7.93 - 8.00 (m, 3H), 7.62 - 7.69 (m, 1H), 7.52 - 7.58 (m, 2H), 4.94 (s, 2H) ^{13}C NMR (126 MHz, CDCl_3) δ 191.0, 167.9, 152.2, 149.8, 144.8, 139.9, 132.8, 131.1, 128.7, 124.5, 122.7, 118.4, 50.5



4-((2,3-dihydro-1H-inden-2-yl)amino)benzaldehyde (232662)

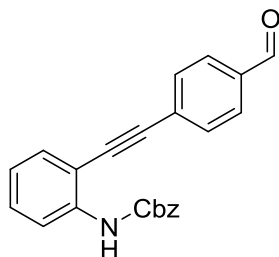
To a pressure tube charged with 3mL of rigorously degassed anhydrous toluene were added, Cs₂CO₃ (528 mg, 1.621 mmol), Pd₂(dba)₃ (37.1 mg, 0.041 mmol), X-Phos (19.32 mg, 0.041 mmol), 2,3-dihydro-1H-inden-2-amine (106 µl, 0.811 mmol), and 4-bromobenzaldehyde (150mg, 0.811 mmol). The mixture was bubbled with argon for a few minutes then the tube was capped and heated to 100°C overnight. The reaction mixture was diluted with ethyl acetate and ran through a plug of celite. The filtrate was further diluted with ethyl acetate and washed with water and brine. The organic portion was dried over sodium sulfate and the solvent removed in vacuo. The crude material was purified by flash chromatography 10-30% EA in Hex. The product was further taken up in hot methanol and the titled compound was obtained as a yellow crystalline solid upon cooling (50mg, 0.211 mmol, 26.0 % yield). ESIMS: 238.1 [M+H]⁺ ¹H NMR (500 MHz, CDCl₃) δ 9.74 (s, 1H), 7.71 (d, J = 8.9 Hz, 2H), 7.28 - 7.23 (m, 2H), 7.23 - 7.18 (m, 2H), 6.64 (d, J = 8.6 Hz, 2H), 4.56 (d, J = 7.4 Hz, 1H), 4.43 (dtd, J = 11.1, 7.1, 4.0 Hz, 1H), 3.42 (dd, J = 16.0, 6.7 Hz, 2H), 2.92 (dd, J = 16.0, 4.1 Hz, 2H). ¹³C NMR (126 MHz, CDCl₃) δ 190.19, 152.37, 140.70, 132.32, 126.92, 124.97, 112.29, 109.99, 53.58, 40.17.



benzyl (2-iodophenyl)carbamate (2.5b)

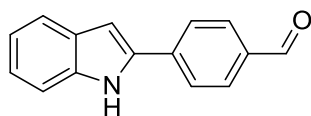
To a flask containing 2-iodoaniline (**2.5a**) (1 g, 4.57 mmol) was added 1N aq. NaOH (4.57 ml, 4.57 mmol). To the suspension was added CBZ-Cl (0.978 ml, 6.85 mmol) dropwise by syringe. The flask was stirred for an additional hour and the mixture was extracted 3 times with DCM and dried over NaSO₄ and concentrated, yielding a yellow oil. The oil was dissolved in minimal

diethyl ether then cooled to -78°C until the titled compound crystallized as a white solid (1.499g, 4.24 mmol, 93 % yield). ^1H NMR is consistent with literature.⁹²



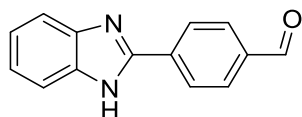
benzyl (2-((4-formylphenyl)ethynyl)phenyl)carbamate (2.5c)

Bis(triphenylphosphine)palladium(II) dichloride (35.1 mg, 0.050 mmol), copper(I) iodide (19.05 mg, 0.100 mmol), **2.5b** (353 mg, 1.000 mmol), and 4-ethynylbenzaldehyde (130 mg, 1 mmol) were added to an flask which was purged and backfilled with N_2 3x. A rigorously deoxygenated solution of triethylamine (1.394 mL, 10.00 mmol) in 2.5 mL toluene was added by syringe and the flask was heated to 70°C for 1 hour, at which point the reaction was observed to be complete by TLC. The reaction mixture was concentrated and the resulting residue was dissolved in ethyl acetate and washed with sat. aq. NH_4Cl then brine. The organic portion was dried over sodium sulfate and concentrated. The crude was dissolved in a ~20 mL of hot ethanol and immediately filtered to remove an insoluble impurity. The titled compound recrystallized as an orange crystalline solid upon cooling (207mg, 0.582 mmol, 58.2 % yield). ^1H NMR (500 MHz, CDCl_3) δ 10.03 (s, 1H), 8.21 (d, $J = 8.31$ Hz, 1H), 7.83 - 7.95 (m, $J = 7.83$ Hz, 2H), 7.62 - 7.74 (m, $J = 7.83$ Hz, 2H), 7.50 (d, $J = 7.34$ Hz, 1H), 7.42 - 7.47 (m, 2H), 7.33 - 7.42 (m, 4H), 7.06 (t, $J = 7.58$ Hz, 1H), 5.26 (s, 2H)



4-(1H-indol-2-yl)benzaldehyde (224256)

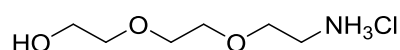
To a degassed solution of (**2.5c**) (207mg, 0.582 mmol) in 5mL THF was added 1M TBAF in THF (1747 μ l, 1.747 mmol) which was sealed in a pressure tube and stirred at 70°C for 1 h at which point the initially red solution turned nearly black. The mixture was concentrated and taken up in EtOAc and washed several times with 1% NaOH until a clear aqueous portion resulted. The organic portion was washed with brine, dried over sodium sulfate and concentrated. The crude product was purified by flash (0-10% EtOAc in Hexanes) yielding the titled compound as an off white solid (12mg, 0.054 mmol, 9.31 % yield). ESIMS: 222.1 [M+H]⁺ ¹H NMR (500 MHz, CDCl₃) δ 10.04 (s, 1H), 8.51 (br. s., 1H), 7.96 (dd, J = 1.30, 8.31 Hz, 2H), 7.83 (d, J = 8.31 Hz, 2H), 7.68 (d, J = 7.83 Hz, 1H), 7.44 (d, J = 8.31 Hz, 1H), 7.23 - 7.29 (m, 1H), 7.13 - 7.21 (m, 1H), 7.02 (s, 1H) ¹³C NMR (126 MHz, CDCl₃) δ 191.6, 138.1, 137.5, 136.2, 135.3, 130.7, 129.2, 125.3, 123.7, 121.3, 120.9, 111.3, 102.8.



4-(1H-benzo[d]imidazol-2-yl)benzaldehyde (224257)

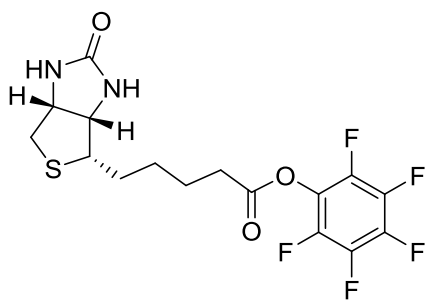
A flask charged with benzene-1,2-diamine (81 mg, 0.746 mmol), terephthalaldehyde (100mg, 0.746 mmol), 3Å M.S., and 10 mL *t*-BuOH was heated to 40°C for 5 min resulting in a bright orange solution. I₂ (237 mg, 0.932 mmol) and K₂CO₃ (309 mg, 2.237 mmol) were added and the mixture was stirred at 70°C. A bright orange precipitate formed and quickly turned rust red. After heating for 2 h, 10% sodium thiosulfate was added to the mixture until the solution turned yellow. The mixture was extracted with DCM and the organic portion was washed with brine and dried over sodium sulfate before removing the solvent in vacuo. The residue was purified by

flash (25-75% EtOAc in Hex) yielding the titled compound as a yellow solid (20mg, 0.089 mmol, 11.95 % yield). ESIMS: 223.1 $[M+H]^+$ 1H NMR (500 MHz, DMSO- d_6) δ 10.09 (s, 1H), 8.43 (d, $J = 7.83$ Hz, 2H), 8.09 (d, $J = 8.31$ Hz, 2H), 7.67 (dd, $J = 2.93, 5.87$ Hz, 1H), 7.23 - 7.31 (m, 2H) ^{13}C NMR (126 MHz, DMSO- d_6) δ 192.6, 149.9, 136.6, 135.3, 130.1, 126.9, 122.7, 115.6, 111.4



2-(2-(2-aminoethoxy)ethoxy)ethanol, HCl (2.8b)

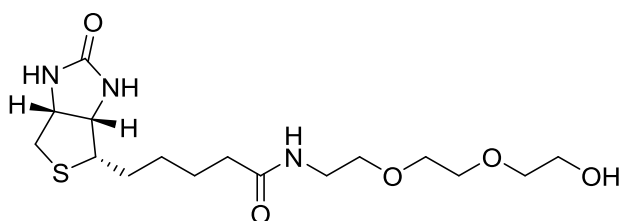
2-(2-(2-azidoethoxy)ethoxy)ethanol (prepared from **2.8a** as previously described⁹³) (1.5 g, 8.56 mmol) was dissolved in 5mL THF to which triphenylphosphine (2.69 g, 10.27 mmol) was added. After stirring for 30 minutes, 1mL water was added and the mixture was stirred overnight. The next day the reaction was taken up in 1N HCl and washed 3x with EtOAc. The aqueous portion was concentrated in vacuo to afford the titled compound as a brown oil (1.4 g, 7.54 mmol, 88 % yield). 1H NMR (400 MHz, Methanol- d_4) δ 3.76 - 3.62 (m, 7H), 3.60 - 3.53 (m, 2H), 3.30 (p, $J = 1.6$ Hz, 2H), 3.12 (t, $J = 5.0$ Hz, 2H).



Perfluorophenyl 5-((3aS,4S,6aR)-2-oxohexahydro-1H-thieno[3,4-d]imidazol-4-yl)pentanoate (2.8d)

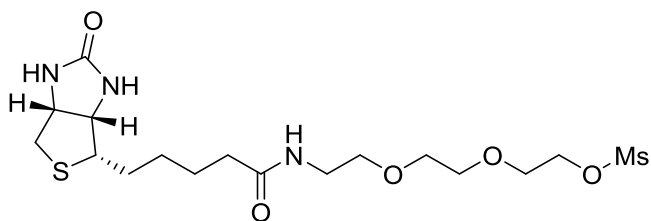
To a solution of Biotin (**2.8c**) (1g, 4.09 mmol) in 5mL DMF at 0°C was added EDC (0.942 g, 4.91 mmol). The mixture was stirred for 1hour at which point 2,3,4,5,6-pentafluorophenol

(0.829 g, 4.50 mmol) was dissolved in 2mL DMF and added by syringe. The slurry was stirred overnight and diluted with 10% citric acid and DCM and the titled compound was collected by filtration as a white solid (1.06 g, 2.58 mmol, 63.1 % yield). ¹H NMR was consistent with literature.⁹⁴



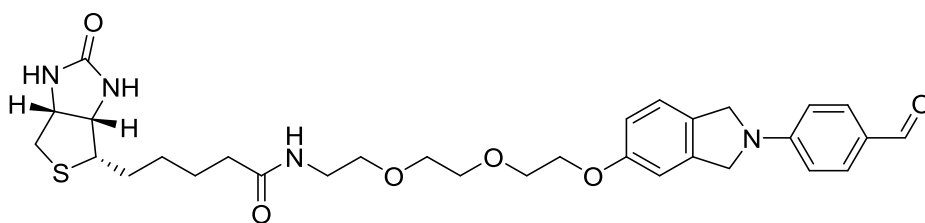
N-(2-(2-(2-hydroxyethoxy)ethoxy)ethyl)-5-((3aS,4S,6aR)-2-oxohexahydro-1H-thieno[3,4-d]imidazol-4-yl)pentanamide (2.8e)

To a flask charged with **2.8d** (300 mg, 0.731 mmol) and **2.8b** (163 mg, 0.877 mmol) in 5mL DMF was added DIPEA (0.153 ml, 0.877 mmol). The mixture was stirred at RT overnight. The next day the DMF was removed in vacuo and the crude residue was purified by flash (0-15% MeOH in DCM) to yield the titled compound as a white solid. (190mg, 0.506 mmol, 69.2 % yield) ¹H NMR (500 MHz, DMSO-*d*₆) δ 7.81 (t, J = 5.8 Hz, 1H), 6.39 (s, 1H), 6.33 (s, 1H), 4.56 (t, J = 5.5 Hz, 1H), 4.28 (dd, J = 7.7, 5.1 Hz, 1H), 4.11 (ddd, J = 7.0, 4.5, 1.8 Hz, 1H), 3.52 - 3.44 (m, 6H), 3.42 - 3.34 (m, 4H), 3.16 (q, J = 5.8 Hz, 2H), 3.08 (ddd, J = 8.8, 6.1, 4.4 Hz, 1H), 2.80 (dd, J = 12.4, 5.1 Hz, 1H), 2.56 (d, J = 12.4 Hz, 1H), 2.04 (t, J = 7.4 Hz, 2H), 1.66 - 1.54 (m, 1H), 1.53 - 1.37 (m, 3H), 1.35 - 1.17 (m, 2H).



2-(2-(2-(5-((3aS,4S,6aR)-2-oxohexahydro-1H-thieno[3,4-d]imidazol-4-yl)pentanamido)ethoxy)ethoxy)ethyl methanesulfonate (2.8f)

2.8e (340mg, 0.905 mmol) was dissolved in 3mL pyridine, to which Ms-Cl (0.085 ml, 1.087 mmol) was added. The mixture turned green immediately then went to brown over the course of the next hour, at which point the reaction was complete by TLC (20% MeOH in DCM, Visualize with permanganate stain. Product is more lipophilic than starting material, UV active spot is dissociated pyridine HCl). The reaction mixture was concentrated and purified by flash (2-10% MeOH in DCM, detect with ELSD) to obtain the titled compound as an oily orange solid (410mg, 0.904 mmol, 100 % yield). ESIMS 454.1677 [M+H]⁺. ¹H NMR (500 MHz, CDCl₃) δ 7.37 - 6.17 (m, 2H), 4.66 - 4.23 (m, 3H), 3.86 - 3.51 (m, 7H), 3.48 - 3.30 (m, 2H), 3.26 - 3.04 (m, 3H), 3.03 - 2.68 (m, 2H), 2.26 (s, 2H), 1.87 - 1.33 (m, 7H).



N-(2-(2-(2-((2-(4-formylphenyl)isoindolin-5-yl)oxy)ethoxy)ethoxy)ethyl)-5-((3aS,4S,6aR)-2-oxohexahydro-1H-thieno[3,4-d]imidazol-4-yl)pentanamide (264441)

A dry flask charged with **2.8f** (410mg, 0.904 mmol), Cs₂CO₃ (295 mg, 0.904 mmol) and 5mL DMF was rigorously deoxygenated under vacuum then heated to 80°C for 2 days under N₂. The solvent was removed in vacuo and the crude residue subjected to flash (Silica gel, 0-20% MeOH in DCM gradient) yielding a dark green solid with reasonable purity by HPLC. The product was further purified by flash (C18 20-50% ACN in Water, 0.1% TFA (Permanently stained the column)) which resulted in >95% purity by HPLC but did not remove the dark green coloration. Decoloration was achieved by flash (Neutral Alumina, 0-20% MeOH in DCM) to yield the titled compound as a yellow residue (12mg, 0.02 mmol, 2.2 % yield). ESIMS 597.2741 [M+H]⁺. ¹H NMR (500 MHz, DMSO-*d*₆) δ 9.71 (s, 1H), 7.82 (t, *J* = 5.6 Hz, 1H), 7.79 – 7.73 (m, 2H), 7.31

(d, $J = 8.3$ Hz, 1H), 7.00 (d, $J = 2.3$ Hz, 1H), 6.91 (dd, $J = 8.3, 2.4$ Hz, 1H), 6.80 – 6.73 (m, 2H), 6.38 (d, $J = 30.6$ Hz, 2H), 4.74 – 4.60 (m, 4H), 4.32 – 4.23 (m, 1H), 4.17 – 4.04 (m, 2H), 3.79 – 3.69 (m, 2H), 3.60 (dd, $J = 5.9, 3.5$ Hz, 2H), 3.54 (dd, $J = 5.7, 3.4$ Hz, 2H), 3.41 (t, $J = 5.9$ Hz, 2H), 3.20 (t, $J = 5.8$ Hz, 2H), 3.07 (ddd, $J = 8.6, 6.1, 4.3$ Hz, 1H), 2.80 (dd, $J = 12.5, 5.1$ Hz, 1H), 2.57 (d, $J = 12.4$ Hz, 1H), 2.06 (t, $J = 7.4$ Hz, 2H), 1.60 (ddt, $J = 12.3, 9.7, 6.1$ Hz, 1H), 1.55 – 1.40 (m, 4H), 1.38 – 1.20 (m, 2H). ^{13}C NMR (126 MHz, DMSO- d_6) δ 190.45, 172.53, 163.12, 158.71, 151.71, 138.63, 132.24, 129.08, 125.49, 124.00, 114.79, 111.89, 108.93, 70.32, 70.03, 69.64, 69.39, 67.85, 61.47, 59.63, 55.86, 53.98, 53.33, 49.04, 38.89, 35.55, 28.64, 28.48, 25.71.

Chapter 3 Development of 1st Generation Pyrazolopyrimidinone Aldehyde Dehydrogenase Inhibitors

3.1. Characterization of Lead Compound CM39

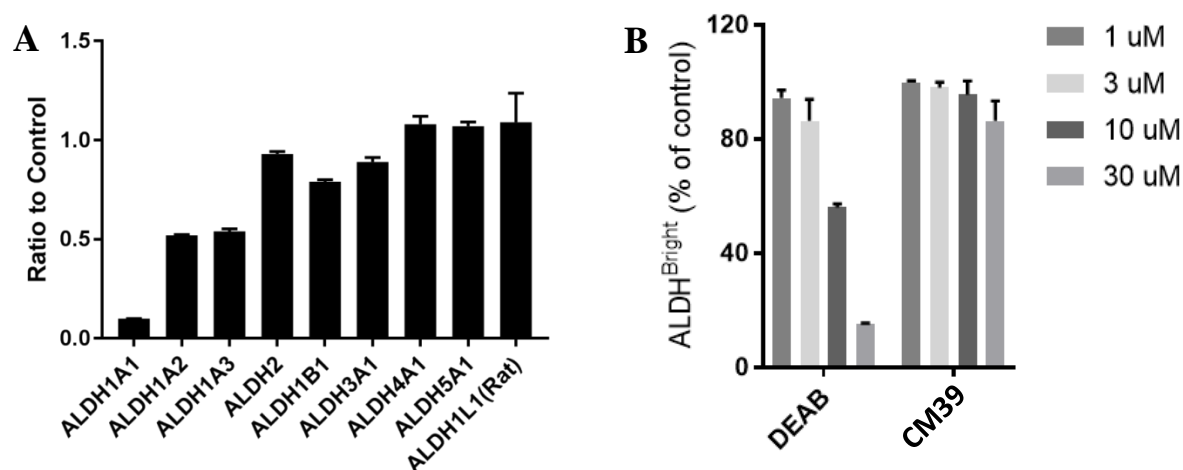


Figure 3.1: Biochemical and Cellular ALDH Inhibition by CM39

(A) Fraction of enzyme activity remaining for 9 ALDH isoforms in the presence of 20 μM **CM39**. (B) Percent control ALDH^{Bright} cells remaining following treatment of PEO1 cells at the specified concentration with DEAB (**1**) or compound **CM39** (N=2). (Unpublished work, courtesy of Hurley and Buckanovich Labs)

The Hurley Lab HTS campaign for 1A1 inhibitors that resulted in discovery of **CM026** and **CM037** also identified **CM39**.⁶⁶ This compound was an attractive lead for the development of pan-ALDH1A inhibitors because it exhibited reasonably ligand-efficient inhibition of 1A1 ($IC_{50} = 0.9 \mu\text{M}$, $LE = 0.32$) and good selectivity (<20% inhibition of ALDH2 and 3A1 at 20μM).⁶⁶ A further screen of selectivity showed ~50% inhibition of 1A2 and 1A3 at 20 μM and little activity against other ALDH isoforms (Figure 3.1A).⁹⁵

Despite the presence of a potentially electrophilic isothiourea, **CM39**-mediated inhibition of 1A1 was fully reversed following gel filtration, indicating it is non-covalent. Similar to other non-covalent inhibitors of 1A1, **CM39** was found to be non-competitive with respect to the substrate acetaldehyde with a $K_i = 0.38 \pm 0.05 \mu\text{M}$ and uncompetitive with respect to NAD^+ .⁶⁷ Liabilities of the lead with regard to its potential as a therapeutic included a half-life of 9 minutes in the presence of MLMs and poor aqueous solubility ($2 \mu\text{M}$), both of which could be attributed to high lipophilicity (cLogP of 5.2).⁹⁵

As shown in Figure 3.1B, compound **CM39** was inferior to the widely-used ALDEFLUOR control compound DEAB (**1**) at reducing ALDH^{Bright} PEO1 cells at concentrations up to $30 \mu\text{M}$, suggesting that ALDH1A1 selective inhibition is not sufficient to inhibit ALDEFLUOR in this 1A3 high cell line, although we cannot rule out poor solubility or cell permeability. It is important to note that while DEAB is a 57 nM 1A1 selective inhibitor, it only inhibits ALDEFLUOR above its 1A3 IC_{50} ($3 \mu\text{M}$).⁴¹ Lower ALDEFLUOR IC_{50} s for DEAB in two 1A1 high cell lines, MIA PaCa-2 ($3.4 \mu\text{M}$) and HT-29 ($1.7 \mu\text{M}$), have previously been reported.⁹⁶

3.2. Crystal Structure of ALDH1A1 complexed with CM39

To guide the design of new analogs, an X-ray crystal structure of **CM39** bound to N121S ALDH1A1 was obtained with a resolution of 2.1 \AA (PDB code 5TEI, Figure 3.2A). The known single nucleotide polymorphism (NCBI rs1049981) resulting in the N121S missense mutation has been found in a small percentage of the HapMap-CEU population. There is no known clinical significance to the mutation and its structure is highly similar to the wild-type.⁶⁶⁻⁶⁷ The N121S enzyme crystallizes under identical conditions to the WT enzyme, but complexes with inhibitors are frequently easier to obtain, presumably due to dynamic fluctuations within the

active site that are not detectable by crystallography and have little impact on observed potency. Furthermore, the IC_{50} of **CM39** was comparable for the WT and N121S (0.9 and 0.7 μ M respectively).

Similar to the complex with **CM026** (PDB code 4WP7), the bicyclic ring binds across the exterior 1/3 of the substrate binding pocket. The 3-fluorobenzyl group extends in towards the catalytic nucleophile (C303) making contacts with aromatic residues F171, W178 and F466. In contrast to **CM026** and **CM037** (PDB code 4X4L), **CM39** does not engage the cleft of the active site adjacent to T129, suggesting it may be possible to gain additional interactions with the active site in this region.⁶⁷ The pyrazolopyrimidinone of **CM39** binds adjacent to G458. Other ALDH1/2 isoenzymes have either an Asn or Asp residue at position 458 which may drive

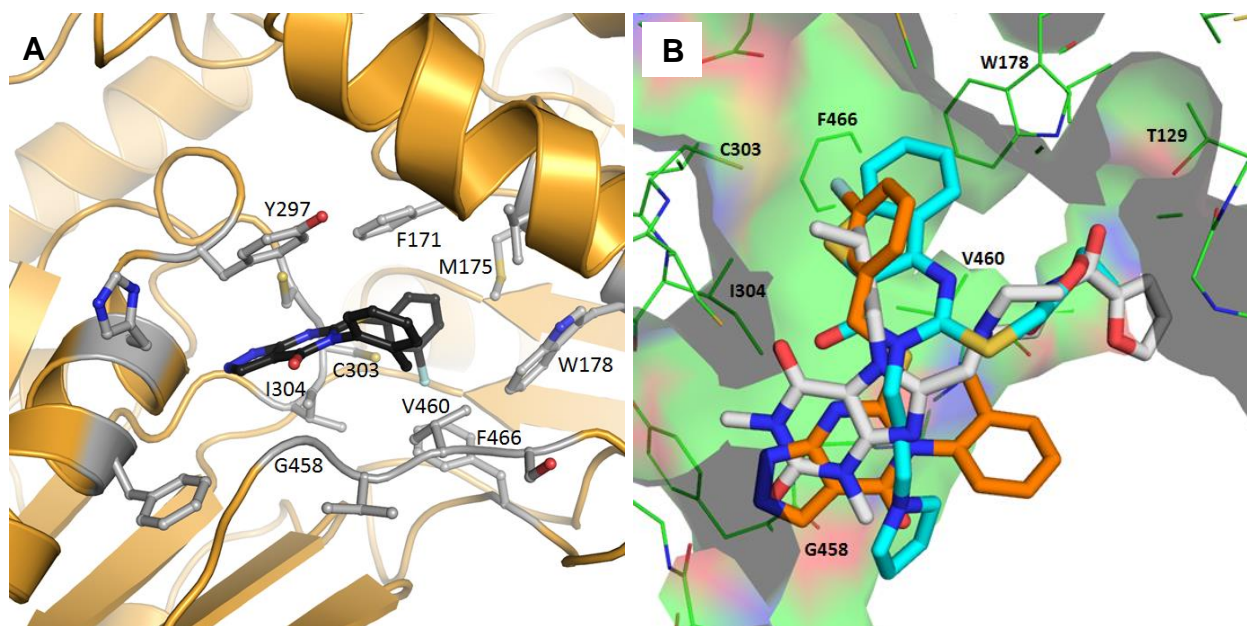


Figure 3.2 Structure of ALDH1A1 N121S with CM39 (2.10 Å, PDB 5TEI)

(A) The fluorophenyl of compound **CM39** projects into the lipophilic pocket towards the catalytic cysteine (C303). Key residues are labelled. (B) Overlay of Compounds **CM026** (Cyan, PDB entry 4WP7), **CM073** (Grey, PDB Entry 4X4L), and **CM39**(Orange) bound in ALDH1A1. (Unpublished work, courtesy Hurley lab)

selectivity by prohibiting a similar binding mode in these isoforms. There appears to be room for small substitutions on the pyrazole at N-1 but not N-2, suggesting that larger substituents at these positions will not be tolerated without alteration of the binding pose. The lipophilic 2-methylphenyl ring binds near a relatively polar region of the 1A1 active site, suggesting that appropriate polar substituents could improve or maintain binding affinity while lowering cLogP. The 3-fluorobenzyl ring attached to the sulfur projects into the deepest section of the active site and maximizes contacts with the aromatic residues near the catalytic nucleophile, C303. The apparent goodness of fit of the 3-fluorobenzyl substituent, as well as its expected metabolic stability, encouraged us to retain it for the initial set of analogs based on **CM39**.

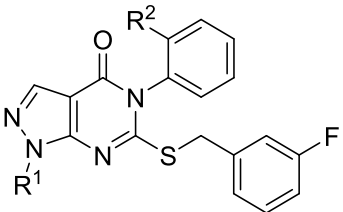
3.3. Optimization of Pyrazole Substituents

We began our SAR campaign by generating N-alkylated analogs to fill the small lipophilic pocket adjacent to Ile304. We also hypothesized that eliminating the moderately acidic ($pK_a = 8.1^{97}$) pyrazole N-H might improve cell permeability. Encouragingly, methylation at N-1 (Table 3.1, **257128**) resulted in a modest improvement in 1A1 inhibition compared to **CM39**. Consistent with a reduction in $cLogP^{97}$ aqueous solubility was also improved. Installing the larger ethyl (**257443**) and cyclopropyl-methyl substituent (**257724**) improved the 1A1 IC_{50} but did not improve potency against 1A2 or 1A3. The unfavorable $cLogPs > 5$ of the two analogs encouraged us to explore less lipophilic oxetanyl analogs **257910-257911**. Importantly, **257911** maintained comparable potency against 1A1 with substantially lower $cLogP$ (4.7). The homologated oxetane **257910** was 2-fold less potent against 1A1, suggesting that larger substituents would not be tolerated.

In an effort to pare down the **CM39** scaffold to the key pharmacophore, we discovered that removing the R^2 *o*-methyl markedly improved inhibition of 1A2 and 1A3 affording

compound **257901**, the first pan-ALDH1A inhibitor in the series. We revisited the panel of N-1 substituents used in the *o*-methyl series (**257723**, **257904**, **257905**, **258082**, **258084**) and observed different SAR trends. The small N-methyl substituent of **257723** afforded the most potent of the four analogs tested but exhibited very poor solubility. The cLogP of **257723** is significantly lower than **257901**; however, as judged by retention times on reverse and normal phase chromatography, the lipophilicity of the two was similar. We believe the poor solubility is best explained by the increased planarity of **257723** upon removal of the *o*-methyl. The MLM stability of **257723** was unchanged relative to **CM39**. The bulkier ethyl, cyclopropyl-methyl, and oxetanyl-methyl substituents resulted in 4-fold or greater reduction in potency against the ALDH1A family relative to **257723**. The smaller oxetanyl substituent of **258082** was only slightly less potent than **257723** and afforded a modest improvement in aqueous solubility. *The divergent SAR trends for N-1 pyrazole substituents upon removal of the o-methyl suggested a new binding mode was accessible.*

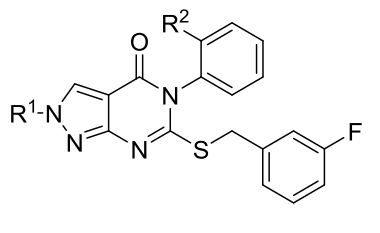
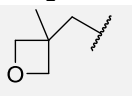
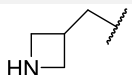
Table 3.1 Characterization of N-1 Pyrazole Substituents

			ALDH IC ₅₀ ^a (μM) or % control at 20 μM ^b				ADME Characterization		
Cmpd No.	R ¹	R ²					cLogP	Aq. Sol. ^c (μM)	MLM t _{1/2} (min)
			1A1	1A2	1A3	2			
CM39	H	Me	0.9 ±0.2	53%	53%	85%	5.2	2	9
257901	H	H	0.45 ±0.03	0.67 ±0.08	0.39 ±0.02	94%	4.7		
257128	Me	Me	0.66 ±0.06	52%	4 ±1	94%	4.8	38	
257443	Et	Me	0.35 ±0.01	>10	>10	100%	5.2		
257724	c-PrCH ₂	Me	0.18 ±0.01	>10	>10	100%	5.6		
257911	3-oxetanyl	Me	0.26 ±0.03	6 ± 1	60%	96%	4.7		
257910	3-oxetanyl- CH ₂	Me	0.42 ±0.01	45%	58%	97%	4.7		
257723	Me	H	0.08 ±0.01	0.15 ±0.01	0.09 ±0.01	100%	4.3	<0.7 (BLQ) ^d	8
257904	Et	H	0.32 ±0.02	0.40 ±0.06	0.25 ±0.02	82%	4.7		
257905	c-PrCH ₂	H	0.56 ±0.03	1.26 ±0.08	0.55 ±0.02	83%	5.1		
258082	3-oxetanyl	H	0.13 ±0.01	0.23 ±0.01	0.17 ±0.01	94%	4.1	8	
258084	3-oxetanyl- CH ₂	H	0.34 ±0.07	1.1 ±0.1	0.61 ±0.09	96%	4.1		

Values are expressed as ^a Mean ± SEM (n=3), ^b Mean (n=3); ^c Thermodynamic solubility analysis was performed by Analiza Inc. using quantitative nitrogen detection.

(www.analiza.com); ^dBLQ = below limit of quantitation. (Unpublished work, courtesy of Hurley and Sun Labs)

Table 3.2 Characterization of N-2 Pyrazole Substituents

			ALDH IC ₅₀ ^a (μM) or % control at 20 μM ^b				ADME Characterization		
Cmpd No.	R ¹	R ²					cLogP	Aq. Sol. ^c (μM)	MLM t _{1/2} (min)
			1A1	1A2	1A3	2			
257432	Me	Me	0.67 ±0.07	6 ±1	2.2 ±0.4	100%	5.3		
257434	Et	Me	0.40 ±0.05	5 ±1	>5	91%	5.6		
257725	c-Pr-CH ₂	Me	0.10 ±0.01	>10	1.0 ±0.1	100%	6.1		
257913	3-oxetanyl	Me	0.44 ±0.06	8 ±1	3.9 ±0.4	100%	5.2		
257912	3-oxetanyl- CH ₂	Me	0.20 ±0.03	3.9 ±0.3	2.6 ±0.3	98%	5.2		
257902	Me	H	0.25 ±0.01	0.34 ±0.05	0.13 ±0.01	94%	4.8	69	13
257903	Et	H	0.17 ±0.07	0.6 ±0.05	0.15± 0.01	98%	5.2		
257906	c-Pr-CH ₂	H	0.13 ±0.03	1.1 ±0.2	0.17 ±0.03	87%	5.6		
258083	3-oxetanyl	H	0.08 ±0.01	0.25 ±0.04	0.12 ±0.02	97%	4.7	5	23
258085	3-oxetanyl- CH ₂	H	0.27 ±0.01	0.48 ±0.04	0.13 ±0.01	99%	4.7	53	27
262701		H	7%	21%	4%	97%	5.0		
262702		H	14%	14%	10%	93%	4.3		

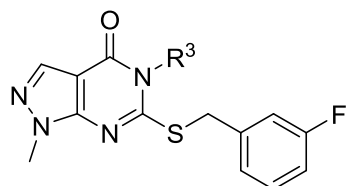
Values are expressed as ^aMean ± SEM (n=3), ^bMean (n=3); ^cThermodynamic solubility analysis was performed by Analiza Inc. using quantitative nitrogen detection.

(www.analiza.com); ^dBLQ = below limit of quantitation. (Unpublished work, courtesy of Hurley and Sun Labs)

N-2 alkylated analogs were also tested to further probe the flexibility of the binding mode depicted in the **CM39** crystal structure (Table 3.2). **257432** exhibited a similar ALDH1A inhibition profile to **257128**. Extending to bulkier substituents (**257434**, **257725**, **257912**, **257913**) resulted in improved 1A1 potency with the cyclopropyl-methyl being optimal, providing strong evidence for an alternative binding mode. These N-2 substituted analogs were more potent against 1A3 than the corresponding N-1 regioisomers, as exemplified by the modestly 1A1/1A3 selective cyclopropyl-methyl analog **257725** vs 1A1-selective **257724**. As we observed previously, removal of the *o*-methyl significantly improved the inhibition of 1A2 and 1A3 in analogs (**257902-257903**, **257906**, **258083**, **258085**). Oxetane was the optimal N-2 substituent to achieve potent pan-ALDH1A inhibition (**258083**), while cyclopropyl-methyl (**257906**) afforded a potent 1A1/1A3 inhibitor with >5-fold selectivity over 1A2. Despite having higher values for cLogP than the corresponding N-1 regioisomers, N-2 analogs were observed to be more polar by both normal and reverse phase chromatography. Consistent with this observation, the solubility of N-2 methyl analog **257902** was substantially improved over regioisomer **257723**. **257902** was also moderately more stable to treatment with MLMs, leading us to prioritize N-2 substituted analogs for further pharmacokinetic studies. Curiously, appending the oxetanyl substituent at N-2 (**258083**) was not favorable for solubility as was observed at N-1 (**258082**). Reasonable aqueous solubility was restored for the homologated analog **258085**. Perhaps resulting from steric blocking of N-dealkylation, **258083** and **258085** were about 2-fold more stable in the MLM assay than **257902**. The branched oxetanyl and azetidiny analogs **262701-262702** maintained reasonable ALDH inhibition but did not offer any particular advantage. Exquisite selectivity over the closely related ALDH2 isoform was

maintained for all tested analogs, positioning the series as a useful set of tool compounds to probe the biological effect of ALDH1A inhibition.

Table 3.3 Characterization of N-phenyl Modifications



Cmpd No.	R ³	ALDH IC ₅₀ ^a (μM) or % control at 20 μM ^b			
		1A1	1A2	1A3	2
257128	2-Me-Ph	0.66 ±0.06	52%	4 ±1	94%
257723	Ph	0.08 ±0.01	0.15 ±0.01	0.09 ±0.01	100%
258463	2-Cl-Ph	0.25 ±0.04	75%	10 ±2	100%
258464	3-Cl-Ph	4.1 ±0.6	0.56 ±0.06	2.6 ±0.3	100%
258465	4-Cl-Ph	69%	1.1 ±0.1	0.75 ±0.05	100%
258962	2-F-Ph	0.11 ±0.01	8% ^c	1% ^c	90%
257727	2-OMe-Ph	0.97 ±0.10	>10	>10	100%
258077	3-OMe-Ph	41%	1.3 ±0.1	44%	82%
258078	4-OMe-Ph	8.2 ±0.7	1.77 ±0.09	0.78 ±0.09	86%
257907	3-Pyridyl	3.83 ±0.03	45%	117%	99%
257908	4-Pyridyl	52%	52%	60%	97%
257914	2-Pyridyl	2.4 ±0.4	64%	67%	99%
257726	Bn	0.89 ±0.13	0.72 ±0.04	>10	100%
258081	Ph-CH ₂ -CH ₂	1.4 ±0.15	0.9 ±0.1	0.18 ±0.04	87%
258074	Me	4.1 ±0.37	79%	66%	95%
258466	Cyclohexyl	37%	36%	43%	N.I.
258467	Cyclopentyl	46%	37%	95%	N.I.
258468	Cyclopropyl	28%	14%	73%	96%

Values are expressed as ^a Mean ± SEM (n=3), ^b Mean (n=3); ^c Dose response curves were not satisfactory for IC₅₀ determination. (Unpublished work, courtesy of Hurley Lab)

The substantial increase in inhibition across the ALDH1A family upon removal of the *o*-methyl at R² (**257723**) encouraged us to further probe the effect of varied substitutions at this position as shown in Table 3.3. We retained the N-1 methyl substituent of **257723** for synthetic ease. Although we had evidence to suggest the binding mode of **CM39** depicted in the crystal structure was flexible, we began by designing R³ analogs according to the crystal structure. The R³ region of **CM39** is flanked by a region of exposed peptide backbone (residues 458-460) and the sidechain of N121 (S121 in WT), suggesting that polar interactions in this region might improve binding over the lipophilic 2-methylphenyl. Additionally, as the R³ methyl-phenyl is partially solvent exposed, polar solubilizing moieties were expected to improve pharmacokinetic properties without substantial loss of potency. Unfortunately, all attempts to alter the phenyl present in **257723** resulted in significant loss of activity across the ALDH1A family. Nevertheless, interesting selectivity trends did emerge. Substituents other than methyl at the ortho position (Cl, OMe) also rendered compounds 1A1 selective, but decreased 1A1 potency (**258463** and **257727**) relative to proteo analog **257723**. Chloro analog **258463** showed a twofold improvement in potency (1A1 IC₅₀ = 250 nM) compared to methyl analog **257128**. Because of the comparable size of Cl and CH₃, this difference suggested a preference for electron withdrawing groups; however, the electron-deficient fluorinated analog **258962** was merely equipotent with **257723** despite the similar size of the ortho substituents. Electron-rich methoxy analog **257727** was four-fold less potent against 1A1 than chloro analog **258463**. Meta substituents rendered analogs **258464** and **258077** modestly 1A2 selective. Addition of a chlorine in the para position resulted in a 1A2/1A3-selective inhibitor vs 1A1 (**258465**), while para methoxy analog **258078** exhibited very modest selectivity for 1A3. Pyridyl analogs **257907-257908**, **257914** were substantially less potent across the ALDH1A family, perhaps

reflecting a desolvation penalty without formation of productive hydrogen bonds within the active site. Benzyl analog **257726** inhibited 1A1 and 1A2 with good selectivity over 1A3. Homologation to phenylethyl analog **258081** resulted in potent inhibition of 1A3 ($IC_{50} = 180$ nM) with more than 5-fold selectivity over 1A1 and 1A2 and greater selectivity over other ALDH isoforms as shown in Figure 3.3. Methyl and cycloalkyl groups at R^3 were not tolerated (**258074**, **258466-258468**). The steep SAR at R^3 , inconsistent with partial solvent exposure, was further evidence that the binding mode depicted in the crystal structure of **CM39** was no longer relevant.

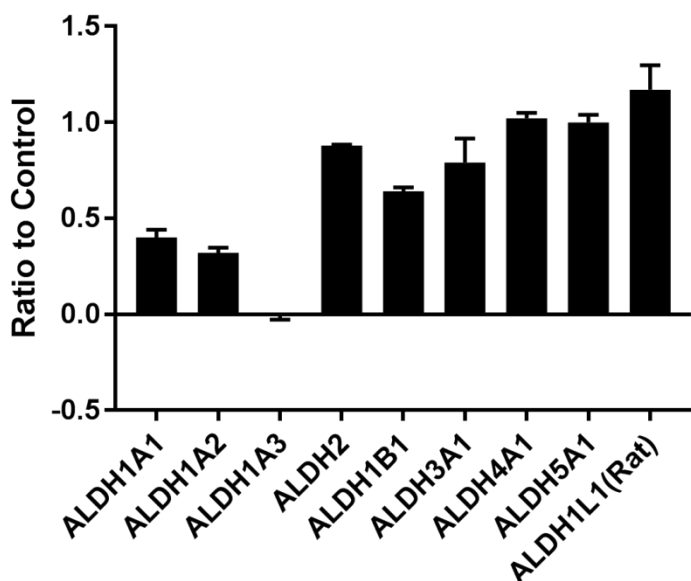


Figure 3.3 Isoform Selectivity of Compound 258081

Fraction of enzyme activity remaining for 9 ALDH isoforms in the presence of 20 μ M **258081**. (Unpublished work, courtesy of Hurley Lab)

3.4. Crystal Structure of ALDH1A1 Complexed with Compound 258083

To elucidate the change in binding mode we suspected, the Hurley lab obtained a co-crystal structure of N121S ALDH1A1 with compound **258083** resolved to 2.0Å (PDB code 6DUM) (Figure 3.4). The structure reveals a dramatically different binding pose for **258083** in which the R³ N-phenyl is situated near the catalytic cysteine. The N-phenyl is flanked by Phe171 and Phe466, potentially explaining why steric bulk and polarity are not tolerated at the ortho and meta positions (Table 3.3). It is more difficult to justify why para substituents are so poorly tolerated. In contrast to the binding pose of compound **CM39**, there is room for fairly large N-2 pyrazole substituents to extend across the mouth of the active site. Consistent with this observation, larger substituents at N-2 improve 1A1 potency (**257906** and **258083**) relative to methyl analog **257902**. As expected, given that large substituents at N-1 would project into solvent, compounds with larger N-1 substituents (e.g. **257904-257905**, **258084**) do not improve potency over methyl analog **257723**.

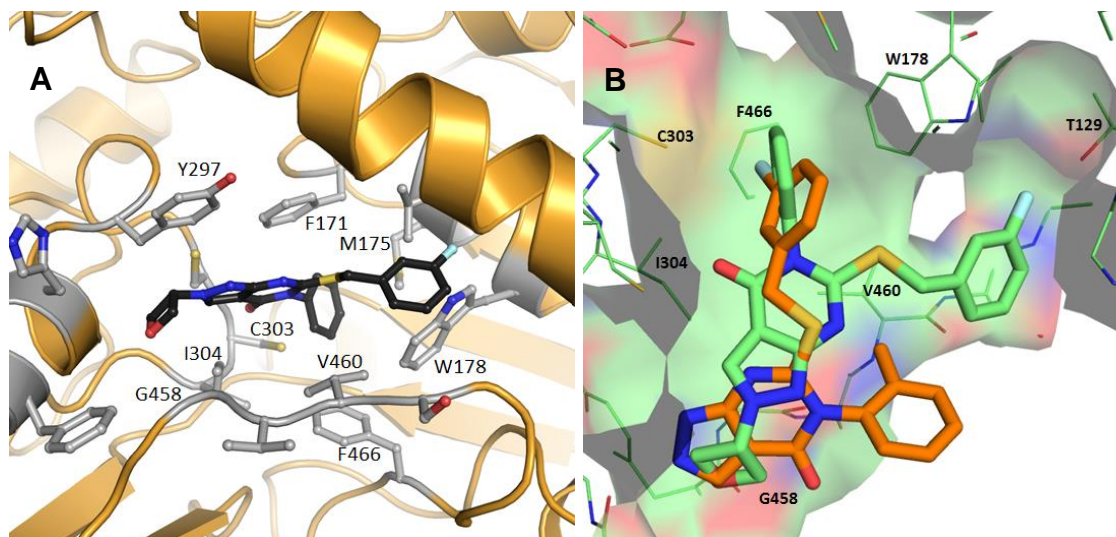


Figure 3.4 258083-1A1 Crystal Structure

(A) X-Ray crystal structure of **258083** bound to ALDH1A1 (PDB code 6DUM). (B) Overlay of compounds **CM39** (PDB code 5TEI) (Orange) and **258083** (Green). (Unpublished work, courtesy of Hurley Lab)

3.5. Homology Models to Explain Isoform Selectivity

Homology models for 1A2 and 1A3 and docking experiments were performed by the Neamati lab to rationalize the selectivity trends we observed among the ALDH1A isoforms. At the time the studies were conducted there were no crystal structures for 1A2 or 1A3 of sufficient quality to inform drug design. We later validated our 1A2 homology model with the recently published 1A2 crystal structure (PDB:6B5H).⁹⁸ The average RMSD between the two 1A2 structures was 0.76 Å, indicative of an excellent homology model. The docking method was validated by comparing the **CM39** and **258083** docking poses in 1A1 to their respective crystallographic poses. Good agreement (1.0 and 0.8 Å) was observed for **CM39** and **258083**, respectively.

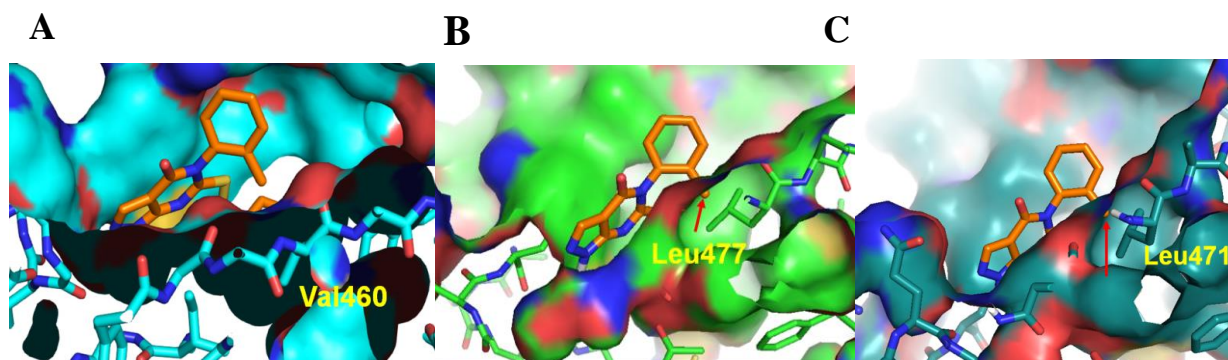


Figure 3.5 1A2 and 1A3 Homology Models Provide Rationale for 1A1 Selectivity of CM39

(A) Val460 does not clash with *o*-methyl substituent of N-Phenyl in ALDH1A1-**CM39** structure. (B, C) Docking poses of **CM39** in ALDH1A2 and ALDH1A3, respectively. Red arrow indicates that in both ALDH1A2 and A3, 2-methyl substituent at phenyl clashes with Leu477/471. (Unpublished work, courtesy Neamati Lab)

As shown in Figure 3.5, the docking studies suggest that the smaller 1A1 specific residue Val460 accommodates the *o*-methyl substituent of **CM39**, while the bulkier leucine at the

corresponding position in 1A2 and 1A3 clashes. This result is consistent with the observed 1A1 selectivity of **CM39**.

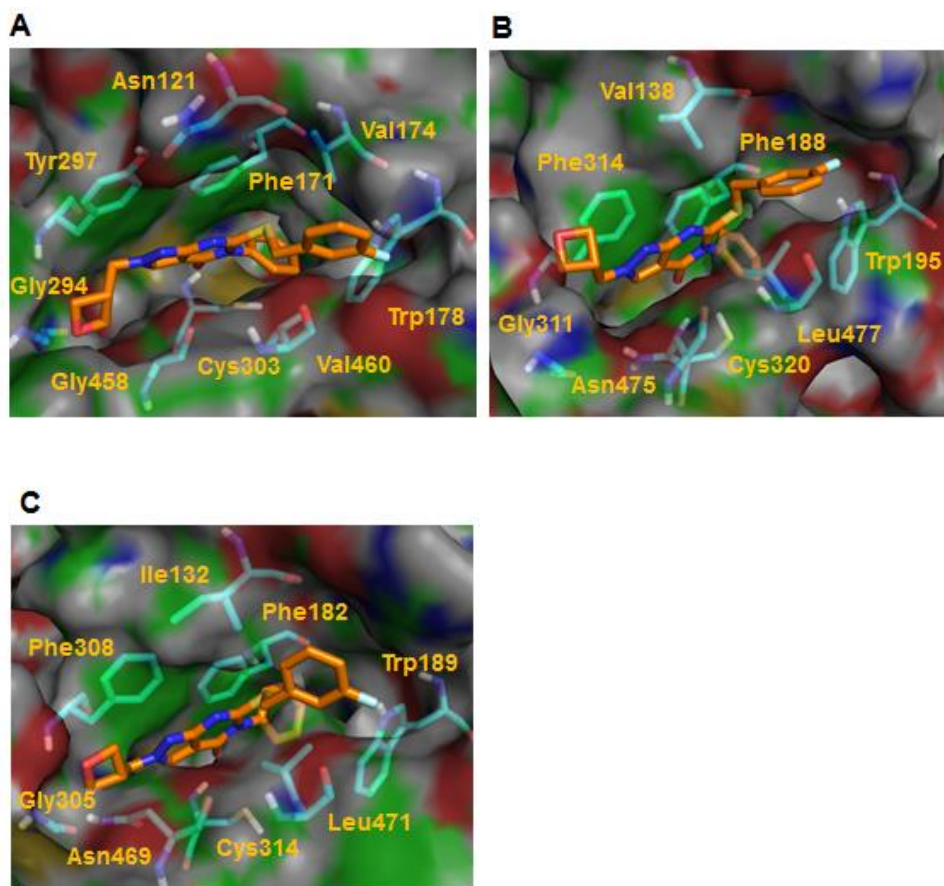


Figure 3.6 Homology Model Docking of **258085**

Compound **258085** docked in the active site of 1A1 (A), 1A2 (B) and 1A3 (C). (Unpublished work, courtesy Neamati Lab)

Given that the large N-2 pyrazole substituents should preclude binding in the **CM39**-like binding mode, we also wanted to rationalize the continued ability of the *o*-methyl substituent to promote 1A1 selectivity in the N-2 substituted analogs. The docking pose for **258085** in the 1A1 active site (Figure 3.6A) agrees with the **258083** crystal structure (Figure 3.4). **258085** docks into 1A2 and 1A3 in a similar manner. For both **258083** and **258085**, the ortho position of the N-

Phenyl is situated near the 1A1 specific Val460 and the bulkier corresponding leucine in 1A2 and 1A3. We hypothesize that the 1A1 selectivity of **257912** and **257913** arises from clash of the *o*-methyl with this leucine in 1A2 and 1A3.

3.6. Confirming Activity in Live Cells

The Buckanovich Lab next performed the ALDEFLUOR assay (Stem Cell Technologies) in PEO1 and OVCAR5 cells, cancer cell lines with high ALDH activity (predominantly 1A3), to confirm ALDH inhibition in live cells (Figure 3.7A, B). PEO-1 is a high grade serous ovarian cancer cell line.⁹⁹ OVCAR5, a commonly used cell line originally classified as high grade serous ovarian, may be gastrointestinal in origin.¹⁰⁰ The pan-ALDH1A inhibitors **258082-258083**, and **258085** all exhibited strong inhibition of ALDEFLUOR signal with significant activity in both cell lines at 1 μ M and reductions of greater than 50% at 10 μ M. Similar to **CM39** (1A1 selective), **258464** (1A2 selective) had little effect on ALDH activity at concentrations up to 30 μ M. In contrast to **CM39**, **258464** had 55 μ M thermodynamic aqueous solubility (Analiza inc.) ruling out poor solubility as an alternative explanation for the lack of activity. Poor cell penetrance is also an unlikely explanation for this lack of activity, as **258464** has a lower TPSA, MW, and fewer rotatable bonds than the efficacious pan-inhibitors.

As mentioned in Chapter 1, the surface glycoprotein CD133 has also been used as a marker of stemness in many cancers including ovarian cancer, and its expression is correlated with poorer patient outcomes in ovarian cancer.^{18, 101} Treating PEO1 and OVCAR5 cells with the pan-ALDH1A inhibitors **258082-258083**, and **258085** also elicited a dose dependent preferential reduction in the percentage of CD133⁺ cells (Figure 3.7C, D). The 1A2 selective **258464** had a

less pronounced effect. Considering that **673A** also depleted CD133⁺ cells, this suggests that the CD133⁺ depletion is indeed an on-target effect.

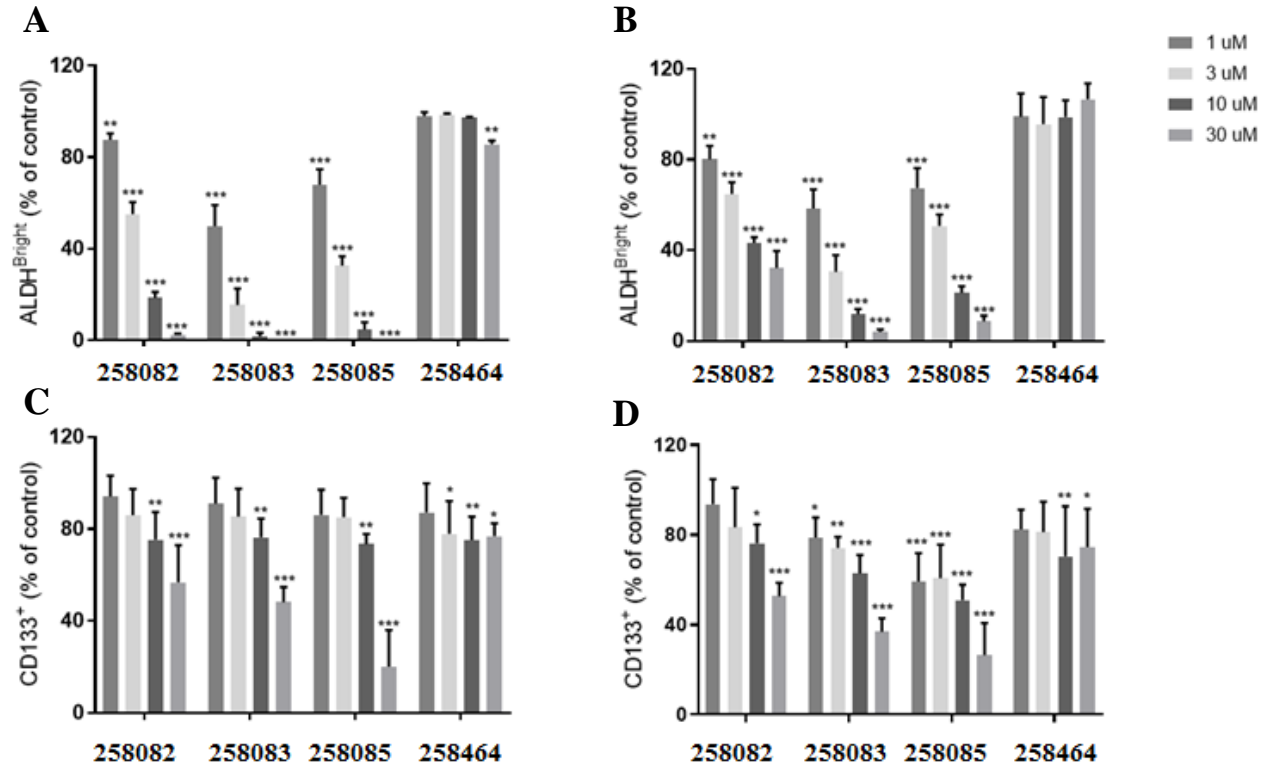


Figure 3.7 Pan-ALDH1A Inhibitors Engage ALDH in Cells and Deplete Cells Bearing Putative CSC Marker CD133

(A, B) Graphs showing changes in ALDEFLUOR activity in PEO1 (A) and OVCAR5 (B) cells following the specified treatment (N=3). (C, D) Graphs showing changes in the CD133⁺ cell population as determined by flow cytometry following 48 h drug treatment of PEO1 (C) and OVCAR5 (D) at the specified concentration (N=3-6). *p ≤ 0.05, **p ≤ 0.01, ***p ≤ 0.0001. (Unpublished work, courtesy Buckanovich Lab)

3.7. Evaluation of Synergy with Cisplatin

ALDH1A family members are known to play a role in resistance to multiple chemotherapy agents,¹⁰²⁻¹⁰⁵ and a reduction in their activity has been shown to restore sensitivity (as shown in Chapter 1 for **673A**).^{32-38, 106-108} Therefore, the Buckanovich lab investigated the

ability of our pan-ALDH1A inhibitors to increase sensitivity to and potentially synergize with cisplatin in PEO1 and OVCAR5 cells. Using the Chou-Talalay method, we determined that the pan-ALDH1A inhibitors **258082-258083**, and **258085** are highly synergistic (Combination Index values <1 indicate synergy with smaller numbers indicating stronger synergy) with cisplatin (Figure 3.7 A,B).¹⁰⁹ The observed synergy for **258082** and **258083** at 1 μ M was already strong but it was improved by increasing the concentration of these compounds to 10 μ M. While **258082** and **258083** alone did not show cytotoxicity at these doses, **258085** did and, therefore, had to be tested at lower doses. Nonetheless, synergy with **258085** was observed at concentrations as low as 0.3 μ M. The ALDH1A2 selective inhibitor, **258464**, also showed synergy but was overall less effective than any of the pan inhibitors.

The Mehta lab evaluated synergy using primary patient derived samples in a 3-D tumor spheroid assay; a platform which mimics in vivo growth (Figure 3.7C).¹¹⁰⁻¹¹¹ As **258085** showed comparable synergy to **258082** and **258083** at 3-fold lower concentrations in the initial synergy studies, we tested this compound. Ovarian cancer spheroids, compared to 2D monolayer culture, are more resistant to standard therapies and express higher levels of ALDH1A1.^{36, 112} Treatment of patient derived ovarian cancer spheroids with 0.3 μ M **258085** did not significantly reduce viability as monotherapy. However it was highly synergistic with all three concentrations of cisplatin tested (Figure 3.7C, Combination indices 0.08-0.27).¹⁰⁹

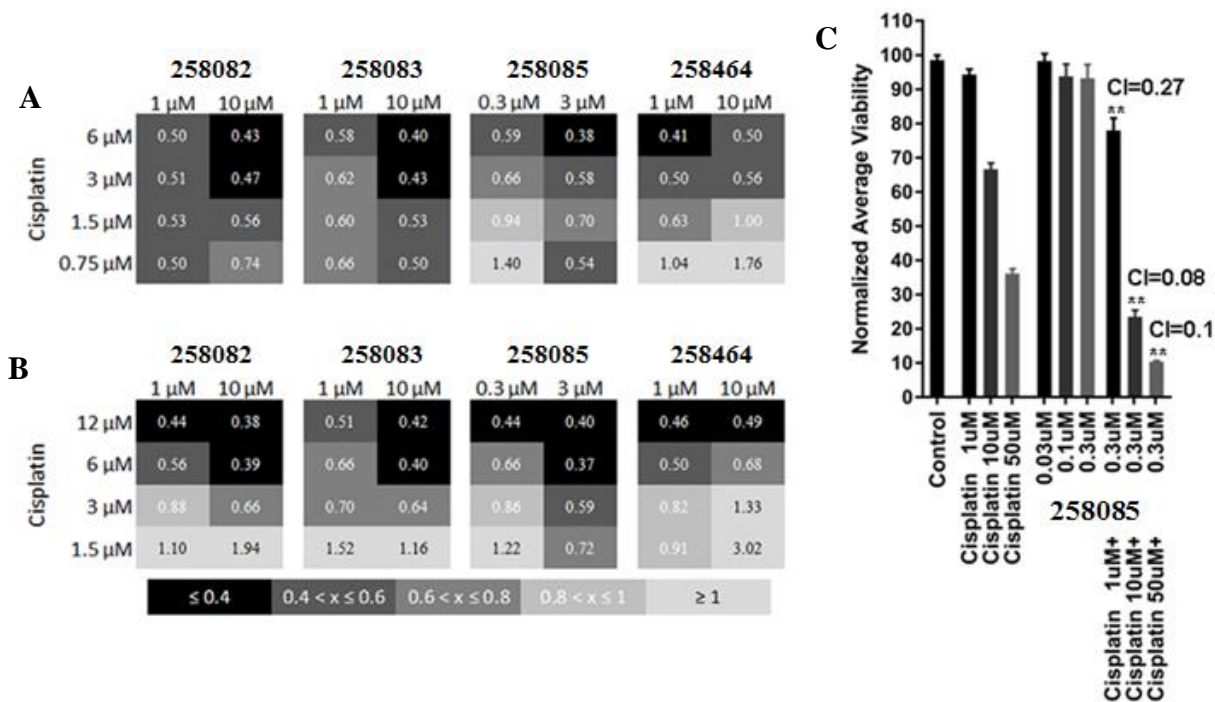


Figure 3.8 Compounds 258082, 258083, and 258085 Synergistically Enhance the Effect of Cisplatin on Ovarian Cancer Cell Lines and Patient Derived Spheroids.

(A, B) Representative heatmaps of combination indices for PEO1 (A) and OVCAR5 (B) cells cultured for 72 h in the presence of cisplatin and the indicated ALDH inhibitor at the concentrations shown. (N=3) (C) Normalized average viability as determined using Alamarblue dye following exposure to the specified compounds for 72 hours. (N=5-8) * $p \leq 0.05$, **** $p \leq 0.0001$ one way ANOVA compared to Control. Combination indices for the specified drug combinations calculated using CompuSyn software. (CI < 1 indicates synergy) (<http://www.combosyn.com>).¹⁰⁹ (Unpublished work, courtesy Buckanovich and Mehta Labs)

3.8. Evaluation of In Vivo Metabolic Stability

Table 3.4 In Vivo Exposure Following IP Injection in Mice.

Compound (dose)	Plasma Concentration (μM)				$\text{AUC}_{0-7\text{h}}^{\text{obs}}$ ($\text{hr}\cdot\mu\text{M}$)
	0.5 h	2 h	4 h	7 h	
257723 (20 mg/kg)	24.3 ± 4.1	5.1 ± 0.7	1.0 ± 0.6	0.2 ± 0.2	36
258083 (10mg/kg)	7.6 ± 0.8	5.2 ± 1.0	3.0 ± 1.3	0.9 ± 0.7	27.8
258085 (10mg/kg)	5.6 ± 0.2	2.6 ± 0.6	0.6 ± 0.2	0.1 ± 0.1	11

Compounds at the specified doses were administered by a single intraperitoneal injection of the specified dose to CD-1 mice. Values expressed as Mean \pm S.D for 3 mice at each timepoint. (Unpublished work, courtesy of Sun Lab)

Our most potent pan-inhibitor at the time (**257723**) and our two most promising compounds in cells (**258083**, **258085**) were submitted for a preliminary study of exposure following IP injection (Table 3.4). **257723** demonstrated the highest AUC, driven by a high C_{max} , but it was given at twice the dose of the other two compounds. It was cleared the fastest of the three compounds, consistent with its short MLM $t_{1/2}$ (8 min). Despite **258083** and **258085** having very similar MLM $t_{1/2}$ (23 and 27 min, respectively), the AUC for **258083** was more than double that of **258085**. **258083** achieved a higher maximal concentration and appeared to be more resistant to clearance. The greater plasma exposure of **258083** could also reflect less partitioning into the tissue (Lower V_D) given its cLogP is lower than **258085**. Importantly, plasma concentrations of **258083** exceeded $1 \mu\text{M}$, the concentration needed for 50% inhibition of ALDEFLUOR (Figure 3.7B), for nearly 7 hours. Compound **258085** exceeded $0.3 \mu\text{M}$, an efficacious dose in the spheroid cisplatin synergy assay (Figure 3.8C), for almost 4 hours.

3.9. Efficacy of 258085 in Xenograft Studies

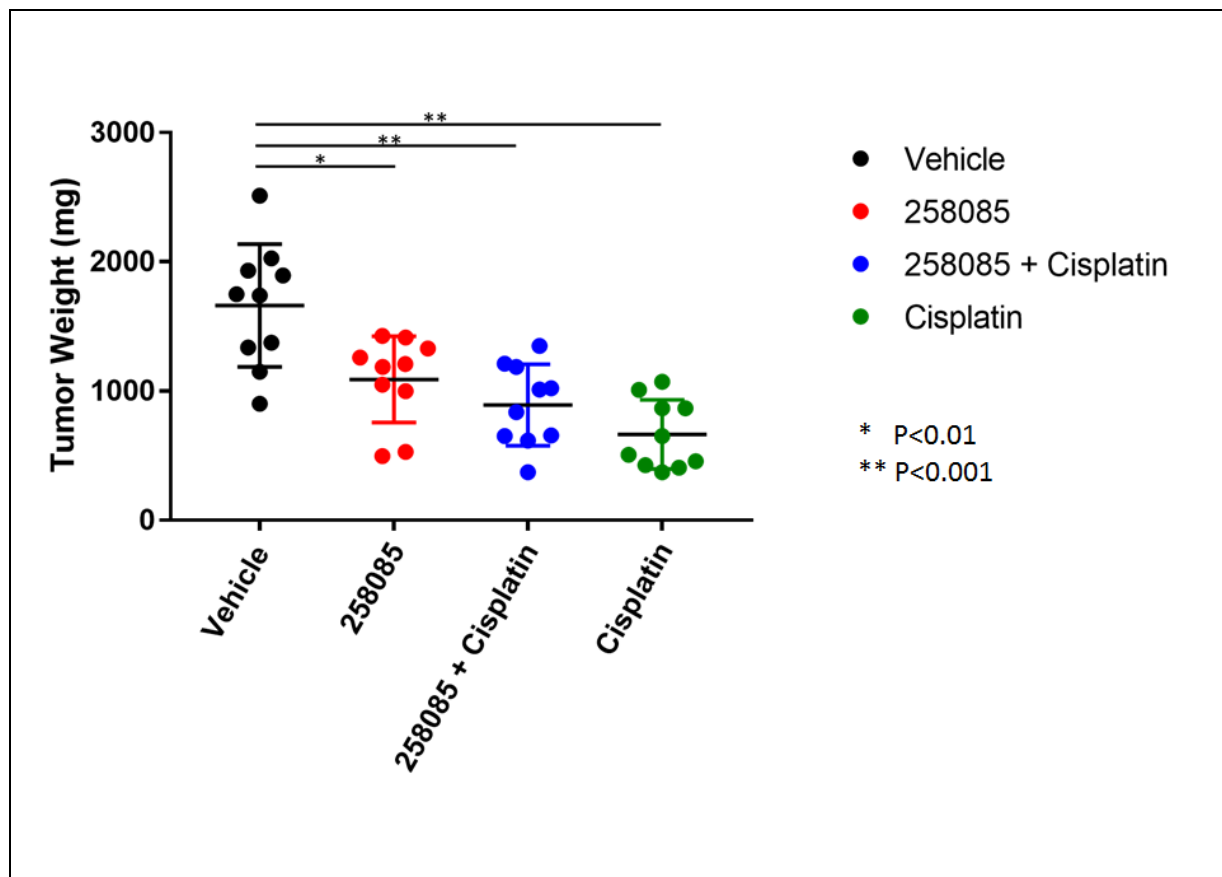


Figure 3.9 258085 Reduces OVSAHO Xenograft Tumor Volume as a Single Agent

Mice were engrafted bilaterally with OVSAHO cells, generating two tumors in each mouse. Five days after engraftment mice were injected with the specified compound(s) or vehicle (258085 10mg/kg i.p. q.d.), (cisplatin 1mg/kg i.p. weekly). 18 days post injection, the mice were sacrificed to obtain tumor weight. (Unpublished work, courtesy Buckanovich Lab)

In light of the promising results in the spheroid assay, the Buckanovich lab next assessed the impact of our pan-ALDH1A inhibitor **258085** against a xenograft of the ovarian cancer cell line OVSAHO in mice. To assess any dose limiting toxicities for **258085**, we treated Nod-*scid* gamma (NSG) mice with 20mg/kg **258085** i.p. q.d. for 7 days. Mice in the treatment group lost 15% body weight compared to 5% for vehicle and showed some enlargement of the spleen.

Because of concern that these effects combined with the adverse effects associated with cisplatin treatment would not be tolerated, we decided to dose at 10mg/kg **258085** in the xenograft studies. As shown in Figure 3.9, as a single agent, **258085** significantly inhibited tumor growth. Disappointingly, cisplatin alone appeared to be slightly more effective at inhibition of tumor growth than combination therapy with cisplatin + **258085** or **258085**. This contrasts significantly with the in vitro results. Compared to the cisplatin cohort, mice in the combination therapy arm exhibited subjectively less of the characteristic behavior associated with cisplatin treatment, suggesting that cisplatin may be reacting with **258085** or the DMSO vehicle and reducing systemic exposure for the drug. Although the two drugs were administered in separate injections in close succession, the reactivity of cisplatin and DMSO is well-known, and **258085** contains aza-heterocycle and thioether motifs which could also potentially inactivate cisplatin.¹¹³⁻¹¹⁵ Future in vivo studies will employ dosing regimens with temporally or spatially separate administration of cisplatin and the ALDH inhibitors.

3.10. Conclusions

In order to assess the suitability of a novel series of pan-ALDH1A inhibitors as a treatment to deplete cancer stem cells and/or potentiate chemotherapy in ovarian cancer, we generated a number of analogs of lead compound **CM39** guided by a co-crystal structure with 1A1. Expedient synthetic routes were developed to allow late-stage diversification at multiple sites. The observation that the ortho-methyl group on the N-phenyl was unfavorable to binding across the ALDH1A family led to the first potent pan ALDH1A inhibitor with excellent selectivity over ALDH2 (**257723**). Small structural changes led to a new binding mode for compound **258083**, explaining SAR trends which did not agree with the 1A1 crystal structure for

lead compound **CM39**. We demonstrated that significant changes in ALDH1A isoform-selectivity can be achieved by minor structural changes to the N-phenyl substituent, which binds in the narrow lipophilic region of the active site near the catalytic cysteine according to the **258083**-1A1 structure. In the course of exploring SAR at this position we discovered the 1A2 selective compounds **258464** and **258077**, and the 1A3 selective compounds **258078** and **258081**. To our knowledge, these are the first examples of 1A2 and 1A3 selective inhibitors with no activity against ALDH2, which should prove useful for probing the function of these specific isoforms.

Our primary objective of obtaining pan-ALDH1A inhibitors with cellular activity was realized with exemplary compounds **258082**, **258083**, and **258085**. The compounds achieved 3- to-10-fold improvements in 1A1 IC₅₀ vs. lead **CM39** and even greater improvements against 1A2 and 1A3 as well as engaging ALDH in cells as determined by the ALDEFLUOR assay. Interestingly the three compounds depleted the CD133⁺ putative stem cell pool in a dose dependent manner, and synergized with cisplatin at a range of concentrations. **258085** also showed synergy with cisplatin in patient derived ovarian cancer spheroids. Notably, 1A2 selective **258464** was much less effective in the ALDEFLUOR and CD133 assays, supporting our hypothesis that pan-ALDH1A inhibitors will be more effective anticancer agents, perhaps due to their ability to overcome any compensating overexpression of alternate ALDH1A isoforms.

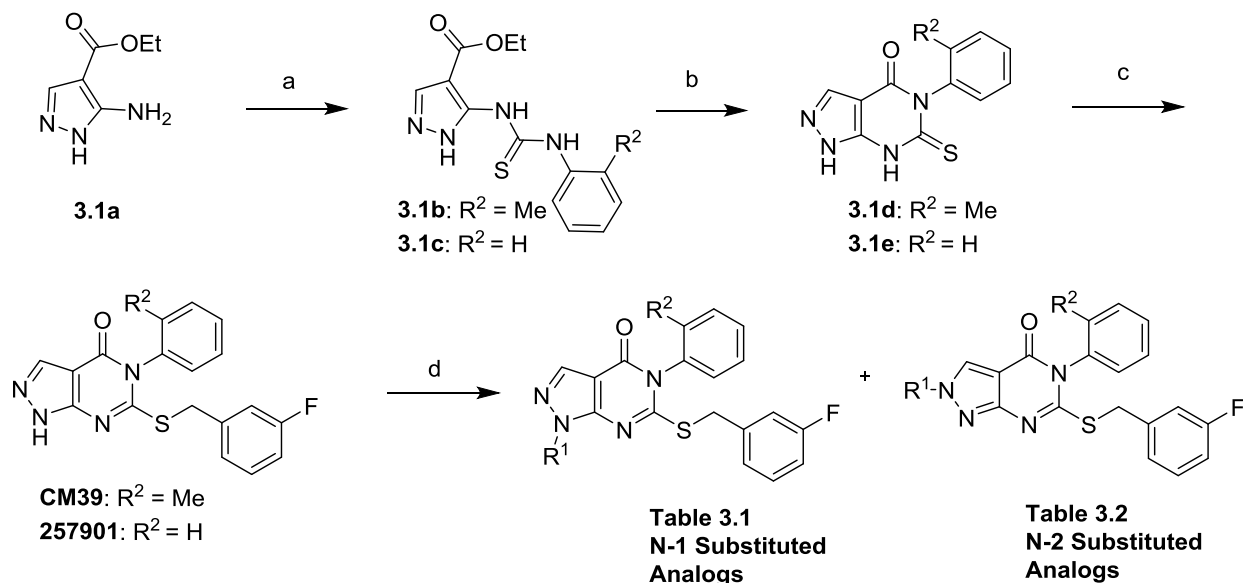
In a preliminary PK study, both **258083** and **258085** cover efficacious concentrations following i.p. administration. Due to its compelling activity in the spheroid assay, **258085** was advanced into a xenograft model. While **258085** was effective at reducing tumor growth as a single agent, it appeared to antagonize the effects of cisplatin. In contrast, **258085** was non-toxic

as a single agent in the spheroid assay but was highly synergistic with cisplatin. We suspect this may result from interaction between **258085** or its vehicle, DMSO, and cisplatin. Future xenograft studies will employ more metabolically stable analogs and may stagger dosing schedules or use a different route of administration than for cisplatin.

The following chapter will disclose further optimization of this series, focusing on further improving enzymatic and cellular potency and pharmacokinetic properties, as well as tuning the selectivity profile among the ALDH1A isoforms in order to generate diverse probes for determining the contribution of individual isoforms to cellular activity.

3.11. Synthesis of CM39 Analogs

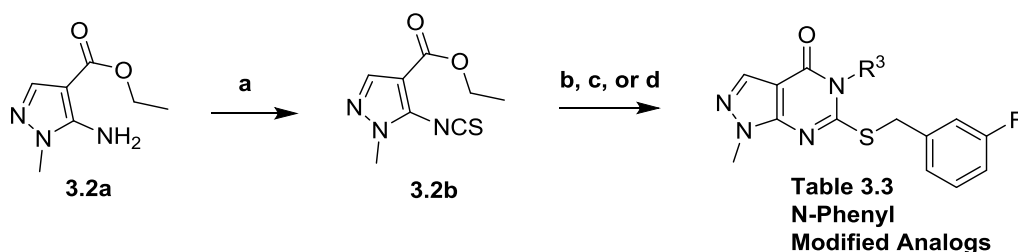
Scheme 3.1 Synthesis of Pyrazole substituted analogs (Table 3.1, Table 3.2).^a



^aReagents and conditions: (a) ArNCS, toluene, reflux; (b) 1N NaOH, reflux; (c) 3-F-PhCH₂Br, K₂CO₃, DMF, RT; (d) R¹-X, K₂CO₃, DMF, 50°C X = Br, OMs

As shown in Scheme 3.1, synthesis of N-1 and N-2 pyrazole substituted analogs (Table 3.1, Table 3.2) began with the commercially available pyrazole **3.1a**.¹¹⁶ Treatment of **3.1a** with the appropriate aryl isothiocyanate in refluxing toluene afforded the thioureas **3.1b-c** which precipitated from the reaction mixture upon cooling. Ring closure to generate thiopyrimidinones **3.1d-e** proceeded in aqueous NaOH at reflux. Selective S-alkylation with 3-fluorobenzyl bromide yielded compounds **CM39** and **257128**. Subsequent N-alkylation resulted in a mixture of regioisomers which were easily separated by flash chromatography on silica. Regioisomeric assignment was made by NOE; in all cases the N-1 substituted analogs eluted before the corresponding N-2 substituted analogs.

Scheme 3.2 Synthesis of N-Phenyl Modifications (Table 3.3)^a



^aReagents and conditions: (a) NaH, CS₂, I₂, THF, 0-40°C; (b) R³-NH₂, 3-F-PhCH₂Br, NaH, DMF, 0-20°C (**257723**, **258463-5**, **258962**, **257727**, **258077-8**, **257907-8**); (c) (i) R³-NH₂, NaH, DMF, 0-20°C (**257914**, **257726**, **258081**, **258466-8**); (ii) 3-F-PhCH₂Br, K₂CO₃, DMF, RT; (d) (i) MeNH₂, EtOH; (ii) 3-F-PhCH₂Br, K₂CO₃, DMF, RT (**258074**).

In a departure from our earlier synthetic strategy, we envisioned an alternative route to R³ analogs that would use readily available amines rather than the corresponding isothiocyanates to introduce diverse R³ substituents as shown in Scheme 3.2. The synthesis of **3.2b** has been previously accomplished by treating commercially available pyrazole **3.2a** with thiophosgene

under Schotten-Baumann conditions; however, we found the low yield, difficult purification, and use of noxious reagents to be unsatisfactory.¹¹⁷ After screening many reported isothiocyanate-forming conditions employing carbon disulfide as the thiocarbonyl source, we found that treatment of **8b** with NaH and CS₂ followed by the slow addition of I₂ afforded **3.2b** in good yield following a simple purification.¹¹⁸ Isothiocyanate **3.2b** reacted with amines rapidly under mild conditions to form thioureas. Subsequent addition of NaH in the same pot facilitated cyclization to the thiopyrimidinone. For the majority of arylamines, adding 3-fluorobenzyl bromide at this point completed the transformation of **3.2b** to afford R³ analogs (**257723**, **258463-5**, **258962**, **257727**, **258077-8**, **257907-8**) in one pot. For alkylamines and 2-aminopyridine (**257914**, **257726**, **258081**, **258466-8**), an aqueous workup prior to S-alkylation with 3-fluorobenzyl bromide reduced the formation of several unidentified side products. The thiourea resulting from treatment of **3.2b** with 8N ethanolic methylamine spontaneously cyclized to form the thiopyrimidinone. Following removal of volatiles, S-alkylation of this intermediate with 3-fluorobenzyl bromide under basic conditions afforded **258074**.

3.12. Experimental Procedures

Crystal Structure Determination (Hurley Lab)

Crystals of ALDH1A1 N121S were grown by equilibrating 4-8 mg/mL ALDH1A1 N121S against 100 mM sodium BisTris, pH 6.2-6.5, 6-11% PEG3350, 200 mM NaCl, and 5-10 mM YbCl₃. The crystal of ALDH1A1 N121S in complex with **CM39** was prepared by soaking approximately 2-week old apo crystals for 6 hr in crystallization solution containing 500 μM **CM39** with 1% (v/v) DMSO and 1 mM NAD. The crystal of ALDH1A1 N121S in complex with **258083** was prepared by soaking apo crystals for 1 hr in crystallization solution containing 1 mM

NAD followed by soaking overnight in crystallization solution containing 500 μM **258083** with 2% (v/v) DMSO and 1 mM NAD. Cryoprotection for flash-freezing was 20% (v/v) ethylene glycol in ligand soaking solution. Diffraction data for **CM39** in complex with ALDH1A1 N121S was collected at Beamline 23-ID-D (GM/CA), National Institute of General Medicine Sciences and National Cancer Institute of the NIH at APS. Diffraction data for **258083** in complex with ALDH1A1 N121S was collected at Beamline 19-ID operated by the Structural Biology Consortium at the Advance Photon Source (APS), Argonne National Laboratory. Diffraction data were indexed, integrated, and scaled using HKL3000.¹¹⁹ The CCP4 program suite was used for molecular replacement and refinement.¹²⁰ The Coot molecular graphic application was used for model building.¹²¹ The TLSMD (translation/libration/screw motion determination) server was used to determine dynamic properties of ALDH1A1 N121S.¹²²⁻¹²³

Protein Purification and Enzymatic Assays (Hurley Lab)

Human ALDH1A1, ALDH1A2, ALDH1A3, ALDH2, ALDH1B1, ALDH3A1, ALDH4A1, ALDH5A1 and rat ALDH1L1 were prepared and purified as previously described.^{41, 124-127}

Inhibition of ALDH activity by compounds and IC_{50} curves were determined by measuring the formation of NAD(P)H spectrophotometrically at 340 nm (molar extinction coefficient of $6200 \text{ M}^{-1} \text{ cm}^{-1}$) on the Beckman DU-640 and Spectramax 340PC spectrophotometers using purified recombinant enzyme. Reaction components for ALDH1A and ALDH2 assays consisted of 100-200 nM enzyme, 200 μM NAD^+ , 100 μM propionaldehyde, and 1% DMSO in 25 mM BES buffer, pH 7.5. For ALDH1B1, the assay included 500 μM NAD^+ and 200 μM propionaldehyde. For ALDH3A1, the assay included 300 μM NADP^+ , 20nM enzyme, and 300 μM benzaldehyde. For ALDH4A1 and ALDH5A1, the assay included 1.5mM NAD^+ , 100nM enzyme, with 20mM

propionaldehyde for ALDH4A1 and 2mM propionaldehyde for ALDH5A1. For rat ALDH1L1, the assay included 0.5mM NADP⁺, 200nM enzyme and 4mM propionaldehyde. All assays were performed at 25°C and were initiated by addition of substrate after a 2 min incubation period. IC₅₀ curves were collected for compounds which substantially inhibited ALDH1A activity at 20 μM compound. Data were fit to the four parameter EC₅₀ equation using SigmaPlot (v12) and the values represent the mean/SEM of three independent experiments (each n=3).

ALDEFLUOR Assay (Buckanovich Lab)

PEO1 and OVCAR5 cells were grown in RPMI 1640 media (Corning) containing 2mM glutamine, 2mM sodium pyruvate (PEO1 only, Gibco), 10% FBS (Sigma), and 1X Pen/Strep (Gibco). When the cells reached 80% confluency they were harvested by trypsinization and assayed for ALDH activity using the aldefluor assay (STEMCELL Technologies). Briefly, the cells were washed with PBS before being centrifuged and resuspended in ALDEFLUOR buffer. Once the cells were resuspended in ALDEFLUOR buffer, the ALDEFLUOR reagent was added. The cells were quickly mixed and evenly distributed into 1.5 mL Eppendorf tubes containing inhibitor or vehicle. The tubes were incubated for 30 minutes at 37 °C. Next, the tubes were centrifuged, the buffer containing the ALDEFLUOR reagent was removed, and the cells were resuspended in fresh ALDEFLUOR buffer that had been kept on ice. The tubes were kept on ice until they were analyzed on an Accuri C6 flow cytometer (BD). The percent of control values were calculated using the percentage of ALDEFLUOR positive cells for a particular sample and the percentage of ALDEFLUOR positive cells in the control sample (vehicle treated). The percentage of ALDEFLUOR positive cells was graphed in Prism 7 (GraphPad) and is displayed as mean ± SD. The Two-way ANOVA with Tukeys multiple comparison test within Prism 7

(GraphPad) was used to determine statistical significance between samples treated with compound or vehicle.

CD133⁺ Cell Assay (Buckanovich Lab)

PEO1 and OVCAR5 cells were grown in RPMI 1640 media (Corning) containing 2mM glutamine, 2mM sodium pyruvate (PEO1 only, Gibco)10% FBS (Sigma), and 1X Pen/Strep (Gibco). When the cells reached 80% confluency they were harvested by trypsinization, washed with PBS, and reseeded in 6-well plates at 1×10^5 cells/well. The cells were allowed to recover for 24 h, inhibitor or vehicle was added, and the cells were put back into the incubator for 48 h. Following the 48 h incubation, the cells were harvested and counted. An equal number of cells were isolated from each sample. The cells were washed with PBS and resuspended in fresh PBS. CD133/2-APC antibody (Miltenyi Biotec) was added at a dilution of 1:100. The cells were mixed and incubated at room temperature for 10 minutes. Next, ten times the volume of PBS was added and the cells were centrifuged. The cells were washed with PBS and resuspended in fresh PBS that had been kept on ice. The tubes were kept on ice until they could be analyzed on a Cytoflex S flow cytometer (BeckmanCoulter). The percentage of CD133 positive cells was graphed in Prism 7 (GraphPad) and is displayed as mean \pm SD. The Two-way ANOVA with Tukeys multiple comparison test within Prism 7 (GraphPad) was used to determine statistical significance between samples treated with compound or vehicle.

Cell Viability and Synergy Assays (Buckanovich Lab)

PEO1 and OVCAR5 cells were grown in RPMI 1640 media (Corning) containing 2mM glutamine, 2mM sodium pyruvate (PEO1 only, Gibco)10% FBS (Sigma), and 1X Pen/Strep (Gibco). When the cells reached 80% confluency they were harvested by trypsinization, washed

with PBS, and reseeded in 96-well plates at 4000 cells/well (PEO1) or 1500 cells/well (OVCAR5). The cells were allowed to recover for 24 h, inhibitor or vehicle was added, cisplatin was added, and the cells were put back into the incubator for 72 h. Following the 72 h incubation, the media was removed and a 1X solution of Cell-Titer Glo 2.0 (Promega) was added. The plates were mixed and allowed to incubate at room temperature for 10 min before luminescence was read. Normalized viability was calculated by comparing the luminescence of drug-treated wells to vehicle treated wells and expressed as a percentage. The percentage of viable cells was graphed in Prism 7 and all data are displayed as mean \pm SD. Synergy was assessed using Chou-Talalay method and the CompuSyn program.¹⁰⁹

Hanging drop culture for patient derived spheroid formation (Mehta Lab)

Graded patient tumor samples (high grade epithelial stage IIC or IV, obtained from IRB approved protocol, and collected from consented patients) were dissected, digested enzymatically using a mixture of Collagenase IV/Dispase, recovered by centrifugation and filtered through a 500 μ m mesh to remove large debris. Resulting patient cells were suspended in serum-free medium (SFM) supplemented with 5ng/ml FGF, 5ng/ml EGF, B27, 1X insulin-transferrin-selenium supplement, 1X nonessential amino acids, antibiotics and antimycotics. Cell counts were obtained using a hemocytometer and adjusted such that a 20 μ L volume contained 100 cells. Similar to previously established protocol, patient derived spheroids were initiated using 100 CD133⁺ ALDH⁺ cells per spheroid.^{110, 112, 128} Spheroids were maintained in SFM for a period of 10 days, and imaged using live phase contrast microscopy to follow spheroid formation and maintenance.

Drug treatment on patient derived spheroids in hanging drop array culture (Mehta Lab)

Patient derived spheroids were initiated in 384-well hanging drop arrays using 100 cells per spheroid. Spheroids were allowed to aggregate and form a 3D microtissue over a period of 10 days. For drug treatment, a 10X stock of drug was prepared independently, and 2 μ L of drug was added to the 20 μ L hanging drop containing spheroids, to result in a final concentration of 1X. Several drug-dosing regimens were carried out, including cisplatin in the range of 1-50 μ M and ALDH inhibitor **258085** in the range of 0.03-.3 μ M.

The effect of drug was assayed on spheroids 72 hours, using the alamarBlue assay to determine viability after drug treatment. Control untreated spheroids were maintained for the same duration in culture. Cell viability after drug treatment was normalized to untreated controls, and quantified. At least 20 spheroids (technical replicates) were assayed per experiment, with 5 to 8 biological replicates. Drug-treated spheroids were imaged using phase-contrast microscopy to observe morphologic differences in spheroids exposed to drug compared with control untreated spheroids.

Metabolic activity in hanging drop ovarian cancer spheroids (Mehta Lab)

AlamarBlue dye (Life Technologies, Carlsbad CA) was added in a 1:10 dilution to 100 cells/drop spheroids. Following 4 hours of alamarblue addition and incubation, the 384 hanging drop array was placed in a fluorescence plate reader (Synergy HT, BioTek Instruments, Winooski, VT). Alamarblue fluorescence readings were obtained at 530 nm excitation and 590 nm emission. To quantify viability within spheroids, alamarblue readings of treated as well untreated spheroids were obtained at Day 10, and compared to the untreated Control spheroids.

Statistical analysis (Mehta Lab)

Drug viability data were determined and quantified using the alamarBlue assay, as outlined previously.^{110, 112} Briefly, normalized viability was calculated by comparing the alamarBlue fluorescence of drug-treated spheroids to control untreated spheroids and expressed as a percentage. Statistical analysis was performed using one-way ANOVAs and levels of statistical significance are indicated in the figures. All data are expressed as mean±SEM and are an average of at least 5 to 8 independent experiments.

Metabolic Stability in Mouse Liver Microsomes (Sun Lab)

The metabolic stability was assessed using CD-1 mouse liver microsomes. 1 µM of each compound was incubated with 0.5 mg/mL microsomes and 1.7 mM cofactor β-NADPH in 0.1 M phosphate buffer (pH = 7.4) containing 3.3 mM MgCl₂ at 37 °C. The DMSO concentration was less than 0.1% in the final incubation system. At 0, 5, 10, 15, 30, 45, and 60 min of incubation, 40 µL of reaction mixture were taken out, and the reaction is quenched by adding 3-fold excess of cold acetonitrile containing 100 ng/mL of internal standard for quantification. The collected fractions were centrifuged at 15000rpm for 10 min to collect the supernatant for LC–MS/ MS analysis, from which the amount of compound remaining was determined. The natural log of the amount of compound remaining was plotted against time to determine the disappearance rate and the half-life of tested compounds.

Pharmacokinetic Studies in Mice (Sun Lab)

All animal experiments in this study were approved by the University of Michigan Committee on Use and Care of Animals and Unit for Laboratory Animal Medicine (ULAM). The abbreviated pharmacokinetics of compounds **257723**, **258083**, and **258085** were determined in female CD-1 mice following intraperitoneal (ip) injection of 10 mg/kg respectively. Compounds were

dissolved in the vehicle containing 20% DMSO, 50% PEG-400, and 30% PBS. Four blood samples (50 μ L) were collected over 7 h (at 0.5h, 2h, 4h, and 7h), centrifuged at 35 00 rpm for 10 min, and plasma was frozen at -80°C for later analysis. Plasma concentrations of the compounds were determined by the LC–MS/MS method developed and validated for this study. The LC–MS/MS method consisted of a Shimadzu HPLC system, and chromatographic separation of tested compound which was achieved using a Waters Xbridge-C18 column (5 cm \times 2.1 mm, 3.5 μ m). An AB Sciex QTrap 4500 mass spectrometer equipped with an electrospray ionization source (ABI-Sciex, Toronto, Canada) in the positive-ion multiple reaction monitoring (MRM) mode was used for detection. All pharmacokinetic parameters were calculated by noncompartmental methods using WinNonlin, version 3.2 (Pharsight Corporation, Mountain View, CA, USA).

Molecular Modeling (Neamati Lab)

Molecular modeling was performed on a Dell Precision T7400n Mini-Tower, Quad Core Xeon Proc X5450 dual processor with 32 nodes computer.

Homology Modeling (Neamati Lab)

Homology models for ALDH1A2 and 1A3 were built on Swiss-Model Workspace (SMW) using ALDH1A1 PDB (PDB code 5TEI) as a template.¹²⁹⁻¹³⁰ The homology modeling on SMW can be briefly described as alignment of a target sequence and a template sequence using the “automated mode” since the similarity between ALDH1A isoforms are approximately 70%. The target/template alignment along with 3D coordinates of the template were used as input for generating an all-atom model for the target sequence using ProMod3, a comparative modelling

engine. Side chains were remodeled using a backbone dependent rotamer library. Finally, the geometry of the resulting model was energy minimized by using the force field OpenMM.¹²⁹⁻¹³⁰

Global and per-residue quality of the model was assessed by the QMEAN scoring function, where several statistical potential terms, i.e., geometrical features of the model as well as each residue (pairwise atomic distances, torsion angles, solvent accessibility, etc.), are compared to statistical parameters obtained from experimental structures.^{129, 131} The local scores are linear combinations of the four statistical potential terms evaluated on a per residue basis. Each residue gets a score between 0 and 1, with 1 being the best. To assess the overall quality of the model, global QMEAN scores were calculated as a Z-score which compares the obtained values to scores calculated from a set of high-resolution X-ray structures. GMQE (Global Model Quality Estimation) is another global quality estimation which combines properties from the target-template alignment.¹³¹ The resulting GMQE score is between 0 and 1 and expresses the accuracy of a model built with that alignment and template. The quality of the model increases as the number approaches 1. Additionally, the model quality was evaluated by a Ramachandran plot within the PROCHECK server.¹³² PROCHECK assesses the stereo-chemical quality of a protein structure. A good quality model would be expected to have over 90% in the most favored regions.¹³³

Molecular Docking (Neamati Lab)

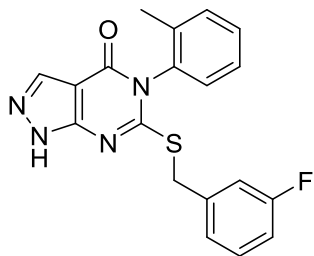
Molecular docking studies were performed using the HYBRID docking program from OpenEye Scientific, Santa Fe, NM against ALDH1A isoforms with co-crystal **CM39** (PDB code 5TEI) or **258083** (PDB code 6DUM) as the reference ligands.¹³⁴ Prior to docking, 500 different conformations were generated for each ligand using Omega (OpenEye Scientific, Santa Fe, NM), a systematic, knowledge-based conformer generator.¹³⁵ HYBRID performs a systematic,

exhaustive, non-stochastic examination of poses within the protein active site. However, HYBRID reduces this search space based on shape and chemical complementarity to reference bound ligands. It treats ligand conformers as rigid during the docking process, although ligand flexibility is implicitly included by docking multiple conformers of each ligand. The input for HYBRID is a protein structure and a multi-conformer representation of the ligand to be docked. In the exhaustive search using the Chemical Gaussian Overlay (CGO) scoring function, each ligand conformation is systematically rotated and translated within the active site at a resolution of 1 Å. Every pose that passes a bump check is scored.¹³⁴

Xenograft Studies (Buckanovich Lab)

50K OVSAHO cells were resuspended in 50 uL of complete media (RPMI containing 10% FBS and 1X pen/strep) and added to a mix of 100 uL of PBS and 100 uL of growth factor reduced Matrigel. This mixture was drawn up into an 1 mL syringe with a 27 g needle and stored on ice until ready to inject. Bilateral subcutaneous injections were performed on four sets of 5 NSG mice such that mice would develop tumors near their front axilli. Tumors were allowed to form for 5 days before treatments were begun. Treatment groups were: 1. 10 mg/kg 258085 + 1mg/kg cisplatin, 2. 10 mg/kg 258085, 3. 1 mg/kg cisplatin, and 4. vehicle only. The cisplatin was delivered in PBS while 258085 prepared such that each injection contained 30 uL DMSO, 75 uL PEG-400, and 45 uL PBS. Cisplatin was delivered weekly while 258085 was given daily. Tumors were measured starting on day 16 post injection with electronic calipers. Tumor volume was determined using the $V=L*W*W$ formula. At the end of the experiment the mice were sacrificed and tumors were removed and weighed.

General Chemistry Information: All reagents were used in the condition received from commercial sources. ^1H NMR and ^{13}C NMR were taken in CDCl_3 or $\text{DMSO}-d_6$ at room temperature on Varian Inova 400 or 500 MHz instruments. Reported chemical shifts are expressed in parts per million (ppm) on the δ scale from an internal standard of tetramethylsilane (0 ppm). Mass spectrometry data were obtained on either an Agilent TOF or Agilent Q-TOF. An Agilent 1100 series HPLC with an Agilent Zorbax Eclipse Plus-C18 column was used to determine purity of biologically tested compounds. All tested compounds were determined to be >95% pure using a 6 minute gradient of 10-90% acetonitrile in water followed by a 2 minute hold at 90% acetonitrile with detection at 254 nm. Flash chromatographic purifications were performed using a Teledyne ISCO Combiflash RF with Redisep Gold RF columns.



6-((3-Fluorobenzyl)thio)-5-(o-tolyl)-1H-pyrazolo[3,4-d]pyrimidin-4(5H)-one (CM39). To a flask charged with potassium carbonate (1.56 g, 11.3 mmol), **3.1b** (1.46 g, 5.7 mmol), and 10 mL DMF was added 3-fluorobenzyl bromide (0.69 mL, 5.7 mmol). After stirring under N_2 for 16 h at RT the reaction was neutralized with sat. aq. NH_4Cl and the mixture was diluted with water

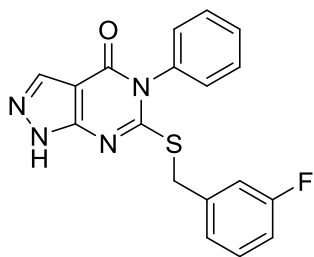
and extracted 2x with EtOAc. The combined organic portions were washed 3x with brine and then dried with sodium sulfate and the solvent removed. The crude was purified by flash (50% EtOAc in Hex) yielding the titled compound as a white solid (1.26g, 61% yield). HRMS (ESI): m/z 367.1022 $[M+H]^+$. 1H NMR (500 MHz, $CDCl_3$) δ 8.40 (br. s, 1H), 8.15 (s, 1H), 7.40 (t, $J = 8.30$ Hz, 1H), 7.34 (d, $J = 7.83$ Hz, 1H), 7.31 (t, $J = 7.83$ Hz, 1H), 7.21 (t, $J = 7.80$ Hz, 1H), 7.18 (d, $J = 7.83$ Hz, 1H), 7.07 (d, $J = 7.34$ Hz, 1H), 7.02 (d, $J = 9.29$ Hz, 1H), 6.90 (dt, $J = 1.96, 8.56$ Hz, 1H), 4.28 (d, $J = 13.69$ Hz, 1H), 4.31 (d, $J = 13.69$ Hz, 1H), 2.10 (s, 3H) ^{13}C NMR (126 MHz, $CDCl_3$) δ 162.59 (d, $J = 246.5$ Hz), 161.52, 157.71, 153.63, 138.25 (d, $J = 7.5$ Hz), 136.92, 135.62, 134.42, 131.40, 130.42, 130.01 (d, $J = 8.2$ Hz), 129.36, 127.37, 124.82 (d, $J = 3.2$ Hz), 116.08 (d, $J = 21.9$ Hz), 114.54 (d, $J = 21.1$ Hz), 102.86, 36.55, 17.28. HPLC Purity: 99%.

Method A: General Method for Synthesis of Pyrazolopyrimidinones 3.1b-c. A solution of the appropriate isothiocyanate (12.9 mmol), and ethyl 5-amino-1H-pyrazole-4-carboxylate (**3.1a**) (12.9 mmol) in 15 mL toluene was refluxed under N_2 for 3 h. The thiourea intermediate, which precipitated upon cooling to RT, was collected and added to 10 mL 1N NaOH and refluxed for 3 h. The product was precipitated by the addition of concentrated HCl and collected by filtration.

6-Mercapto-5-(o-tolyl)-1H-pyrazolo[3,4-d]pyrimidin-4(5H)-one (3.1b). Method A. White solid. 44% yield. 1H NMR (400 MHz, $DMSO-d_6$) δ 13.77 (br. s., 1H), 13.41 (br. s., 1H), 8.57 (br. s., 1H), 7.19 - 7.31 (m, 3H), 7.09 (d, $J = 5.87$ Hz, 1H), 1.99 (s, 3H).

5-Phenyl-6-thioxo-6,7-dihydro-1H-pyrazolo[3,4-d]pyrimidin-4(5H)-one (3.1c). Method A.

White solid. 64% yield. ^1H NMR (500 MHz, $\text{DMSO-}d_6$) δ 13.73 (s, 1H), 13.37 (s, 1H), 8.58 (s, 1H), 7.44 (t, $J = 7.6$ Hz, 2H), 7.37 (t, $J = 7.4$ Hz, 1H), 7.20 (d, $J = 7.7$ Hz, 2H).



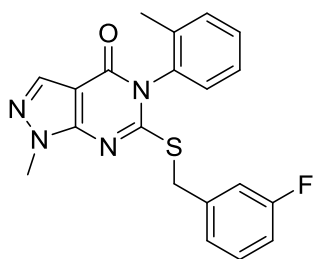
6-((3-Fluorobenzyl)thio)-5-phenyl-1H-pyrazolo[3,4-d]pyrimidin-4(5H)-one (257901).

Starting from compound **3.1c** the titled compound was synthesized and purified in a similar manner to compound **CM39** and obtained as a white solid. 69% yield. HRMS (ESI): m/z

353.0867 $[\text{M}+\text{H}]^+$. ^1H NMR (400 MHz, CDCl_3) δ 12.54 (br. s., 1H), 8.08 (s, 1H), 7.47 (s, 3H), 7.30 (s, 2H), 7.14 - 7.22 (m, 1H), 7.06 (d, $J = 7.83$ Hz, 1H), 7.02 (d, $J = 9.39$ Hz, 1H), 6.89 (t, $J = 8.60$ Hz, 1H), 4.22 - 4.35 (m, 2H), ^{13}C NMR (101 MHz, CDCl_3) δ 162.46 (d, $J = 246.6$ Hz), 161.46, 158.34, 153.26, 138.12 (d, $J = 7.6$ Hz), 135.27, 135.13, 129.98, 129.91 (d, $J = 9.0$ Hz), 129.60, 129.27, 124.84 (d, $J = 2.9$ Hz), 116.07 (d, $J = 21.8$ Hz), 114.42 (d, $J = 21.1$ Hz), 102.73, 36.68. HPLC Purity: 99%.

Method B. General Method for Synthesis of Pyrazole Substituted Analogs (Table 3.1, Table 3.2).

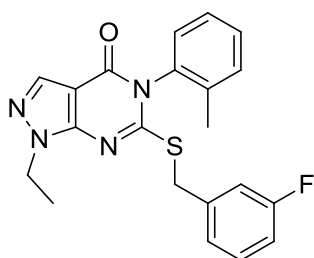
To a dry flask charged with **CM39** or **257128** (0.27 mmol) and potassium carbonate (0.55 mmol) under N₂ was added 2 mL DMF and the appropriate alkyl halide or mesylate (0.34 mmol) by syringe. The mixture was heated to 50 °C for 16 h at which point starting material was consumed by HPLC. The mixture was diluted with ethyl acetate and washed with water and 3x with brine. The organic portion was dried over sodium sulfate and the solvent removed. The regioisomers were separated by flash (EtOAc in Hex gradient). The 1-alkyl pyrazoles (Table 3.1) eluted more quickly than the 2-alkyl pyrazoles (Table 3.2). The alkylating reagents used are designated below for each compound. All were commercially available except for oxetan-3-ylmethyl methanesulfonate,¹³⁶ (3-methyloxetan-3-yl)methyl methanesulfonate,¹³⁶ and tert-butyl 3-(((methylsulfonyl)oxy)methyl)azetidine-1-carboxylate¹³⁷ which were prepared as previously described.



6-((3-Fluorobenzyl)thio)-1-methyl-5-(o-tolyl)-1H-pyrazolo[3,4-d]pyrimidin-4(5H)-one (257128).

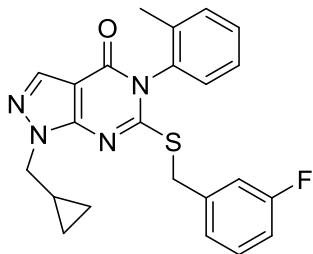
Method B. Methyl iodide. White solid. 43% yield. HRMS (ESI): *m/z* 381.1179 [M+H]⁺ ¹H NMR (400 MHz, DMSO-*d*₆) δ 8.06 (s, 1H), 7.41 (dt, *J* = 1.20, 6.40 Hz, 2H), 7.31 - 7.38 (m, 2H),

7.23 - 7.31 (m, 3H), 7.06 (tt, $J = 1.60, 8.60$ Hz, 1H), 4.38 (d, $J = 13.30$ Hz, 1H), 4.43 (d, $J = 13.30$ Hz, 1H), 3.96 (s, 3H), 1.95 (s, 3H) ^{13}C NMR (126 MHz, CDCl_3) δ 162.63 (d, $J = 246.5$ Hz), 161.21, 157.07, 151.01, 138.62 (d, $J = 7.4$ Hz), 136.93, 135.40, 134.49, 131.41, 130.40, 130.01 (d, $J = 8.4$ Hz), 129.35, 127.37, 124.67 (d, $J = 2.9$ Hz), 116.05 (d, $J = 22.0$ Hz), 114.54 (d, $J = 21.0$ Hz), 102.86, 36.56 (d, $J = 2.0$ Hz), 34.09, 17.29. HPLC Purity: 97%.



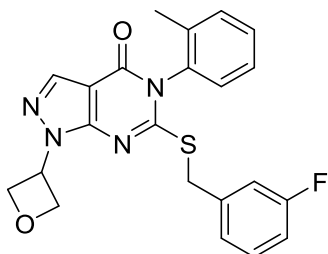
**1-ethyl-6-((3-fluorobenzyl)thio)-5-(o-tolyl)-1H-pyrazolo[3,4-d]pyrimidin-4(5H)-one
(257433)**

Method B. Iodoethane. White solid (52mg, 0.132 mmol, 48.3 % yield) MS (ESI): m/z 395.1
[$\text{M}+\text{H}$] $^+$ ^1H NMR (400 MHz, CDCl_3) δ 8.04 (s, 1H), 7.42 (t, $J = 7.70$ Hz, 1H), 7.30 - 7.39 (m, 2H), 7.25 (s, 1H), 7.16 (d, $J = 7.83$ Hz, 1H), 7.13 (d, $J = 7.83$ Hz, 1H), 7.09 (d, $J = 9.78$ Hz, 1H), 6.94 (dt, $J = 1.57, 8.41$ Hz, 1H), 4.41 (q, $J = 7.04$ Hz, 2H), 4.26 - 4.36 (m, 2H), 2.11 (s, 3H), 1.53 (t, $J = 7.24$ Hz, 3H) ^{13}C NMR (101 MHz, CDCl_3) δ 162.7, 161.0, 157.2, 150.4, 138.8, 137.0, 135.4, 134.6, 131.4, 130.4, 130.1, 129.4, 127.4, 124.6, 116.0, 114.5, 102.9, 42.4, 36.6, 17.4, 15.0
HPLC Purity: 98%.



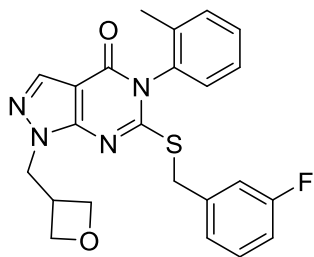
1-(Cyclopropylmethyl)-6-((3-fluorobenzyl)thio)-5-(o-tolyl)-1H-pyrazolo[3,4-d]pyrimidin-4(5H)-one (257724).

Method B. Cyclopropylmethyl bromide. Colorless oil. 32% yield. HRMS (ESI): m/z 421.1493
 $[M+H]^+$ 1H NMR (500 MHz, $CDCl_3$) δ 8.05 (s, 1H), 7.42 (t, $J = 7.80$ Hz, 1H), 7.31 - 7.39 (m, 2H), 7.21 - 7.28 (m, 1H), 7.17 (d, $J = 7.34$ Hz, 1H), 7.12 (d, $J = 7.83$ Hz, 1H), 7.07 (d, $J = 9.78$ Hz, 1H), 6.94 (dt, $J = 2.20, 8.44$ Hz, 1H), 4.32 (d, $J = 13.69$ Hz, 1H), 4.29 (d, $J = 14.18$ Hz, 1H), 4.19 (d, $J = 7.20$ Hz, 2H), 2.12 (s, 3H), 1.32 - 1.44 (m, 1H), 0.62 (td, $J = 5.50, 7.80$ Hz, 2H), 0.44 (dt, $J = 4.80, 5.50$ Hz, 2H) ^{13}C NMR (126 MHz, $CDCl_3$) δ 162.66 (d, $J = 246.7$ Hz), 160.99, 157.09, 150.50, 138.64 (d, $J = 7.4$ Hz), 136.96, 135.33, 134.53, 131.37, 130.36, 130.01 (d, $J = 8.2$ Hz), 129.34, 127.33, 124.45 (d, $J = 2.7$ Hz), 115.81 (d, $J = 22.1$ Hz), 114.47 (d, $J = 21.0$ Hz), 102.82, 52.05, 36.49 (d, $J = 1.9$ Hz), 17.33, 11.16, 3.97. HPLC Purity: 96%.



6-((3-Fluorobenzyl)thio)-1-(oxetan-3-yl)-5-(o-tolyl)-1H-pyrazolo[3,4-d]pyrimidin-4(5H)-one (257911).

Method B. 3-Bromoioxetane. White solid. 18% yield. HRMS (ESI): m/z 423.1292 $[M+H]^+$ 1H NMR (500 MHz, $CDCl_3$) δ 8.14 (s, 1H), 7.41 - 7.46 (m, 1H), 7.32 - 7.39 (m, 2H), 7.24 - 7.29 (m, 1H), 7.11 - 7.17 (m, 2H), 7.06 - 7.10 (m, 1H), 6.95 (dt, $J = 2.20, 8.44$ Hz, 1H), 5.91 - 5.99 (m, 1H), 5.28 - 5.35 (m, 2H), 5.04 - 5.09 (m, 2H), 4.30 (d, $J = 13.69$ Hz, 1H), 4.34 (d, $J = 13.69$ Hz, 1H), 2.10 (s, 1H) ^{13}C NMR (126 MHz, $CDCl_3$) δ 162.71 (d, $J = 246.9$ Hz), 161.93, 156.91, 151.04, 138.31 (d, $J = 7.6$ Hz), 136.85, 136.37, 134.35, 131.51, 130.55, 130.10 (d, $J = 8.4$ Hz), 129.26, 127.47, 124.57 (d, $J = 2.9$ Hz), 115.92 (d, $J = 22.0$ Hz), 114.66 (d, $J = 21.1$ Hz), 103.38, 76.85, 50.69, 36.62, 17.32. HPLC Purity: 98%.



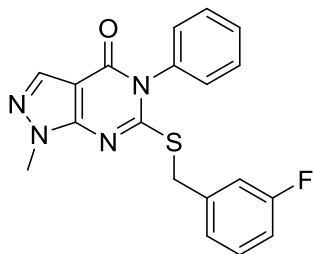
6-((3-Fluorobenzyl)thio)-1-(oxetan-3-ylmethyl)-5-(o-tolyl)-1H-pyrazolo[3,4-d]pyrimidin-4(5H)-one (257910).

Method B. Oxetan-3-ylmethyl methanesulfonate. White crystalline solid. 42% yield. HRMS (ESI): m/z 437.1449 $[M+H]^+$ 1H NMR (500 MHz, $CDCl_3$) δ 8.03 (s, 1H), 7.42 - 7.47 (m, 1H), 7.33 - 7.40 (m, 2H), 7.25 - 7.31 (m, 1H), 7.17 (d, $J = 7.34$ Hz, 1H), 7.14 (d, $J = 7.34$ Hz, 1H),

7.06 - 7.11 (m, 1H), 6.97 (dt, $J = 2.45, 8.31$ Hz, 1H), 4.86 (dt, $J = 1.47, 7.09$ Hz, 2H), 4.59 - 4.66 (m, 4H), 4.35 (d, $J = 13.69$ Hz, 1H), 4.31 (d, $J = 14.18$ Hz, 1H), 3.52 - 3.61 (m, 1H), 2.12 (s, 3H)
 ^{13}C NMR (126 MHz, CDCl_3) δ 162.68 (d, $J = 246.7$ Hz), 161.69, 156.89, 150.99, 138.43 (d, $J = 7.5$ Hz), 136.90, 135.82, 134.41, 131.44, 130.46, 130.08 (d, $J = 8.2$ Hz), 129.28, 127.40, 124.50 (d, $J = 2.9$ Hz), 115.86 (d, $J = 22.0$ Hz), 114.58 (d, $J = 21.3$ Hz), 102.85, 74.85, 74.77, 49.40, 36.64 (d, $J = 1.9$ Hz), 35.21, 17.32. HPLC Purity: 99%.

Method C. General Synthesis of Selected R^3 analogs (Table 3.3)

To a dry flask under N_2 charged with **3.2b** (0.24 mmol) and 2 mL dry DMF was added the appropriate amine (0.24 mmol) by syringe. The reaction was stirred at RT for 1hr and then cooled to 0°C . 60 wt.% NaH in mineral oil(0.24 mmol) was added and the flask was stirred at 0°C for 20min then allowed to warm to RT and stirred for 3 h. The flask was once again cooled to 0°C and 3-fluorobenzyl bromide (0.24 mmol) was added by syringe. The mixture was stirred at 0°C for 30 min at which point the reaction was complete by HPLC. The reaction was diluted with 10 mL water and extracted 2x with 10 mL EtOAc. The combined organic portion was washed 3x with brine, dried over sodium sulfate and the solvent removed. The crude product was purified by flash (0-100% EtOAc in Hexanes).



6-((3-Fluorobenzyl)thio)-1-methyl-5-phenyl-1H-pyrazolo[3,4-d]pyrimidin-4(5H)-one

(257723).

Method C. White crystalline solid. 84 % yield. HRMS (ESI): m/z 367.1023 $[M+H]^+$ 1H NMR

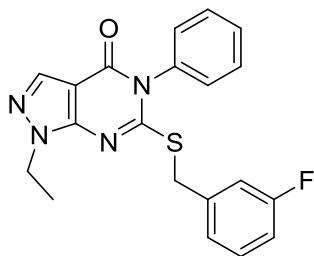
(500 MHz, $CDCl_3$) δ 8.03 (s, 1H), 7.47 - 7.58 (m, 3H), 7.22 - 7.30 (m, 3H), 7.13 (d, $J = 7.83$ Hz,

1H), 7.09 (d, $J = 9.78$ Hz, 1H), 6.95 (dt, $J = 2.20, 8.44$ Hz, 1H), 4.34 (s, 2H), 4.01 (s, 3H) ^{13}C

NMR (126 MHz, $CDCl_3$) δ 162.67 (d, $J = 246.6$ Hz), 161.31, 157.68, 150.89, 138.47 (d, $J = 7.4$

Hz), 135.50, 135.42, 130.11, 130.06 (d, $J = 8.3$ Hz), 129.75, 129.36, 124.76 (d, $J = 3.1$ Hz),

116.15 (d, $J = 21.9$ Hz), 114.61 (d, $J = 21.0$ Hz), 102.95, 36.88, 34.12. HPLC Purity: 98%.

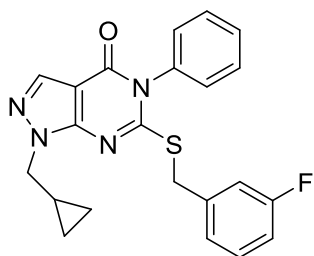


1-ethyl-6-((3-fluorobenzyl)thio)-5-phenyl-1H-pyrazolo[3,4-d]pyrimidin-4(5H)-one (257904)

Method B. Iodoethane. White Solid (43mg, 0.113 mmol, 49.8 % yield) MS (ESI): m/z 381.1175

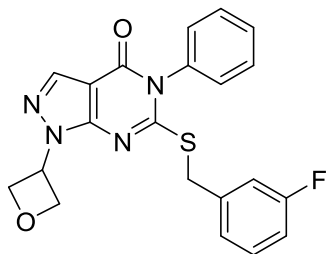
$[M+H]^+$ 1H NMR (400 MHz, $CDCl_3$) δ 8.06 (s, 1H), 7.46 - 7.56 (m, 3H), 7.24 - 7.31 (m, 2H),

7.21 (dd, $J = 6.26, 7.83$ Hz, 1H), 7.12 (d, $J = 7.83$ Hz, 1H), 7.06 (d, $J = 9.78$ Hz, 1H), 6.91 (dt, $J = 1.76, 8.51$ Hz, 1H), 4.40 (s, 2H), 4.33 (q, $J = 7.43$ Hz, 2H), 1.61 (t, $J = 7.43$ Hz, 3H) ^{13}C NMR (101 MHz, CDCl_3) δ 162.7, 159.9, 158.7, 158.1, 138.5, 135.6, 130.0, 130.0, 129.9, 129.6, 127.8, 125.0, 116.3, 114.5, 104.6, 48.6, 37.0, 15.4. HPLC Purity: 99%



1-(Cyclopropylmethyl)-6-((3-fluorobenzyl)thio)-5-phenyl-1H-pyrazolo[3,4-d]pyrimidin-4(5H)-one (257905)

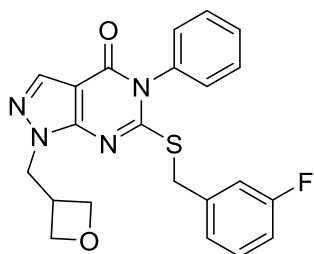
Method B. Cyclopropylmethyl bromide. White Solid. 47.7 % yield. HRMS (ESI): m/z 407.1335
[$\text{M}+\text{H}$] $^+$ ^1H NMR (400 MHz, CDCl_3) δ 8.05 (s, 1H), 7.48 - 7.57 (m, 3H), 7.20 - 7.33 (m, 3H), 7.12 (d, $J = 7.83$ Hz, 1H), 7.08 (d, $J = 9.39$ Hz, 1H), 6.95 (t, $J = 8.41$ Hz, 1H), 4.31 (s, 2H), 4.19 (d, $J = 7.04$ Hz, 2H), 1.38 (s, 1H), 0.54 - 0.69 (m, 2H), 0.36 - 0.50 (m, 2H) ^{13}C NMR (101 MHz, CDCl_3) δ 162.69 (d, $J = 246.7$ Hz), 161.07, 157.71, 150.37, 138.46 (d, $J = 7.6$ Hz), 135.53, 135.35 (d, $J = 3.7$ Hz), 130.07, 130.05 (d, $J = 8.1$ Hz), 129.72, 129.35, 124.55 (d, $J = 2.9$ Hz), 115.92 (d, $J = 21.9$ Hz), 114.54 (d, $J = 21.3$ Hz), 102.91, 52.05, 36.82, 11.22, 3.98. HPLC Purity: 99%.



**6-((3-Fluorobenzyl)thio)-1-(oxetan-3-yl)-5-phenyl-1H-pyrazolo[3,4-d]pyrimidin-4(5H)-one
(258082)**

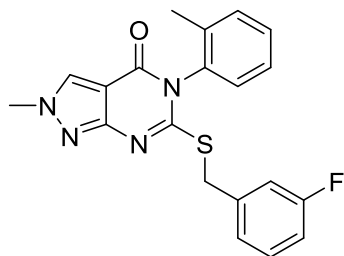
Method B. 3-bromooxetane. White solid. 15.5 % yield. HRMS (ESI): m/z 409.1131 $[M+H]^+$

^1H NMR (500 MHz, CDCl_3) δ 8.13 (s, 1H), 7.50 - 7.57 (m, 3H), 7.21 - 7.31 (m, 3H), 7.12 (d, $J = 7.83$ Hz, 1H), 7.08 (d, $J = 9.29$ Hz, 1H), 6.92 - 6.99 (m, 1H), 5.94 (quin, $J = 7.21$ Hz, 1H), 5.30 (t, $J = 6.36$ Hz, 2H), 5.06 (t, $J = 7.09$ Hz, 2H), 4.33 (s, 2H) ^{13}C NMR (126 MHz, CDCl_3) δ 162.71 (d, $J = 246.6$ Hz), 161.98, 157.48, 150.90, 138.14 (d, $J = 7.4$ Hz), 136.33, 135.33, 130.22, 130.12 (d, $J = 8.3$ Hz), 129.82, 129.25, 124.64 (d, $J = 2.9$ Hz), 115.99 (d, $J = 22.1$ Hz), 114.69 (d, $J = 21.1$ Hz), 103.47, 76.81, 50.75, 36.91. HPLC Purity: 96%.



6-((3-Fluorobenzyl)thio)-1-(oxetan-3-ylmethyl)-5-phenyl-1H-pyrazolo[3,4-d]pyrimidin-4(5H)-one (258084)

Method B. Oxetan-3-ylmethyl methanesulfonate. White solid. 32.5 % yield. HRMS (ESI): m/z 423.1289 $[M+H]^+$ 1H NMR (500 MHz, $CDCl_3$) δ 8.00 (s, 1H), 7.48 - 7.56 (m, 3H), 7.23 - 7.31 (m, 3H), 7.14 (d, $J = 7.83$ Hz, 1H), 7.08 (d, $J = 9.78$ Hz, 1H), 6.92 - 6.98 (m, 1H), 4.83 (t, $J = 7.09$ Hz, 2H), 4.62 (d, $J = 7.34$ Hz, 2H), 4.60 (t, $J = 6.10$ Hz, 2H), 4.32 (s, 2H), 3.48 - 3.59 (m, 1H) ^{13}C NMR (126 MHz, $CDCl_3$) δ 162.59 (d, $J = 246.6$ Hz), 161.67, 157.39, 150.77, 138.22 (d, $J = 7.6$ Hz), 135.68, 135.34, 130.05, 130.2 (d, $J = 7.6$), 129.99, 129.67, 129.21, 124.51 (d, $J = 3.0$ Hz), 115.84 (d, $J = 22.0$ Hz), 114.52 (d, $J = 21.0$ Hz), 102.84, 74.67, 49.29, 36.85, 35.15. HPLC Purity: 99%.

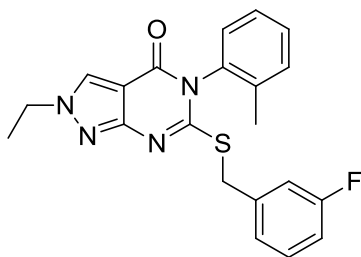


**6-((3-Fluorobenzyl)thio)-2-methyl-5-(o-tolyl)-2H-pyrazolo[3,4-d]pyrimidin-4(5H)-one
(257432)**

Method B. Methyl iodide. Colorless Oil. 27% yield. HRMS (ESI): m/z 381.1179 $[M+H]^+$ 1H NMR (500 MHz, $CDCl_3$) δ 8.03 (s, 1H), 7.40 (t, $J = 7.58$ Hz, 1H), 7.29 - 7.36 (m, 2H), 7.19 - 7.25 (m, 1H), 7.17 (d, $J = 7.83$ Hz, 1H), 7.13 (d, $J = 7.83$ Hz, 1H), 7.07 (d, $J = 9.78$ Hz, 1H), 6.91 (dt, $J = 2.00, 8.30$ Hz, 1H), 4.33 - 4.42 (m, 2H), 4.07 (s, 3H), 2.10 (s, 3H) ^{13}C NMR (126 MHz, $CDCl_3$) δ 162.61 (d, $J = 246.1$ Hz), 159.88, 158.40, 157.99, 138.73 (d, $J = 7.4$ Hz), 137.12,

134.53, 131.25, 130.26, 129.89 (d, $J = 8.5$ Hz), 129.59, 129.31, 127.20, 124.93 (d, $J = 2.9$ Hz), 116.09 (d, $J = 21.6$ Hz), 114.34 (d, $J = 21.1$ Hz), 104.89, 40.29, 36.60 (d, $J = 2.1$ Hz), 17.29.

HPLC Purity: 99%.



2-ethyl-6-((3-fluorobenzyl)thio)-5-(o-tolyl)-2H-pyrazolo[3,4-d]pyrimidin-4(5H)-one

(257434)

Method B. Iodoethane. Colorless oil (30mg, 0.076 mmol, 27.9 % yield) MS (ESI): m/z 395.1

$[M+H]^+$ 1H NMR (400 MHz, $CDCl_3$) δ 8.08 (s, 1H), 7.41 (t, $J = 7.40$ Hz, 1H), 7.28 - 7.37 (m,

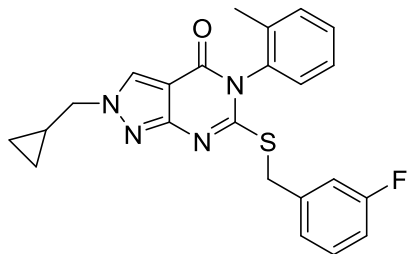
2H), 7.19 - 7.26 (m, 1H), 7.17 (d, $J = 7.83$ Hz, 1H), 7.12 (d, $J = 7.83$ Hz, 1H), 7.06 (d, $J = 9.78$

Hz, 1H), 6.91 (t, $J = 8.41$ Hz, 1H), 4.40 (s, 2H), 4.33 (q, $J = 7.43$ Hz, 2H), 2.11 (s, 3H), 1.61 (t, J

= 7.43 Hz, 3H) ^{13}C NMR (101 MHz, $CDCl_3$) δ 162.7, 159.9, 158.3, 158.2, 138.7, 137.2, 134.6,

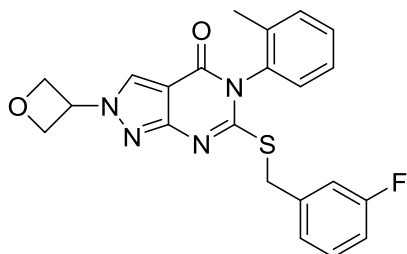
131.3, 130.3, 130.0, 129.6, 127.9, 127.3, 125.0, 116.2, 114.4, 104.6, 48.6, 36.7, 17.4, 15.4.

HPLC Purity: 98%



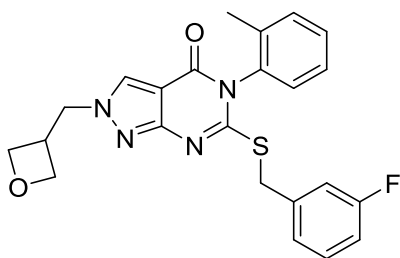
2-(Cyclopropylmethyl)-6-((3-fluorobenzyl)thio)-5-(o-tolyl)-2H-pyrazolo[3,4-d]pyrimidin-4(5H)-one (257725)

Method B. Cyclopropylmethyl bromide. White Crystalline solid. 38% yield. HRMS (ESI): m/z 421.1492 $[M+H]^+$ 1H NMR (500 MHz, $CDCl_3$) δ 8.21 (s, 1H), 7.40 (t, $J = 7.34$ Hz, 1H), 7.28 - 7.36 (m, 2H), 7.19 - 7.25 (m, 1H), 7.17 (d, $J = 7.83$ Hz, 1H), 7.12 (d, $J = 7.83$ Hz, 1H), 7.06 (d, $J = 9.78$ Hz, 1H), 6.91 (t, $J = 8.31$ Hz, 1H), 4.41 (d, $J = 14.18$ Hz, 1H), 4.38 (d, $J = 14.20$ Hz, 1H), 4.13 (d, $J = 6.85$ Hz, 2H), 2.12 (s, 3H), 1.36 - 1.47 (m, 1H), 0.69 - 0.78 (m, 2H), 0.42 - 0.49 (m, 2H) ^{13}C NMR (126 MHz, $CDCl_3$) δ 162.58 (d, $J = 246.2$ Hz), 159.74, 158.16, 158.10, 138.60 (d, $J = 7.3$ Hz), 137.13, 134.55, 131.22, 130.21, 129.87 (d, $J = 8.4$ Hz), 129.58, 127.85, 127.17, 124.90 (d, $J = 3.1$ Hz), 116.08 (d, $J = 21.9$ Hz), 114.32 (d, $J = 21.2$ Hz), 104.54, 58.20, 36.64, 17.30, 10.71, 4.19. HPLC Purity: 97%.



6-((3-Fluorobenzyl)thio)-2-(oxetan-3-yl)-5-(o-tolyl)-2H-pyrazolo[3,4-d]pyrimidin-4(5H)-one (257913)

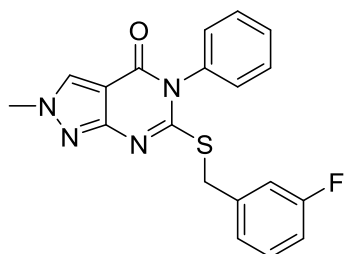
Method B. 3-Bromooxetane. White solid. 15% yield. HRMS (ESI): m/z 423.1295 $[M+H]^+$ 1H NMR (500 MHz, $CDCl_3$) δ 8.21 (s, 1H), 7.39 - 7.45 (m, 1H), 7.30 - 7.37 (m, 2H), 7.23 (dt, $J = 5.87, 7.83$ Hz, 1H), 7.15 - 7.19 (m, 1H), 7.12 (d, $J = 7.83$ Hz, 1H), 7.04 - 7.09 (m, 1H), 6.92 (dt, $J = 1.96, 8.56$ Hz, 1H), 5.53 - 5.62 (m, 1H), 5.23 (t, $J = 6.60$ Hz, 2H), 5.10 (t, $J = 7.34$ Hz, 2H), 4.38 - 4.46 (m, 2H), 2.11 (s, 3H) ^{13}C NMR (126 MHz, $CDCl_3$) δ 162.70 (d, $J = 246.7$ Hz), 160.89, 158.58, 157.91, 138.34 (d, $J = 7.8$ Hz), 137.11, 134.40, 131.36, 130.41, 130.00 (d, $J = 8.2$ Hz), 129.58, 128.09, 127.31, 124.97 (d, $J = 3.2$ Hz), 116.18 (d, $J = 22.2$ Hz), 114.51 (d, $J = 21.0$ Hz), 105.25, 76.81 (d, $J = 2.7$ Hz), 56.83, 36.87, 17.34. HPLC Purity: 96%.



6-((3-Fluorobenzyl)thio)-2-(oxetan-3-ylmethyl)-5-(o-tolyl)-2H-pyrazolo[3,4-d]pyrimidin-4(5H)-one (257912)

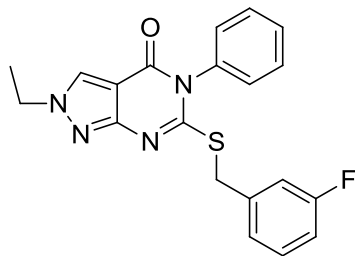
Method B. Oxetan-3-ylmethyl methanesulfonate. Colorless oil. 24.3 % yield. HRMS (ESI): m/z 437.1449 $[M+H]^+$ 1H NMR (500 MHz, $CDCl_3$) δ 8.07 (s, 1H), 7.38 - 7.44 (m, 1H), 7.29 - 7.37 (m, 2H), 7.22 (dt, $J = 6.11, 7.95$ Hz, 1H), 7.16 (d, $J = 7.34$ Hz, 1H), 7.10 (d, $J = 7.83$ Hz, 1H),

7.05 (dd, $J = 1.96, 9.78$ Hz, 1H), 6.91 (dt, $J = 2.45, 8.31$ Hz, 1H), 4.88 (t, $J = 7.09$ Hz, 2H), 4.59 (d, $J = 7.83$ Hz, 2H), 4.55 (t, $J = 6.36$ Hz, 2H), 4.35 - 4.43 (m, 2H), 3.62 - 3.71 (m, 1H), 2.11 (s, 3H) ^{13}C NMR (126 MHz, CDCl_3) δ 162.66 (d, $J = 246.2$ Hz), 160.42, 158.56, 157.96, 138.42 (d, $J = 7.7$ Hz), 137.13, 134.45, 131.32, 130.36, 129.96 (d, $J = 8.3$ Hz), 129.57, 128.70, 127.28, 124.95 (d, $J = 2.6$ Hz), 116.18 (d, $J = 21.9$ Hz), 114.45 (d, $J = 21.1$ Hz), 104.89, 74.48 (d, $J = 2.7$ Hz), 55.85, 36.79, 35.36, 17.35. HPLC Purity: 99%.



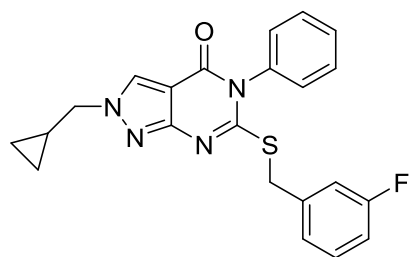
**6-((3-Fluorobenzyl)thio)-2-methyl-5-phenyl-2H-pyrazolo[3,4-d]pyrimidin-4(5H)-one
(257902)**

Method B. Methyl Iodide. White solid. 24.0 % yield. HRMS (ESI): m/z 367.1021 $[\text{M}+\text{H}]^+ \text{ } ^1\text{H}$ NMR (500 MHz, CDCl_3) δ 8.02 (s, 1H), 7.46 - 7.56 (m, 3H), 7.26 - 7.31 (m, 2H), 7.23 (q, $J = 7.34$ Hz, 1H), 7.14 (d, $J = 7.83$ Hz, 1H), 7.08 (d, $J = 9.29$ Hz, 1H), 6.92 (t, $J = 8.07$ Hz, 1H), 4.39 (s, 2H), 4.07 (s, 3H) ^{13}C NMR (126 MHz, CDCl_3) δ 162.64 (d, $J = 246.3$ Hz), 159.88, 158.52, 158.23, 138.61 (d, $J = 7.6$ Hz), 135.54, 129.91 (d, $J = 8.3$ Hz), 129.91, 129.57, 129.54, 129.25, 124.98 (d, $J = 3.2$ Hz), 116.17 (d, $J = 21.9$ Hz), 114.38 (d, $J = 21.3$ Hz), 104.95, 40.28, 36.90. HPLC Purity: 96%.



2-Ethyl-6-((3-fluorobenzyl)thio)-5-phenyl-2H-pyrazolo[3,4-d]pyrimidin-4(5H)-one (257903)

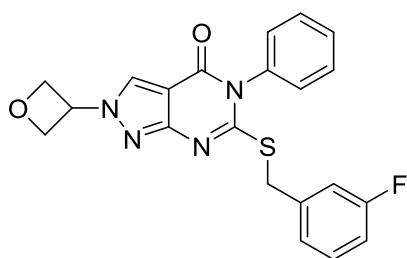
Method B. Iodoethane White Solid (8mg, 0.021 mmol, 9.26 % yield) M+H found: MS (ESI): m/z 381.1178 $[M+H]^+$ 1H NMR (500 MHz, $CDCl_3$) δ 8.04 (s, 1H), 7.49 - 7.57 (m, 3H), 7.23 - 7.32 (m, 3H), 7.14 (d, $J = 7.83$ Hz, 1H), 7.10 (d, $J = 9.78$ Hz, 1H), 6.95 (dt, $J = 2.20, 8.44$ Hz, 1H), 4.41 (q, $J = 7.01$ Hz, 2H), 4.33 (s, 2H), 1.53 (t, $J = 7.09$ Hz, 3H) ^{13}C NMR (126 MHz, $CDCl_3$) δ 162.7, 161.1, 157.7, 150.2, 138.7, 135.6, 135.4, 130.1, 130.1, 129.8, 129.4, 124.7, 116.1, 114.6, 103.0, 42.5, 36.8, 15.0 HPLC Purity: 96%



2-(Cyclopropylmethyl)-6-((3-fluorobenzyl)thio)-5-phenyl-2H-pyrazolo[3,4-d]pyrimidin-4(5H)-one (257906)

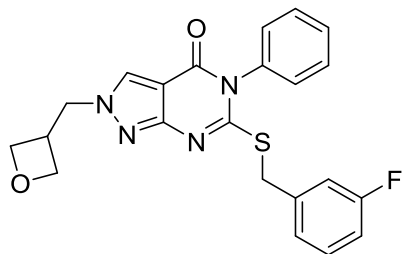
Method B. Cyclopropylmethyl bromide. White Solid. 36.8 % yield. HRMS (ESI): m/z 407.1334 $[M+H]^+$ 1H NMR (400 MHz, $CDCl_3$) δ 8.19 (s, 1H), 7.42 - 7.58 (m, 3H), 7.27 (d, $J = 4.30$ Hz,

2H), 7.16 - 7.24 (m, 1H), 7.11 (d, $J = 7.43$ Hz, 1H), 7.06 (d, $J = 9.78$ Hz, 1H), 6.90 (t, $J = 8.41$ Hz, 1H), 4.39 (s, 2H), 4.12 (d, $J = 7.04$ Hz, 2H), 1.34 - 1.49 (m, 1H), 0.72 (d, $J = 7.83$ Hz, 2H), 0.44 (d, $J = 4.30$ Hz, 2H) ^{13}C NMR (101 MHz, CDCl_3) δ 162.7, 159.8, 158.8, 158.0, 138.5, 135.6, 130.0, 129.9, 129.6, 129.6, 127.9, 125.0, 116.2, 114.4, 104.7, 58.3, 37.0, 10.5, 4.3. HPLC Purity: 99%.



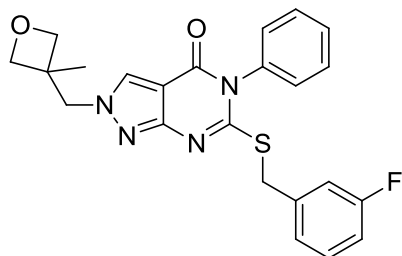
6-((3-Fluorobenzyl)thio)-2-(oxetan-3-yl)-5-phenyl-2H-pyrazolo[3,4-d]pyrimidin-4(5H)-one (258083)

Method B. 3-bromooxetane. White solid. 21.6 % yield. HRMS (ESI): m/z 409.1130 $[\text{M}+\text{H}]^+$
 ^1H NMR (500 MHz, CDCl_3) δ 8.20 (s, 1H), 7.46 - 7.54 (m, 3H), 7.26 - 7.31 (m, 2H), 7.19 - 7.25 (m, 1H), 7.12 (d, $J = 7.34$ Hz, 1H), 7.06 (d, $J = 9.78$ Hz, 1H), 6.92 (dt, $J = 1.71, 8.44$ Hz, 1H), 5.56 (quin, $J = 6.97$ Hz, 1H), 5.21 (t, $J = 6.60$ Hz, 2H), 5.07 (t, $J = 7.34$ Hz, 2H), 4.42 (s, 2H) ^{13}C NMR (126 MHz, CDCl_3) δ 162.71 (d, $J = 246.3$ Hz), 160.83, 158.50, 158.42, 138.22 (d, $J = 7.4$ Hz), 135.42, 130.09, 130.02 (d, $J = 6.8$ Hz), 129.68, 129.58, 128.18, 125.05 (d, $J = 3.0$ Hz), 116.26 (d, $J = 21.9$ Hz), 114.55 (d, $J = 21.1$ Hz), 105.26, 76.82, 56.81, 37.17. HPLC Purity: 96%.



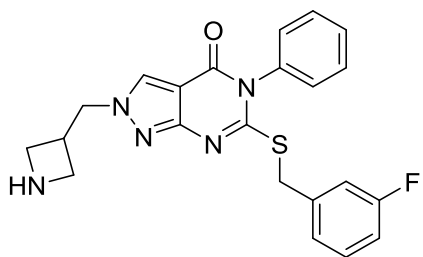
6-((3-Fluorobenzyl)thio)-2-(oxetan-3-ylmethyl)-5-phenyl-2H-pyrazolo[3,4-d]pyrimidin-4(5H)-one (258085)

Method B. Oxetan-3-ylmethyl methanesulfonate. White solid. 22.5 % yield. HRMS (ESI): m/z 423.1286 $[M+H]^+$ 1H NMR (500 MHz, $CDCl_3$) δ 8.07 (s, 1H), 7.47 - 7.54 (m, 3H), 7.25 - 7.30 (m, 2H), 7.19 - 7.25 (m, 1H), 7.11 (d, $J = 7.34$ Hz, 1H), 7.05 (d, $J = 9.29$ Hz, 1H), 6.92 (dt, $J = 1.47, 8.31$ Hz, 1H), 4.86 (t, $J = 7.09$ Hz, 2H), 4.57 (d, $J = 7.34$ Hz, 2H), 4.54 (t, $J = 6.11$ Hz, 2H), 4.38 (s, 2H), 3.58 - 3.70 (m, 1H) ^{13}C NMR (126 MHz, $CDCl_3$) δ 162.63 (d, $J = 246.5$ Hz), 160.34, 158.48, 158.36, 138.26 (d, $J = 7.5$ Hz), 135.42, 129.98, 129.95 (d, $J = 7.8$ Hz), 129.59, 129.52, 128.68, 124.98 (d, $J = 2.9$ Hz), 116.21 (d, $J = 21.9$ Hz), 114.45 (d, $J = 21.0$ Hz), 104.90, 74.41, 55.76, 37.03, 35.31. HPLC Purity: 99%.



6-((3-fluorobenzyl)thio)-2-((3-methyloxetan-3-yl)methyl)-5-phenyl-2H-pyrazolo[3,4-d]pyrimidin-4(5H)-one (262701)

Method B. (3-Methyloxetan-3-yl)methyl methanesulfonate. White solid (30mg, 0.069 mmol, 24.22 % yield) MS (ESI): m/z 437.1444 $[M+H]^+$ 1H NMR (500 MHz, $CDCl_3$) δ 8.05 (s, 1H), 7.55 - 7.46 (m, 3H), 7.31 - 7.25 (m, 2H), 7.22 (q, $J = 7.5$ Hz, 1H), 7.10 (d, $J = 7.7$ Hz, 1H), 7.05 (d, $J = 9.6$ Hz, 1H), 6.91 (t, $J = 8.3$ Hz, 1H), 4.78 (d, $J = 6.3$ Hz, 2H), 4.47 (s, 2H), 4.45 (d, $J = 6.4$ Hz, 2H), 4.39 (s, 2H), 1.29 (s, 3H). ^{13}C NMR (126 MHz, $CDCl_3$) δ 162.68 (d, $J = 246.5$ Hz), 160.34, 158.62, 158.34, 138.20 (d, $J = 7.6$ Hz), 135.49, 130.03, 130.01 (d, $J = 8.0$ Hz), 129.65, 129.57, 129.50, 125.06 (d, $J = 2.9$ Hz), 116.31 (d, $J = 21.8$ Hz), 114.52 (d, $J = 21.0$ Hz), 104.86, 80.24, 60.07, 40.49, 37.18, 21.52. HPLC Purity: 98%

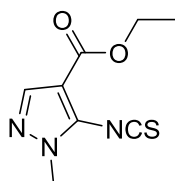


3-(((6-((3-fluorobenzyl)thio)-4-oxo-5-phenyl-4,5-dihydro-2H-pyrazolo[3,4-d]pyrimidin-2-yl)methyl)azetidinium-1-ium sulfate (262702)

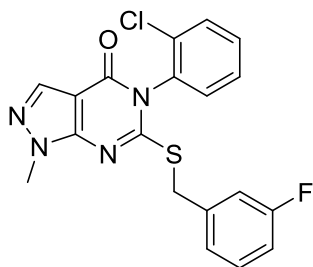
Method B afforded tert-butyl 3-(((6-((3-fluorobenzyl)thio)-4-oxo-5-phenyl-4,5-dihydro-2H-pyrazolo[3,4-d]pyrimidin-2-yl)methyl)azetidinium-1-ium sulfate using tert-butyl 3-

((methylsulfonyl)oxy)methyl)azetidine-1-carboxylate. White solid (230mg, 0.441 mmol, 15.54 % yield). ^1H NMR (400 MHz, CDCl_3) δ 8.06 (s, 1H), 7.59 - 7.46 (m, 3H), 7.25 - 7.17 (m, 3H), 7.11 (d, $J = 7.6$ Hz, 1H), 7.06 (d, $J = 9.6$ Hz, 1H), 6.93 (dt, $J = 9.8, 4.9$ Hz, 1H), 4.47 (d, $J = 7.6$ Hz, 2H), 4.39 (s, 2H), 4.08 (t, $J = 8.5$ Hz, 2H), 3.77 (dd, $J = 8.9, 5.0$ Hz, 2H), 3.23 (q, $J = 8.0, 6.8$ Hz, 1H), 1.45 (s, 9H).

Tert-butyl 3-((6-((3-fluorobenzyl)thio)-4-oxo-5-phenyl-4,5-dihydro-2H-pyrazolo[3,4-d]pyrimidin-2-yl)methyl)azetidine-1-carboxylate (230mg, 0.441 mmol), 5mL toluene and 0.5 mL concentrated sulfuric acid was stirred for 1 hour at RT. The toluene layer was discarded and the sulfuric acid layer was washed with 10mL Diethyl ether before being dissolved in 5mL hot methanol. The product crystallized out upon cooling. The product was further washed with cold methanol to remove residual sulfuric acid yielding the titled compound as a white solid (50mg, 0.118 mmol, 26.8 % yield). MS (ESI): m/z 422.1445 $[\text{M}+\text{H}]^+$ ^1H NMR (500 MHz, $\text{DMSO}-d_6$) δ 9.11 (s, 3H), 8.68 (s, 1H), 7.52 (d, $J = 5.3$ Hz, 3H), 7.41 - 7.34 (m, 2H), 7.34 - 7.29 (m, 1H), 7.23 (t, $J = 9.2$ Hz, 2H), 7.07 (t, $J = 8.7$ Hz, 1H), 4.61 (d, $J = 7.2$ Hz, 2H), 4.35 (s, 2H), 4.03 (t, $J = 9.6$ Hz, 2H), 3.91 (t, $J = 8.6$ Hz, 2H), 3.33 (dq, $J = 15.3, 7.6$ Hz, 1H). ^{13}C NMR (126 MHz, $\text{DMSO}-d_6$) δ 162.38 (d, $J = 244.0$ Hz), 159.53, 158.25, 157.93, 139.95 (d, $J = 7.9$ Hz), 136.15, 130.96, 130.81 (d, $J = 8.6$ Hz), 130.28, 130.24, 129.85, 125.71, 116.35 (d, $J = 21.9$ Hz), 114.60 (d, $J = 21.1$ Hz), 104.54, 54.06, 48.89, 35.98, 32.39. HPLC Purity: 96%.

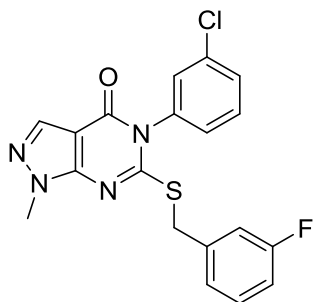


Ethyl 5-isothiocyanato-1-methyl-1H-pyrazole-4-carboxylate (3.2b). To a dry flask under N₂ at 0°C charged with 60 wt.% NaH in mineral oil (296 mg, 7.39 mmol) and **3.2a** (500 mg, 2.96 mmol) was added 10 mL THF. The mixture was stirred for 10 min at which point CS₂ (1.8 mL, 29.6 mmol) was added by syringe. The mixture was allowed warm to room temperature then heated to 40°C and stirred for 3 h. After cooling the flask to 0°C, iodine was added portion-wise over 10 min. The mixture was stirred for 1 h at 0°C then 30 mL diethyl ether was added and the precipitate was filtered off. The filtrate was washed 3x with 1N HCl, 1x with brine and the organic portion was dried over sodium sulfate and the solvent removed yielding a reddish black solid. The crude product was purified by flash (0-30% EA in Hex) yielding the titled compound as a yellow solid (460 mg, 2.18 mmol, 74% yield). MS (ESI): *m/z* 212.0 [M+H]⁺ ¹H NMR (400 MHz, CDCl₃) δ 7.81 (s, 1H), 4.25 - 4.44 (m, 2H), 3.80 (s, 3H), 1.30 - 1.44 (m, 3H).



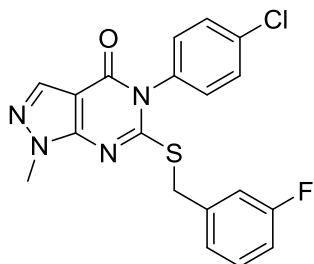
5-(2-Chlorophenyl)-6-((3-fluorobenzyl)thio)-1-methyl-1H-pyrazolo[3,4-d]pyrimidin-4(5H)-one (258463)

Method C. White crystalline solid. 83% yield. HRMS (ESI): m/z 401.0629 $[M+H]^+$ 1H NMR (500 MHz, $CDCl_3$) δ 8.04 (s, 1H), 7.58 (dd, $J = 1.47, 7.83$ Hz, 1H), 7.48 (dt, $J = 1.71, 7.70$ Hz, 1H), 7.43 (dt, $J = 1.47, 7.58$ Hz, 1H), 7.33 (d, $J = 7.83$ Hz, 1H), 7.23 - 7.30 (m, 1H), 7.15 (d, $J = 7.34$ Hz, 1H), 7.10 (d, $J = 9.78$ Hz, 1H), 6.95 (dt, $J = 1.96, 8.31$ Hz, 1H), 4.32 - 4.42 (m, 2H), 4.01 (s, 3H) ^{13}C NMR (126 MHz, $CDCl_3$) δ 162.67 (d, $J = 246.8$ Hz), 160.82, 156.77, 150.91, 138.29 (d, $J = 7.3$ Hz), 135.54, 133.78, 133.22, 131.56, 131.21, 130.73, 130.05 (d, $J = 8.5$ Hz), 128.07, 124.69 (d, $J = 2.9$ Hz), 116.07 (d, $J = 22.1$ Hz), 114.63 (d, $J = 21.0$ Hz), 102.72, 36.59, 34.15. HPLC Purity: 99%.



5-(3-Chlorophenyl)-6-((3-fluorobenzyl)thio)-1-methyl-1H-pyrazolo[3,4-d]pyrimidin-4(5H)-one (258464)

Method C. White crystalline solid. 44% yield. HRMS (ESI): m/z 401.0629 $[M+H]^+$ 1H NMR (500 MHz, $CDCl_3$) δ 8.03 (s, 1H), 7.51 (td, $J = 1.60, 8.00$ Hz, 1H), 7.47 (t, $J = 8.00$ Hz, 1H), 7.26 - 7.32 (m, 2H), 7.18 (td, $J = 1.53, 7.70$ Hz, 1H), 7.15 (d, $J = 7.83$ Hz, 1H), 7.11 (td, $J = 2.08, 9.54$ Hz, 1H), 6.98 (dt, $J = 2.69, 8.44$ Hz, 1H), 4.32 - 4.41 (m, 2H), 4.02 (s, 3H) ^{13}C NMR (126 MHz, $CDCl_3$) δ 162.70 (d, $J = 246.8$ Hz), 160.84, 157.42, 150.77, 138.20 (d, $J = 7.6$ Hz), 136.53, 135.47, 135.27, 130.66, 130.47, 130.15 (d, $J = 8.1$ Hz), 129.77, 127.77, 124.78 (d, $J = 3.2$ Hz), 116.19 (d, $J = 21.7$ Hz), 114.74 (d, $J = 21.0$ Hz), 102.80, 36.93, 34.18. HPLC Purity: 98%.



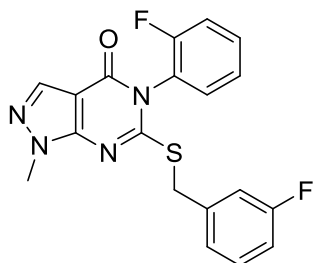
5-(4-Chlorophenyl)-6-((3-fluorobenzyl)thio)-1-methyl-1H-pyrazolo[3,4-d]pyrimidin-4(5H)-one (258465)

Method C. White crystalline solid. 44% yield. HRMS (ESI): m/z 401.0629 $[M+H]^+$ 1H NMR (500 MHz, $CDCl_3$) δ 8.02 (s, 1H), 7.49 (d, $J = 8.31$ Hz, 2H), 7.24 - 7.30 (m, 1H), 7.20 (d, $J = 8.31$ Hz, 2H), 7.13 (d, $J = 7.34$ Hz, 1H), 7.09 (d, $J = 9.78$ Hz, 1H), 6.96 (dt, $J = 2.45, 8.31$ Hz, 1H), 4.34 (s, 2H), 4.01 (s, 3H) ^{13}C NMR (126 MHz, $CDCl_3$) δ 162.69 (d, $J = 246.7$ Hz), 160.96,

157.53, 150.81, 138.22 (d, $J = 7.6$ Hz), 136.33, 135.44, 133.89, 130.75, 130.17, 130.11, 124.76

(d, $J = 2.9$ Hz), 116.16 (d, $J = 22.1$ Hz), 114.73 (d, $J = 21.0$ Hz), 102.81, 36.92, 34.16. HPLC

Purity: 99%.



6-((3-Fluorobenzyl)thio)-5-(2-fluorophenyl)-1-methyl-1H-pyrazolo[3,4-d]pyrimidin-4(5H)-one (258962)

Method C. White crystalline solid. 70% yield. HRMS (ESI): m/z 385.0932 $[M+H]^+$ 1H NMR

(500 MHz, $CDCl_3$) δ 8.03 (s, 1H), 7.57 - 7.49 (m, 1H), 7.36 - 7.20 (m, 4H), 7.14 (d, $J = 7.6$ Hz,

1H), 7.10 (d, $J = 9.5$ Hz, 1H), 6.96 (td, $J = 8.4, 2.5$ Hz, 1H), 4.40 (d, $J = 13.7$ Hz, 1H), 4.34 (d, J

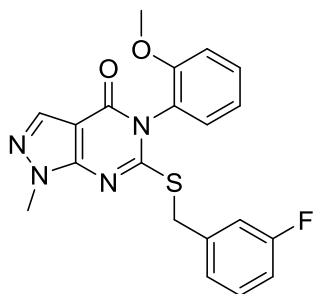
= 13.6 Hz, 1H), 4.01 (s, 3H). ^{13}C NMR (126 MHz, $CDCl_3$) δ 162.70 (d, $J = 247.0$ Hz), 161.09,

158.28 (d, $J = 253.4$ Hz), 156.94, 150.92, 138.20 (d, $J = 7.6$ Hz), 135.52, 132.33 (d, $J = 8.0$ Hz),

131.24, 130.12 (d, $J = 8.5$ Hz), 125.05 (d, $J = 3.9$ Hz), 124.75 (d, $J = 3.1$ Hz), 123.11 (d, $J = 14.1$

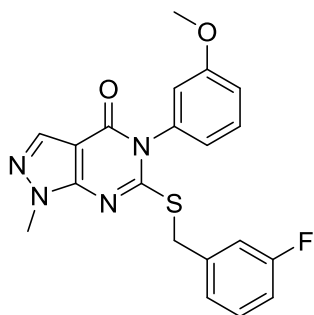
Hz), 117.03 (d, $J = 19.5$ Hz), 116.15 (d, $J = 22.2$ Hz), 114.71 (d, $J = 21.0$ Hz), 102.69, 36.73,

34.18. HPLC Purity: 98%.



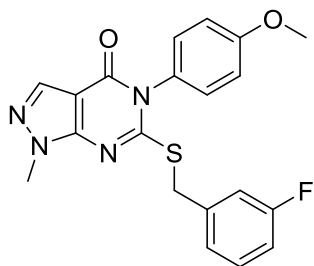
6-((3-Fluorobenzyl)thio)-5-(2-methoxyphenyl)-1-methyl-1H-pyrazolo[3,4-d]pyrimidin-4(5H)-one (257727)

Method C. White crystalline solid. 19% yield. HRMS (ESI): m/z 397.1127 $[M+H]^+$ (400 MHz, $CDCl_3$) δ 8.02 (s, 1H), 7.49 (t, $J = 8.02$ Hz, 1H), 7.22 - 7.29 (m, 1H), 7.19 (d, $J = 7.83$ Hz, 1H), 7.02 - 7.16 (m, 4H), 6.94 (t, $J = 8.22$ Hz, 1H), 4.33 (s, 2H), 3.99 (s, 3H), 3.78 (s, 3H) ^{13}C NMR (101 MHz, $CDCl_3$) δ 162.64 (d, $J = 246.3$ Hz), 161.76, 157.31, 155.40, 151.04, 138.76 (d, $J = 7.6$ Hz), 135.39, 131.80, 130.64, 129.92 (d, $J = 8.4$ Hz), 124.70 (d, $J = 2.9$ Hz), 123.89, 121.08, 116.00 (d, $J = 21.9$ Hz), 114.44 (d, $J = 21.0$ Hz), 112.34, 102.95, 55.82, 36.48, 34.06. HPLC Purity: 99%.



6-((3-Fluorobenzyl)thio)-5-(3-methoxyphenyl)-1-methyl-1H-pyrazolo[3,4-d]pyrimidin-4(5H)-one (258077)

Method C. White Solid. 80% yield. HRMS (ESI): m/z 397.1125 $[M+H]^+$ 1H NMR (400 MHz, $CDCl_3$) δ 7.99 (s, 1H), 7.41 (t, $J = 8.22$ Hz, 1H), 7.21 - 7.30 (m, 1H), 7.07 - 7.17 (m, 2H), 7.04 (dd, $J = 2.35, 8.22$ Hz, 1H), 6.90 - 6.98 (m, 1H), 6.85 (dd, $J = 0.78, 7.83$ Hz, 1H), 6.80 (d, $J = 1.96$ Hz, 1H), 4.33 (s, 2H), 3.99 (s, 3H), 3.80 (s, 3H) ^{13}C NMR (101 MHz, $CDCl_3$) δ 162.55 (d, $J = 246.6$ Hz), 161.20, 160.39, 157.50, 150.73, 138.41 (d, $J = 7.5$ Hz), 136.38, 135.24, 130.29, 129.97 (d, $J = 8.3$ Hz), 124.72 (d, $J = 3.0$ Hz), 121.31, 116.06 (d, $J = 21.8$ Hz), 115.82, 114.83, 114.48 (d, $J = 21.1$ Hz), 102.79, 55.39, 36.74, 34.04. HPLC Purity: 97%.

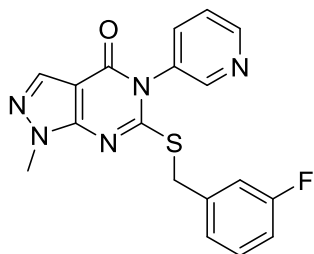


6-((3-Fluorobenzyl)thio)-5-(4-methoxyphenyl)-1-methyl-1H-pyrazolo[3,4-d]pyrimidin-4(5H)-one (258078)

Method C. White needles. 47% yield. HRMS (ESI): m/z 397.1123 $[M+H]^+$ 1H NMR (400 MHz, $CDCl_3$) δ 8.01 (s, 1H), 7.22 - 7.30 (m, 1H), 7.07 - 7.19 (m, 4H), 6.98 - 7.04 (m, 2H), 6.95 (dt, $J = 2.35, 8.41$ Hz, 1H), 4.32 (s, 2H), 4.00 (s, 3H), 3.85 (s, 3H) ^{13}C NMR (101 MHz, $CDCl_3$) δ 162.64 (d, $J = 246.4$ Hz), 161.92, 160.63, 157.91, 150.86, 138.52 (d, $J = 7.4$ Hz), 135.38, 130.40,

130.00, 127.75, 124.76 (d, $J = 2.7$ Hz), 116.16 (d, $J = 22.6$ Hz), 114.96, 114.56 (d, $J = 21.0$ Hz),

102.91, 55.45, 36.93, 34.14. HPLC Purity: 96%.



**6-((3-Fluorobenzyl)thio)-1-methyl-5-(pyridin-3-yl)-1H-pyrazolo[3,4-d]pyrimidin-4(5H)-one
(258907)**

Method C. White solid. 64 % yield. HRMS (ESI): m/z 368.0972 $[M+H]^+$ (500 MHz, $CDCl_3$) δ

8.72 (d, $J = 4.40$ Hz, 1H), 8.52 (s, 1H), 7.97 (s, 1H), 7.63 (d, $J = 8.31$ Hz, 1H), 7.45 (dd, $J =$

4.89, 7.83 Hz, 1H), 7.21 - 7.30 (m, 1H), 7.12 (d, $J = 7.34$ Hz, 1H), 7.07 (d, $J = 9.78$ Hz, 1H),

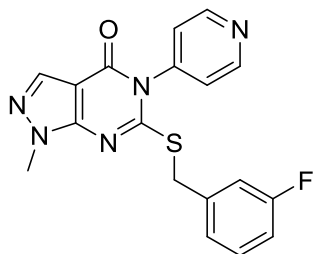
6.94 (t, $J = 8.30$ Hz, 1H), 4.37 (d, $J = 14.18$ Hz, 1H), 4.33 (d, $J = 14.18$ Hz, 1H), 4.00 (s, 3H) ^{13}C

NMR (126 MHz, $CDCl_3$) δ 162.54 (d, $J = 246.9$ Hz), 160.65, 157.29, 150.83, 150.64, 150.08,

137.96 (d, $J = 7.6$ Hz), 137.13, 135.25, 132.31, 130.05 (d, $J = 8.2$ Hz), 124.66 (d, $J = 3.2$ Hz),

124.07, 116.02 (d, $J = 21.9$ Hz), 114.64 (d, $J = 21.0$ Hz), 102.54, 36.80, 34.09. HPLC Purity:

99%.



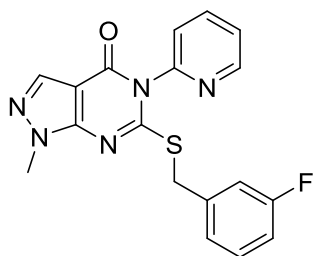
**6-((3-Fluorobenzyl)thio)-1-methyl-5-(pyridin-4-yl)-1H-pyrazolo[3,4-d]pyrimidin-4(5H)-one
(257908)**

Method C. Off white solid. 62% yield. HRMS (ESI): m/z 368.0974 [M+H]⁺ ¹H NMR (500 MHz, CDCl₃) δ 8.82 (d, J = 4.89 Hz, 2H), 8.00 (s, 1H), 7.26 - 7.32 (m, 1H), 7.25 (d, J = 5.38 Hz, 2H), 7.13 (d, J = 7.83 Hz, 1H), 7.09 (d, J = 9.78 Hz, 1H), 6.96 (dt, J = 2.45, 8.31 Hz, 1H), 4.37 (s, 2H), 4.01 (s, 3H) ¹³C NMR (101 MHz, CDCl₃) δ 162.48 (d, J = 246.8 Hz), 162.30, 159.50, 156.74, 151.49, 150.51, 143.30, 137.86 (d, J = 7.5 Hz), 135.19, 130.03 (d, J = 8.3 Hz), 124.62 (d, J = 3.0 Hz), 124.20, 115.96 (d, J = 22.1 Hz), 114.63 (d, J = 21.0 Hz), 102.45, 36.28, 34.06 (d, J = 4.9 Hz). HPLC Purity: 99%.

Method D. General Synthesis of Selected R³ analogs (Table 3.3)

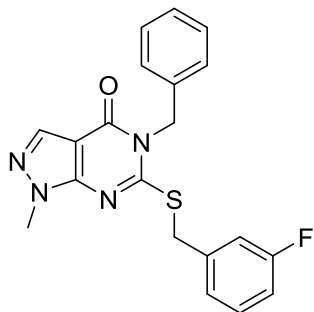
To a dry flask under N₂ charged with **3.2b** (0.24 mmol) and 2 mL dry DMF was added the appropriate amine (0.24 mmol) by syringe. The reaction was stirred at RT for 1 h and then cooled to 0°C. 60 wt. % NaH in mineral oil (0.71 mmol) was added and the flask was stirred at 0°C for 20 min then allowed to warm to RT and stirred for 3 h. The reaction was quenched with sat. aq. NH₄Cl and extracted 2x with ethyl acetate. The combined organics were dried with sodium sulfate and the solvent removed. The residue was dissolved in 2 mL DMF and 3-fluorobenzyl bromide (0.03 mL, 0.24 mmol), sodium bicarbonate (80 mg, 0.95 mmol) were added. The mixture was stirred at RT overnight at which point the reaction was complete by

HPLC. The mixture was diluted with water and extracted 2x with EtOAc. The combined organics were washed 3x with brine, dried over sodium sulfate, and the solvent removed. The crude product was purified by flash chromatography (0-100% EtOAc in Hex) yielding the titled compounds.



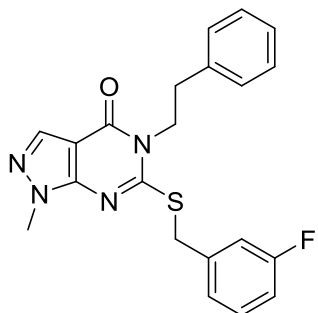
6-((3-Fluorobenzyl)thio)-1-methyl-5-(pyridin-2-yl)-1H-pyrazolo[3,4-d]pyrimidin-4(5H)-one (257914).

Method D. White needles. 40% yield. HRMS (ESI): m/z 368.0977 $[M+H]^+$ 1H NMR (500 MHz, $CDCl_3$) δ 8.69 (dd, $J = 1.47, 4.89$ Hz, 1H), 8.03 (s, 1H), 7.92 (dt, $J = 1.96, 7.58$ Hz, 1H), 7.44 - 7.49 (m, 1H), 7.38 (d, $J = 7.83$ Hz, 1H), 7.21 - 7.29 (m, 1H), 7.13 (d, $J = 7.83$ Hz, 1H), 7.06 - 7.11 (m, 1H), 6.95 (dt, $J = 2.20, 8.44$ Hz, 1H), 4.38 (s, 2H), 4.01 (s, 3H) ^{13}C NMR (126 MHz, $CDCl_3$) δ 162.70 (d, $J = 246.7$ Hz), 160.19, 157.59, 150.88, 150.26, 149.38, 138.83, 138.17 (d, $J = 7.6$ Hz), 135.52, 130.10 (d, $J = 8.5$ Hz), 125.06, 124.86, 124.81 (d, $J = 3.1$ Hz), 116.19 (d, $J = 22.0$ Hz), 114.70 (d, $J = 21.4$ Hz), 102.96, 36.66, 34.18. HPLC Purity: 98%.



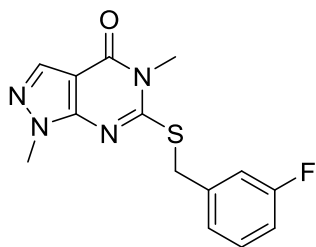
**5-Benzyl-6-((3-fluorobenzyl)thio)-1-methyl-1H-pyrazolo[3,4-d]pyrimidin-4(5H)-one
(257726).**

Method D. White crystalline solid. 57% yield. HRMS (ESI): m/z 381.1180 $[M+H]^+$ 1H NMR (500 MHz, $CDCl_3$) δ 8.02 (s, 1H), 7.22 - 7.35 (m, 6H), 7.16 (d, $J = 7.83$ Hz, 1H), 7.11 (d, $J = 9.78$ Hz, 1H), 6.97 (t, $J = 8.31$ Hz, 1H), 5.36 (br. s., 2H), 4.43 (s, 2H), 3.96 (s, 3H) ^{13}C NMR (126 MHz, $CDCl_3$) δ 162.69 (d, $J = 246.9$ Hz), 160.36, 157.77, 150.44, 138.33 (d, $J = 7.5$ Hz), 135.33, 135.20, 130.09 (d, $J = 8.3$ Hz), 128.57, 127.67, 127.28, 124.70 (d, $J = 3.1$ Hz), 116.09 (d, $J = 22.0$ Hz), 114.70 (d, $J = 21.0$ Hz), 102.58, 46.60, 36.51, 33.97. HPLC Purity: 99%.



**6-((3-Fluorobenzyl)thio)-1-methyl-5-phenethyl-1H-pyrazolo[3,4-d]pyrimidin-4(5H)-one
(258081)**

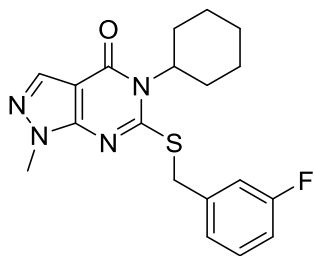
Method D. White Needles. 72% yield. HRMS (ESI): m/z 395.1341 $[M+H]^+$ 1H NMR (500 MHz, $CDCl_3$) δ 8.00 (s, 1H), 7.27 - 7.36 (m, 5H), 7.23 (t, $J = 7.58$ Hz, 2H), 7.17 (d, $J = 9.78$ Hz, 1H), 7.00 (dt, $J = 2.20, 8.44$ Hz, 1H), 4.48 (s, 2H), 4.24 - 4.31 (m, 2H), 3.96 (s, 3H), 2.97 - 3.04 (m, 2H) ^{13}C NMR (126 MHz, $CDCl_3$) δ 162.76 (d, $J = 246.8$ Hz), 159.65, 157.37, 150.47, 138.42 (d, $J = 7.6$ Hz), 137.64, 135.00, 130.18 (d, $J = 8.3$ Hz), 128.90, 128.65, 126.81, 124.76 (d, $J = 2.9$ Hz), 116.19 (d, $J = 22.0$ Hz), 114.78 (d, $J = 21.2$ Hz), 102.75, 45.68, 36.34, 34.23, 33.98. HPLC Purity: 99%.



6-((3-Fluorobenzyl)thio)-1,5-dimethyl-1H-pyrazolo[3,4-d]pyrimidin-4(5H)-one (258074)

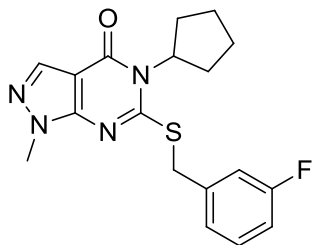
Compound **3.2b** (100mg, 0.47 mmol) was dissolved in 1 mL 8N methylamine in ethanol and stirred at RT for 1 h. The volatiles were removed and the residue was dissolved in 1 mL DMF to which sodium bicarbonate (80 mg, 0.947 mmol) and 3-fluorobenzyl bromide (70 μ l, 0.57 mmol) were added. The reaction was stirred for 1 h at which point the product was precipitated out by the addition of water. The precipitate was collected by filtration, washed with water and then hexanes. The precipitate was then taken up in dichloromethane and dried with sodium sulfate. The solvent was removed to yield the titled compound as a white crystalline solid (122mg, 0.40

mmol, 85 % yield). HRMS (ESI): m/z 305.0864 $[M+H]^+$ 1H NMR (500 MHz, $CDCl_3$) δ 7.99 (s, 1H), 7.29 - 7.35 (m, 1H), 7.24 (d, $J = 7.83$ Hz, 1H), 7.19 (d, $J = 9.78$ Hz, 1H), 7.00 (dt, $J = 2.45$, 8.56 Hz, 1H), 4.49 (s, 2H), 3.96 (s, 3H), 3.55 (s, 3H) ^{13}C NMR (126 MHz, $CDCl_3$) δ 162.74 (d, $J = 246.7$ Hz), 160.32, 157.62, 150.46, 138.42 (d, $J = 7.5$ Hz), 134.95, 130.17 (d, $J = 8.2$ Hz), 124.75 (d, $J = 2.9$ Hz), 116.17 (d, $J = 22.0$ Hz), 114.77 (d, $J = 21.0$ Hz), 102.44, 36.28, 33.95, 29.70. HPLC Purity: 99%.



**5-cyclohexyl-6-((3-fluorobenzyl)thio)-1-methyl-1H-pyrazolo[3,4-d]pyrimidin-4(5H)-one
(258466)**

Method D. White Needles (22mg, 0.059 mmol, 20.80 % yield) MS (ESI): m/z 373.1498 $[M+H]^+$ 1H NMR (500 MHz, $CDCl_3$) δ 7.93 (br. s., 1H), 7.28 - 7.37 (m, 1H), 7.23 (d, $J = 7.34$ Hz, 1H), 7.18 (d, $J = 9.29$ Hz, 1H), 7.00 (t, $J = 7.83$ Hz, 1H), 4.44 (br. s., 2H), 4.07 - 4.19 (m, 1H), 3.92 (s, 3H), 2.69 (d, $J = 10.27$ Hz, 2H), 1.88 (br. s., 2H), 1.59 - 1.77 (m, 3H), 1.30 (br. s., 3H) ^{13}C NMR (126 MHz, $CDCl_3$) δ 162.8, 160.2, 158.4, 150.0, 138.3, 134.8, 130.2, 124.9, 116.2, 114.7, 104.2, 62.2, 37.2, 33.9, 28.8, 26.5, 25.0 HPLC Purity: 96%



5-cyclopentyl-6-((3-fluorobenzyl)thio)-1-methyl-1H-pyrazolo[3,4-d]pyrimidin-4(5H)-one

(258467)

Method D. Clear faintly yellow sheets. (44mg, 0.123 mmol, 43.2 % yield) MS (ESI): m/z

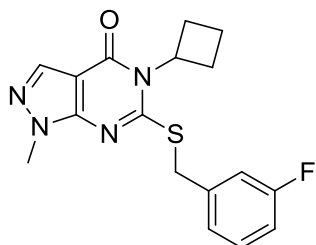
359.1346 $[M+H]^+$ 1H NMR (500 MHz, $CDCl_3$) δ 7.93 (s, 2H), 7.32 (dq, $J = 1.90, 7.30$ Hz, 1H),

7.23 (d, $J = 7.34$ Hz, 1H), 7.18 (d, $J = 9.29$ Hz, 1H), 7.00 (dt, $J = 1.90, 8.30$ Hz, 1H), 4.79 (quin,

$J = 8.44$ Hz, 1H), 4.45 (s, 2H), 3.93 (s, 3H), 2.25 - 2.37 (m, 2H), 2.01 - 2.12 (m, 2H), 1.85 - 1.96

(m, 2H), 1.55 - 1.66 (m, 2H) ^{13}C NMR (126 MHz, $CDCl_3$) δ 162.8, 160.5, 157.8, 150.1, 138.3,

134.7, 130.1, 124.8, 116.2, 114.7, 104.0, 60.5, 37.1, 33.9, 28.8, 26.0. HPLC Purity: 99%



5-cyclobutyl-6-((3-fluorobenzyl)thio)-1-methyl-1H-pyrazolo[3,4-d]pyrimidin-4(5H)-one

(258468)

Method D. White crystalline solid. (11mg, 0.032 mmol, 11.24 % yield) MS (ESI): m/z 345.1182
[M+H]⁺ ¹H NMR (500 MHz, CDCl₃) δ 7.95 (s, 1H), 7.31 (q, J = 7.5 Hz, 1H), 7.22 (d, J = 7.7 Hz, 1H), 7.17 (d, J = 9.6 Hz, 1H), 6.99 (td, J = 8.4, 2.4 Hz, 1H), 4.91 (p, J = 8.7 Hz, 1H), 4.44 (s, 2H), 3.92 (s, 3H), 3.24 (pd, J = 9.6, 2.7 Hz, 3H), 2.40 - 2.24 (m, 3H), 2.11 - 1.94 (m, 2H), 1.76 (h, J = 9.4 Hz, 1H). ¹³C NMR (126 MHz, CDCl₃) δ 162.73 (d, J = 246.7 Hz), 160.20, 158.96, 149.94, 138.38 (d, J = 7.4 Hz), 134.87, 130.14 (d, J = 8.2 Hz), 124.81 (d, J = 3.1 Hz), 116.19 (d, J = 22.0 Hz), 114.71 (d, J = 21.0 Hz), 103.87, 53.45, 36.93, 33.91, 27.66, 14.72. HPLC Purity: 97%

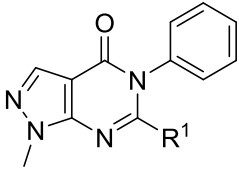
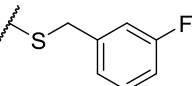
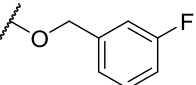
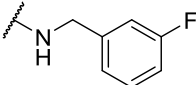
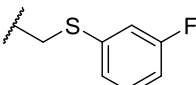
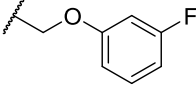
Chapter 4 Development of 2nd Generation CM39 Analogs

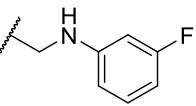
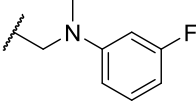
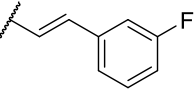
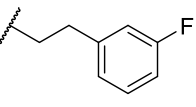
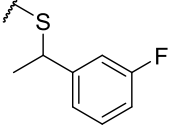
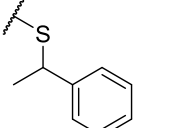
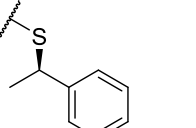
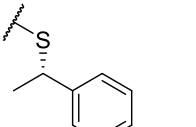
4.1. Rationale

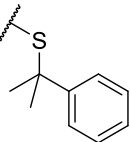
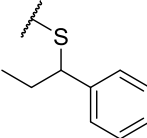
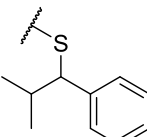
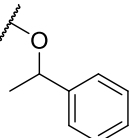
Although exemplary compounds from Chapter 3, **258083** and **258085**, provided promising ALDEFLUOR inhibition, depletion of CD133⁺ cells, and synergy with chemotherapy, several challenges in the development of compounds with in vivo efficacy remained. Namely, the relatively high ALDEFLUOR IC_{50s} (~1 μM) combined with modest solubility and metabolic stability limited our ability to cover efficacious concentrations for > 7 h. We felt that the dose limiting toxicity (weight loss) of **258085** may result from its toxicity as a single agent in 2-D cell assays, which we believe is not ALDH mediated (see Section 4.2). It is impractical to perform multi-week xenograft studies with more than one i.p. injection each day, so we sought to achieve more durable coverage of efficacious concentrations by: 1) improving cellular potency to reduce the necessary drug concentration, 2) improving solubility to enable greater exposure following i.p. administration and the potential for dose escalation, and 3) optimizing metabolic stability. Our main approach to improving the solubility and metabolic stability was to eliminate the lipophilic thioether and engage ALDH in new polar interactions to lower cLogP while improving or maintaining potency. We also explored TPSA-lowering modifications to the core heterocycle and conformational restriction as a potential avenue to improve cellular activity by improving ALDH potency and/or cell permeability. Promising compounds were tested for ALDEFLUOR and CD133 inhibition in PEO-1 cells. We performed the ALDEFLOUR assay at 1 μM, the concentration at which the exemplary compounds in Chapter 3 inhibited ~50% in the assay. A

concentration of 10 μM for the CD133 assay was chosen for the same reason. No analogs inhibited ALDH2 by $> 20\%$ at 20 μM , so the values have been removed from the tables for clarity. (All results shown are unpublished, courtesy of Buckanovich, Hurley, and Sun labs)

4.2. Optimization of Thioether Linker

Table 4.1 Optimization of the Thioether Linker								
								
CMPD No. / R ¹	ALDH ^a IC ₅₀ or ^b % Control at 20 μM			ADME Characterization			^d PEO-1 Cell Assays % Control	
	1A1	1A2	1A3	MLM t _{1/2} (min)	^c Aq. Sol (μM)	cLogP	ALDH 1 μM	CD133 10 μM
257723 	0.08 ± 0.01	0.15 ± 0.01	0.09 ± 0.01	8	< 0.7	4.3		
259011 	0.775 ± 0.031	3.7 ± 0.64	1.7 ± 0.1			3.6		
263868 	69%	73%	58%			3.0		
258475 	0.7 ± 0.2	71%	86%			3.3		
258079 	8.2 ± 0.7	1.77 ± 0.09	0.78 ± 0.09		194	2.8		

258473 	0.57 ±0.03	2.3 ±0.1	1.05 ±0.08		64	2.5		
259123 	88%	72%	74%			3.1		
258471 	0.27 ±0.06	0.44 ±0.03	79%		4	3.7		
258472 	1.0 ±0.1	41%	2.5 ±0.2		126	3.6		
262741 	0.151 ±0.003	0.11 ±0.01	0.128 ±0.005	8		4.6		
259122 	0.13 ±0.03	0.11 ±0.02	0.073 ±0.005	8	8	4.5	53 ±5	83 ±2
262548 	0.07 ±0.04	0.04 ±0.01	0.034 ±0.001	8		4.5	29 ±5	75 ±5
262703 	1.41 ±0.09	1.48 ±0.07	1.64 ±0.07			4.5	98 ±3	82 ±3

263057 	1.9 ±0.3	2.2 ±0.3	1.39 ±0.09			4.7		
262704 	0.150 ±0.003	0.179 ±0.011	0.119 ±0.001			5.0		
263639 	0.38 ±0.07	0.3 ±0.1	0.13 ±0.04			5.4		
262561 	2.4 ±0.6	^c 42%	0.6 ±0.2			3.9		
Values are expressed as ^a Mean ± SEM (n=3), ^b Mean (n=3); ^c Thermodynamic solubility analysis was performed by Analiza Inc. using quantitative nitrogen detection. (www.analiza.com), ^d Mean ± SD as determined by flow cytometry (N=3), ^e Obtained at 5 μM.(Unpublished work, courtesy of Buckanovich, Hurley and Sun labs.)								

Due to the predicted metabolic lability and calculated lipophilicity of the thioether, we reasoned that finding an alternative linker could substantially improve the metabolic stability and solubility of the series. Direct replacement of the sulfur with oxygen led to a 10-20 fold loss of potency across the ALDH1A family (Table 4.1, **259011**). Nitrogen fared worse; **263868** failed to inhibit any 1A isoforms by 50% at 5 μM.

As shown in Figure 4.1A the lack of tolerance for hydrophilic linkers by ALDH1A1 can be justified by the crystal structure 5DUM in which the four closest contacts of the sulfur are lipophilic sidechains (F171, V174, W178, V460). Conversely, the linker carbon is situated 4.1Å

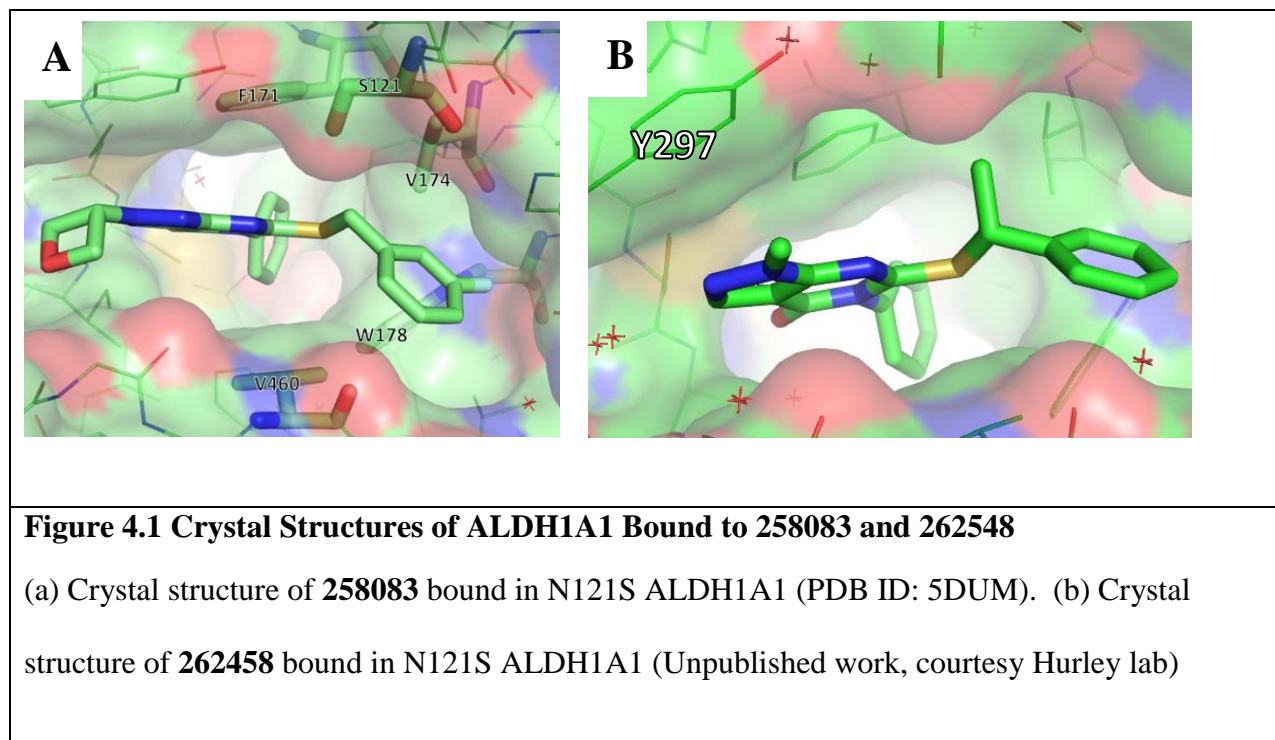
from the polar S121 sidechain (N121 in wild type ALDH1A1), suggesting that it might be favorable to reverse the position of the carbon and heteroatom in the linker. Flipping the orientation of the thioether, as in **258475**, results in greater predicted partial charge on the carbon and a significantly lower cLogP vs. **257723**; unfortunately, this change was poorly tolerated by ALDH1A.⁹⁷ Oxygen and nitrogen analogs **258079** and **258473** evidently did not engage in a favorable interaction with N121, but exhibited much improved aqueous solubility, consistent with their lower cLogP. Methylated analog **259123** abolished the remaining weak 1A1 activity of **258473**, perhaps due to an unfavorable effect of the methyl on the linker conformation.

The methylene group more closely matches the electronegativity, lipophilicity, and bond angle of sulfur than nitrogen or oxygen.¹³⁸ We next assessed the ALDH activity of alkenyl and alkyl C-C linker analogs **258471-2**. Based on the non-planar active conformation of the thioether **258083** in crystal structure 5DUM, we were surprised that rigidifying the linker in a planar conformation was only modestly detrimental to the ALDH1A1 and 1A2 binding of **258471**. Despite a moderate reduction in cLogP, this analog did not show enough improvement in aqueous solubility to justify the loss of potency and was not pursued further. We also felt that increasing the planarity was unattractive for further development. The less conformationally constrained analog **258472** was 4-fold less potent against 1A1, although it did exhibit excellent aqueous solubility. Sulfur provides unique bond geometries that are difficult to mimic with simple single atom replacements; a more sophisticated and synthetically complex bioisostere is likely required to satisfactorily mimic the sulfur.¹³⁹

Since the thioether linker proved difficult to replace while maintaining potent ALDH1A inhibition in the series, we next turned to alkyl branching as a strategy to improve solubility by reducing planarity and sterically blocking metabolism of the thioether. Methyl-branched analog

262741 was nearly equipotent against all 3 members of the 1A family. To assess whether we could simplify synthesis of further analogs, we synthesized des-fluoro analog **259122**, which gratifyingly retained potency relative to **262741** and showed a modest improvement in solubility relative to **257723**. We observed a 20:1 eudismic favoring R-enantiomer **262548** over S-enantiomer **262703**. We did not observe any difference in MLM stability between the racemate and the R-enantiomer.

Throughout the project, we observed single-agent toxicity for a number of compounds that did not seem to correlate with ALDH activity. As discussed in Chapter 3, despite having similar ALDEFLUOR activity, **258085** had single agent toxicity, while **258083** didn't. The pair of enantiomers provided the strongest evidence yet that the toxicity was off-target; inactive enantiomer **262703** was one of the most toxic compounds in the series (OVSAHO $CC_{50} = 1 \mu\text{M}$), while **262548** was non-toxic at relevant concentrations (OVSAHO $CC_{50} > 30 \mu\text{M}$). At the time, **262548** exhibited the strongest inhibition of ALDEFLUOR at 1 μM of any compound tested; conversely, **262703** was inactive.



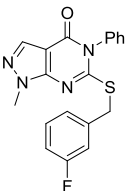
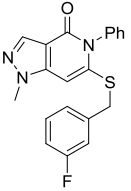
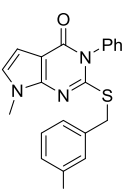
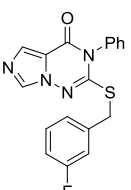
We obtained a crystal structure of **262548** (Figure 4.1 B) which indicates that **262548** adopts a very similar binding pose to **258083**. Gem-dimethyl analog **263057**, which likely presents a methyl in the same orientation as **262703** was not tolerated. The crystal structure of **262548** indicated a small cleft adjacent to the methyl which might accommodate further branching; however, ethyl-branched analog **262704** lost modest activity relative to **259122**. The bulkier isopropyl analog **263639** lost further potency against 1A1/1A2 but retained similar inhibition of 1A3. Revisiting the sulfur to oxygen substitution with our newly optimized linker resulted in a 0.6 μM 1A3 selective compound (**262561**).

Before we knew which enantiomer was active, we submitted **259122** to broad safety profiling and kinase inhibition screening (Eurofins SafteyScreen44, Eurofins Broad Oncology Kinase Panel) to assess off-target liabilities. Using 50% ligand displacement or 50% enzyme inhibition at 10 μM as a cutoff, **259122** only exhibited significant (66% ligand displacement)

binding to the CB₂ receptor. Importantly < 10% displacement of the ligand dofetilide in the hERG binding assay was observed at 10 μM. Interestingly, **259122** increased the binding of the agonist ligand to the GABA_A receptor by 51%, indicating possible positive allosteric modulation. Eurofins advises that increased binding in these assays is most frequently the result of assay interference. We also assessed permeability and PGP efflux liability utilizing the MDR1-MDCK assay (Alliance Pharma). **259122** has excellent permeability ($P_{app, A>B} = 28 \times 10^{-6}$ cm/s) and is not a PGP substrate (Efflux Ratio = 1.2).

4.3. Exploring Alternative Heterocyclic Cores

Table 4.2 Characterization of Alternative Heterocyclic Core Analogs

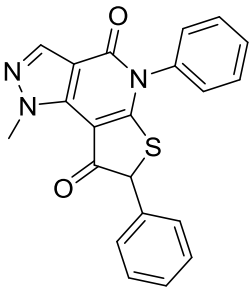
CMPD No. / Structure	^a ALDH IC ₅₀			ADME Characterization			^c PEO-1 Cell Assays % Control	
	1A1	1A2	1A3	MLM	^b Aq. Sol	cLogP	ALDH 1 μM	CD133 10 μM
257723 	0.08 ±0.01	0.15 ±0.01	0.09 ±0.01	8	<0.7	4.3		
258469 	0.240 ±0.007	0.24 ±0.02	0.14 ±0.02	9	178	4.4	97 ±1	81 ±2
258470 	0.93 ±0.05	0.81 ±0.04	0.6 ±0.1		23	5.2		
259010 	2.2 ±0.2	1.60 ±0.04	0.50 ±0.02		47	3.4		

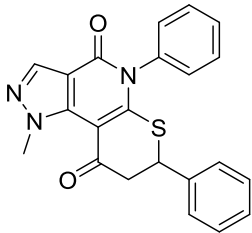
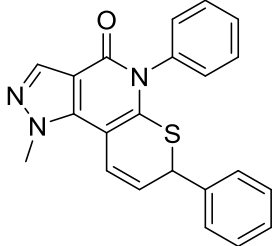
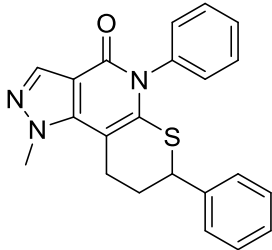
Values are expressed as ^a Mean ± SEM (n=3), ^b Thermodynamic solubility analysis was performed by Analiza Inc. using quantitative nitrogen detection. (www.analiza.com) ^c Mean ± SD as determined by flow cytometry (N=3) (Unpublished work, courtesy of Buckanovich, Hurley, and Sun labs.)

In a parallel effort to our optimization of the linker, we explored TPSA-lowering changes to the pyrazolopyrimidinone core to improve cell penetrance. As shown in Table 4.2, de-aza analog **258469** was 4-fold less potent against 1A1 than **257723**, but had substantially better aqueous solubility. Unfortunately, it was inactive against ALDELFUOR at 1 μ M. Given the similar cLogP of **258469** compared to **257723**, we hypothesize that the nitrogen of **257723** stabilizes the crystal packing leading to poorer solubility. Pyrrole and imidazole analogs **258470** and **259010** lost significantly more ALDH activity. The steep SAR for pyrazole modifications contrasts with the relatively flat SAR for pyrazole substituents. Perhaps modifying the electronics of the heterocycle unfavorably impacts the offset-parallel π - π interaction with Y297.

4.4. Conformational Restriction of the Thioether

Table 4.3 Characterization of Conformationally Restricted Analogs

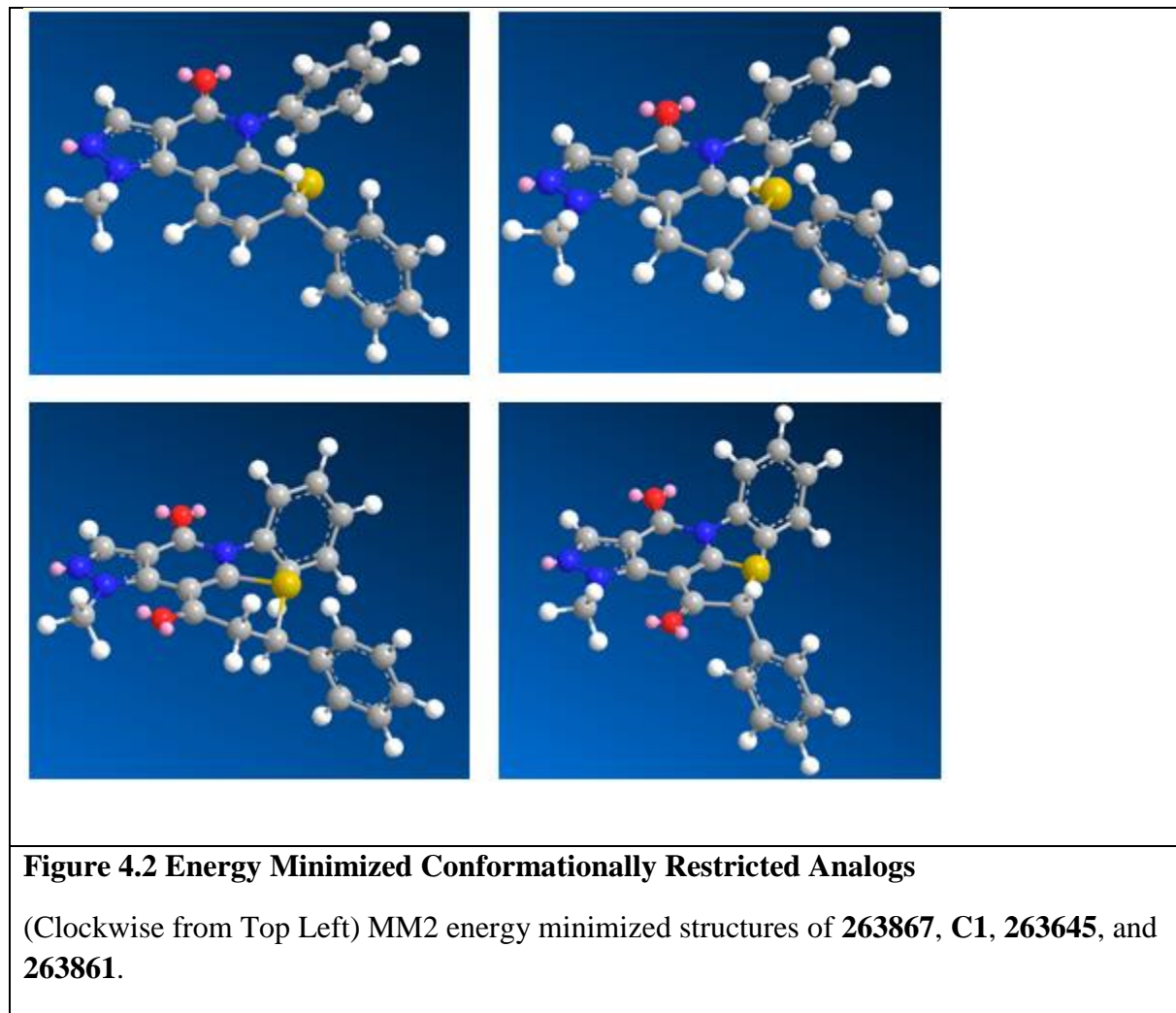
CMPD No./ Structure	ALDH ^a IC ₅₀ or ^b % Control at 20 μ M			ADME Characterization			^d PEO-1 Cell Assays % Control	
	1A1	1A2	1A3	MLM	^c Aq. Sol	cLogP	ALDH 1 μ M	CD133 10 μ M
263861 	1.0 ± 0.1	0.17 ± 0.02	0.15 ± 0.05	5	38	3.7	46 ± 3	77 ± 5

<p>263645</p> 	0.206 ±0.06	0.4 ±0.1	0.69 ±0.08	8		3.9	98 ±2	80 ±5
<p>263867</p> 	0.8 ±0.1	0.27 ±0.01	0.24 ±0.01			4.2	89 ±1	70 ±3
<p>C1</p> 						4.4		
<p>Values are expressed as ^a Mean ± SEM (n=3), ^b Mean (n=3); ^c Thermodynamic solubility analysis was performed by Analiza Inc. using quantitative nitrogen detection. (www.analiza.com) ^d Mean ± SD as determined by flow cytometry (N=3) (Unpublished work, courtesy of Buckanovich, Hurley and Sun labs.)</p>								

Upon examination of the **262548** crystal structure (as shown in 4.1B), we envisioned restricting the thioether into the active conformation by forming a 5 or 6 membered ring joining the benzylic carbon of the thioether to the 7 position of the heterocyclic core. Appropriately applied conformational restriction can lead to significant gains in potency; locking the ligand in the active conformation reduces the entropic penalty of enzyme binding which results from a loss of

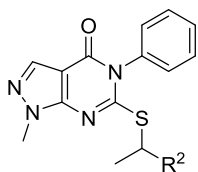
rotational degrees of freedom. Conformational restriction may also reduce binding to metabolic enzymes and other unwanted targets due to elimination of induced fit.¹⁴⁰ As shown in Table 4.3, the more rigidified analogs **263861** and **263867** favored binding to 1A2 and 1A3 with 3-to-5-fold selectivity over 1A1. Conversely the more flexible **263645** was slightly 1A1 selective.

Unfortunately the most flexible analog, **C1**, was too insoluble in DMSO or water to test. Only **263861**, the most potent 1A3 inhibitor from the series inhibited ALDEFLUOR at 1 μ M. As shown in Figure 4.1B, the C-S-C bonds of the thioether are essentially co-planar with the heterocyclic ring, while the the C-Ph bond comes slightly out of this plane to position the phenyl favorably in the 1A1 active site. Energy minimization of the 4 conformationally restricted analogs revealed that the insoluble 6-membered alkane analog **C1** most closely reproduces this geometry(Figure 4.2). 1A1 selective compound **263645** was unique among the four analogs in that the R-enantiomer most closely replicated the active conformation of **262548**. The benzylic carbon puckers out of plane to position the phenyl pseudo-equatorial. 1A2/1A3 selective analogs **263867** and **263861** project the phenyl more dramatically downward. If these minimized structures are predictive of the bound conformations, it suggests that 1A2/1A3 prefer a somewhat different conformation of the thioether than 1A1. According to the 1A1 and 1A2 crystal structures, there are not obvious differences between the 1A1 and 1A2 active sites in this region to explain this difference. The energy minimization also reveals that, due to a pseudo-biphenyl interaction between the phenyl and the 5 or 6 membered rings, the phenyl is oriented nearly perpendicular to the heterocyclic core. In the **262548** the phenyl is about 30-45 degrees out of plane. The phenyl may not be the optimal substituent for these conformationally restricted analogs.



4.5. Optimization of the Benzyl Pendant

Table 4.4 Characterization of Benzyl Pendant Modifications



CMPD. No / R ²	ALDH ^a IC ₅₀ or ^b % Control at 5 μM			ADME Characterization				^c PEO-1 Cell Assays % Control	
	1A1	1A2	1A3	MLM	^c Aq. Sol	cLogP	^d LLE	ALDH 1 μM	CD133 10 μM
259122 Phenyl	0.13 ±0.03	0.11 ±0.02	0.073 ±0.005	8	8	4.5	2.5	53 ±5	83 ± 2
263118 2-Pyridyl	0.242 ±0.02	0.063 ±0.006	0.089 ±0.007	50	20	3.4	3.2	3 ± 1	87 ± 3
264623 3-Cl-2- Pyridyl	0.46 ±0.03	0.144 ±0.004	0.33 ±0.03			4.2	2.1		
264624 3-F-2- Pyridyl	0.20 ±0.03	0.108 ±0.03	0.28 ±0.03			3.9	2.7		
263119 3-Pyridyl	0.139 ±0.001	0.089 ±0.005	0.095 ±0.016	7	209	3.3	3.6	5 ±2	89 ± 3
263640 3,5-Pyr imidinyl	0.094 ±0.007	0.38 ±0.08	0.10 ±0.03			2.6	4.4		
263350 4-Pyridyl	0.451 ±0.031	68%	45%			3.3	3.0		
C2 2-OH Phenyl									
263117 3-OH Phenyl	0.130 ±0.004	0.100 ±0.002	0.091 ±0.001	4	21	4.2	2.7	39 ±5	76 ± 4

263351 2-OMe Phenyl	0.445 ±0.021	0.136 ±0.009	0.112 ±0.011			4.3	2.1		
263353 3-OMe Phenyl	0.451 ±0.031	0.108 ±0.008	0.174 ±0.015	6	< 2	4.3	2.0		
263352 4-OMe Phenyl	0.352 ±0.024	41%	39%			4.3	2.2		
<p>Values are expressed as ^a Mean ± SEM (n=3), ^b Mean (n=3); ^c Thermodynamic solubility analysis was performed by Analiza Inc. using quantitative nitrogen detection. (www.analiza.com) ^dLLE = Lipophilic Ligand Efficiency (1A1 pIC₅₀ – cLogP) ^e Mean ± SD as determined by flow cytometry (N=3). (Unpublished work, courtesy of Buckanovich, Hurley and Sun labs.)</p>									

For synthetic ease, we retained our N-1 methyl pyrazolopyrimidinone core as we turned our attention to the optimization of the benzyl pendant with the alkyl branched linker (

Table 4.4). The crystal structure of **262548** indicated the opportunity to engage the side chains of T129 and W178 in polar interactions and potentially improve the lipophilic efficiency of our compounds, as shown in Figure 4.3. Gratifyingly, 2 and 3 pyridyl analogs (**263118-9**) retained potent biochemical inhibition of the ALDH1A family and improved the lipophilic ligand efficiency substantially. Consistent with a reduced cLogP, **263118** was more than 2-fold more soluble and 6-fold more stable in the MLM assay than **259122**.

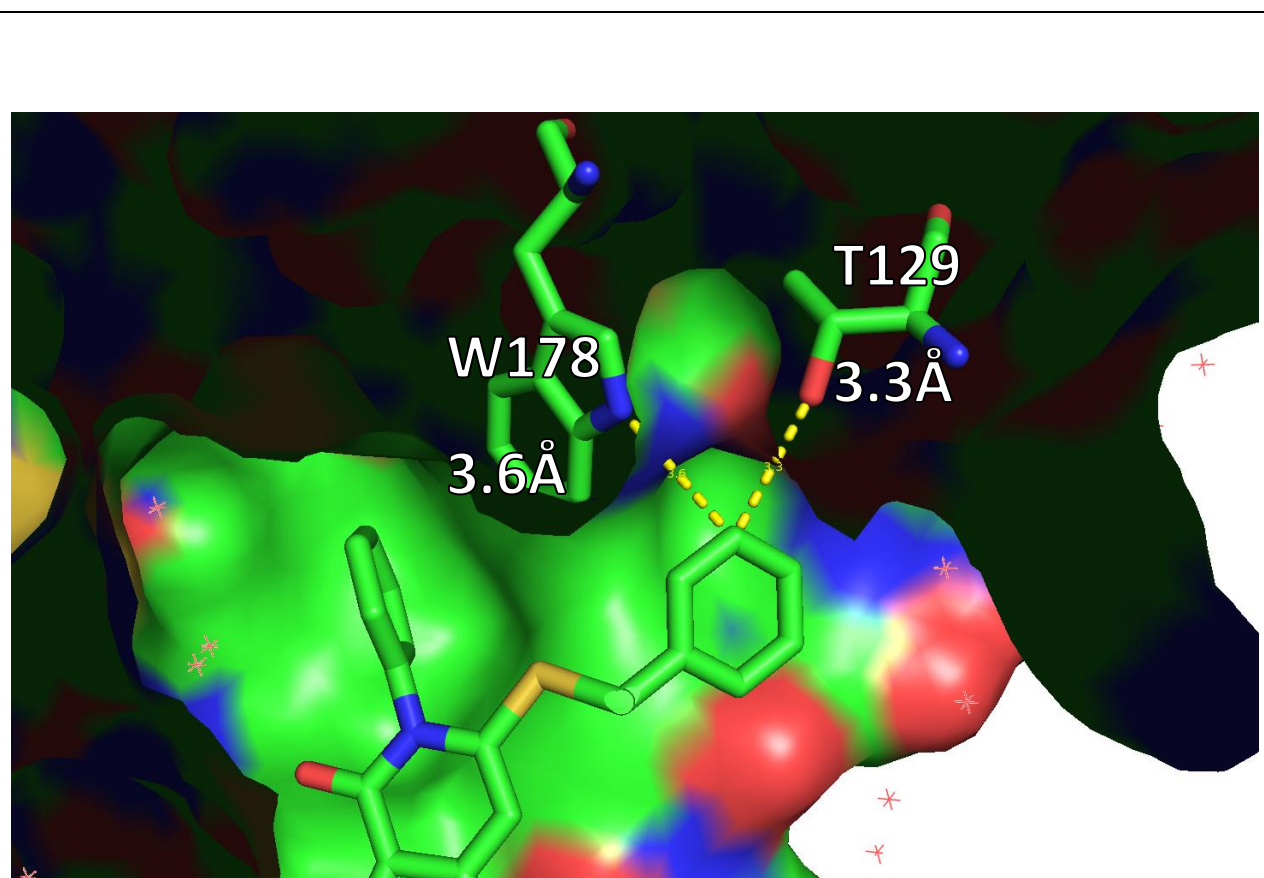


Figure 4.3 The 1A1 Crystal Structure of 262548 Indicates Potential to Engage Polar Side Chains of W178 and T129

The benzyl pendant is in close contact with polar residues W178 and T129 in ALDH1A1. (Unpublished work, courtesy Hurley lab.)

A preliminary assessment of a **263118-1A1** crystal structure (data not shown, refinement in progress) indicates a slight rightward shift in the binding mode compared to that of **262548** depicted in (Figure 4.3). This shift brings the pyridyl nitrogen in closer contact with the W178 N-H and suggests that there is indeed a hydrogen bonding interaction. Because the meta position of **262548** is already in the optimal location for hydrogen bonding with **W178** and **T129** we predict that **263119** would not exhibit the same shift in binding mode. The 3,5-pyrimidinyl analog **263640** retained strong 1A1 and 1A3 inhibition but was 4-fold less effective against 1A2. Driven by a substantial reduction in cLogP, this compound has the best lipophilic efficiency, with respect to 1A1, of any compound to date. The 4-pyridyl was not expected to make productive polar interactions and showed diminished activity across the ALDH1A family. 3-phenol analog **263117** was similarly potent against the 1A family as the 3-pyridyl analog, but was less soluble and stable in the MLM assay. Examination of a preliminary crystal structure of **263117** (data not shown, refinement in progress) indicates that this compound engages W178 and T129 without the shift in binding mode observed for **263118**. Interestingly, the 2-phenol analog **C2** was unstable under basic conditions in organic solvent and in PBS buffer, rapidly decomposing to afford the thiol **S4.1b** (See Scheme 4.1). Presumably a small amount of the phenoxide was formed under neutral conditions and was able to abstract the nearby proton β to the sulfide leading to an irreversible elimination. The methoxy analogs (**263351**, **263353**) were tolerated by 1A2 and 1A3 but somewhat disfavorable to 1A1 binding. The 4-methoxy analog was a weak 1A1 selective inhibitor, similar to the 4-pyridyl analog. Overall, polar substituents at the 3-position (**263119**, **263117**, **263353**) had little impact on metabolic stability, while 2-pyridyl substituted **263118** was substantially more stable. While both pyridyl analogs should reduce CYP 450 mediated metabolism at distant sites by reducing cLogP, the less hindered 3-pyridyl of

263119 may be susceptible to N-Oxidation.¹³⁷ Gratifyingly, both pyridyl substituted analogs inhibited ALDEFLUOR by >90% at 1 μ M. The more potent ALDEFLUOR inhibition did not translate to greater CD133⁺ depletion relative to **259122**.

4.6. Exploring Polar *p*-Phenyl Substituents

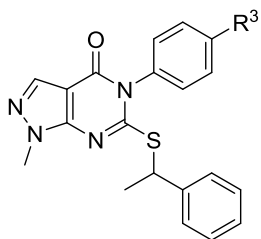
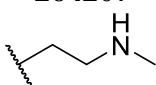
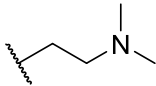
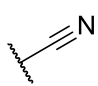

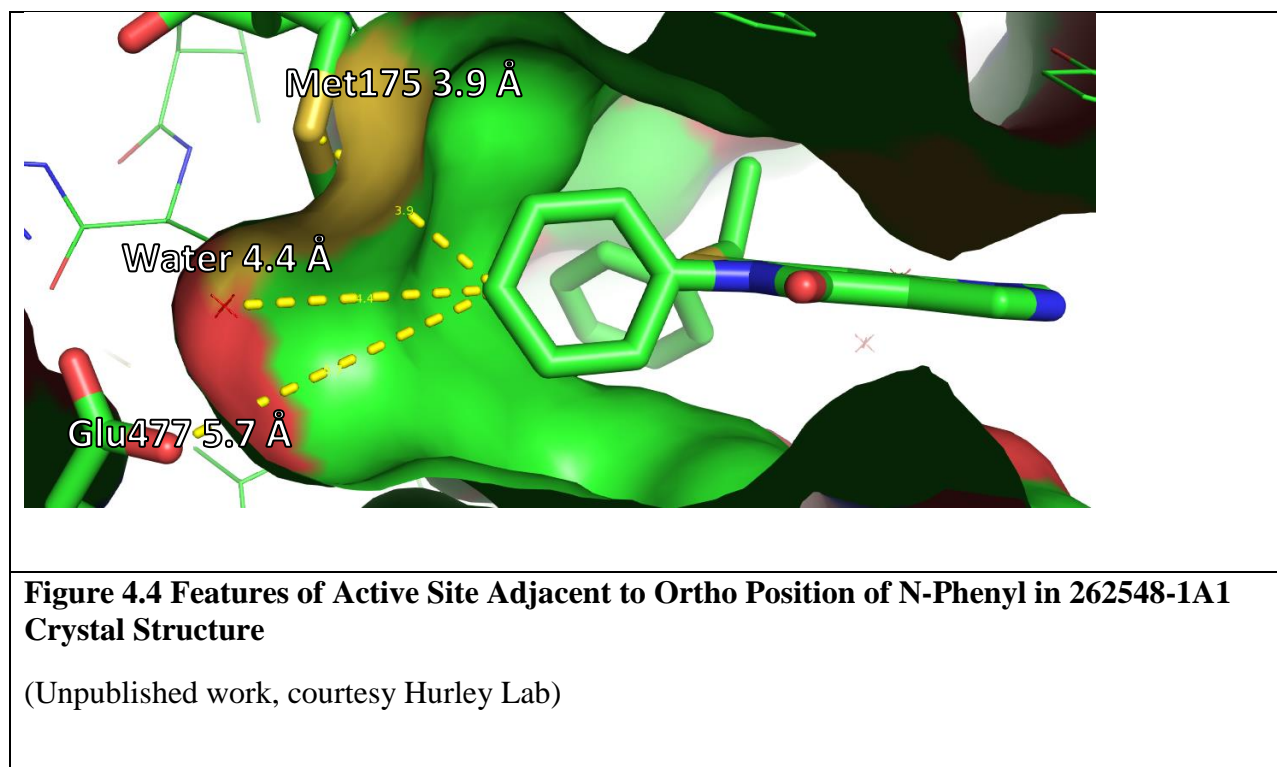


Table 4.5 Characterization of *p*-Phenyl Substituted Analogs

CMPD No./ R ³	ALDH ^a IC ₅₀ or ^b % Control at 5 μM			ADME Characterization	
	1A1	1A2	1A3	MLM	cLogP
263642 	0.6 ±0.2	0.60 ±0.05	1.0 ±0.5		3.7
263862 	65%	61%	8 ±8		4.4
263863 	0.36 ±0.09	0.216 ±0.003	3.0 ±0.1		4.0
263864 	27%	54%	34%		4.6
264203 	47%	64%	56%		3.6
264200 	58%	70%	57%		4.0
264201 	47%	86%	53%		4.4
264205 	39%	45%	50%		3.9

264207 	89%	94%	80%		4.3
264206 	100%	91%	61%		4.7
264202 	55% ^c	3.1 ± 0.2	0.200 ± 0.009	1	4.3
264626 	N.I. ^c	0.8 ± 0.1	0.52 ± 0.05		4.6

Values are expressed as ^a Mean ± SEM (n=3), ^b Mean (n=3); ^c % Control at 20 μM. (Unpublished work, courtesy of Hurley and Sun labs.)



The **262548** crystal structure also indicated the presence of a water and E477 4.4 and 5.7 Å and away from distal carbon of the N-phenyl substituent, respectively (Figure 4.4). Although none of our attempts to engage these features improved the potency relative to proteo analog **259122**, comparison of alcohols **263642**, **263863** and ethers **263862**, **263864**, indicates a clear preference by ALDH1A for hydrogen bond donors in this region. In contrast to the 1A3 selectivity observed for –Cl and –OMe substituents (see **Table 3.3**), **263863** achieved 10-fold selectivity for 1A1-1A2 over 1A3. Examination of a **263642-1A1** crystal structure (data not shown, refinement in progress) indicates that the methylene of the benzyl alcohol substituent is situated very close to Met175 with the OH pointed in the direction of the water and Glu477 as we predicted. Appending basic amines, in an attempt to form a salt bridge with Glu477, was not tolerated across the 1A family (**264200-1**, **264203-7**). We postulate that the desolvation penalty for the charged species is too great to be offset by a non-optimal polar interaction. The ability of Glu477 to interact with basic amines is likely diminished by the neighboring Lys179. Serendipitously, nitrile **264202**, an intermediate in an abandoned synthetic route to **264203**, is the most potent, selective 1A3 inhibitor disclosed to our knowledge. We performed docking studies using the 1A2 crystal structure and 1A3 homology model to rationalize the observed selectivity. As shown in Figure 4.5, our docking model indicates that the nitrile of **264202** projects deep into the active site of 1A3 and is able to engage the catalytic cysteine. The predicted binding mode in 1A2 is shallower, preventing engagement of the catalytic cysteine. The pyrimidinone carbonyl engages the adjacent non-catalytic cysteine in both models. Due to a clash between the nitrile and Met175, we predict that **264202** could not adopt the “new” binding mode with the N-Phenyl substituent pointing toward the catalytic cysteine in 1A1. Given the typical metabolic stability of electron rich aryl nitriles, we speculate that the poor stability (MLM $t_{1/2}$ = 1 min) of this

compound may result from the nitrile forming a favorable interaction with a metabolic enzyme, promoting metabolism at a distant site. Terminal alkynes possess similar linear geometry as nitriles, but are not sufficiently electrophilic to participate in semi-covalent interactions with cysteine. In support of our binding hypothesis, the alkyne **264626** was 2-fold less potent against 1A3 than the nitrile, consistent with loss of cysteine engagement. **264626** was greater than 3-fold more potent against 1A2. The increase in potency against 1A2 suggests that there is a significant desolvation penalty for the polar nitrile to bind deep in the active site. This desolvation penalty may partially offset the favorable interaction with the cysteine in 1A3, explaining why a greater increase in potency was not observed upon engaging the cysteine. The alkyne substituent is about 1 Å longer than the nitrile, likely worsening the clash with Met175 in 1A1.

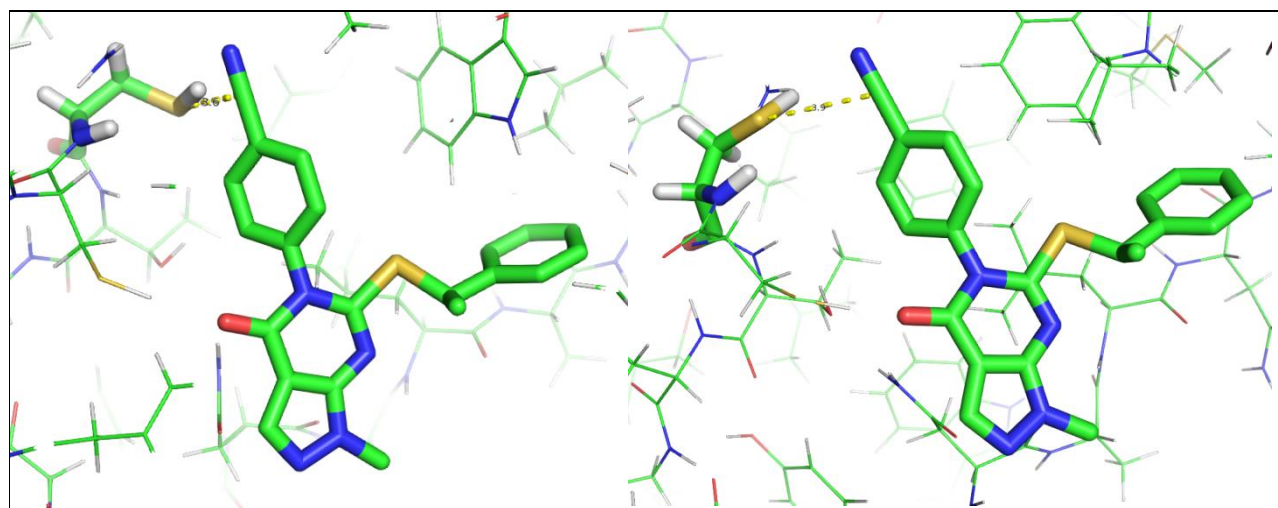
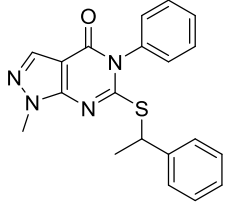
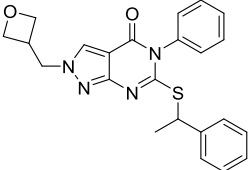
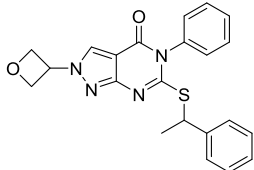
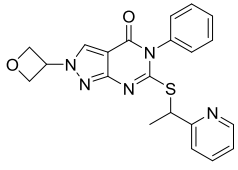
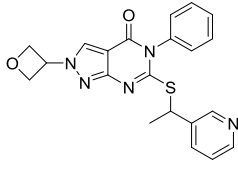


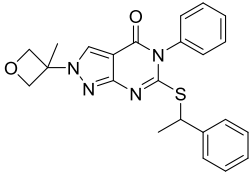
Figure 4.5 Homology Model Docking to Rationalize 1A3 Selectivity of Nitrile 264202

(Left) Docking **264202** into ALDH1A3 homology model active site indicates the nitrile carbon is near the catalytic cysteine sulfur (3.6 Å). (Right) Docking **264202** into 1A2 (PDB ID: 6B5H) predicts a shallower binding mode with the cysteine sulfur 3.9 Å away from the nitrile carbon. (Unpublished work, courtesy Neamati lab.)

4.7. Combining Optimal Thiol and Pyrazole Substituents

Table 4.6 Characterization of Optimized Compounds

CMPD No. Structure	ALDH ^a IC ₅₀			ADME Characterization				^c PEO-1 Cell Assays % Control	
	1A1	1A2	1A3	MLM	^b Aq. Sol	cLogP	LLE	ALDH 1 μM	CD133 10 μM
259122 	0.13 ±0.03	0.11 ±0.02	0.073 ±0.005	8	8	4.5	2.5	53 ±5	83 ±3
262547 	0.10 ±0.04	0.08 ±0.02	0.060 ±0.01	19	77	4.8	2.5	13 ±3	86 ±9
263052 	0.109 ±0.004	0.065 ±0.006	0.109 ±0.004	47	26	4.8	2.2	2 ±0.3	74 ±1
263646 	0.068 ±0.02	0.021 ±0.01	0.048 ±0.013	>60	60	3.7	3.5	0.8 ±0.5	79 ±3
264627 	0.118 ±0.008	0.058 ±0.001	0.25 ±0.02			3.6	3.3		

264199	0.093 ±0.02	0.112 ±0.012	0.050 ±0.003	>60		5.1	1.9	10 ±3	64 ±1
									
Values are expressed as ^a Mean ± SEM (n=3), ^b Thermodynamic solubility analysis was performed by Analiza Inc. using quantitative nitrogen detection. (www.analiza.com) ^c LLE = Lipophilic Ligand Efficiency (1A1 pIC ₅₀ – cLogP) ^c Mean ± SD as determined by flow cytometry (N=3) (Unpublished work, courtesy of Buckanovich, Hurley and Sun labs.)									

As shown in Table 4.6, we combined our optimized thiol substituents with the pyrazole substituents disclosed in Chapter 3. Homologated oxetanyl analog **262547** exhibited potent pan-ALDH1A inhibition, as well as improved solubility and metabolic stability relative to **259122**. Oxetanyl analog **263052** maintained comparable ALDH1A activity and more than doubled the MLM stability of **259122**. As discussed below, the improved MLM stability did not correlate well with in vivo exposure.

To aid in understanding this discrepancy, we obtained in vivo metabolite ID for **263052** which revealed the oxetane and thioether to be the two sites of metabolism (Figure 4.6). Interestingly, the presence of **M6** may suggest the role of epoxide hydrolase in the metabolism of the oxetane; however, such a transformation has also been attributed to CYP mediated metabolism alone.¹⁴¹⁻¹⁴³ The most abundant **M8**, **M9** species resulted from metabolism of both the oxetane and thioether.

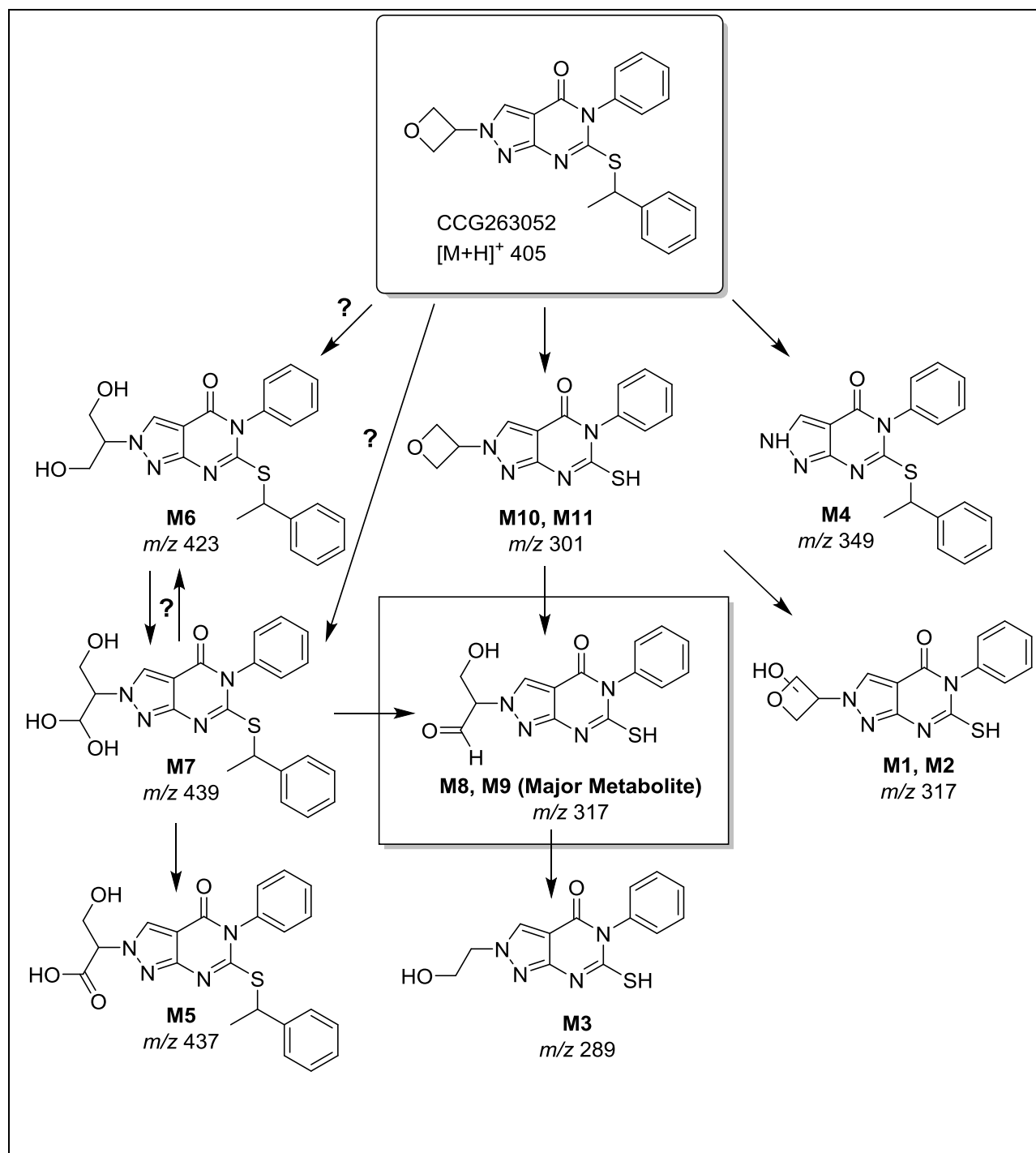


Figure 4.6 In Vivo Metabolites Identified for 263052

Ambiguous metabolic pathways denoted with question marks.
 (Unpublished work, courtesy Sun Lab)

With the intent of reducing overall metabolism by reducing cLogP, we synthesized 2-pyridyl analog **263646** which gratifyingly exhibited excellent MLM stability and good solubility. Relative to **263118**, **263646** improved inhibition across the 1A family. 3-pyridyl analog **264627** did not gain potency relative to **263119**. As discussed above, the 2-pyridyl substituent requires a subtle change in binding mode to form a hydrogen bond with W178, while the 3-pyridyl is aligned without such a shift. Comparison of the binding modes for **258083** and **262548** (Figure 4.7) indicates a subtle shift in the orientation of the heterocyclic core, likely to accommodate the N-2 pyrazole substituent in **258083**. The changes to accommodate the pyridyl and oxetanyl substituents are likely complementary, explaining the increased potency. In contrast, the shift facilitated by the oxetane is not favorable for the 3-pyridyl substituent because the binding mode of **262548** already presents the 3 position in the optimal geometry to interact with W178 and T129.

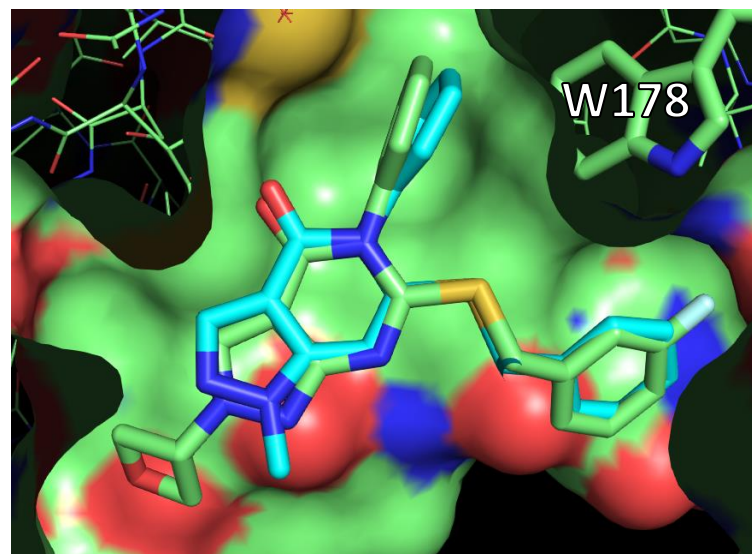


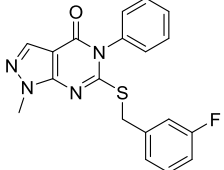
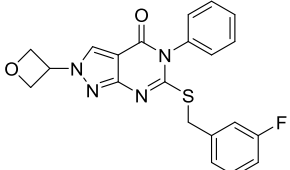
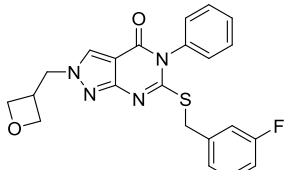
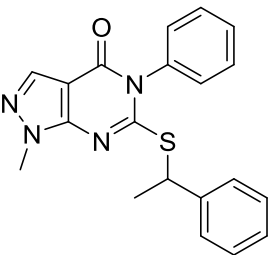
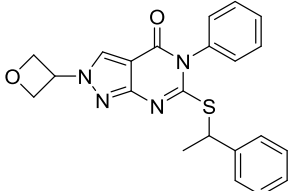
Figure 4.7 Overlay 258083 and 262548 From Their Respective 1A1 Crystal Structures

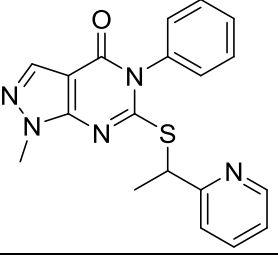
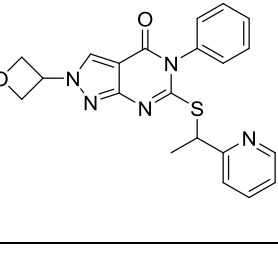
Compound **258083** (PDB ID: 5DUM, green) and **262548** (Unpublished work, courtesy Hurley lab, blue) overlaid in 1A1 active site.

264199 demonstrates that sterically blocking the oxetane is also effective at improving MLM stability. All of the N-2 pyrazole substituted analogs were potent inhibitors of ALDEFLUOR and **264199** exhibited especially strong depletion of CD133⁺ cells.

4.8. Analysis of Pharmacokinetic Data for the CM39 Series

Table 4.7 Pharmacokinetic Characterization of Selected Compounds

CMPD No./ Structure	^b Pharmacokinetic Parameters							
	ADME Properties			10mg/kg i.p.			20mg/kg p.o.	
	cLogP	^a Aq. Sol	MLM	AUC _{0-7h} ^{obs} (hr·μM)	^c t _{1/2} (h)	CMax (μM)	AUC _{0-7h} ^{obs} (hr·μM)	CMax (μM)
257723 	4.3	<0.7	8	36 ^d	0.9	24.3 ^d		
258083 	4.7	5	23	27.8	2.6	7.6		
258085 	4.7	53	27	11	0.9	5.6		
259122 	4.5	8	8	4.9	1.8	2.3	3.9	0.8
263052 	4.8	26	47	19.5	2.1	7.9		
263118	3.4	20	50	7.9	1.2	3.9	17.4	7.3

								
263646	3.7	60	>60	3.5	0.6	3.3	6.2	3.9
								
264199	5.1		>60	23	1.6	7.0		
^a Thermodynamic solubility analysis was performed by Analiza Inc. using quantitative nitrogen detection. (www.analiza.com), ^b Results expressed as Mean (N=3) following a single administration as specified, ^c Calculated using 2 and 4 hour timepoints only, ^d Compound administered at 20 mg/kg i.p. (Unpublished work, courtesy Sun Lab)								

As shown in Table 4.7, despite significant improvements in MLM stability and aqueous solubility, none of the compounds attained the level of exposure observed for **258083**. Analysis of the 7 compounds (Figure 4.8) administered at 10 mg/kg i.p. indicated poor correlation between the MLM stability and AUC (**257723** was excluded because it was administered at 20 mg/kg). Comparing the in vivo and MLM half-lives for all 8 compounds revealed a similar lack of correlation. Conversely, increased cLogP was associated with increased AUC and in vivo half-life. None of the compounds with $c\text{LogP} \leq 4.5$ exceeded an AUC of $10 \text{ hr} \cdot \mu\text{M}$ following 10 mg/kg i.p. injection (**257723** ($c\text{LogP} 4.3$) would have exceeded $10 \text{ hr} \cdot \mu\text{M}$ at 10 mg/kg assuming

a linear relationship between dose and exposure). These preliminary PK studies measure the total drug level in the plasma following protein precipitation with acetonitrile; they do not consider plasma protein binding or volume of distribution. A possible explanation for these results is that lowering the cLogP is decreasing partitioning into tissue and/or plasma protein binding, leading to decreased volume of distribution. The higher fraction of unbound drug in the plasma would facilitate greater clearance. Additionally, MLM studies may not correlate to intrinsic clearance because 1) hepatocytes contain metabolic enzymes not present in microsomes, 2) hepatocytes may uptake drugs via active transport mechanisms increasing clearance, 3) ALDH1 isoforms comprise about 0.4% of the soluble protein in human liver tissue, potentially leading to further partitioning of potent ALDH inhibitors into the liver.¹⁴⁴⁻¹⁴⁵ The better oral exposure for **263118** and **264646** relative to the i.p. study conflicts with the hypothesis that the unbound drug is rapidly cleared since following oral administration, compounds are subjected to first pass metabolism. Compounds with low plasma protein binding and high intrinsic clearance are expected to be very susceptible to first pass metabolism. It is possible that solubility limited exposure in the i.p. study of the two compounds but that the pyridyl promoted greater solubility in the low pH of the stomach. Consistent with this, compound **259122**, which does not contain a pyridyl, exhibited worse exposure following oral administration relative to i.p., although extensive first pass metabolism could also explain this result.

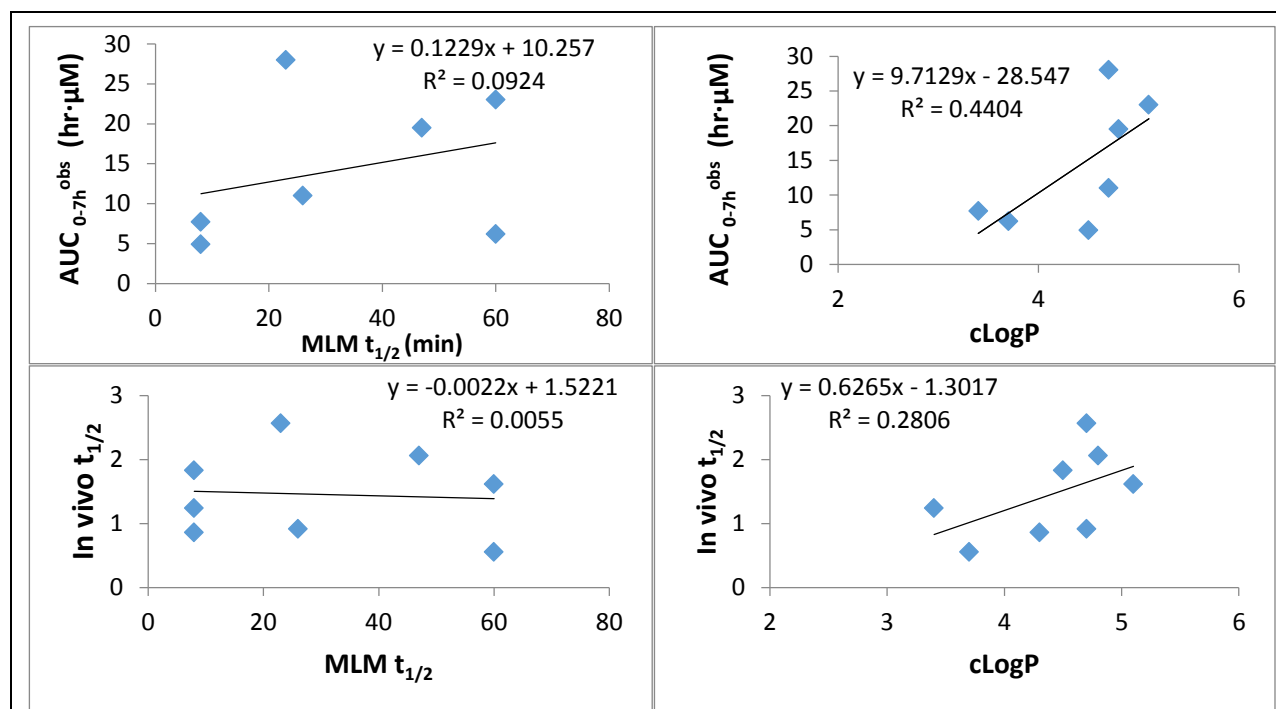


Figure 4.8 Analysis of Correlation Between cLogP, MLM stability, and In Vivo Exposure and Stability.

(Top) Plot and trendline depicting the correlation between AUC and MLM $t_{1/2}$ or cLogP for the 7 compounds in Table 4.7 (excluding 257723). (Bottom) Plot and trendline depicting the correlation between in vivo half-life and MLM $t_{1/2}$ or cLogP for the 8 compounds in Table 4.7.

4.9. Conclusions

Encouraged by the promising synergy with cisplatin for several analogs discussed in Chapter 3, we set out to create analogs of **CM39** with improved ALDEFLUOR activity and pharmacokinetic properties. While replacement of the metabolically labile and lipophilic thioether linker was not successful, disrupting planarity with alkyl branching resulted in improved solubility for **259122** relative to **257723**. Synthesis of the two enantiomers **262548** and **262703** revealed that the R-enantiomer **262548** possessed 20-fold greater ALDH activity and greater ALDEFLUOR inhibition. Inactive enantiomer **262703** was potentially cytotoxic as a single

agent, indicating that the single agent cytotoxicity possessed by some analogs in the series is very likely off target. Efforts to alter the pyrazolopyrimidinone core or conformationally restrict the thioether did not afford any advantageous compounds. Exploring polar substituents to engage the W179 and T129 was more fruitful. While 2 and 3 pyridyl substituents did not result in increased enzymatic 1A1 potency relative to phenyl, they improved solubility, lipophilic efficiency, and ALDEFLUOR potency. Crystal structures of the 2-pyridyl and 3-hydroxyl analogs **263117-8** indicate engagement with W179 in 1A1, but a desolvation penalty may counteract this favorable interaction. The 2-pyridyl analog **263118** also improved metabolic stability 6-fold relative to phenyl analog **259122**. Pyrimidinyl analog **263640** demonstrated that further increases in polarity in this region are tolerated, and more polar substituents will be explored in this region.

While attempts to engage polar residues deep in the active site were not successful in improving potency, they did result in compounds with interesting isoform selectivity. To our knowledge, nitrile analog **264202** is the most potent and selective ALDH1A3 selective inhibitor to date. Finally combining the optimal linker and pyridyl substituents with the oxetane substituents discussed in Chapter 3 resulted in compounds with excellent MLM stability and ALDEFLUOR inhibition. Steric blocking of the oxetane, which was identified as a site of in vivo metabolism also resulted in improved MLM stability. Studies to determine the synergy with cisplatin for optimal compounds are underway.

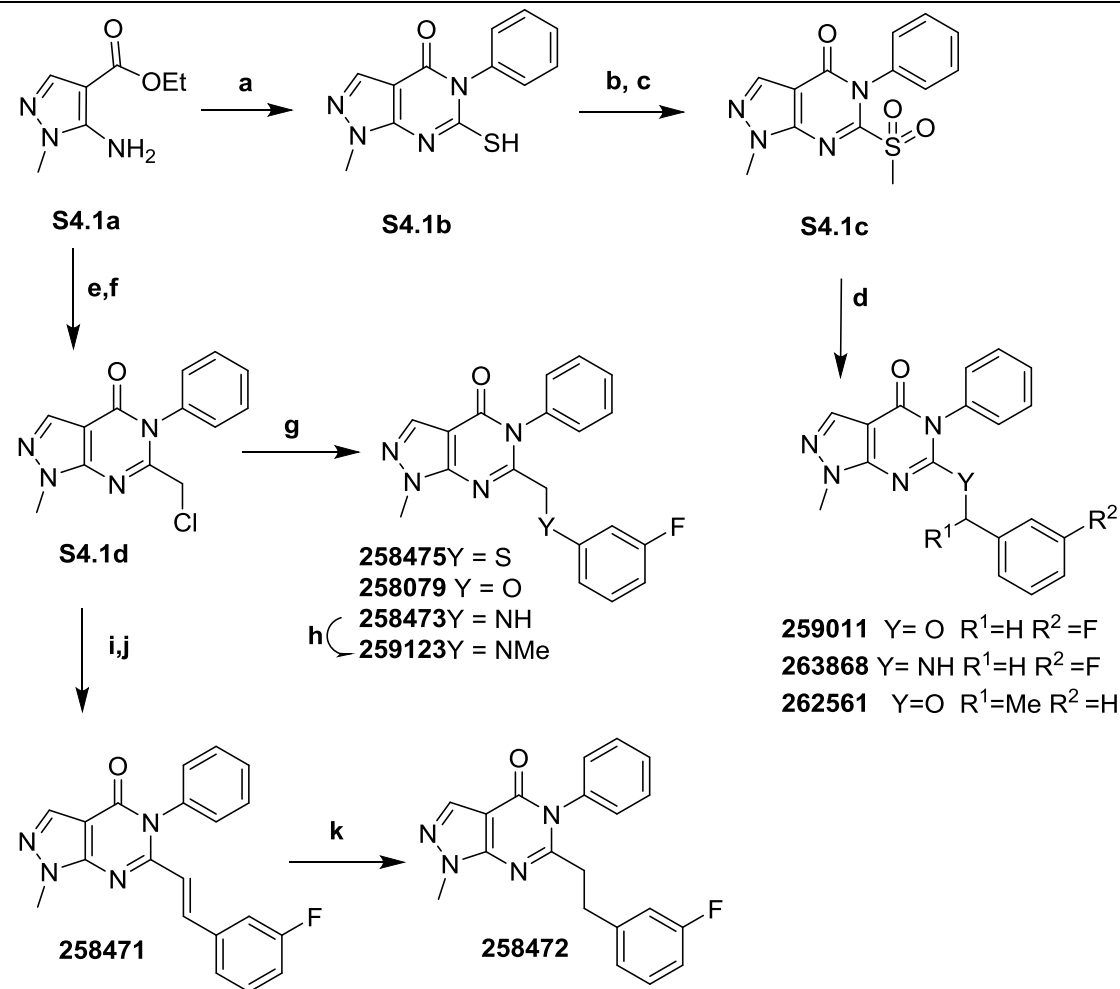
Unfortunately, analysis of the short PK studies obtained for analogs in this series indicated a poor correlation between MLM stability and in vivo exposure. There was a stronger correlation between cLogP and in vivo exposure. The 4 aromatic rings in the series are a significant liability in terms of clinical developability. Employing the property forecast index

(PFI, $\text{ChromLogD}_{7.4} + \text{\#Aromatic Rings}$), compounds with 4 aromatic rings would need a measured LogD of < 1 in order to have a reasonable probability of success (PFI < 5) in pre-clinical development.¹⁴⁶ Major factors in devising the PFI were susceptibility to clearance and poor solubility associated with highly aromatic, lipophilic compounds. Early efforts to reduce the aromatic ring count will be disclosed in the following chapter.

4.10. Chemistry

As shown in Scheme 4.1, synthesis of analogs **259011**, **262562**, and **263868** started with addition of commercially available pyrazole **S4.1a** to phenyl isothiocyanate in the presence of NaH followed by spontaneous cyclization. Methylation of the thiol followed by *m*CPBA-mediated oxidation of resulting sulfide afforded the sulfone **S4.1c**, which could be displaced with the appropriate amine or alcohol under basic conditions to afford **259011**, **262562**, and **263868**. Synthesis of reversed linker analogs began with the *n*BuLi mediated addition elimination reaction between ester **4.1a** and aniline to afford the phenyl amide. Subsequently, treatment with chloroacetyl chloride in a melt of chloroacetic acid to afforded compound **S4.1d**. Employing acetic acid as a solvent exclusively afforded the des-chloro analog, presumably resulting from formation of a mixed anhydride and subsequent nucleophilic attack at the less hindered acetate. The chloride could be directly displaced with the appropriate phenol, thiophenol, or aniline at moderate temperatures to afford analogs **258475**, **258079**, **258473**. Alkylation of amine **258473** with methyl iodide afforded the tertiary aniline **258471**. Alkenyl analog **258471** was generated by displacement of the **S4.1d** with P(OEt)₃ and subsequent Horner-Wadsworth-Emmons olefination with 3-fluorobenzaldehyde. Pd-C catalyzed hydrogenation of the alkene afforded **258472**.

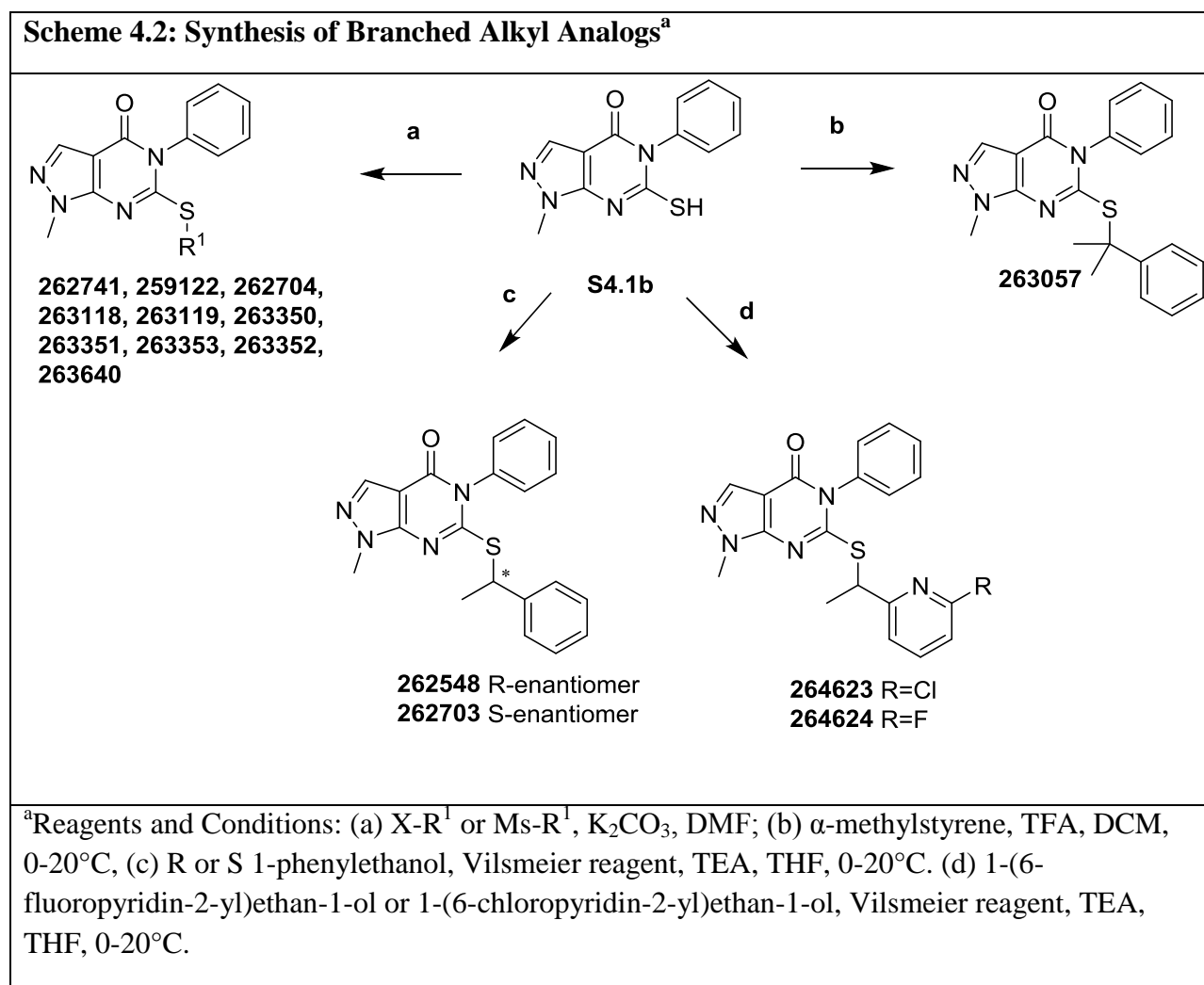
Scheme 4.1 Synthesis of Modified Linker Analogs^a



^aReagents and Conditions: (a) PhNCS, NaH, DMF, 0-50°C; (b) K₂CO₃, MeI, DMF; (c) *m*CPBA, DCM; (d) NaH, 3-fluorobenzylamine or 3-fluorobenzyl alcohol, DMF, 0-20°C; (e) *n*BuLi, aniline, THF, -78°C to RT; (f) chloroacetic acid, chloroacetyl chloride, 80-120°C; (g) 3-fluorophenol or 3-fluorothiophenol or 3-fluoroaniline, K₂CO₃, DMF, 50 or 70°C; (h) MeI, K₂CO₃, DMF, 50°C; (i) P(OEt)₃, DMF, 150°C; (j) NaH, 3-fluorobenzaldehyde, DMF, 0-20°C; (k) Pd-C, H₂, MeOH.

As shown in Scheme 4.2, the 10 listed branched alkyl analogs were generated by displacing the appropriate halide or mesylate with thiol **S4.1b** in the presence of potassium carbonate. The R and S enantiomers of **259122** were obtained by first activating enantiopure 1-phenylethanol with the Vilsmeier reagent. Subsequent displacement by thiol **S4.1b** with

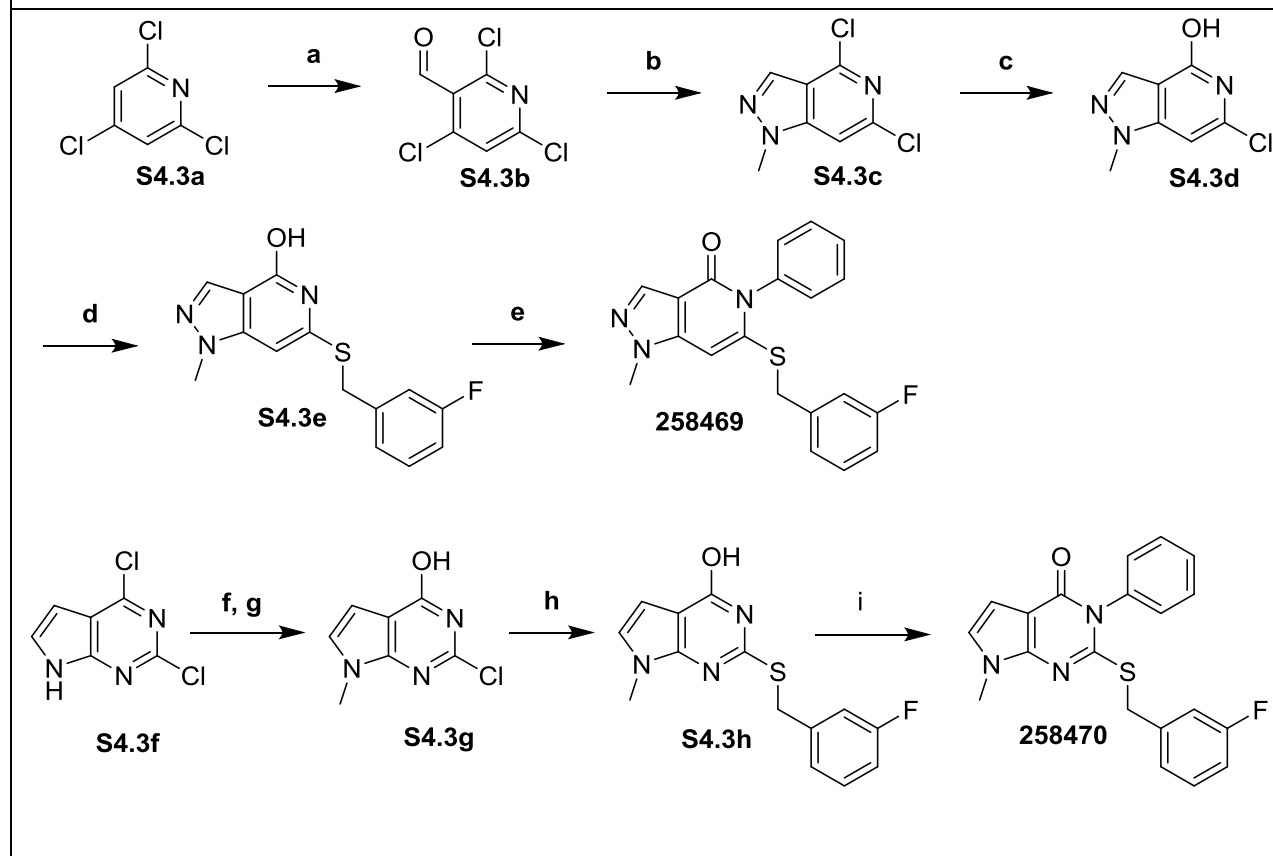
complete inversion of stereochemistry afforded enantiomers **262548** and **262703**.¹⁴⁷ Mitsunobu conditions provided the products in inferior yield and enantiopurity. The pyridine halide analogs **264623-4** were generated under the analogous Vilsmeier reagent mediated conditions with the appropriate benzyl alcohol. The gem-dimethyl analog **263057** was formed by treating thiol **S4.1b** with α -methylstyrene under acidic conditions.



As shown in Scheme 4.3, Synthesis of de-aza analog **258469** began by lithiating **S4.3a** and quenching with ethyl formate to afford aldehyde **S4.3b**. The pyrazole was formed by treating **S4.3c** with methyl hydrazine. The 4-chloro was selectively hydrolyzed by briefly

heating a slurry of **S4.3c** in aqueous NaOH to 140°C in a microwave synthesizer.¹⁴⁸ Vigorous heating was required to displace the remaining chloride with 3-fluorobenzyl mercaptan forming **S4.3e**. Finally, Chan-Lam coupling with phenylboronic acid afforded **258469**. Pyrrole **258470** was prepared in a similar manner following methylation of commercially available **S4.3f**.

Scheme 4.3: Synthesis of De-aza Analogs 258469-70^a

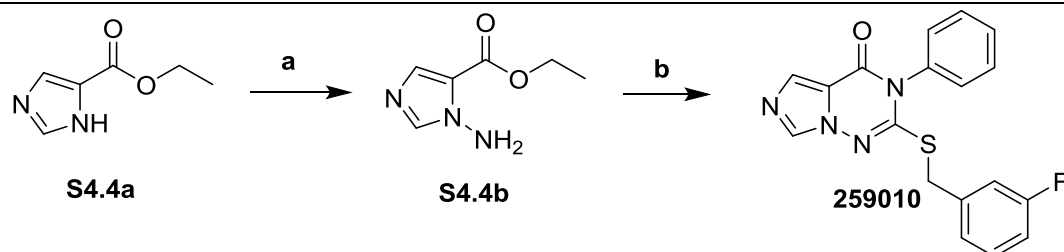


^aReagents and Conditions: (a) *n*-BuLi, ethyl formate, THF, -78 – 20°C; (b) methyl hydrazine, TEA, EtOH, -78 – 20°C; (c) 10% aq. NaOH 140°C Microwave; (d) 3-fluorobenzyl mercaptan, DIPEA, *n*-BuOH, 170°C Microwave; (e) PhB(OH)₂, Cu(OAc)₂, pyridine, TEMPO, 3 Å MS, Air, DCE; (f) MeI, NaH, THF, 0 – 20°C; (g) 10% aq. NaOH, Reflux; (h) 3-fluorobenzyl mercaptan, DIPEA, EtOH, 100°C; (i) PhB(OH)₂, Cu(OAc)₂, pyridine, 3 Å MS, Air, DCM.

Synthesis of analog **259010** began by treating imidazole **S4.4a** with the electrophilic NH₂ source *O*-(diphenylphosphinyl)hydroxylamine and LiHDMS (Scheme 4.4).¹⁴⁹ Subsequently,

thiourea formation, cyclization and displacement of 3-fluorobenzyl bromide in one pot afforded imidazole analog **259010**.

Scheme 4.4: Synthesis of Analog 259010^a

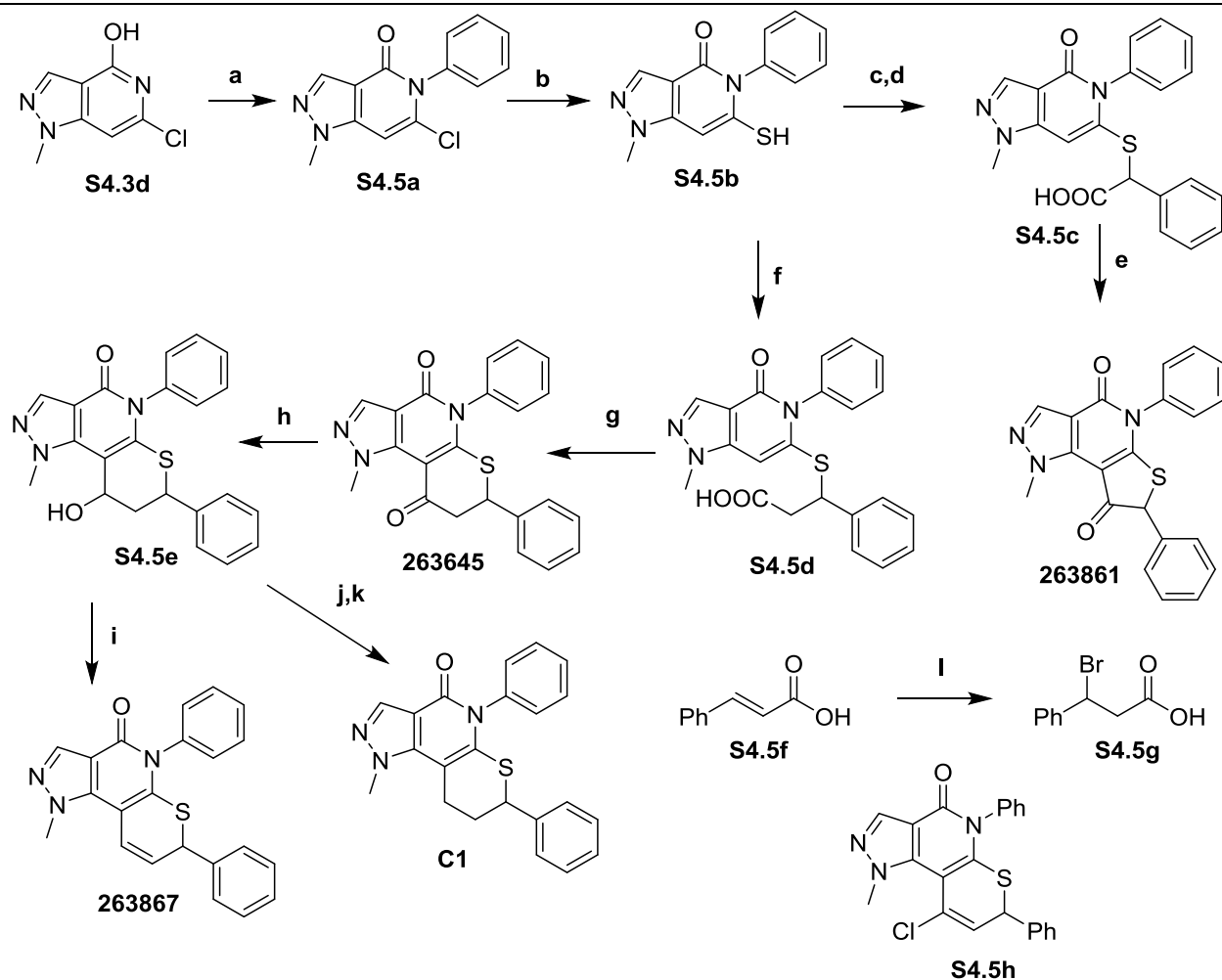


^aReagents and Conditions: (a) *O*-(diphenylphosphinyl)hydroxylamine, LiHDMS, DMF, -10 – 20°C; (b) PhNCS, NaH, 3-fluorobenzyl bromide, DMF, 0 - 20°C.

As shown in Scheme 4.5, synthesis of the conformationally restricted analogs began with Chan-Lam coupling of **S4.3d** with phenylboronic acid followed by displacement of the chloride with Na₂S. Synthesis of the 5 membered ring analog proceeded by alkylating the thiol with the ethyl 2-bromo-2-phenyl acetate then hydrolyzing the ester to afford acid **S4.5c**. Generating the acid chloride resulted in a spontaneous intramolecular Friedel-Crafts acylation to afford **263861**. To generate the 6-membered ring analogs, a survey of 1,4 conjugate addition conditions employing cinnamate esters did not afford the desired product. We postulate that under basic conditions the carbanion intermediate formed following addition of the thiol undergoes a retro-Michael elimination to regenerate starting materials faster than it can be protonated. Gratifyingly, treating cinnamic acid with HBr in HOAc affords bromide **S4.5g** which efficiently alkylates thiol **S4.5b** in the presence of NaHCO₃. Upon generating the acid chloride by treating **S4.5d** with oxalyl chloride, we found heat was required to promote formation of the 6-membered ring. Unfortunately the Vilsmeier reagent formed from residual DMF in the starting material resulted in significant amounts of the undesirable chloroalkene side product **S4.5h**. Generating the

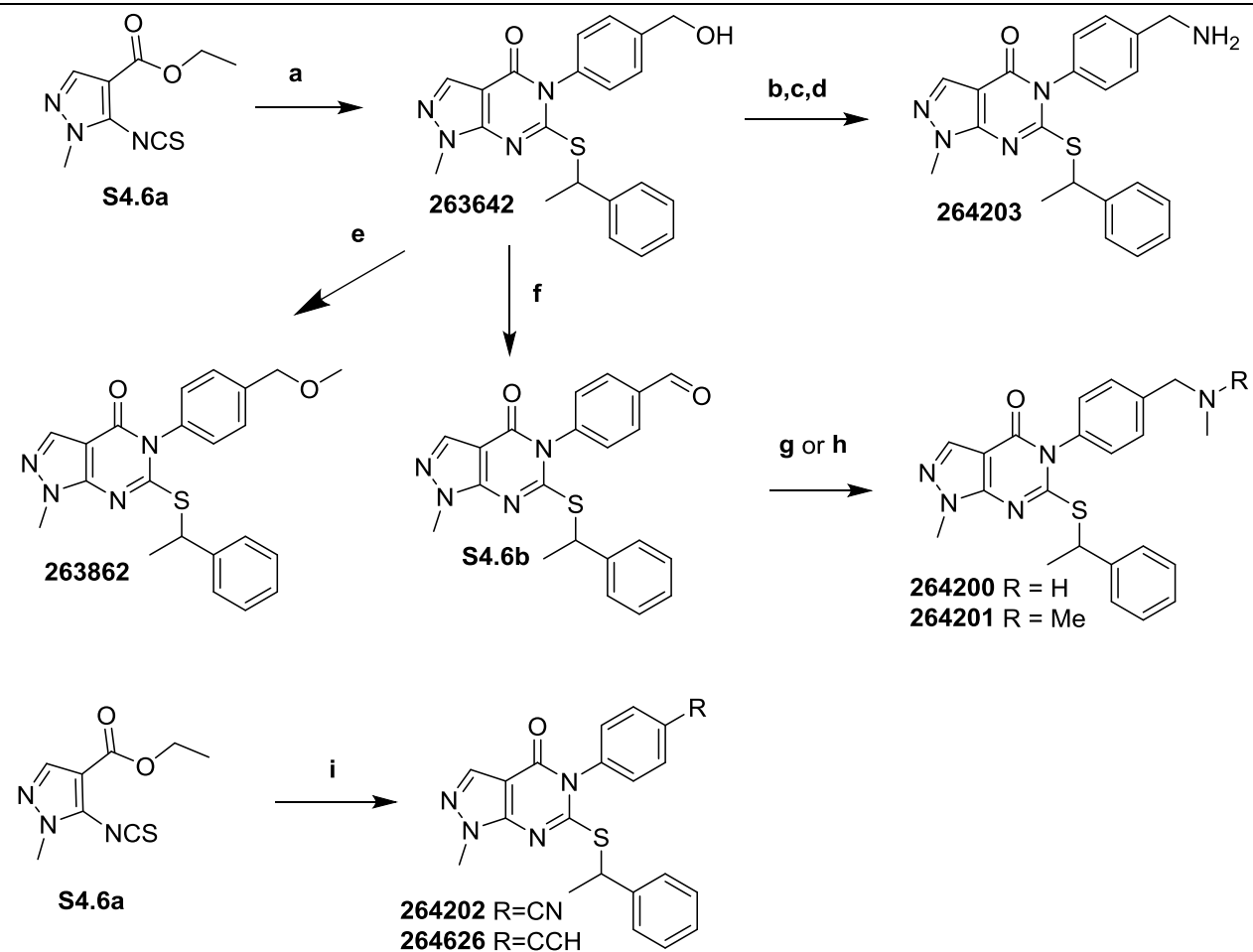
mesylic mixed anhydride by treatment with Ms_2O in DCE at 85°C promoted the cyclization to **263645** without the undesired side reaction.¹⁵⁰ Treatment of the resulting ketone with NaBH_4 afforded **S4.5e** as an inconsequential, inseparable mix of diastereomers. We first tried deoxygenation of the alcohol with chlorodiphenylsilane and InCl_3 but obtained the unexpected elimination product **263867**.¹⁵¹ Barton-McCombie deoxygenation afforded the desired saturated linker analog **C1**.

Scheme 4.5: Synthesis of Conformationally Restricted Analogs^a



^aReagents and Conditions: (a) PhB(OH)_2 , Cu(OAc)_2 , pyridine, 3 Å MS, O_2 , DCE; (b) Na_2S , DMF, 140°C ; (c) ethyl-2-bromo-2-phenylacetate, K_2CO_3 , DMF; (d) Aq. LiOH, EtOH, THF; (e) $(\text{COCl})_2$, cat. DMF, DCM; (f) 3-bromo-3-phenylpropanoic acid, NaHCO_3 , DMF, 50°C ; (g) methanesulfonic anhydride, DCE, 85°C ; (h) NaBH_4 , EtOH; (i) chlorodiphenyl silane, InCl_3 , DCM; (j) CS_2 , NaH, MeI, THF, 0°C ; (k) tributyltin hydride, AIBN, toluene, reflux (l) HBr/HOAc, 70°C , sealed tube.

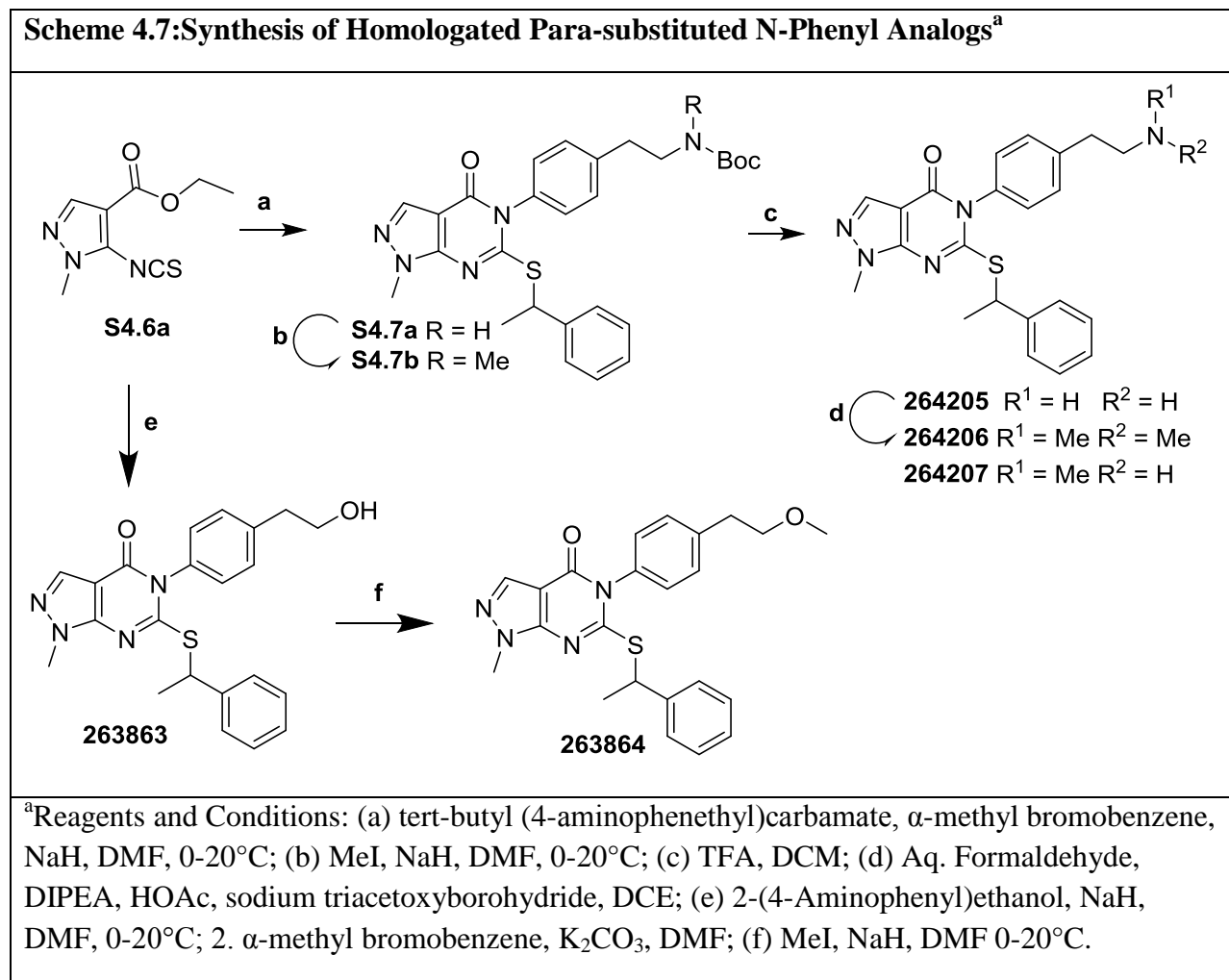
Scheme 4.6: Synthesis of Para-substituted N-Phenyl Analogs^a



^aReagents and Conditions: (a) 4-aminobenzyl alcohol, α -methyl bromobenzene, NaH, DMF, 0-20°C; (b) Ms-Cl, DIPEA, DCM, 0-20°C; (c) NaN₃, DMF; (d) PS-PPh₃, H₂O, THF; (e) MeI, NaH, DMF 0-20°C; (f) Dess-Martin periodinane, DCM; (g) titanium isopropoxide, MeNH₂ in EtOH, NaBH₄, MeOH; (h) titanium isopropoxide, Me₂NH in EtOH, NaBH₄, MeOH; (i) 4-amino benzonitrile, NaH, α -methyl bromobenzene, DMF 0-20°C.

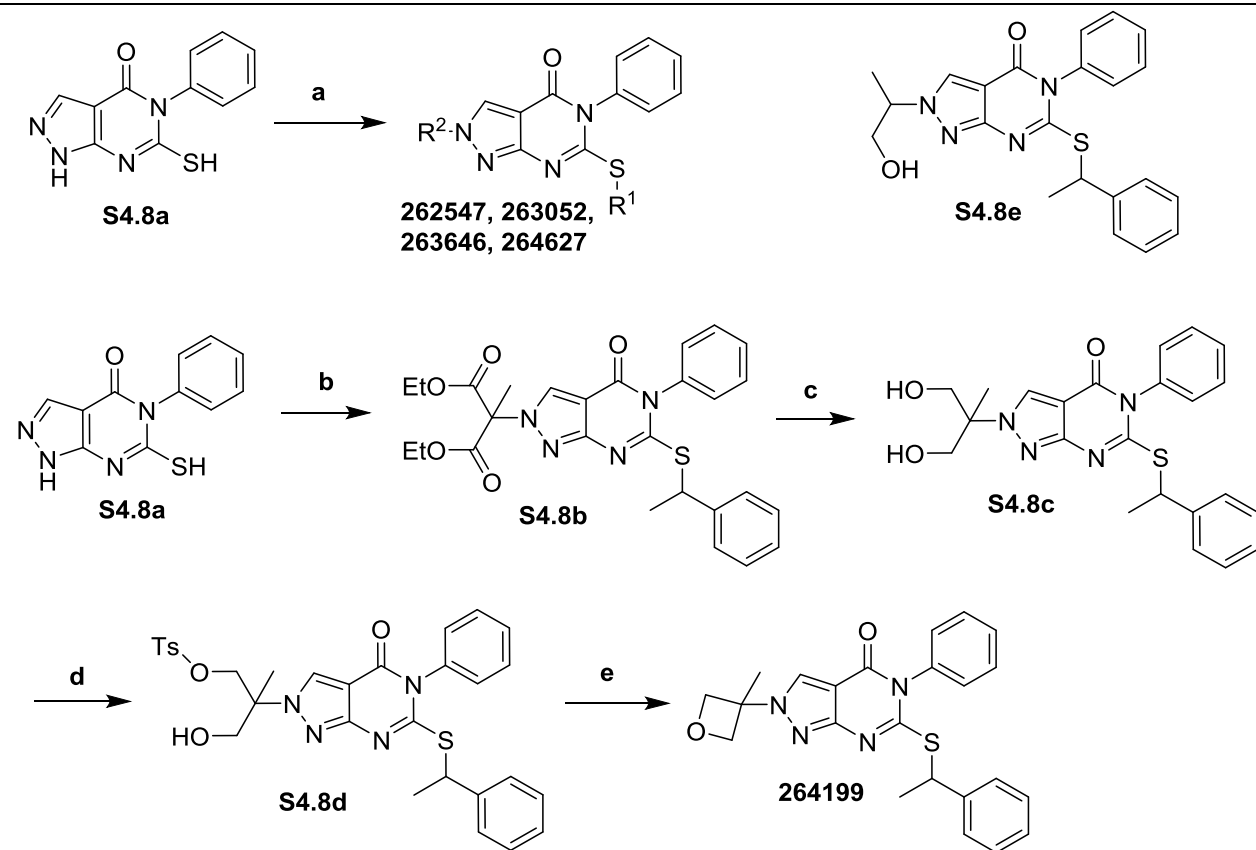
As shown in Scheme 4.6, compound **263642** was generated from isothiocyanate **S4.6a** by addition of aniline then cyclization and alkylation of the resulting thiol under basic conditions in two pots as previously described in Chapter 3. The resulting alcohol afforded primary amine **264203** upon mesylation, displacement with sodium azide, and Staudinger reduction. Dess-Martin oxidation of the alcohol **263642** and reductive amination with methyl or dimethylamine

afforded **264200-1**. Synthesis of the nitrile and alkynyl analogs **264202** and **264626** was affected from **S4.6a** in one pot as previously described in Chapter 3.



Synthesis of **264205-7** began with the addition of tert-butyl (4-aminophenethyl)carbamate¹⁵² to isothiocyanate **S4.6a** according to Scheme 4.7, generating **S4.7a** as described in chapter 3. Alkylation with MeI under basic conditions which furnished **S4.7b** upon deprotection. Deprotection of **S4.7a** afforded **264205** which was bis-methylated under reductive amination conditions to generate **264206**. Deprotection of **S4.7b** yielded **264207**. Compounds **263863-4** were prepared analogously to **263642** and **263862**.

Scheme 4.8: Synthesis of N-2 Pyrazole Substituted Analogs^a



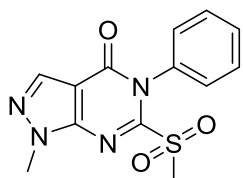
^aReagents and Conditions: (a) R^1 -Br, R^2 -Br or R^2 -OMs, K_2CO_3 , DMF, 20-80°C; (b) 1-bromoethylbenzene, diethyl 2-bromo-2-methylmalonate, K_2CO_3 , DMF, 20-50°C; (c) NaBH_4 , Br_2 , dimethoxyethane, -20°C to RT; (d) $n\text{BuLi}$, Ts-Cl , THF, -78°C to RT; (e) $n\text{BuLi}$, THF, 0-80°C.

As shown in Scheme 4.8, synthesis of oxetanyl analogs **263052**, **263646**, and **264627** and homologated oxetane analog **262547** was accomplished in 1 pot as previously described in chapter 3. Synthesis of methyl-oxetane analog **264199** similarly began with the 1-pot double alkylation of **S4.8a**. Fortuitously, in contrast to other electrophiles which alkylated both positions of the pyrazole with a slight preference for the 1 position, diethyl 2-bromo-2-methylmalonate alkylated exclusively at the 2 position. The challenging reduction of the malonate ester **S4.8b** was completed by *in situ* generation of BH_3 in dimethoxyethane from NaBH_4 and Br_2 .¹⁵³ **S4.8b**

was unaffected by fresh, commercially-obtained $\text{BH}_3\text{-THF}$ or 9-BBN at temperatures up to 70°C , while reduction with NaBH_4 , LiBH_4 , and L-Selectride resulted primarily in the decarboxylated analog **S4.8e**. Reduction with aluminum-based reagents LiAlH_4 , or DIBAL-H resulted in rapid decomposition, even at -78°C . With **S4.8c** in hand, mono-tosylation and cyclization afforded oxetane **264199**.

4.11. Experimentals

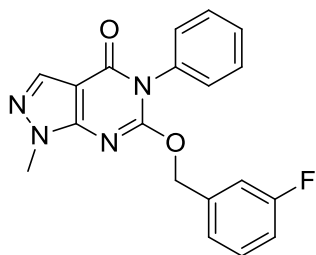
General chemistry information, protocols for crystallography, cellular, enzymatic, and pharmacokinetic assays are reported in Chapter 3.



1-Methyl-6-(methylsulfonyl)-5-phenyl-1H-pyrazolo[3,4-d]pyrimidin-4(5H)-one (S4.1c)

MeI (116 μl , 1.858 mmol) was added to a solution of **S4.1b** (prepared as described in chapter 3)(400mg, 1.549 mmol) and K_2CO_3 (321 mg, 2.323 mmol) in 5mL DMF. The mixture was stirred for 2 hours at which point it was diluted with water, cooled to 0°C and stirred for 30 minutes. The resulting white precipitate was filtered and taken up in 5mL DCM to which mCPBA (896 mg, 3.64 mmol) was added. The mixture was stirred overnight at RT then 5mL Aq. Sodium Thiosulfate was added at which point the mixture was stirred an additional 1 H. The mixture was diluted with more DCM and the aqueous portion was discarded. The aqueous portion was washed with sat. aq. bicarbonate followed by brine and dried over sodium sulfate

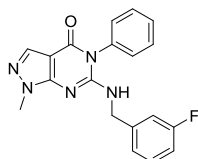
and concentrated. The reaction was redissolved in 5mL DCM, filtered and the filtrate concentrated. The residue was taken up in hot ethanol and slowly cooled to 0°C to afford the titled compound as a white solid (360mg, 1.183 mmol, 76 % yield).



6-((3-Fluorobenzyl)oxy)-1-methyl-5-phenyl-1H-pyrazolo[3,4-d]pyrimidin-4(5H)-one (259011)

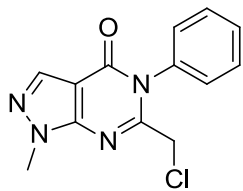
To a dry flask at 0°C under N₂ charged with 60 wt.% NaH in mineral oil (16.43 mg, 0.411 mmol) was added 1 mL of DMF and (3-fluorophenyl)methanol (0.038 mL, 0.353 mmol) by syringe. The mixture was stirred for 10 minutes at which point solid **s4.1c** (100mg, 0.329 mmol) was added quickly. The mixture was stirred overnight and gradually warmed to RT. The following day the mixture was diluted with EtOAc and washed with water. The water was back extracted with a small portion of EtOAc and the combined organics were washed 3x with brine before drying over sodium sulfate and concentrating. The crude was purified by flash (0-100% EtOAc in Hex) yielding the titled compound as a white solid (10mg, 0.029 mmol, 8.69 % yield). MS (ESI): *m/z* 351.1252 [M+H]⁺ ¹H NMR (500 MHz, CDCl₃) δ 8.00 (s, 1H), 7.59 - 7.43 (m, 3H), 7.32 - 7.24 (m, 1H), 7.22 (d, J = 7.5 Hz, 2H), 7.04 - 6.90 (m, 2H), 6.84 (d, J = 9.6 Hz, 1H), 5.41 (s, 2H), 3.94 (s, 3H). ¹³C NMR (126 MHz, CDCl₃) δ 162.73 (d, J = 246.7 Hz), 157.90, 155.24, 150.75, 137.55 (d, J = 7.6 Hz), 135.64, 134.86, 130.08 (d, J = 8.3 Hz), 129.38, 128.95,

128.35, 122.58 (d, J = 3.0 Hz), 115.15 (d, J = 21.1 Hz), 114.12 (d, J = 22.3 Hz), 102.06, 69.24, 33.90. HPLC Purity: 97%



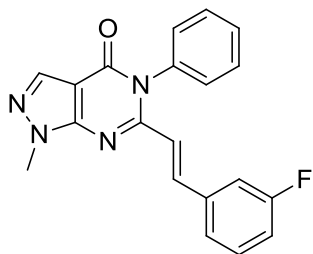
6-((3-Fluorobenzyl)amino)-1-methyl-5-phenyl-1H-pyrazolo[3,4-d]pyrimidin-4(5H)-one
(263868)

To a solution of (3-fluorophenyl)methanamine (0.112 ml, 0.986 mmol) in 5mL DMF at 0°C was added 60 wt.% NaH in mineral oil (32.9 mg, 0.821 mmol). The mixture turned purple and after 5 minutes and **4.1c** (200mg, 0.657 mmol) was added. The mixture turned immediately yellow and was stirred at 0°C for an hour at which point it was allowed to warm to RT. After another hour it was quenched with sat. ammonium chloride and diluted with water and extracted 2x with ethyl acetate. The combined organics were washed with brine 3x and dried over sodium sulfate before concentrating to yield a yellow solid. The crude solid was recrystallized from hot ethanol to yield a white crystalline solid. (29mg, 0.083 mmol, 12.63 % yield) MS (ESI): m/z 350.1410 [M+H]⁺ ¹H NMR (500 MHz, CDCl₃) δ 7.96 - 7.90 (m, 1H), 7.64 - 7.56 (m, 2H), 7.56 - 7.50 (m, 1H), 7.34 - 7.27 (m, 3H), 7.01 (d, J = 7.6 Hz, 1H), 6.98 - 6.92 (m, 2H), 4.67 - 4.54 (m, 3H), 3.85 (s, 3H). ¹³C NMR (126 MHz, CDCl₃) δ 162.93 (d, J = 246.7 Hz), 158.16, 152.49, 152.47, 140.69 (d, J = 6.9 Hz), 135.47, 134.63, 130.74, 130.20 (d, J = 8.1 Hz), 130.05, 129.15, 122.77 (d, J = 2.8 Hz), 114.48 (d, J = 21.1 Hz), 114.27 (d, J = 21.9 Hz), 100.24, 45.20 (d, J = 1.9 Hz), 33.57. HPLC Purity: 99%



6-(chloromethyl)-1-methyl-5-phenyl-1H-pyrazolo[3,4-d]pyrimidin-4(5H)-one (4.1d)

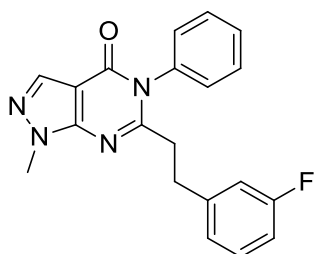
A flask under N₂ charged with chloroacetic acid (12.76 g, 135 mmol) and 5-amino-1-methyl-N-phenyl-1H-pyrazole-4-carboxamide (1.46 g, 6.75 mmol) was heated at 80°C until a homogenous melt was obtained. Chloroacetyl chloride (1.352 mL, 16.88 mmol) was added dropwise and the mixture was stirred at 80°C for 1 hour. The flask was then fitted with a reflux condenser and heated to 120°C overnight. The next day the flask was removed from the oil bath and immediately poured into 100 mL water. The mixture was stirred vigorously until cool to the touch then filtered yielding the titled compound as an off white solid (1.22 g, 4.44 mmol, 65.8 % yield). ¹H NMR (400 MHz, CDCl₃) δ 8.10 (s, 1H), 7.48 - 7.64 (m, 3H), 7.28 - 7.37 (m, 2H), 4.23 (s, 2H), 4.05 (s, 3H)



(E)-6-(3-fluorostyryl)-1-methyl-5-phenyl-1H-pyrazolo[3,4-d]pyrimidin-4(5H)-one (258471)

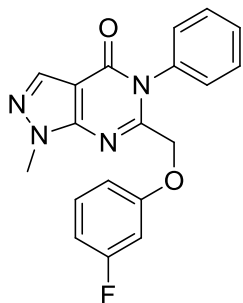
(4.1d) (250mg, 0.910 mmol) and Triethyl Phosphite (318 μ l, 1.820 mmol) were dissolved in 2mL DMF and heated to 150°C for 3 hours. The mixture was concentrated under vacuum and the crude residue was purified by flash chromatography (EA in Hex) yielding diethyl ((1-methyl-4-oxo-5-phenyl-4,5-dihydro-1H-pyrazolo[3,4-d]pyrimidin-6-yl)methyl)phosphonate as a yellow solid (250mg, 0.664 mmol, 73.0 % yield).

A dry flask charged with 60% NaH in mineral oil (11.16 mg, 0.279 mmol) and diethyl ((1-methyl-4-oxo-5-phenyl-4,5-dihydro-1H-pyrazolo[3,4-d]pyrimidin-6-yl)methyl)phosphonate (100mg, 0.266 mmol) was cooled to 0°C and DMF was added by syringe. After stirring for 10 min 3-fluorobenzaldehyde (0.031 ml, 0.292 mmol) was added by syringe and the flask was allowed to warm to RT. After an hour the reaction went from yellow to brownish red and was complete by HPLC. Water was added to precipitate product which was collected by filtration, washed with additional water and hexanes, and then recrystallized from hot ethanol yielding the titled compound as a yellow crystalline solid (50mg, 0.144 mmol, 54.3 % yield). MS (ESI): m/z 347.1305 [M+H]⁺ ¹H NMR (500 MHz, CDCl₃) δ 8.10 (s, 1H), 7.91 (d, J = 15.65 Hz, 2H), 7.53 - 7.64 (m, 3H), 7.22 - 7.34 (m, 3H), 7.09 (d, J = 7.83 Hz, 1H), 7.02 (dt, J = 2.45, 8.31 Hz, 1H), 6.96 (d, J = 9.78 Hz, 1H), 6.34 (d, J = 15.16 Hz, 2H), 4.10 (s, 3H) ¹³C NMR (126 MHz, CDCl₃) δ 162.92 (d, J = 247.3 Hz), 158.17, 154.11, 151.05, 139.17, 137.23 (d, J = 7.5 Hz), 136.73, 135.40, 130.38 (d, J = 8.4 Hz), 129.96, 129.54, 128.88, 123.80 (d, J = 2.6 Hz), 120.96, 116.75 (d, J = 21.5 Hz), 114.04 (d, J = 21.8 Hz), 104.23, 34.17. HPLC Purity: 97%



6-(3-Fluorophenethyl)-1-methyl-5-phenyl-1H-pyrazolo[3,4-d]pyrimidin-4(5H)-one (258472)

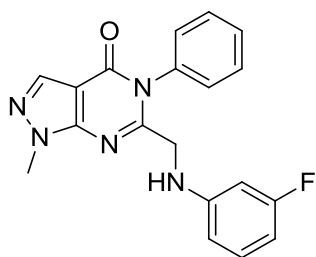
A solution of **258471** (40mg, 0.115 mmol) and 10% Pd-C (36.9 mg, 0.035 mmol) in 5mL methanol was degassed under vacuum and the flask backfilled with an H₂ balloon. The mixture was stirred vigorously for 2 hours then filtered through Celite and concentrated yielding the titled compound as a white solid (27mg, 0.078 mmol, 67.1 % yield). MS (ESI): *m/z* 349.1461 [M+H]⁺
¹H NMR (400 MHz, CDCl₃) δ 8.05 (s, 1H), 7.44 - 7.62 (m, 3H), 7.10 - 7.23 (m, 3H), 6.86 (t, *J* = 8.41 Hz, 1H), 6.81 (d, *J* = 7.83 Hz, 1H), 6.74 (d, *J* = 10.17 Hz, 1H), 4.04 (s, 3H), 3.04 (t, *J* = 7.83 Hz, 2H), 2.68 (t, *J* = 7.83 Hz, 2H) ¹³C NMR (101 MHz, CDCl₃) δ 162.7, 158.9, 158.3, 150.8, 142.8, 136.9, 135.1, 130.0, 129.8, 129.4, 128.4, 123.9, 115.3, 113.2, 104.0, 37.2, 34.1, 32.3.
HPLC Purity: 95%



6-((3-Fluorophenoxy)methyl)-1-methyl-5-phenyl-1H-pyrazolo[3,4-d]pyrimidin-4(5H)-one (258079)

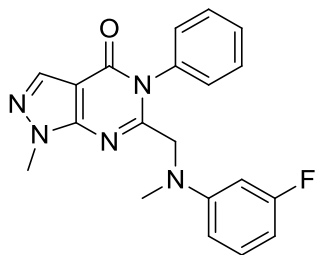
To a dry vial charged with K₂CO₃ (55.3 mg, 0.400 mmol) and **S4.1d** (55 mg, 0.200 mmol) was added 1 mL DMF followed by 3-fluorophenol (0.027 mL, 0.300 mmol). The vial was flushed with argon, sealed, and heated to 70°C for 3 h at which point the reaction was complete by HPLC. The mixture was diluted with 20 mL water and extracted 2x with EtOAc. The combined organics were washed 3x with brine and dried over sodium sulfate. Removal of solvent yielded

a colorless oil which was subjected to flash (eluted at 40% EA/Hex) yielding the titled compound as a white crystalline solid (58mg, 0.166 mmol, 83 % yield). MS (ESI): m/z 351.1255 [M+H]⁺ ¹H NMR (400 MHz, CDCl₃) δ 8.10 (s, 1H), 7.43 - 7.55 (m, 3H), 7.28 (d, J = 7.04 Hz, 2H), 7.12 - 7.21 (m, 1H), 6.66 (dt, J = 1.57, 8.22 Hz, 1H), 6.52 - 6.58 (m, 1H), 6.46 - 6.52 (m, 1H), 4.71 (s, 2H), 4.02 (s, 3H) ¹³C NMR (101 MHz, CDCl₃) δ 163.3, 158.7, 158.0, 153.9, 150.5, 135.6, 135.4, 130.3, 129.8, 129.7, 128.5, 110.3, 108.7, 104.7, 102.6, 68.3, 34.3 HPLC Purity: 98%



6-(((3-Fluorophenyl)amino)methyl)-1-methyl-5-phenyl-1H-pyrazolo[3,4-d]pyrimidin-4(5H)-one (258473)

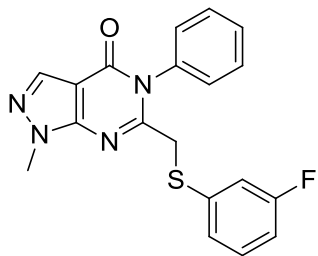
A flask was charged with 1 mL DMF, K₂CO₃ (151 mg, 1.092 mmol), KI (18.13 mg, 0.109 mmol), **S4.1d** (150 mg, 0.546 mmol) and was briefly vacuum degassed and put under nitrogen at which point 3-fluoroaniline (0.063 ml, 0.655 mmol) was added by syringe. The flask was heated at 50°C for 24 hours. Water was added to precipitate the product which was collected by filtration yielding the titled compound as a light pink powder (177mg, 0.507 mmol, 93 % yield). MS (ESI): m/z 350.1415 [M+H]⁺ ¹H NMR (500 MHz, CDCl₃) δ 8.07 (s, 1H), 7.54 - 7.65 (m, 3H), 7.26 (d, J = 6.36 Hz, 2H), 7.07 (q, J = 7.83 Hz, 1H), 6.41 (t, J = 8.07 Hz, 1H), 6.29 (d, J = 7.83 Hz, 1H), 6.18 (d, J = 11.25 Hz, 1H), 5.00 (br. s., 1H), 4.05 (s, 3H), 3.88 (d, J = 5.20 Hz, 2H) ¹³C NMR (126 MHz, CDCl₃) δ 163.9, 157.9, 156.2, 150.3, 148.4, 135.6, 135.4, 130.4, 130.3, 130.1, 128.3, 109.0, 104.8, 104.3, 99.9, 46.8, 34.3 HPLC Purity: 95%



6-(((3-Fluorophenyl)(methyl)amino)methyl)-1-methyl-5-phenyl-1H-pyrazolo[3,4-d]pyrimidin-4(5H)-one (259123)

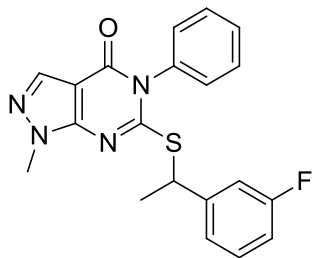
A flask containing K_2CO_3 (24.72 mg, 0.179 mmol), MeI (9.40 μ l, 0.150 mmol), **258473** (50mg, 0.143 mmol), and 1mL DMF was heated to 50°C and stirred overnight. The next day the mixture was diluted with water and extracted 2x with EtOAc. The combined organic portion was washed 3x with brine, dried over sodium sulfate, and concentrated. The crude mixture was purified by flash chromatography (EtOAc in Hex) and the product obtained was further purified by recrystallization from ethanol yielding the titled compound as a white solid (10mg, 0.028 mmol, 19.23 % yield). MS (ESI): m/z 364.1568 $[M+H]^+$ 1H NMR (500 MHz, $CDCl_3$) δ 8.05 (s, 1H), 7.59 (t, $J = 7.5$ Hz, 2H), 7.53 (t, $J = 7.4$ Hz, 1H), 7.28 (d, $J = 8.1$ Hz, 2H), 7.10 (q, $J = 7.9$ Hz, 1H), 6.41 (t, $J = 8.3$ Hz, 1H), 6.29 (dd, $J = 16.8, 10.6$ Hz, 2H), 4.16 (s, 2H), 3.87 (s, 3H), 2.99 (s, 3H). ^{13}C NMR (126 MHz, $CDCl_3$) δ 163.94 (d, $J = 242.4$ Hz), 158.37, 156.25, 150.80, 150.59 (d, $J = 10.6$ Hz), 136.07, 135.24, 130.30, 130.07 (d, $J = 10.3$ Hz), 129.73, 128.15, 107.78 (d, $J = 2.3$ Hz), 104.16, 103.66 (d, $J = 21.5$ Hz), 99.46 (d, $J = 26.3$ Hz), 55.73, 39.56, 33.91.

HPLC Purity: 96%



6-(((3-Fluorophenyl)thio)methyl)-1-methyl-5-phenyl-1H-pyrazolo[3,4-d]pyrimidin-4(5H)-one (258475)

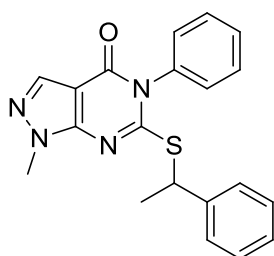
S4.1d (60mg, 0.218 mmol), K_2CO_3 (45.3 mg, 0.328 mmol), 3-fluorobenzenethiol (0.025 ml, 0.306 mmol) and 1mL DMF were stirred overnight at 50°C. The product was precipitated by the addition of water and collected by filtration. The filtrate was recrystallized from EtOH yielding the titled compound as a white crystalline solid (24mg, 0.066 mmol, 30.0 % yield). MS (ESI): m/z 367.1025 $[M+H]^+$ 1H NMR (400 MHz, $CDCl_3$) δ 8.06 (s, 1H), 7.49 - 7.60 (m, 3H), 7.28 - 7.34 (m, 2H), 7.15 - 7.24 (m, 2H), 7.08 (d, $J = 7.83$ Hz, 1H), 6.92 (dt, $J = 1.96, 8.41$ Hz, 1H), 3.95 (s, 3H), 3.86 (s, 2H) ^{13}C NMR (101 MHz, $CDCl_3$) δ 164.1, 163.9, 161.4, 158.2, 155.9, 136.3, 135.3, 130.1, 129.9, 129.7, 128.9, 125.9, 117.2, 114.1, 104.3, 38.7, 34.1 HPLC Purity: 97%



6-((1-(3-fluorophenyl)ethyl)thio)-1-methyl-5-phenyl-1H-pyrazolo[3,4-d]pyrimidin-4(5H)-one (262741)

Prepared as described for **257723** in chapter 3. White solid. (106mg, 0.279 mmol, 67.9 % yield).

MS (ESI): m/z 381.1182 $[M+H]^+$ 1H NMR (500 MHz, Chloroform- d) δ 7.99 (s, 1H), 7.60 - 7.45 (m, 3H), 7.32 - 7.23 (m, 2H), 7.19 (dd, $J = 4.8, 2.2$ Hz, 1H), 7.17 (d, $J = 8.3$ Hz, 1H), 7.10 (dt, $J = 10.0, 2.1$ Hz, 1H), 6.93 (td, $J = 8.4, 2.5$ Hz, 1H), 4.99 (q, $J = 7.2$ Hz, 1H), 3.98 (s, 3H), 1.67 (d, $J = 7.0$ Hz, 3H). ^{13}C NMR (126 MHz, Chloroform- d) δ 162.69 (d, $J = 246.1$ Hz), 161.07, 157.70, 150.94, 144.96 (d, $J = 7.4$ Hz), 135.45 (d, $J = 23.9$ Hz), 135.38, 130.02, 129.96, 129.73 (d, $J = 9.7$ Hz), 129.37 (d, $J = 2.6$ Hz), 123.07 (d, $J = 2.9$ Hz), 114.59 (d, $J = 19.2$ Hz), 114.42 (d, $J = 18.5$ Hz), 102.92, 46.26, 34.10, 21.78. HPLC Purity: 99%

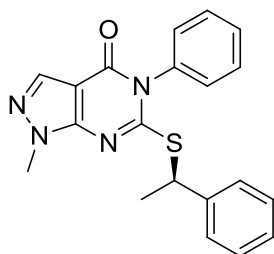


1-methyl-5-phenyl-6-((1-phenylethyl)thio)-1H-pyrazolo[3,4-d]pyrimidin-4(5H)-one (259122)

Prepared as described for **257723** in chapter 3. White Solid (183 mg, 0.505 mmol, 65.2 % yield)

MS (ESI): m/z 363.1278 $[M+H]^+$ 1H NMR (500 MHz, Chloroform- d) δ 7.99 (s, 1H), 7.64 - 7.45

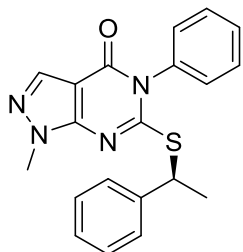
(m, 3H), 7.42 - 7.35 (m, 2H), 7.34 - 7.22 (m, 4H), 7.18 (d, J = 6.9 Hz, 1H), 5.02 (q, J = 7.2 Hz, 1H), 4.00 (s, 3H), 1.70 (d, J = 7.1 Hz, 3H). ¹³C NMR (126 MHz, Chloroform-d) δ 161.50, 157.82, 151.05, 142.12, 135.64, 135.36, 129.93, 129.72, 129.65, 129.41, 129.38, 128.53, 127.56, 127.52, 102.88, 46.89, 34.07, 21.97. HPLC Purity: 98%



(R)-1-methyl-5-phenyl-6-((1-phenylethyl)thio)-1H-pyrazolo[3,4-d]pyrimidin-4(5H)-one (262548)

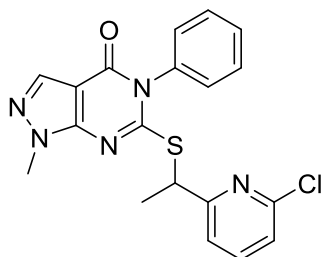
To a flask under N₂ charged with 3mL DCM and DMF (0.096 ml, 1.239 mmol) was added oxalyl chloride (0.102 ml, 1.161 mmol) dropwise by syringe. The mixture was stirred for 15 minutes at which point the solvent was removed and residual acid removed with an additional DCM chase. The solid obtained was suspended in 3mL THF and cooled to 0°C and (S)-1-phenylethanol (0.140 ml, 1.161 mmol) was added and stirred for ~1 minute until a homogenous solution was obtained. TEA (0.324 ml, 2.323 mmol) and **S4.1b** (200 mg, 0.774 mmol) were added. The mixture was stirred for 2h at which point the reaction was done by HPLC. The reaction was quenched with water and extracted 2x with ethyl acetate. The combined organics were washed with brine, dried over sodium sulfate, and concentrated. The crude solid obtained was taken up in hot ethanol and the titled compound crystallized as a yellow solid upon cooling (156mg, 0.430 mmol, 55.6 % yield). HPLC Purity: 96%, >95% EE as determined by Chiral

HPLC (15% IPA in Hexanes, 1 mL/min, RT = 19 min). NMR and MS data were verified to be identical to the racemate.



(S)-1-methyl-5-phenyl-6-((1-phenylethyl)thio)-1H-pyrazolo[3,4-d]pyrimidin-4(5H)-one (262703)

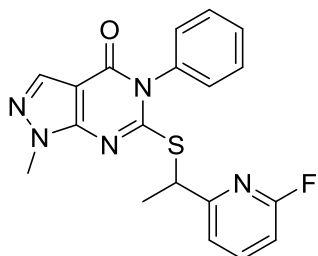
Prepared in the same manner as **262548** employing (R)-1-phenylethanol. (80mg, 0.221 mmol, 28.5 % yield) HPLC Purity: 98%, >95% EE as determined by Chiral HPLC (15% IPA in Hexanes, 1 mL/min, RT = 16 min). NMR and MS data were verified to be identical to the racemate.



6-((1-(6-chloropyridin-2-yl)ethyl)thio)-1-methyl-5-phenyl-1H-pyrazolo[3,4-d]pyrimidin-4(5H)-one (264623)

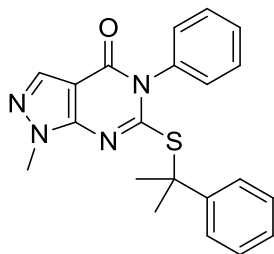
Prepared in a similar manner as 262548 from 1-(6-chloropyridin-2-yl)ethanol. Yellow solid. (150mg, 0.377 mmol, 59.4 % yield). MS (ESI): m/z 398.0836 $[M+H]^+$ 1H NMR (500 MHz, $CDCl_3$) δ 7.99 (s, 1H), 7.60 (t, $J = 7.8$ Hz, 1H), 7.57 - 7.50 (m, 3H), 7.35 (d, $J = 7.6$ Hz, 1H), 7.31 - 7.27 (m, 1H), 7.24 - 7.16 (m, 2H), 5.08 (q, $J = 7.3$ Hz, 1H), 3.95 (s, 3H), 1.67 (d, $J = 7.3$

Hz, 3H). ^{13}C NMR (126 MHz, CDCl_3) δ 162.76, 160.94, 157.70, 150.83, 150.76, 139.31, 135.47, 135.37, 130.08, 129.37, 129.33, 122.89, 119.81, 102.81, 47.87, 34.02, 20.50. HPLC Purity: 99%



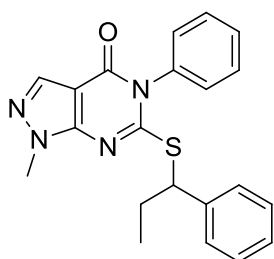
6-((1-(6-fluoropyridin-2-yl)ethyl)thio)-1-methyl-5-phenyl-1H-pyrazolo[3,4-d]pyrimidin-4(5H)-one (264624)

Prepared in a similar manner to **262548** using 1-(6-fluoropyridin-2-yl)ethanol prepared as previously described.¹⁵⁴ White solid (45 mg, 0.118 mmol, 24.98 % yield) MS (ESI): m/z 382.1135 $[\text{M}+\text{H}]^+$ ^1H NMR (500 MHz, CDCl_3) δ 8.02 - 7.96 (m, 1H), 7.73 (q, $J = 8.3$ Hz, 1H), 7.57 - 7.47 (m, 3H), 7.33 - 7.27 (m, 2H), 7.24 - 7.19 (m, 1H), 6.81 (dd, $J = 8.1, 2.8$ Hz, 1H), 5.08 (dd, $J = 4861.1, 7.2$ Hz, 1H), 3.96 (s, 3H), 1.68 (d, $J = 7.3$ Hz, 3H). ^{13}C NMR (126 MHz, CDCl_3) δ 163.04 (d, $J = 240.6$ Hz), 161.12, 160.55 (d, $J = 12.9$ Hz), 157.70, 150.86, 141.60 (d, $J = 7.8$ Hz), 135.44, 135.39, 130.07, 129.78 (d, $J = 3.8$ Hz), 129.35, 118.83 (d, $J = 4.3$ Hz), 108.15 (d, $J = 36.9$ Hz), 102.85, 47.47, 34.02, 20.42. HPLC Purity: 97%



1-methyl-5-phenyl-6-((2-phenylpropan-2-yl)thio)-1H-pyrazolo[3,4-d]pyrimidin-4(5H)-one
(263057)

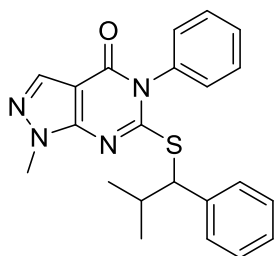
To a slurry of **S4.1b** (75 mg, 0.290 mmol) and prop-1-en-2-ylbenzene (0.038 ml, 0.290 mmol) in DCM at 0°C was added TFA (0.224 ml, 2.90 mmol) dropwise. The resulting homogenous solution was stirred for 30 min at 0°C and 30 min at RT. The reaction was diluted with DCM and washed with saturated bicarb. The organic portion was dried over sodium sulfate and concentrated. The crude product was purified by flash (eluting around 40-50% EtOAc in Hex) yielding a white solid. (65mg, 0.173 mmol, 59.5 % yield) MS (ESI): m/z 377.1434 [M+H]⁺ ¹H NMR (500 MHz, CDCl₃) δ 7.91 (s, 1H), 7.62 - 7.50 (m, 5H), 7.31 (t, J = 7.6 Hz, 2H), 7.25 - 7.14 (m, 3H), 3.71 (s, 3H), 1.89 (s, 6H). ¹³C NMR (126 MHz, CDCl₃) δ 160.48, 157.80, 150.72, 145.95, 135.76, 135.19, 129.82, 129.65, 129.43, 127.91, 126.59, 126.28, 102.90, 54.87, 33.99, 29.71. HPLC Purity: 95%



1-methyl-5-phenyl-6-((1-phenylpropyl)thio)-1H-pyrazolo[3,4-d]pyrimidin-4(5H)-one

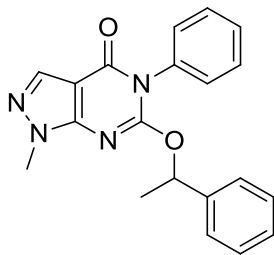
(262704)

White solid. (110mg, 0.292 mmol, 75 % yield) MS (ESI): m/z 377.1321 $[M+H]^+$ 1H NMR (500 MHz, $CDCl_3$) δ 7.99 (s, 1H), 7.58 - 7.46 (m, 3H), 7.37 - 7.32 (m, 2H), 7.30 (t, $J = 7.7$ Hz, 2H), 7.28 - 7.22 (m, 2H), 7.17 (d, $J = 7.2$ Hz, 1H), 4.77 (dd, $J = 9.1, 6.1$ Hz, 1H), 4.00 (s, 3H), 2.16 - 2.02 (m, 1H), 1.97 - 1.83 (m, 1H), 0.92 (t, $J = 7.3$ Hz, 3H). ^{13}C NMR (126 MHz, $CDCl_3$) δ 161.60, 157.83, 151.02, 140.91, 135.72, 135.34, 129.90, 129.70, 129.63, 129.42, 129.36, 128.40, 128.08, 127.46, 102.86, 53.65, 34.03, 29.25, 12.29. HPLC Purity: 98%



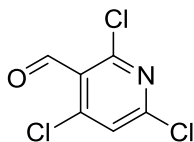
1-methyl-6-((2-methyl-1-phenylpropyl)thio)-5-phenyl-1H-pyrazolo[3,4-d]pyrimidin-4(5H)-one (263639)

Prepared from (1-bromo-2-methylpropyl)benzene¹⁵⁵ as described for **257723** in chapter 3. White solid (29mg, 0.074 mmol, 28.1 % yield) MS (ESI): m/z 413.1418 $[M+H]^+$ 1H NMR (500 MHz, $CDCl_3$) δ 7.95 (d, $J = 1.1$ Hz, 1H), 7.60 - 7.46 (m, 3H), 7.35 - 7.26 (m, 5H), 7.25 - 7.20 (m, 1H), 7.16 (d, $J = 7.8$ Hz, 1H), 4.74 (d, $J = 7.8$ Hz, 1H), 3.96 (s, 3H), 2.14 (dtt, $J = 7.2, 6.8$ Hz, 1H), 1.04 (d, $J = 6.7$ Hz, 3H), 0.85 (d, $J = 6.7$ Hz, 3H). ^{13}C NMR (126 MHz, $CDCl_3$) δ 161.57, 157.86, 150.95, 140.89, 135.87, 135.29, 129.88, 129.70, 129.64, 129.43, 129.37, 128.61, 127.98, 127.13, 102.81, 59.22, 34.04, 33.39, 21.07, 20.57. HPLC Purity: 99%



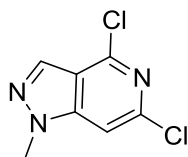
1-methyl-5-phenyl-6-(1-phenylethoxy)-1H-pyrazolo[3,4-d]pyrimidin-4(5H)-one (262561)

60% NaH in mineral oil (7.89 mg, 0.197 mmol) was added to a solution of 1-phenylethanol (0.026 ml, 0.214 mmol) in DMF at 0°C. The mixture was stirred for 10 min at which point 1-methyl-6-(methylsulfonyl)-5-phenyl-1H-pyrazolo[3,4-d]pyrimidin-4(5H)-one (50mg, 0.164 mmol) was added and the mixture was allowed to warm to room temperature and stirred overnight. The mixture was diluted with water and extracted 2x with EtOAc. The combined organics were washed 3x with brine, dried over sodium sulfate, and concentrated. The crude residue was purified by flash (EtOAc and Hexanes) yielding the titled compound as a white solid (5mg, 0.014 mmol, 8.79 % yield). MS (ESI): m/z 347.1504 $[M+H]^+$ 1H NMR (500 MHz, $CDCl_3$) δ 7.97 (s, 1H), 7.60 - 7.44 (m, 3H), 7.28 (dd, $J = 10.4, 7.1$ Hz, 4H), 7.14 (d, $J = 7.0$ Hz, 3H), 6.20 (q, $J = 6.6$ Hz, 1H), 3.90 (s, 3H), 1.50 (d, $J = 6.6$ Hz, 3H). ^{13}C NMR (126 MHz, $CDCl_3$) δ 158.07, 154.93, 151.02, 141.03, 135.55, 135.21, 129.23, 128.72, 128.48, 128.44, 128.39, 128.02, 125.70, 109.99, 101.91, 33.77, 22.59. HPLC Purity: 96%



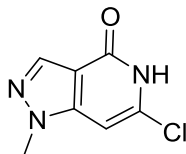
2,4,6-Trichloronicotinaldehyde (S4.3b)

A hot, oven-dried flask was charged with **S4.3a** (5 g, 27.4 mmol), vacuum purged, and backfilled with N₂, at which point 50mL anhydrous THF was added by syringe. The flask was cooled to -78°C and nBuLi (2.6M in Hexanes, 10.96 ml, 27.4 mmol) was added by syringe down the side of the flask over 10 min. The green solution was stirred for 10min before adding ethyl formate (dried over sodium sulfate, 2.90 ml, 35.6 mmol) dropwise by syringe over 10 minutes. The mixture was stirred for 1 h and then removed from the cooling bath and cold quenched with 5mL saturated aqueous ammonium sulfate. The mixture was concentrated and taken up in ethyl acetate and washed with water. The aqueous portion was back extracted and the combined organics were washed with brine and dried over sodium sulfate yielding a yellow solid upon concentration that was used in the next step without further purification (product will slowly sublime in vacuo) (5.98 g, 28.4 mmol, 104 % yield). ¹H NMR (500 MHz, CDCl₃) δ 10.42 (d, J = 1.1 Hz, 1H), 7.46 (d, J = 1.0 Hz, 1H).



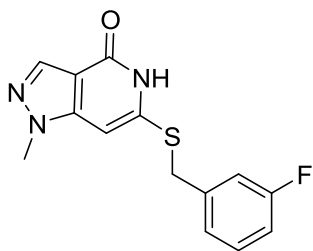
4,6-Dichloro-1-methyl-1H-pyrazolo[4,3-c]pyridine (S4.3c)

A flask under N₂ was charged with **S4.3b** (5.72 g, 27.2 mmol) dissolved in 150mL Abs. EtOH using a sonicator. Triethylamine (11.37 ml, 82 mmol) was added and the flask was cooled to -40°C at which point methylhydrazine (1.574 ml, 29.9 mmol) was added by syringe. The flask was allowed to gradually warm to RT over 2 h then stirred at RT for an additional 3 h. The reaction was concentrated and taken up in ethyl acetate and washed 2x with 1N HCl and 1X with brine, dried over magnesium sulfate, and concentrated. The crude residue was purified by flash affording the titled compound as a yellow solid (1.83 g, 9.06 mmol, 33.3 % yield). ¹H NMR (500 MHz, CDCl₃) δ 8.10 (s, 1H), 7.28 (s, 1H), 4.05 (s, 3H).



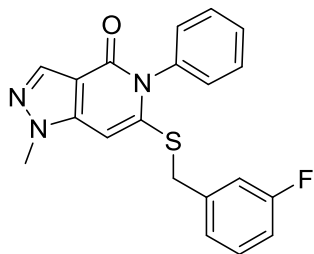
6-chloro-1-methyl-1H-pyrazolo[4,3-c]pyridin-4(5H)-one (S4.3d)

A microwave vessel was charged with **S4.3c** (1.83 g, 9.06 mmol) and 10mL 10% NaOH. The vessel was heated in a microwave synthesizer for 30 minutes at which point the mixture was acidified with conc. HCl and the resulting precipitate collected by filtration affording the titled compound as a white solid (1.48 g, 8.06 mmol, 89 % yield). ¹H NMR (500 MHz, DMSO-*d*₆) δ 7.98 (s, 1H), 6.87 (s, 1H), 3.89 (s, 3H).



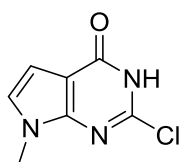
6-((3-Fluorobenzyl)thio)-1-methyl-1H-pyrazolo[4,3-c]pyridin-4(5H)-one (S4.3e)

A microwave tube was charged with **S4.3d** (300 mg, 1.634 mmol), DIPEA (1.142 ml, 6.54 mmol), (3-fluorophenyl)methanethiol (0.404 ml, 3.27 mmol), and 3mL n-Butanol. The headspace was purged with Ar and the tube was capped and heated to 170°C in a microwave synthesizer for 48 h. Upon cooling a white precipitate formed which was collected by filtration and washed with water and hexanes to afford the titled compound (300mg, 1.037 mmol, 63.5 % yield). ¹H NMR (500 MHz, DMSO-*d*₆) δ 11.37 (br. s., 1H), 7.95 (s, 1H), 7.31 - 7.41 (m, 1H), 7.16 - 7.25 (m, 2H), 7.09 (t, J = 8.56 Hz, 1H), 6.67 (s, 1H), 4.38 (s, 2H), 3.88 (s, 3H)



6-((3-Fluorobenzyl)thio)-1-methyl-5-phenyl-1H-pyrazolo[4,3-c]pyridin-4(5H)-one (258469)

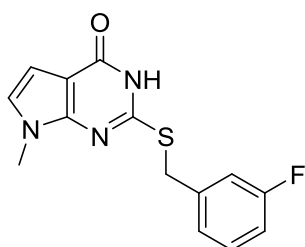
A flask was charged with 2mL DCE, Pyridine (0.028 ml, 0.346 mmol), TEMPO (29.7 mg, 0.190 mmol), **S4.3e** (50mg, 0.173 mmol), Cu(II)OAc hydrate (6.90 mg, 0.035 mmol), phenylboronic acid (42.1 mg, 0.346 mmol), and 3Å molecular sieves and stirred under air for 24 h at RT. The mixture was filtered with celite and the filter pad washed with DCM. The filtrate was washed with 1N HCl and brine, dried over sodium sulfate, and concentrated. The crude mixture was purified by flash (Elutes at 60% EtOAc in Hexanes) affording the titled compound as a white solid (32mg, 0.088 mmol, 50.7 % yield). MS (ESI): m/z 366.1066 $[M+H]^+$ 1H NMR (400 MHz, $CDCl_3$) δ 8.09 (s, 1H), 7.45 - 7.55 (m, 3H), 7.23 - 7.31 (m, 3H), 7.04 (d, $J = 7.43$ Hz, 1H), 6.94 - 7.01 (m, 2H), 6.20 (s, 1H), 3.99 (s, 2H), 3.91 (s, 3H), ^{13}C NMR (101 MHz, $CDCl_3$) δ 162.8, 159.0, 144.9, 143.2, 137.6, 136.9, 130.3, 129.6, 129.3, 124.6, 115.9, 115.0, 111.5, 90.8, 38.5, 35.8. HPLC Purity: 95%



2-chloro-7-methyl-3H-pyrrolo[2,3-d]pyrimidin-4(7H)-one (S4.3g)

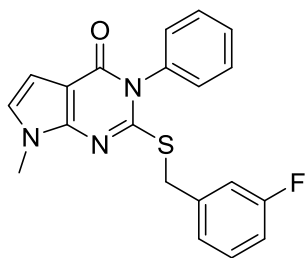
To a flask charged with 10mL THF and 60 wt.% NaH (117 mg, 2.93 mmol) under N_2 at $0^\circ C$ was added **S4.3f** (500mg, 2.66 mmol) dissolved in 10mL THF by syringe. The flask was stirred at $0^\circ C$ for an hour at which point MeI (183 μ l, 2.93 mmol) was added by syringe. The flask was allowed to gradually warm to RT overnight and the next day the solvent was removed and the

residue was treated with 20mL 2N NaOH and refluxed overnight. The product was precipitated by addition of conc. HCl, filtered, and washed with water and hexane. To afford the titled compound as a white solid (415mg, 2.260 mmol, 85 % yield). ¹H NMR (400 MHz, DMSO-d₆) δ 12.83 (br. s., 1H), 7.10 (d, *J* = 2.74 Hz, 1H), 6.45 (d, *J* = 3.13 Hz, 1H), 3.66 (s, 3H).



2-((3-Fluorobenzyl)thio)-7-methyl-3H-pyrrolo[2,3-d]pyrimidin-4(7H)-one (S4.3h)

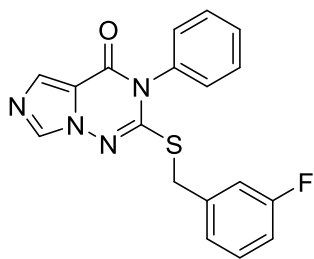
A pressure tube was charged with **S4.3g** (100mg, 0.545 mmol), DIPEA (0.190 ml, 1.089 mmol), (3-fluorophenyl)methanethiol (0.101 ml, 0.817 mmol) and 1mL abs. EtOH. The headspace was purged with Ar and the tube was heated to 100°C overnight. Upon cooling a white precipitate formed which was collected by filtration and washed with an additional 1mL ice cold EtOH to afford the titled compound as a white solid (110mg, 0.380 mmol, 69.8 % yield). ¹H NMR (400 MHz, DMSO-d₆) δ 12.12 (s, 1H), 7.41 - 7.24 (m, 3H), 7.06 (ddt, *J* = 9.5, 7.5, 2.1 Hz, 1H), 6.97 (d, *J* = 3.4 Hz, 1H), 6.35 (d, *J* = 3.3 Hz, 1H), 4.45 (s, 2H), 3.70 (s, 3H).



2-((3-Fluorobenzyl)thio)-7-methyl-3-phenyl-3H-pyrrolo[2,3-d]pyrimidin-4(7H)-one (258470)

A flask was charged with **S4.3h** (50mg, 0.173 mmol), phenylboronic acid (23.18 mg, 0.190 mmol), Cu(II)OAc hydrate (51.8 mg, 0.259 mmol), pyridine (28.0 μl, 0.346 mmol), 3Å

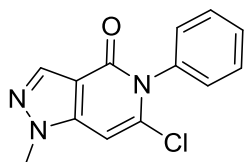
molecular sieves and 2mL DCM and stirred at RT under air for 5 days. The mixture was filtered through celite and the pad washed with additional DCM. The filtrate was washed with 1N HCl and brine before drying over sodium sulfate and concentrating. The crude residue was taken up in hot EtOH and the titled compound recrystallized as a white solid upon cooling (25 mg, 0.068 mmol, 39.6 % yield). MS (ESI): m/z 366.1073 $[M+H]^+$ 1H NMR (500 MHz, $CDCl_3$) δ 7.66 - 7.41 (m, 3H), 7.33 - 7.22 (m, 3H), 7.18 - 7.08 (m, 2H), 6.94 (td, $J = 8.7, 2.5$ Hz, 1H), 6.80 - 6.71 (m, 1H), 6.67 - 6.61 (m, 1H), 4.34 (s, 2H), 3.80 (s, 3H). ^{13}C NMR (126 MHz, $CDCl_3$) δ 162.67 (d, $J = 245.7$ Hz), 162.41, 159.18, 155.59, 146.87, 139.27, 136.39, 129.93 (d, $J = 8.2$ Hz), 129.70, 129.55, 129.49, 124.71 (d, $J = 2.9$ Hz), 123.06, 116.20, 114.35 (d, $J = 21.1$ Hz), 104.59, 102.96, 36.60 (d, $J = 2.0$ Hz), 31.52.



2-((3-fluorobenzyl)thio)-3-phenylimidazo[5,1-f][1,2,4]triazin-4(3H)-one (259010)

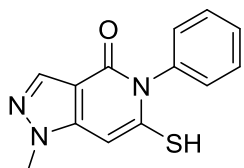
Ethyl 1-amino-1H-imidazole-5-carboxylate (**4.4b**) (12mg, 0.077 mmol), prepared as previously described,¹⁵⁶ was dissolved in dry DMF to which isothiocyanatobenzene (10.16 μ l, 0.085 mmol) was added. The reaction was stirred under N_2 overnight. The next day, 60 wt.% NaH (6.19 mg, 0.155 mmol) was added and the mixture was stirred for 2 h, at which point the flask was chilled to $0^\circ C$ and 3-fluorobenzyl bromide (10.44 μ l, 0.085 mmol) was added. The mixture was stirred overnight. The reaction was diluted with brine and extracted with ethyl acetate. The organic portion was dried over sodium sulfate and the solvent removed. The crude product was purified by Flash (Eluting 50-70% EtOAc in Hexanes) yielding the titled compound as a colorless residue

(14mg, 0.040 mmol, 51.4 % yield). MS (ESI): m/z 353.0870 $[M+H]^+$ 1H NMR (500 MHz, $CDCl_3$) δ 8.11 (s, 1H), 7.91 (s, 1H), 7.59 - 7.47 (m, 3H), 7.33 - 7.25 (m, 3H), 7.12 (d, $J = 7.7$ Hz, 1H), 7.05 (d, $J = 9.4$ Hz, 1H), 6.96 (t, $J = 8.8$ Hz, 1H), 4.26 (s, 2H). ^{13}C NMR (126 MHz, $CDCl_3$) δ 162.71 (d, $J = 246.7$ Hz), 153.51, 153.22, 137.36 (d, $J = 7.6$ Hz), 133.72, 133.52, 130.48, 130.20 (d, $J = 8.4$ Hz), 129.93, 129.74, 129.49, 124.95 (d, $J = 3.2$ Hz), 118.02, 116.24 (d, $J = 22.2$ Hz), 114.95 (d, $J = 21.0$ Hz), 36.59. HPLC Purity 98%



6-chloro-1-methyl-5-phenyl-1H-pyrazolo[4,3-c]pyridin-4(5H)-one (S4.5a)

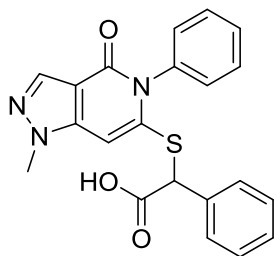
A dry flask was charged with 25mL DCE, 3Å molecular sieves, phenylboronic acid (1.966 g, 16.12 mmol), **S4.3d** (1.48 g, 8.06 mmol), copper(II) acetate hydrate (0.322 g, 1.612 mmol), and pyridine (1.304 ml, 16.12 mmol). The flask was vacuum purged and backfilled with an O_2 balloon and stirred vigorously for 3 d. The crude reaction mixture was filtered with Celite and the filter pad washed with DCM. The filtrate was washed with sat. aq. NH_4Cl and dried over sodium sulfate. Following concentration, the crude residue was washed with 10mL diethyl ether yielding an orange solid which was taken forward without further purification (1.05 g, 4.04 mmol, 50.2 % yield).



6-mercapto-1-methyl-5-phenyl-1H-pyrazolo[4,3-c]pyridin-4(5H)-one (S4.5b)

A flask containing 6-chloro-1-methyl-5-phenyl-1H-pyrazolo[4,3-c]pyridin-4(5H)-one (1.05 g, 4.04 mmol), Na_2S (400 mg, 4.4 mmol) and 20mL DMF was rigorously deoxygenated under

vacuum, backfilled with N₂ and heated to 140°C for 12 h. The reaction was diluted with 1N HCl and EtOAc forming an emulsion. The entire mixture was filtered, affording the titled compound as a white solid (620mg, 2.410 mmol, 59.6 % yield). ¹H NMR (400 MHz, DMSO-*d*₆) δ 7.97 (s, 1H), 7.55 – 7.42 (m, 3H), 7.25 (d, *J* = 7.3 Hz, 2H), 6.89 (s, 1H), 3.87 (s, 3H).

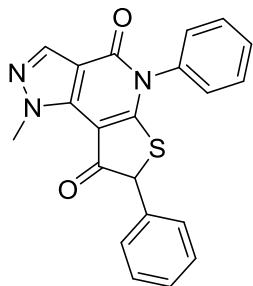


2-((1-Methyl-4-oxo-5-phenyl-4,5-dihydro-1H-pyrazolo[4,3-c]pyridin-6-yl)thio)-2-phenylacetic acid (S4.5c)

To a suspension of **S4.5b** (180 mg, 0.700 mmol) and K₂CO₃ (135 mg, 0.979 mmol) in 3mL DMF was added ethyl 2-bromo-2-phenylacetate (147 μl, 0.839 mmol). The mixture was stirred at RT overnight. The next day the mixture was diluted with water and extracted 2x with EtOAc. The combined organics were washed 3x with brine, dried over sodium sulfate, and concentrated. The crude mixture was purified by flash (Eluting at 50% EtOAc in Hexanes) to afford ethyl 2-((1-methyl-4-oxo-5-phenyl-4,5-dihydro-1H-pyrazolo[4,3-c]pyridin-6-yl)thio)-2-phenylacetate as a white solid (213mg, 0.508 mmol, 72.6 % yield). ¹H NMR (500 MHz, CDCl₃) δ 8.10 (s, 1H), 7.56 - 7.46 (m, 3H), 7.34 - 7.23 (m, 7H), 6.47 (s, 1H), 4.69 (s, 1H), 4.23 - 4.02 (m, 2H), 3.93 (s, 3H), 1.18 (t, *J* = 7.1 Hz, 3H).

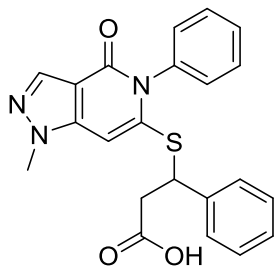
A slurry of ethyl 2-((1-methyl-4-oxo-5-phenyl-4,5-dihydro-1H-pyrazolo[4,3-c]pyridin-6-yl)thio)-2-phenylacetate (213 mg, 0.508 mmol) in 2mL 1N LiOH and 3mL THF was stirred for 2

hours at which point the reaction was complete by HPLC. Following removal of THF, the mixture was acidified with 1N HCl and extracted 3x with EtOAc. The combined organics were washed with brine, dried over sodium sulfate, and concentrated to afford the titled compound as a white solid (202mg, 0.516 mmol, 102 % yield).



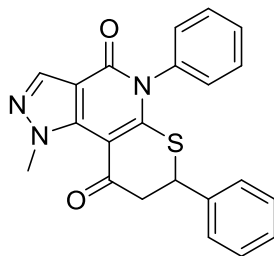
1-Methyl-5,7-diphenyl-1H-pyrazolo[3,4-d]thieno[2,3-b]pyridine-4,8(5H,7H)-dione (263861)

S4.5c (138 mg, 0.353 mmol) was dissolved in 5mL DCM and cooled to 0°C under nitrogen at which point (COCl)₂ (0.037 ml, 0.423 mmol) and DMF (2.73 μl, 0.035 mmol) were added sequentially. The mixture was stirred for 10 minutes at 0°C and then allowed to warm to room temperature and left overnight. The next day the solvent was removed and the residue was purified by flash (EA in Hex) to yield (90mg, 0.241 mmol, 68.4 % yield) as an oily white solid. MS (ESI): m/z 374.0956 [M+H]⁺ ¹H NMR (500 MHz, CDCl₃) δ 8.17 (s, 1H), 7.63 - 7.53 (m, 3H), 7.44 - 7.34 (m, 5H), 7.34 - 7.28 (m, 2H), 4.97 (s, 1H), 4.48 (s, 3H). ¹³C NMR (126 MHz, CDCl₃) δ 192.45, 171.74, 158.04, 138.91, 138.16, 136.11, 134.16, 130.45, 130.00, 129.20, 128.86, 128.53, 128.34, 110.79, 101.00, 58.53, 41.37. HPLC Purity: 96%.



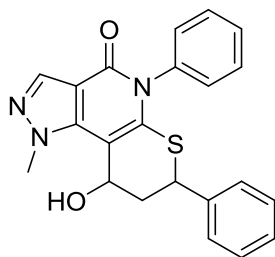
3-((1-Methyl-4-oxo-5-phenyl-4,5-dihydro-1H-pyrazolo[4,3-c]pyridin-6-yl)thio)-3-phenylpropanoic acid (S4.5d)

Cinnamic acid (535 mg, 3.61 mmol) was heated to 70°C in a sealed tube with 1mL 33% HBr/HOAc overnight. The next day the reaction was diluted with DCM and washed with water and brine, dried over sodium sulfate, and concentrated affording a white solid. The solid dissolved in 10mL DMF to which **S4.5b** (620mg, 2.410 mmol) and sodium bicarbonate (304 mg, 3.61 mmol) were added. After 2 h the thiol was all dissolved and the reaction was complete by HPLC and the reaction was neutralized with a couple drops of conc. HCl. The DMF was removed in vacuo and the crude product was purified by flash (5-10% MeOH in DCM) yielding the titled compound as a yellow oil. (670mg, 1.652 mmol, 68.6 % yield). ¹H NMR (500 MHz, CDCl₃) δ 8.04 (d, *J* = 0.9 Hz, 1H), 7.52 – 7.40 (m, 3H), 7.32 – 7.19 (m, 5H), 7.13 (d, *J* = 7.0 Hz, 2H), 6.53 (s, 1H), 4.48 (t, *J* = 7.2 Hz, 1H), 3.86 (s, 3H), 2.97 – 2.83 (m, 2H).



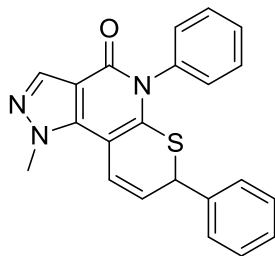
1-Methyl-5,7-diphenyl-7,8-dihydropyrazolo[3,4-d]thiopyrano[2,3-b]pyridine-4,9(1H,5H)-dione (263645)

To a dry pressure tube was added a suspension of **S4.5d** (630mg, 1.554 mmol) in 10mL DCE. Methanesulfonic anhydride (541 mg, 3.11 mmol) was added and the headspace was flushed with N₂ and the tube sealed. The tube was heated to 70°C for 2 h. The next day the reaction was diluted with DCM and washed with saturated Sodium Bicarbonate and brine before drying over sodium sulfate and concentrating. The crude brown oil was purified by flash (Elutes around 50% EA/Hex) yielding the product as a white-yellow foam (250mg, 0.645 mmol, 41.5 % yield). MS (ESI): *m/z* 388.1114 [M+H]⁺ ¹H NMR (400 MHz, CDCl₃) δ 8.17 (s, 1H), 7.57 - 7.46 (m, 3H), 7.40 - 7.30 (m, 5H), 7.29 - 7.21 (m, 3H), 4.66 (dd, J = 12.6, 4.5 Hz, 1H), 4.19 (s, 3H), 3.31 - 3.11 (m, 2H). ¹³C NMR (101 MHz, CDCl₃) δ 189.64, 159.55, 157.89, 141.28, 137.06, 136.73, 135.76, 130.17, 129.87, 129.77, 129.20, 129.15 (d, J = 1.1 Hz), 129.08, 127.79, 112.19, 105.21, 46.86, 45.66, 42.30. HPLC Purity: 99%



9-hydroxy-1-methyl-5,7-diphenyl-5,7,8,9-tetrahydropyrazolo[3,4-d]thiopyrano[2,3-b]pyridin-4(1H)-one (S4.5e)

NaBH₄ (5.86 mg, 0.155 mmol), and **263645** (50 mg, 0.129 mmol) were added to 1mL abs. EtOH at 0°C. The mixture was stirred for 30 minutes at the same temperature then quenched with saturated aqueous NH₄Cl. The mixture was concentrated and taken up in EtOAc, washed with water and brine, dried over sodium sulfate, and concentrated to afford the titled compound (mixture of diastereomers) as a white solid (42mg, 0.108 mmol, 84 % yield).

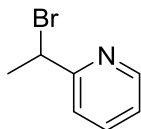


1-Methyl-5,7-diphenyl-5,7-dihydropyrazolo[3,4-d]thiopyrano[2,3-b]pyridin-4(1H)-one

(263867)

To a solution of **S4.5e** (24mg, 0.062 mmol) and InCl_3 (1.363 mg, 6.16 μmol) in 1mL DCM was added chlorodiphenylsilane (0.022 mL, 0.123 mmol). The mixture was stirred for 2 hours at room temperature at which point the mixture was concentrated and purified by flash (Eluting at 70% EA/Hex) to yield the titled compound as a yellow solid (14mg, 0.038 mmol, 61.2 % yield).

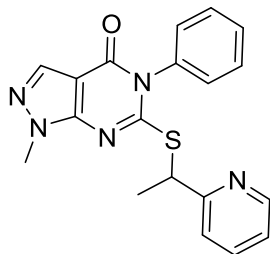
MS (ESI): m/z 372.1162 $[\text{M}+\text{H}]^+$ ^1H NMR (500 MHz, CDCl_3) δ 8.12 (s, 1H), 7.53 - 7.47 (m, 1H), 7.47 - 7.40 (m, 2H), 7.38 - 7.34 (m, 2H), 7.34 - 7.27 (m, 4H), 7.13 (dt, $J = 7.7, 2.3$ Hz, 1H), 7.03 (dd, $J = 9.8, 1.7$ Hz, 1H), 5.81 (dd, $J = 9.8, 4.8$ Hz, 1H), 4.87 (dd, $J = 4.8, 1.7$ Hz, 1H), 4.21 (s, 3H). ^{13}C NMR (126 MHz, CDCl_3) δ 158.29, 143.28, 141.58, 138.56, 138.02, 136.92, 129.44, 129.40, 129.39, 129.23, 128.79, 128.75, 128.40, 128.09, 123.47, 118.72, 112.30, 101.99, 45.63, 39.57. HPLC Purity: 99%



2-(1-Bromoethyl)pyridine

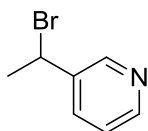
2-ethylpyridine (1.067 ml, 9.33 mmol), AIBN (0.153 g, 0.933 mmol), and NBS (1.744 g, 9.80 mmol) were refluxed in 20mL of CCl_4 for 1 h. The reaction was cooled and filtered and the solid was taken up in DCM and filtered again. The filtrate was washed with saturated aqueous sodium

bicarbonate and brine before drying over sodium sulfate and concentrating. The resulting orange oil was carried forward without further purification.



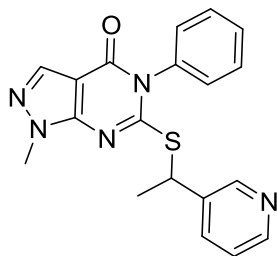
1-Methyl-5-phenyl-6-((1-(pyridin-2-yl)ethyl)thio)-1H-pyrazolo[3,4-d]pyrimidin-4(5H)-one (263118)

Prepared from 2-(1-Bromoethyl)pyridine in a manner similar to **257723** in chapter 3. White solid (56mg, 0.154 mmol, 39.8 % yield) MS (ESI): m/z 364.1225 $[M+H]^+$ 1H NMR (500 MHz, $CDCl_3$) δ 8.55 (d, $J = 4.8$ Hz, 1H), 8.00 (s, 1H), 7.64 (t, $J = 7.7$ Hz, 1H), 7.57 – 7.45 (m, 3H), 7.40 (d, $J = 7.8$ Hz, 1H), 7.28 (d, $J = 7.5$ Hz, 1H), 7.22 (d, $J = 6.5$ Hz, 1H), 7.16 (t, $J = 6.2$ Hz, 1H), 5.14 (q, $J = 7.2$ Hz, 1H), 3.96 (s, 3H), 1.73 (d, $J = 7.1$ Hz, 3H). ^{13}C NMR (126 MHz, $CDCl_3$) δ 161.52, 161.07, 157.78, 150.96, 149.52, 136.66, 135.53, 135.37, 129.96, 129.75, 129.38, 122.34, 121.76, 102.83, 48.47, 34.00, 20.95. HPLC Purity: 99%



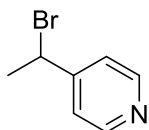
3-(1-Bromoethyl)pyridine

Prepared in a similar manner to 2-(1-Bromoethyl)pyridine. The resulting orange oil was carried forward without further purification.



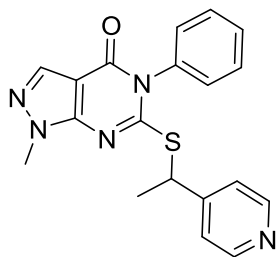
1-Methyl-5-phenyl-6-((1-(pyridin-3-yl)ethyl)thio)-1H-pyrazolo[3,4-d]pyrimidin-4(5H)-one (263119)

Prepared from 3-(1-Bromoethyl)pyridine in a manner similar to **257723** in chapter 3. White solid (90mg, 0.248 mmol, 64.0 % yield) MS (ESI): m/z 364.1225 $[M+H]^+$ 1H NMR (500 MHz, $CDCl_3$) δ 8.72 (d, $J = 2.2$ Hz, 1H), 8.49 (d, $J = 4.8$ Hz, 1H), 7.99 (s, 1H), 7.70 (d, $J = 7.9$ Hz, 1H), 7.59 – 7.47 (m, 3H), 7.29 – 7.21 (m, 2H), 7.18 (d, $J = 7.1$ Hz, 1H), 5.01 (q, $J = 7.3$ Hz, 1H), 3.99 (s, 3H), 1.68 (d, $J = 7.3$ Hz, 3H). ^{13}C NMR (126 MHz, $CDCl_3$) δ 160.67, 157.61, 150.85, 149.37, 148.81, 138.32, 135.47, 135.37, 134.47, 130.10, 129.79, 129.72, 129.37, 129.35, 123.49, 102.96, 44.04, 34.20, 21.59. HPLC Purity: 99%



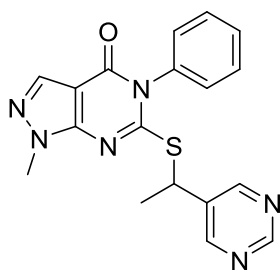
4-(1-bromoethyl)pyridine

Prepared in a similar manner to 2-(1-Bromoethyl)pyridine. The resulting orange oil was carried forward without further purification.



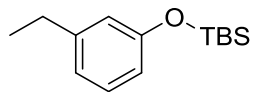
1-methyl-5-phenyl-6-((1-(pyridin-4-yl)ethyl)thio)-1H-pyrazolo[3,4-d]pyrimidin-4(5H)-one (263650)

Prepared from 4-(1-Bromoethyl)pyridine in a manner similar to **257723** in chapter 3. White solid (31mg, 0.085 mmol, 29.4 % yield). MS (ESI): m/z 364.1229 $[M+H]^+$ 1H NMR (500 MHz, $CDCl_3$) δ 8.55 (d, $J = 4.9$ Hz, 2H), 7.99 (s, 1H), 7.61 - 7.48 (m, 3H), 7.36 - 7.30 (m, 2H), 7.29 - 7.22 (m, 1H), 7.23 - 7.15 (m, 1H), 4.95 (q, $J = 7.3$ Hz, 1H), 3.95 (s, 3H), 1.64 (d, $J = 7.3$ Hz, 3H). ^{13}C NMR (126 MHz, $CDCl_3$) δ 160.55, 157.58, 151.66, 150.79, 150.04, 135.43, 135.41, 130.15, 129.79 (d, $J = 9.4$ Hz), 129.35 (d, $J = 3.2$ Hz), 122.37, 102.95, 45.48, 34.10, 21.20. HPLC Purity: 99%



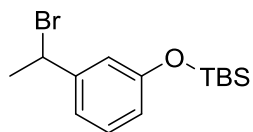
1-methyl-5-phenyl-6-((1-(pyrimidin-5-yl)ethyl)thio)-1H-pyrazolo[3,4-d]pyrimidin-4(5H)-one (263640)

S4.1b (75mg, 0.290 mmol), 5-(1-iodoethyl)pyrimidine (95 mg, 0.407 mmol), and K_2CO_3 (60.2 mg, 0.436 mmol) were stirred at room temperature in 2mL DMF overnight. The next day the mixture was diluted with water and extracted 2x with ethyl acetate. The combined organic portion was washed 3x with brine and dried over sodium sulfate. The crude solid obtained upon concentration was recrystallized from hot ethanol yielding the titled compound as a white solid (41mg, 0.113 mmol, 38.7 % yield). MS (ESI): m/z 387.1010 $[M+H]^+$ 1H NMR (500 MHz, $CDCl_3$) δ 9.10 (s, 1H), 8.82 (s, 2H), 7.99 (s, 1H), 7.61 - 7.49 (m, 3H), 7.30 - 7.23 (m, 1H), 7.21 - 7.15 (m, 1H), 4.94 (q, $J = 7.6$ Hz, 1H), 3.98 (s, 3H), 1.68 (d, $J = 7.4$ Hz, 3H). ^{13}C NMR (126 MHz, $CDCl_3$) δ 160.07, 157.69, 157.41, 155.97, 150.67, 136.63, 135.42, 135.25, 130.29, 129.91, 129.80, 129.34, 103.07, 41.63, 34.31, 21.05.



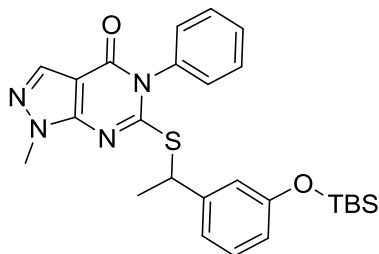
tert-butyl(3-ethylphenoxy)dimethylsilane

3-Ethylphenol (1 g, 8.19 mmol), TBS-Cl (1.357 g, 9.00 mmol), and imidazole (1.226 g, 18.01 mmol) were stirred overnight in 10mL DMF. Diluted with 25mL water and extracted with 25mL Ethyl acetate. The organic portion was dried over sodium sulfate and the solvent was removed. The crude oil was filtered through a pad of silica using ~5% EA in Hex yielding (1.8 g, 7.61 mmol, 93 % yield) as a colorless oil.



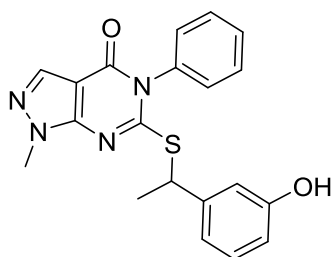
(3-(1-bromoethyl)phenoxy)(tert-butyl)dimethylsilane

A suspension of tert-butyl(3-ethylphenoxy)dimethylsilane (1.8 g, 7.61 mmol), benzoyl peroxide (0.277 g, 1.142 mmol), and NBS (1.355 g, 7.61 mmol) in 15mL CCl₄ was refluxed for 3 h. The mixture was cooled, filtered and the filtrate was diluted with DCM and washed with water and brine before drying over sodium sulfate. The mixture was concentrated and the resulting residue was filtered through a pad of silica eluting with hexanes yielding the titled compound as a colorless oil (1.2 g, 3.81 mmol, 50.0 % yield). ¹H NMR (500 MHz, CDCl₃) δ 7.19 (t, J = 7.9 Hz, 1H), 7.01 (d, J = 7.6 Hz, 1H), 6.92 (d, J = 2.1 Hz, 1H), 6.75 (dd, J = 8.1, 2.4 Hz, 1H), 5.15 (q, J = 6.9 Hz, 1H), 2.02 (d, J = 6.9 Hz, 3H), 1.00 - 0.95 (s, 9H), 0.21 (s, 6H).



6-((1-(3-((tert-butyldimethylsilyl)oxy)phenyl)ethyl)thio)-1-methyl-5-phenyl-1H-pyrazolo[3,4-d]pyrimidin-4(5H)-one

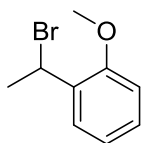
Prepared in a manner similar to **257723** in chapter 3. Yellow oil. (195mg, 0.396 mmol, 82 % yield)



6-((1-(3-hydroxyphenyl)ethyl)thio)-1-methyl-5-phenyl-1H-pyrazolo[3,4-d]pyrimidin-4(5H)-one (263117)

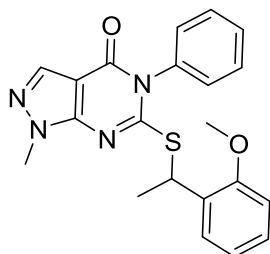
To an HDPE vial was added 6-((1-(3-((tert-butyldimethylsilyl)oxy)phenyl)ethyl)thio)-1-methyl-5-phenyl-1H-pyrazolo[3,4-d]pyrimidin-4(5H)-one (195 mg, 0.396 mmol) dissolved in 3mL THF. 70% HF in pyridine (250 μ l, 10.15 mmol) was added and the vial was sealed under N₂ and left overnight. The next morning the reaction was diluted with 15mL water and extracted with EtOAc. The organic portion was washed with saturated aqueous sodium bicarbonate and brine then dried over sodium sulfate and concentrated yielding the titled compound as a white solid (123mg, 0.325 mmol, 82 % yield). MS (ESI): m/z 379.1218 [M+H]⁺ ¹H NMR (500 MHz, DMSO-*d*₆) δ 9.43 (s, 1H), 8.04 (s, 1H), 7.59 - 7.53 (m, 1H), 7.53 - 7.48 (m, 2H), 7.38 (d, J = 7.6 Hz, 1H), 7.33 - 7.26 (m, 1H), 7.10 (t, J = 7.8 Hz, 1H), 6.83 (d, J = 7.7 Hz, 1H), 6.78 (s, 1H), 6.63 (dd, J = 8.1, 2.4 Hz, 1H), 4.94 (q, J = 7.0 Hz, 1H), 3.97 (s, 3H), 1.64 (d, J = 7.0 Hz, 3H). ¹³C

NMR (126 MHz, DMSO-*d*₆) δ 161.31, 157.80, 157.30, 150.87, 143.59, 136.14, 135.10, 130.26, 130.07, 129.98, 129.95, 118.52, 114.93, 114.74, 102.80, 46.84, 34.34, 22.09. HPLC Purity: 98%



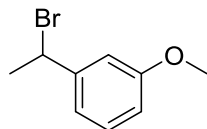
1-(1-bromoethyl)-2-methoxybenzene

1-ethyl-2-methoxybenzene (0.311 ml, 2.203 mmol), NBS (412 mg, 2.313 mmol), and AIBN (72.3 mg, 0.441 mmol) were suspended in 5mL CCl₄ and refluxed for 3 h. The mixture was cooled and filtered. The filtrate was washed with sat. sodium carbonate and brine, then dried over sodium sulfate and concentrated to afford the titled compound as a colorless oil which was used in the next step without further purification (520mg, 2.418 mmol, 110 % yield).



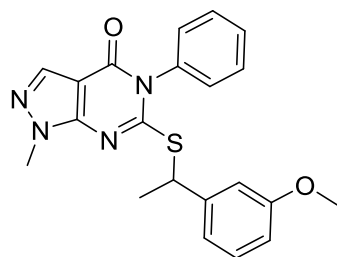
6-((1-(2-methoxyphenyl)ethyl)thio)-1-methyl-5-phenyl-1H-pyrazolo[3,4-d]pyrimidin-4(5H)-one (263351)

Prepared from 1-(1-bromoethyl)-2-methoxybenzene in a manner similar to **257723** in chapter 3. White solid. MS (ESI): *m/z* 393.1383 [M+H]⁺ ¹H NMR (500 MHz, CDCl₃) δ 8.00 (s, 1H), 7.61 - 7.43 (m, 3H), 7.33 (d, *J* = 7.6 Hz, 1H), 7.30 - 7.25 (m, 1H), 7.25 - 7.18 (m, 2H), 6.90 (t, *J* = 7.7 Hz, 1H), 6.87 (d, *J* = 8.0 Hz, 1H), 5.45 (q, *J* = 7.2 Hz, 1H), 3.98 (s, 3H), 3.85 (s, 3H), 1.69 (d, *J* = 7.1 Hz, 3H). ¹³C NMR (126 MHz, CDCl₃) δ 162.17, 157.95, 156.54, 151.18, 135.77, 135.34, 129.94, 129.81, 129.62 (d, *J* = 4.8 Hz), 129.40 (d, *J* = 2.2 Hz), 128.62, 127.98, 120.63, 110.74, 102.76, 55.52, 41.03, 33.78, 21.14. (60 mg, 0.153 mmol, 52.7 % yield) HPLC Purity: 98%



1-(1-Bromoethyl)-3-methoxybenzene

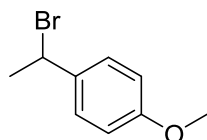
Prepared in a similar manner as 1-(1-bromoethyl)-2-methoxybenzene from 1-ethyl-3-methoxybenzene prepared as previously described.¹⁵⁷ Colorless oil. (550mg, 4.04 mmol, 99 % yield)



6-((1-(3-Methoxyphenyl)ethyl)thio)-1-methyl-5-phenyl-1H-pyrazolo[3,4-d]pyrimidin-4(5H)-one (263353)

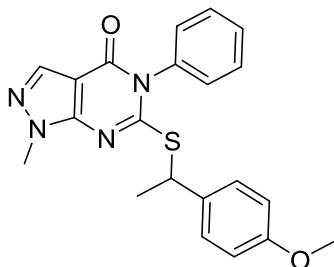
Prepared from 1-(1-bromoethyl)-3-methoxybenzene in a manner similar to **257723** in chapter 3.

White solid. (29mg, 0.074 mmol, 25.4 % yield). MS (ESI): m/z 393.1383 [M+H]⁺ ¹H NMR (500 MHz, CDCl₃) δ 8.00 (s, 1H), 7.60 - 7.43 (m, 3H), 7.27 (d, J = 6.7 Hz, 1H), 7.23 (t, J = 8.1 Hz, 1H), 7.21 - 7.17 (m, 1H), 6.97 (d, J = 7.6 Hz, 1H), 6.95 - 6.90 (m, 1H), 6.78 (d, J = 8.4 Hz, 1H), 4.99 (q, J = 7.2 Hz, 1H), 4.00 (s, 3H), 3.79 (s, 3H), 1.70 (d, J = 7.2 Hz, 3H). ¹³C NMR (126 MHz, CDCl₃) δ 161.49, 159.62, 157.82, 151.04, 143.66, 135.62, 135.36, 129.93, 129.68 (d, J = 9.5 Hz), 129.53, 129.38 (d, J = 5.0 Hz), 119.84, 113.81, 112.35, 102.88, 55.22, 46.85, 34.08, 21.91. HPLC Purity: 98%



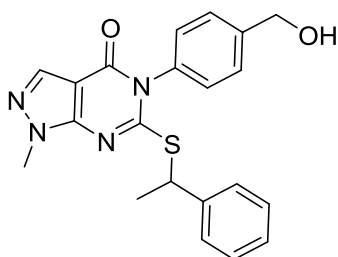
1-(1-Bromoethyl)-4-methoxybenzene

Prepared in a similar manner as 1-(1-bromoethyl)-2-methoxybenzene from 1-ethyl-4-methoxybenzene prepared as previously described.¹⁵⁸ Colorless oil. (490mg, 2.278 mmol, 103 % yield)



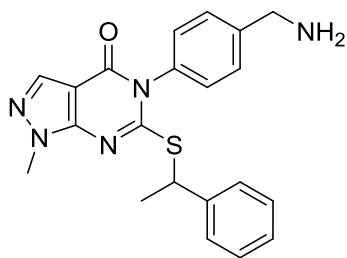
6-((1-(4-Methoxyphenyl)ethyl)thio)-1-methyl-5-phenyl-1H-pyrazolo[3,4-d]pyrimidin-4(5H)-one (263352)

Prepared from 1-(1-Bromoethyl)-4-methoxybenzene in a manner similar to **257723** in chapter 3. White solid. (38mg, 0.097 mmol, 33.3 % yield) MS (ESI): m/z 393.1381 $[M+H]^+$ 1H NMR (500 MHz, $CDCl_3$) δ 8.01 (s, 1H), 7.61 - 7.40 (m, 3H), 7.30 (d, $J = 8.4$ Hz, 2H), 7.28 - 7.24 (m, 1H), 7.18 (d, $J = 6.6$ Hz, 1H), 6.83 (d, $J = 8.4$ Hz, 2H), 5.00 (q, $J = 7.1$ Hz, 1H), 4.02 (s, 3H), 3.78 (s, 3H), 1.71 (d, $J = 7.1$ Hz, 3H). ^{13}C NMR (126 MHz, $CDCl_3$) δ 161.69, 158.95, 157.85, 151.09, 135.65, 135.37, 133.82, 129.88, 129.65 (d, $J = 9.4$ Hz), 129.37 (d, $J = 5.7$ Hz), 128.66, 113.87, 102.87, 55.25, 46.44, 34.06, 21.98. HPLC Purity: 96%



5-(4-(Hydroxymethyl)phenyl)-1-methyl-6-((1-phenylethyl)thio)-1H-pyrazolo[3,4-d]pyrimidin-4(5H)-one (263642)

S4.6a (250 mg, 1.183 mmol), and (4-aminophenyl)methanol (146 mg, 1.183 mmol) were stirred in 2mL DMF for 1 h. The flask was cooled in an ice bath and 60 wt.% NaH (99 mg, 2.485 mmol) was added. The mixture was stirred for 30 min at 0°C and 1 h at RT. The reaction was quenched with a few drops of Sat. NH₄Cl and diluted with water and ethyl acetate (Aq. Layer pH=7). The organic layer was discarded and the aqueous layer was acidified with 1N HCl and extracted 2x with EtOAc. The combined organics were washed 3x with brine, dried over sodium sulfate and concentrated. The crude sulfide was dissolved in 2mL DMF to which K₂CO₃ (164 mg, 1.183 mmol) and (1-bromoethyl)benzene (0.161 ml, 1.183 mmol) were added. The mixture was stirred for 2 h and diluted with water and extracted 2x with EtOAc. The combined organics were washed 3x with brine and dried over sodium sulfate and concentrated. The crude was purified by flash (eluting 50% EtOAc in Hexanes) yielding the product as a white solid. (100mg, 0.255 mmol, 21.53 % yield) MS (ESI): m/z 393.1380 [M+H]⁺ ¹H NMR (500 MHz, CDCl₃) δ 7.95 (d, J = 3.0 Hz, 1H), 7.46 (dd, J = 8.1, 2.0 Hz, 1H), 7.41 (dd, J = 8.1, 1.9 Hz, 1H), 7.37 (d, J = 8.2 Hz, 2H), 7.32 - 7.25 (m, 3H), 7.22 (dd, J = 7.5, 1.9 Hz, 2H), 7.13 (dd, J = 8.1, 2.2 Hz, 1H), 5.00 (q, J = 7.1 Hz, 1H), 4.65 (d, J = 3.3 Hz, 2H), 3.97 (d, J = 1.7 Hz, 3H), 3.38 (d, J = 24.4 Hz, 1H), 1.69 (dd, J = 7.2, 1.3 Hz, 4H). ¹³C NMR (126 MHz, CDCl₃) δ 161.70, 158.05, 151.06, 143.53, 142.09, 135.26, 134.33, 129.25, 128.54, 127.88 (d, J = 7.7 Hz), 127.57, 127.52, 102.79, 64.08, 46.94, 34.06, 21.97. HPLC Purity: 96%



5-(4-(aminomethyl)phenyl)-1-methyl-6-((1-phenylethyl)thio)-1H-pyrazolo[3,4-d]pyrimidin-4(5H)-one hydrochloride (264203)

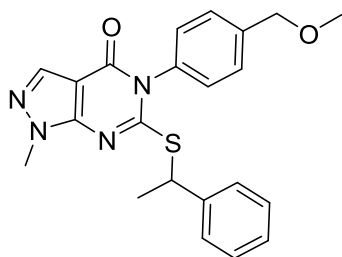
DIPEA (200 μ l, 1.147 mmol), and Ms-Cl (74.5 μ l, 0.955 mmol) were added sequentially by syringe to a solution of **263642** (300mg, 0.764 mmol) in 1.5mL DCM at -10°C . The mixture was stirred for 10 min then taken out of the cooling bath and stirred for 3 h. The reaction was diluted with DCM and washed with water and brine before drying the organic portion over sodium sulfate and concentrating to yield 4-(1-methyl-4-oxo-6-((1-phenylethyl)thio)-1H-pyrazolo[3,4-d]pyrimidin-5(4H)-yl)benzyl methanesulfonate as a colorless oil (347mg, 0.737 mmol, 96 % yield).

A degassed solution of NaN_3 (24.87 mg, 0.383 mmol) and 4-(1-methyl-4-oxo-6-((1-phenylethyl)thio)-1H-pyrazolo[3,4-d]pyrimidin-5(4H)-yl)benzyl methanesulfonate (150 mg, 0.319 mmol) was stirred in 2mL DMF at 60°C overnight. The next day the mixture was diluted with water, and extracted 2x into EtOAc. The combined organics were washed 3x with brine and dried over sodium sulfate. The crude was purified by flash (eluting around 60% EA/Hex) to yield 5-(4-(azidomethyl)phenyl)-1-methyl-6-((1-phenylethyl)thio)-1H-pyrazolo[3,4-d]pyrimidin-4(5H)-one

as a white foam (62mg, 0.149 mmol, 46.6 % yield). ^1H NMR (400 MHz, CDCl_3) δ 8.00 (s, 1H), 7.48 (d, J = 8.0 Hz, 1H), 7.44 (d, J = 8.5 Hz, 1H), 7.38 (d, J = 7.6 Hz, 2H), 7.34 - 7.27 (m, 3H), 7.22 - 7.17 (m, 1H), 5.02 (q, J = 7.2 Hz, 1H), 4.47 (s, 2H), 4.00 (s, 3H), 1.71 (d, J = 7.2 Hz, 3H).

5-(4-(azidomethyl)phenyl)-1-methyl-6-((1-phenylethyl)thio)-1H-pyrazolo[3,4-d]pyrimidin-4(5H)-one (62mg, 0.149 mmol) was taken up in 3mL THF to which polystyrene bound triphenylphosphine (Sigma Aldrich, 3mmol/g, .3mmol) and a few drops of water was added. The mixture was agitated on an orbit shaker for 2 days at which point 1 mL of water was

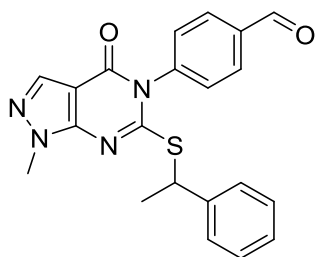
added. The mixture was filtered after an hour and the resin washed with DCM. The filtrate was concentrated and purified by flash (5% MeOH/94% DCM/1% TEA) to yield a yellow oil. The product was additionally purified by C18 flash (30%-50% ACN in Water, 0.1% TFA) to yield the TFA salt as an oil. Residue was taken up in Ethyl Acetate and washed with sat. sodium carbonate. The organic portion was concentrated, taken up in EtOH, treated with a few drops Conc. HCl and then concentrated again to yield the titled compound as a yellow residue (7 mg, 0.016 mmol, 11.01 % yield). MS (ESI): m/z 392.1542 $[M+H]^+$ 1H NMR (500 MHz, Methanol- d_4) δ 7.96 (s, 1H), 7.66 (d, $J = 8.0$ Hz, 1H), 7.62 (d, $J = 8.0$ Hz, 1H), 7.44 (d, $J = 7.9$ Hz, 1H), 7.40 - 7.32 (m, 3H), 7.29 (t, $J = 7.4$ Hz, 2H), 7.22 (t, $J = 7.3$ Hz, 1H), 5.07 (q, $J = 6.9$ Hz, 1H), 4.21 (s, 2H), 3.99 (s, 3H), 1.71 (d, $J = 6.9$ Hz, 3H). ^{13}C NMR (126 MHz, Methanol- d_4) δ 161.48, 158.37, 151.06, 141.70, 136.38, 135.21, 134.48, 130.19 (d, $J = 4.2$ Hz), 130.05 (d, $J = 3.7$ Hz), 128.23, 127.32, 127.18, 102.33, 46.97, 42.44, 33.01, 20.76. HPLC Purity 98%



5-(4-(methoxymethyl)phenyl)-1-methyl-6-((1-phenylethyl)thio)-1H-pyrazolo[3,4-d]pyrimidin-4(5H)-one (263862)

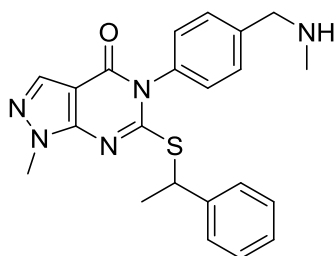
To a solution of **263642** (133mg, 0.339 mmol) in 3mL dry DMF at 0°C was added 60 wt.% NaH (13.55 mg, 0.339 mmol). MeI (42.4 μ l, 0.678 mmol) was added immediately and the mixture was stirred for 10 min then allowed to warm to RT and stirred for 1 h. The reaction was diluted

with water and extracted 2x with EtOAc. The combined organics were washed 3x with brine and dried over sodium sulfate. The crude product was purified by flash (eluting around 50% EtOAc in Hexanes) to yield the titled compound as a colorless oil which solidified over several days (45mg, 0.111 mmol, 32.7 % yield). MS (ESI): m/z 407.1533 $[M+H]^+$ 1H NMR (500 MHz, $CDCl_3$) δ 7.96 (s, 1H), 7.50 (dd, $J = 8.1, 1.9$ Hz, 1H), 7.45 (dd, $J = 8.1, 1.9$ Hz, 1H), 7.41 - 7.35 (m, 2H), 7.33 - 7.27 (m, 2H), 7.27 - 7.21 (m, 2H), 7.17 (dd, $J = 8.1, 2.3$ Hz, 1H), 5.01 (q, $J = 7.2$ Hz, 1H), 4.53 (s, 2H), 3.99 (s, 3H), 3.45 (s, 3H), 1.70 (d, $J = 7.2$ Hz, 3H). ^{13}C NMR (126 MHz, $CDCl_3$) δ 161.56, 157.82, 151.03, 142.13, 140.38, 135.30, 134.80, 129.36, 129.34, 128.57, 128.52, 128.50, 127.55, 127.51, 102.83, 73.99, 58.55, 46.89, 34.06, 21.98. HPLC Purity: 96%



4-(1-Methyl-4-oxo-6-((1-phenylethyl)thio)-1H-pyrazolo[3,4-d]pyrimidin-5(4H)-yl)benzaldehyde (S6.4b)

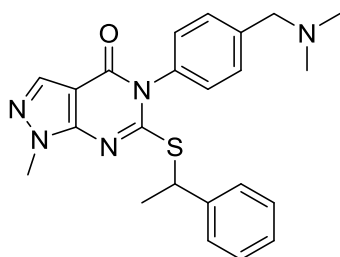
A solution of **263642** (500mg, 1.274 mmol) and Dess-Martin periodinane (648 mg, 1.529 mmol) was stirred in 10mL DCM overnight. The next day, 1mL sat. aq. sodium bicarbonate was added and the mixture vigorously stirred for 1 h then filtered. The organic portion of the filtrate was washed with water and brine then dried over sodium sulfate and concentrated to afford the titled compound as a white solid. (300mg, 0.768 mmol, 60.3 % yield). 1H NMR (500 MHz, $DMSO-d_6$) δ 10.06 (s, 1H), 8.06 (dd, $J = 8.1, 1.9$ Hz, 1H), 8.04 (s, 1H), 8.02 (dd, $J = 8.1, 2.0$ Hz, 1H), 7.66 (dd, $J = 8.1, 2.1$ Hz, 1H), 7.56 (dd, $J = 8.1, 2.1$ Hz, 1H), 7.45 - 7.39 (m, 2H), 7.30 (dd, $J = 8.4, 6.8$ Hz, 2H), 7.25 - 7.13 (m, 1H), 5.06 (q, $J = 7.1$ Hz, 1H), 3.96 (s, 3H), 1.66 (d, $J = 7.1$ Hz, 3H).



1-methyl-5-(4-((methylamino)methyl)phenyl)-6-((1-phenylethyl)thio)-1H-pyrazolo[3,4-d]pyrimidin-4(5H)-one (264200)

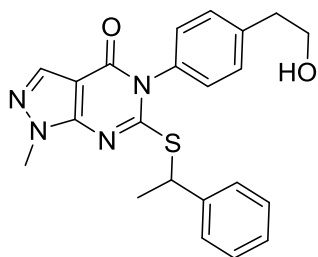
To a flask charged with 1mL MeOH and **S6.4b** (50 mg, 0.128 mmol) was added 33% methylamine in EtOH (0.032 ml, 0.256 mmol) and titanium isopropoxide (0.038 ml, 0.128 mmol) by syringe. The starting material gradually went into solution, and then a white precipitate formed over the course of an hour. At this point NaBH₄ (7.27 mg, 0.192 mmol) was added and the mixture was stirred for 15 minutes at which point the reaction was once again homogenous and the starting material was consumed by HPLC. The mixture was diluted with water and extracted 3x with ethyl acetate. The combined organic portion was washed with brine and dried over sodium sulfate. Upon concentrating, 45mg of an oily residue was obtained which was taken up in 1mL Et₂O and a few drops of hexane was added until the mixture became slightly cloudy. Upon cooling in the freezer, a precipitate formed which was collected by filtration yielding the titled compound as a white solid (9mg, 0.022 mmol, 17.33 % yield). (ESI): m/z 406.1693 [M+H]⁺ ¹H NMR (500 MHz, CDCl₃) δ 7.99 (s, 1H), 7.49 (dd, J = 8.1, 2.0 Hz, 1H), 7.44 (dd, J = 8.1, 1.9 Hz, 1H), 7.38 (d, J = 7.1 Hz, 2H), 7.30 (t, J = 7.5 Hz, 2H), 7.25 - 7.18 (m, 2H), 7.13 (dd, J = 8.1, 2.3 Hz, 1H), 5.01 (q, J = 7.2 Hz, 1H), 3.99 (s, 3H), 3.83 (s, 2H), 2.51 (s, 3H), 1.83 (br. s, 1H), 1.70 (d, J = 7.2 Hz, 3H). ¹³C NMR (126 MHz, CDCl₃) δ 161.62, 157.85,

151.04, 142.13 (d, J = 2.2 Hz), 135.34, 134.27, 129.33, 129.28, 129.26, 128.50, 127.53, 127.51, 102.86, 55.55, 46.87, 36.21, 34.04, 21.95. HPLC Purity 96%



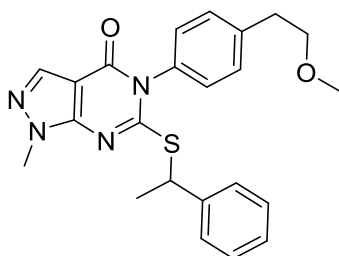
5-(4-((dimethylamino)methyl)phenyl)-1-methyl-6-((1-phenylethyl)thio)-1H-pyrazolo[3,4-d]pyrimidin-4(5H)-one (264201)

Prepared in a similar manner to **264200** using 5.6M dimethylamine in EtOH. (52mg, 0.124 mmol, 48.4 % yield) (ESI): m/z 420.1849 [M+H]⁺ ¹H NMR (500 MHz, CDCl₃) δ 7.98 (s, 1H), 7.47 (dd, J = 8.1, 1.9 Hz, 1H), 7.42 (dd, J = 8.1, 2.0 Hz, 1H), 7.40 - 7.34 (m, 2H), 7.33 - 7.27 (m, 2H), 7.25 - 7.18 (m, 2H), 7.12 (dd, J = 8.1, 2.3 Hz, 1H), 5.01 (q, J = 7.1 Hz, 1H), 3.99 (s, 3H), 3.49 (s, 2H), 2.29 (s, 6H), 1.70 (d, J = 7.2 Hz, 3H). ¹³C NMR (126 MHz, CDCl₃) δ 161.67, 157.84, 151.06, 142.20, 141.17, 135.34, 134.31, 130.10, 130.02, 129.19, 129.17, 128.51, 127.53, 127.51, 102.89, 63.89, 46.87, 45.59, 34.05, 21.99. HPLC Purity: 96%



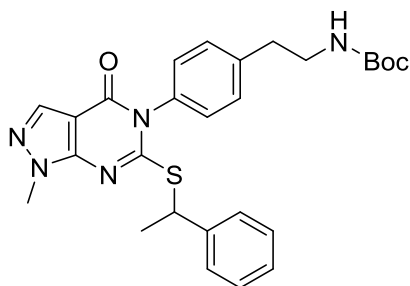
5-(4-(2-hydroxyethyl)phenyl)-1-methyl-6-((1-phenylethyl)thio)-1H-pyrazolo[3,4-d]pyrimidin-4(5H)-one (263863)

S4.6a (200mg, 0.947 mmol) and 2-(4-aminophenyl)ethanol (130 mg, 0.947 mmol) were stirred in 5 mL DMF for 2 h at which point the reaction was cooled to 0°C and 60 wt.% NaH (76 mg, 1.894 mmol) was added. The mixture was stirred at the same temperature for 30 min then allowed to warm to RT and stirred for 2 h. The mixture was diluted with 1N HCl and extracted 2x with EtOAc. The combined organics were washed with brine and dried over sodium sulfate before concentrating and suspending the solid in 2.5 mL DMF and adding K₂CO₃ (196 mg, 1.420 mmol) and (1-bromoethyl)benzene (0.129 ml, 0.947 mmol). The mixture was stirred at RT overnight. The following day the mixture was diluted with water and extracted 2x with EtOAc. The combined organics were washed 3x with brine and dried over sodium sulfate. The crude solid was purified by flash (Eluting at 50% EtOAc in Hexanes) to afford the titled compound as a white foam (125 mg, 0.308 mmol, 32.5 % yield). MS (ESI): m/z 407.1536 [M+H]⁺ ¹H NMR (500 MHz, CDCl₃) δ 7.99 (s, 1H), 7.42 - 7.36 (m, 3H), 7.37 - 7.27 (m, 3H), 7.27 - 7.21 (m, 1H), 7.19 (dd, J = 8.0, 2.3 Hz, 1H), 7.11 (dd, J = 8.0, 2.3 Hz, 1H), 5.02 (q, J = 7.2 Hz, 1H), 3.99 (s, 3H), 3.90 (q, J = 5.7, 5.2 Hz, 2H), 2.93 (t, J = 6.6 Hz, 2H), 1.71 (d, J = 7.2 Hz, 3H). ¹³C NMR (126 MHz, CDCl₃) δ 161.60, 157.91, 151.04, 142.07, 140.80, 135.34, 133.82, 130.39, 130.34, 129.36, 129.33, 128.52, 127.56, 127.53, 102.84, 63.21, 46.91, 38.96, 34.05, 21.92. HPLC Purity 97%



5-(4-(2-methoxyethyl)phenyl)-1-methyl-6-((1-phenylethyl)thio)-1H-pyrazolo[3,4-d]pyrimidin-4(5H)-one (263864)

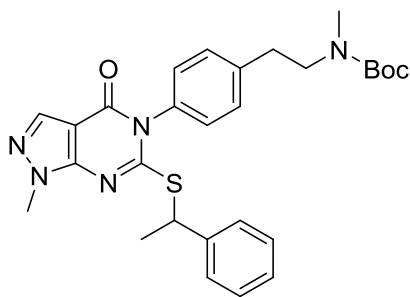
Prepared from **263863** in a similar manner to **263862**. Colorless oil. (54mg, 0.128 mmol, 49.7 % yield) MS (ESI): m/z 421.1689 $[M+H]^+$ 1H NMR (500 MHz, $CDCl_3$) δ 7.96 (s, 1H), 7.43 - 7.36 (m, 3H), 7.36 - 7.27 (m, 3H), 7.27 - 7.21 (m, 1H), 7.18 (dd, $J = 8.1, 2.3$ Hz, 1H), 7.10 (dd, $J = 8.1, 2.3$ Hz, 1H), 5.01 (q, $J = 7.1$ Hz, 1H), 3.99 (s, 3H), 3.66 (t, $J = 7.0$ Hz, 2H), 3.38 (s, 3H), 2.96 (t, $J = 7.0$ Hz, 2H), 1.71 (d, $J = 7.2$ Hz, 3H). ^{13}C NMR (126 MHz, $CDCl_3$) δ 161.68, 157.85, 151.03, 142.16, 141.10, 135.30, 135.28, 133.64, 130.15 (d, $J = 7.6$ Hz), 129.18 (d, $J = 4.5$ Hz), 128.51, 127.53, 102.85, 73.06, 58.70, 46.87, 35.94, 34.04, 21.95. HPLC Purity: 97%



tert-butyl 4-((1-methyl-4-oxo-6-((1-phenylethyl)thio)-1H-pyrazolo[3,4-d]pyrimidin-5(4H)-yl)phenethyl)carbamate (S4.7a)

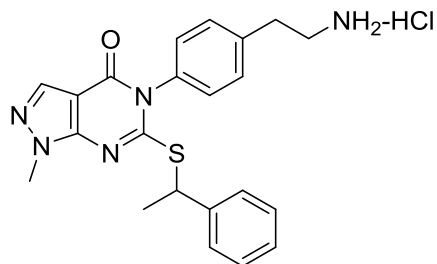
Tert-butyl 4-aminophenethylcarbamate (prepared as previously described¹⁵², 290mg, 1.227 mmol) was added to a solution of **S6.4a** (259 mg, 1.227 mmol) in 5mL DMF. After stirring for 2 h the mixture was cooled to 0°C and 60 wt.% NaH (54.0 mg, 1.350 mmol) was added. The reaction was stirred at the same temperature for 15 min then allowed to warm to RT and stirred for 2 h. The flask was cooled to 0°C and (1-bromoethyl)benzene (184 μ l, 1.350 mmol) was added by syringe. The flask was warmed to RT and stirred for 1 h at which point the solvent was removed in vacuo. The residue was taken up in EtOAc and washed with water and brine before drying over sodium sulfate and concentrating. The crude residue was purified by flash (Eluting

at 60% EtOAc in Hexanes) then further purified by taking up the solid in 30mL hot EtOH, adding 5mL water, and allowing the mixture to cool to RT affording the titled compound as a white crystalline solid (330mg, 0.653 mmol, 53.2 % yield). $^1\text{H NMR}$ (500 MHz, CDCl_3) δ 8.00 (s, 1H), 7.39 (d, $J = 7.6$ Hz, 2H), 7.37 - 7.28 (m, 3H), 7.25 - 7.22 (m, 1H), 7.19 (dd, $J = 8.2, 2.2$ Hz, 1H), 7.11 (dd, $J = 8.1, 2.3$ Hz, 1H), 5.02 (q, $J = 7.2$ Hz, 1H), 4.62 (s, 1H), 4.00 (s, 3H), 3.49 - 3.29 (m, 2H), 2.88 (t, $J = 6.9$ Hz, 2H), 1.71 (d, $J = 7.2$ Hz, 3H), 1.45 (s, 9H).



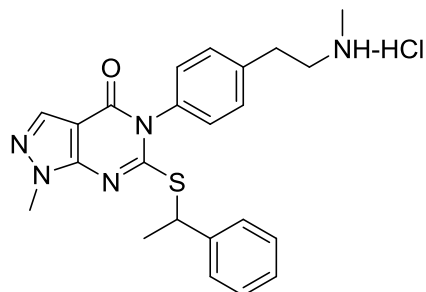
tert-butyl methyl(4-(1-methyl-4-oxo-6-((1-phenylethyl)thio)-1H-pyrazolo[3,4-d]pyrimidin-5(4H)-yl)phenethyl)carbamate (S4.7b)

To a solution of **S4.7a** (48mg, 0.095 mmol) in 1 mL DMF at 0°C was added 60 wt.% NaH (4.94 mg, 0.123 mmol). The mixture was stirred under N_2 at the same temperature for 30 min at which point MeI (7.12 μl , 0.114 mmol) was added by syringe. The mixture was stirred for an hour at RT then quenched with a few drops of sat. Aq. NH_4Cl and concentrated in vacuo. The residue obtained was taken up in water and extracted 3x with EtOAc. The combined organics were washed 3x with brine and dried over sodium sulfate. The crude residue was purified by flash (Eluting around 50% EA in Hex) to yield the titled compound as a white foam (35mg, 0.067 mmol, 70.9 % yield). $^1\text{H NMR}$ (400 MHz, CDCl_3) δ 7.97 (s, 1H), 7.42 - 7.14 (m, 8H), 7.10 (d, $J = 7.8$ Hz, 1H), 5.00 (q, $J = 7.1$ Hz, 1H), 3.98 (s, 3H), 3.47 (br.s, 2H), 2.98 - 2.72 (m, 4H), 1.70 (d, $J = 7.1$ Hz, 3H), 1.45 (s, 9H).



5-(4-(2-Aminoethyl)phenyl)-1-methyl-6-((1-phenylethyl)thio)-1H-pyrazolo[3,4-d]pyrimidin-4(5H)-one hydrochloride (264205)

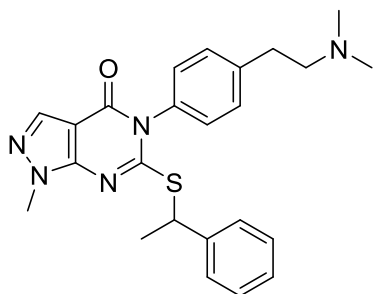
S4.7a (105 mg, 0.208 mmol) was dissolved in 1mL DCM to which 1mL TFA was added. The mixture was stirred overnight then concentrated in vacuo. The residue was taken up in 1:3 conc. HCl and EtOH and evaporated 3 times to exchange TFA salt for HCl to afford the titled compound as an off white solid (70mg, 0.158 mmol, 76 % yield). (ESI): m/z 406.1695 $[M+H]^+$
 1H NMR (500 MHz, DMSO- d_6) δ 8.01 (s, 1H), 7.91 (br. s, 3H), 7.44 - 7.39 (m, 3H), 7.39 - 7.27 (m, 4H), 7.26 - 7.19 (m, 2H), 5.03 (q, $J = 7.1$ Hz, 1H), 3.95 (s, 3H), 3.11 (p, $J = 5.3$ Hz, 2H), 2.96 - 2.88 (m, 2H), 1.66 (d, $J = 7.1$ Hz, 3H). ^{13}C NMR (126 MHz, DMSO- d_6) δ 161.26, 157.34, 150.84, 142.33, 139.55, 135.10, 134.70, 130.19, 130.12, 128.96, 128.06, 127.94, 102.77, 46.86, 39.92, 34.34, 33.16, 21.95. HPLC Purity: 98%



1-methyl-5-(4-(2-(methylamino)ethyl)phenyl)-6-((1-phenylethyl)thio)-1H-pyrazolo[3,4-d]pyrimidin-4(5H)-one hydrochloride (264207)

S4.7b (120mg, 0.231 mmol) was dissolved in 1mL DCM and 1mL TFA. The mixture was stirred for 2 h at which point the starting material was consumed by TLC. The reaction was concentrated and the residue taken up in sat. aq. sodium bicarbonate and extracted 3x into EtOAc. The combined organics were washed with brine, and dried over sodium sulfate. A few drops of 4N HCl in dioxane were added and the mixture was concentrated to yield the titled compound as a white solid (105mg, 0.230 mmol, 100 % yield).

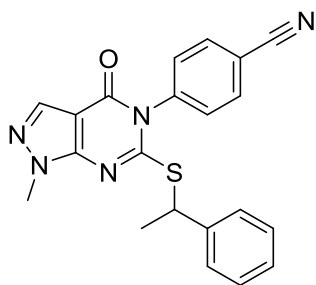
(ESI): m/z 420.1853 $[M+H]^+$ 1H NMR (500 MHz, DMSO- d_6) δ 9.09 (s, 2H), 8.01 (s, 1H), 7.45 - 7.40 (m, 3H), 7.37 (dd, $J = 8.1, 2.0$ Hz, 1H), 7.35 - 7.27 (m, 3H), 7.26 - 7.20 (m, 2H), 5.02 (q, $J = 7.1$ Hz, 1H), 3.95 (s, 3H), 3.17 (dq, $J = 10.9, 6.3, 5.9$ Hz, 2H), 3.02 (dd, $J = 10.0, 6.5$ Hz, 2H), 2.56 (t, $J = 5.3$ Hz, 3H), 1.65 (d, $J = 7.1$ Hz, 3H). ^{13}C NMR (126 MHz, DMSO- d_6) δ 161.27, 157.32, 150.84, 142.37, 139.50, 135.09, 134.67, 130.20 (d, $J = 6.5$ Hz), 130.15, 128.95, 128.06, 127.92, 102.77, 49.02, 46.86, 34.35, 32.76, 31.48, 21.97. HPLC Purity: 98%



5-(4-(2-(dimethylamino)ethyl)phenyl)-1-methyl-6-((1-phenylethyl)thio)-1H-pyrazolo[3,4-d]pyrimidin-4(5H)-one (264206)

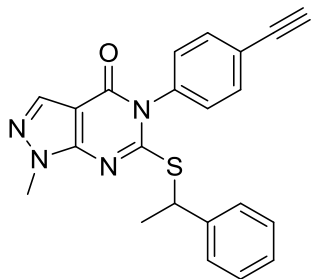
264205 (62mg, 0.140 mmol) was dissolved in 2mL DCE and treated with DIPEA (0.025 ml, 0.140 mmol), stirred for 5 min, then 37% aq. formaldehyde (0.031 ml, 0.421 mmol) and acetic acid (0.024 ml, 0.421 mmol) were added sequentially. The mixture was stirred for 10 min at which point sodium triacetoxyborohydride (89 mg, 0.421 mmol) was added and the mixture was stirred overnight. The next day the mixture was diluted with 10% aq. Na_2CO_3 and extracted

with EtOAc. The organic portion was washed with brine, dried over sodium sulfate, and concentrated to yield the pure product as an off white foam (59mg, 0.136 mmol, 97 % yield). (ESI): m/z 434.2009 [M+H]⁺ ¹H NMR (500 MHz, CDCl₃) δ 7.99 (s, 1H), 7.37 (ddd, J = 15.8, 8.3, 1.8 Hz, 3H), 7.33 - 7.28 (m, 3H), 7.25 (d, J = 8.9 Hz, 1H), 7.16 (dd, J = 8.1, 2.3 Hz, 1H), 7.08 (dd, J = 8.1, 2.3 Hz, 1H), 5.01 (q, J = 7.1 Hz, 1H), 3.99 (s, 3H), 2.89 - 2.80 (m, 2H), 2.65 - 2.52 (m, 2H), 2.32 (s, 6H), 1.71 (d, J = 7.2 Hz, 3H). ¹³C NMR (126 MHz, CDCl₃) δ 161.69, 157.86, 151.04, 142.47, 142.14, 135.35, 133.42, 129.98, 129.90, 129.18, 129.15, 128.50, 127.53, 127.52, 102.87, 61.08, 46.86, 45.47, 34.17, 34.03, 21.93. HPLC Purity: 98%



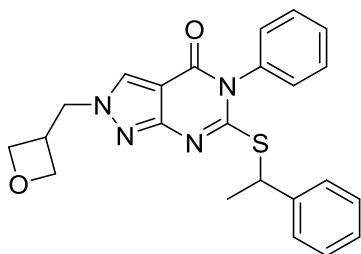
4-(1-methyl-4-oxo-6-((1-phenylethyl)thio)-1H-pyrazolo[3,4-d]pyrimidin-5(4H)-yl)benzotrile (264202)

Prepared from 4-aminobenzotrile in a similar manner to **S4.7a** affording the titled compound as a white solid (50mg, 0.129 mmol, 15.76 % yield). (ESI): m/z 388.1225 [M+H]⁺ ¹H NMR (400 MHz, CDCl₃) δ 7.99 (s, 1H), 7.83 (ddd, J = 8.2, 2.0, 0.6 Hz, 1H), 7.79 (ddd, J = 8.1, 2.0, 0.6 Hz, 1H), 7.42 (ddd, J = 8.1, 2.2, 0.6 Hz, 1H), 7.39 - 7.35 (m, 2H), 7.35 - 7.29 (m, 3H), 7.27 (d, J = 7.7 Hz, 1H), 5.04 (q, J = 7.2 Hz, 1H), 4.01 (s, 3H), 1.73 (d, J = 7.2 Hz, 3H). ¹³C NMR (101 MHz, CDCl₃) δ 160.20, 157.34, 150.88, 141.55, 139.74, 135.44 (d, J = 2.8 Hz), 133.55 (d, J = 6.9 Hz), 130.69, 128.65, 127.83, 127.44, 117.81, 114.08, 102.61, 47.28 (d, J = 8.1 Hz), 34.22, 21.94. HPLC Purity: 99%



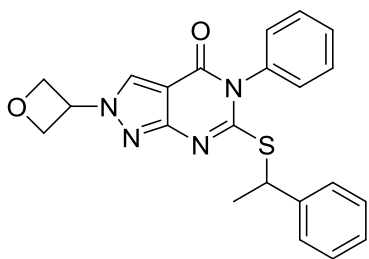
5-(4-ethynylphenyl)-1-methyl-6-((1-phenylethyl)thio)-1H-pyrazolo[3,4-d]pyrimidin-4(5H)-one (264626)

Prepared from 4-aminobenzonitrile in a similar manner to **S4.7a** affording the titled compound as a yellow solid. (117mg, 0.303 mmol, 32.0 % yield) (ESI): m/z 387.1276 $[M+H]^+$ 1H NMR (500 MHz, $CDCl_3$) δ 7.99 (s, 1H), 7.64 (dd, $J = 8.2, 1.8$ Hz, 1H), 7.60 (dd, $J = 8.2, 1.9$ Hz, 1H), 7.38 (d, $J = 7.1$ Hz, 2H), 7.31 (t, $J = 7.5$ Hz, 2H), 7.28 - 7.22 (m, 2H), 7.15 (dd, $J = 8.2, 2.2$ Hz, 1H), 5.02 (q, $J = 7.1$ Hz, 1H), 4.00 (s, 3H), 3.17 (s, 1H), 1.71 (d, $J = 7.0$ Hz, 3H). ^{13}C NMR (126 MHz, $CDCl_3$) δ 161.08, 157.62, 150.99, 141.93, 135.83, 135.39, 133.42 (d, $J = 9.6$ Hz), 129.51 (d, $J = 2.9$ Hz), 128.57, 127.64, 127.46, 124.07, 102.77, 82.53, 79.01, 47.01, 34.09, 21.97. HPLC Purity: 98%



2-(oxetan-3-ylmethyl)-5-phenyl-6-((1-phenylethyl)thio)-2H-pyrazolo[3,4-d]pyrimidin-4(5H)-one (262547)

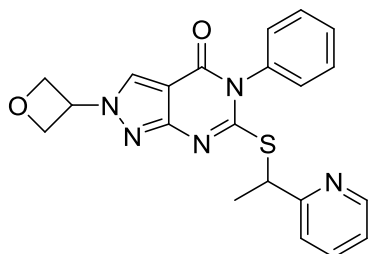
S4.8a (100mg, 0.409 mmol), K₂CO₃ (141 mg, 1.023 mmol), and (1-bromoethyl)benzene (55.9 µl, 0.409 mmol) were stirred in 2mL DMF at room temperature for 1 h. Oxetan-3-ylmethyl methanesulfonate (prepared as previously described¹³⁶), 68.0 mg, 0.409 mmol) was added by syringe and the mixture was heated to 60°C overnight. The next morning the mixture was diluted with water and extracted 2x with EtOAc. The combined organic portions were washed 3x with brine, dried over sodium sulfate, and concentrated. The crude residue was purified by flash (Eluting at 60% EtOAc in Hex) yielding the titled compound as a colorless oil (26mg, 0.062 mmol, 15.18 % yield). MS (ESI): *m/z* 419.1537 [M+H]⁺ ¹H NMR (500 MHz, CDCl₃) δ 8.06 (s, 1H), 7.56 - 7.40 (m, 3H), 7.35 (d, J = 7.6 Hz, 2H), 7.31 - 7.25 (m, 3H), 7.24 - 7.14 (m, 2H), 5.18 (q, J = 7.0 Hz, 1H), 4.87 (t, J = 7.2 Hz, 2H), 4.57 (d, J = 7.5 Hz, 2H), 4.54 (q, J = 5.7 Hz, 2H), 3.66 (h, J = 6.9 Hz, 1H), 1.75 (d, J = 7.0 Hz, 3H). ¹³C NMR (126 MHz, CDCl₃) δ 160.53, 158.69, 158.62, 141.62, 135.57, 129.82, 129.62, 129.59, 129.56, 129.51, 128.62, 128.54, 127.70, 127.48, 105.00, 74.46, 55.80, 46.52, 35.38, 22.10. HPLC Purity: 99%



2-(oxetan-3-yl)-5-phenyl-6-((1-phenylethyl)thio)-2H-pyrazolo[3,4-d]pyrimidin-4(5H)-one (263052)

Prepared in a similar manner to **262547** employing 3-bromooxetane. White Solid. (14mg, 0.035 mmol, 8.45 % yield) MS (ESI): *m/z* 405.1381 [M+H]⁺ ¹H NMR (500 MHz, CDCl₃) δ 8.19 (s, 1H), 7.55 - 7.42 (m, 3H), 7.36 (d, J = 7.6 Hz, 2H), 7.31 - 7.26 (m, 3H), 7.25 - 7.16 (m, 2H), 5.57 (p, J = 6.9 Hz, 1H), 5.26 - 5.18 (m, 3H), 5.09 (t, J = 7.3 Hz, 2H), 1.77 (d, J = 6.9 Hz, 3H). ¹³C

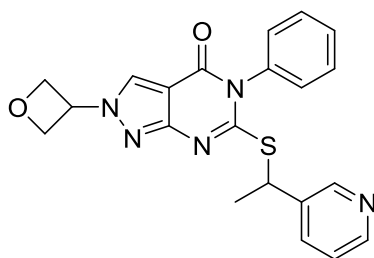
NMR (126 MHz, CDCl₃) δ 160.97, 158.63, 141.50, 135.49, 129.87, 129.61, 129.54, 129.53, 128.57, 127.96, 127.70, 127.52, 105.33, 76.86, 76.82, 56.78, 46.58, 22.15. HPLC Purity: 98%



2-(oxetan-3-yl)-5-phenyl-6-((1-(pyridin-2-yl)ethyl)thio)-2H-pyrazolo[3,4-d]pyrimidin-4(5H)-one (263646)

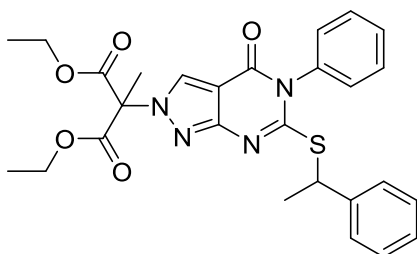
A dry flask was charged with **S4.8a** (250mg, 1.023 mmol), K₂CO₃ (424 mg, 3.07 mmol), 2-(1-bromoethyl)pyridine (190 mg, 1.023 mmol), and 3mL DMF. The mixture was stirred for 1 h= at RT at which point 3-bromooxetane (0.127 ml, 1.535 mmol) was added before heating the mixture to 80°C. After 48 hours the mixture was diluted with water and extracted 2x with EtOAc. The combined organic portion was washed 3x with brine and dried over sodium sulfate. The mixture was purified by flash (60% EtOAc in Hex) yielding the mostly pure product as the later peak. The product was recrystallized from ethanol to obtain the titled compound as a white solid (45mg, 0.111 mmol, 10.84 % yield). MS (ESI): *m/z* 406.1340 [M+H]⁺ ¹H NMR (500 MHz, CDCl₃) δ 8.51 (d, J = 4.3 Hz, 1H), 8.19 (s, 1H), 7.60 (td, J = 7.7, 1.9 Hz, 1H), 7.54 - 7.42 (m, 3H), 7.40 (d, J = 7.8 Hz, 1H), 7.28 (dt, J = 7.7, 1.8 Hz, 1H), 7.19 (dt, J = 7.2, 2.0 Hz, 1H), 7.12 (ddd, J = 7.6, 4.9, 1.2 Hz, 1H), 5.65 - 5.47 (m, 1H), 5.33 (q, J = 6.9 Hz, 1H), 5.21 (q, J = 6.2 Hz, 2H), 5.08 (td, J = 7.4, 1.5 Hz, 2H), 1.78 (d, J = 7.0 Hz, 3H). ¹³C NMR (126 MHz, CDCl₃) δ

161.14, 160.59, 158.64, 158.58, 149.59, 136.65, 135.36, 129.89, 129.67, 129.64, 129.60, 129.54, 128.00, 122.44, 122.31, 105.30, 76.87, 76.83, 56.77, 48.08, 21.49. HPLC Purity 97%



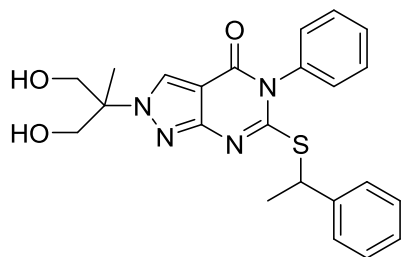
2-(oxetan-3-yl)-5-phenyl-6-((1-(pyridin-3-yl)ethyl)thio)-2H-pyrazolo[3,4-d]pyrimidin-4(5H)-one (264627)

Prepared in a similar manner to **263646** White solid. (100mg, 0.247 mmol, 12.05 % yield) MS (ESI): m/z 406.1335 $[M+H]^+$ 1H NMR (500 MHz, $CDCl_3$) δ 8.68 (d, $J = 2.3$ Hz, 1H), 8.47 (dd, $J = 4.8, 1.6$ Hz, 1H), 8.19 (s, 1H), 7.69 (dt, $J = 8.0, 2.0$ Hz, 1H), 7.56 - 7.45 (m, 3H), 7.30 - 7.24 (m, 1H), 7.22 (dd, $J = 7.9, 4.8$ Hz, 1H), 7.18 (dt, $J = 8.2, 1.8$ Hz, 1H), 5.65 - 5.46 (m, 1H), 5.29 - 5.13 (m, 3H), 5.09 (td, $J = 7.5, 1.3$ Hz, 2H), 1.74 (d, $J = 7.1$ Hz, 3H). NOE at 5.6 when irradiating at 8.19. ^{13}C NMR (126 MHz, $CDCl_3$) δ 160.13, 158.50, 158.40, 149.30, 148.71, 137.73, 135.33, 135.07, 130.04, 129.68, 129.60, 129.58, 129.52, 127.97, 123.33, 105.34, 76.81, 56.82, 43.75, 21.54. HPLC Purity: 99%



Diethyl 2-methyl-2-(4-oxo-5-phenyl-6-((1-phenylethyl)thio)-4,5-dihydro-2H-pyrazolo[3,4-d]pyrimidin-2-yl)malonate (S4.8b)

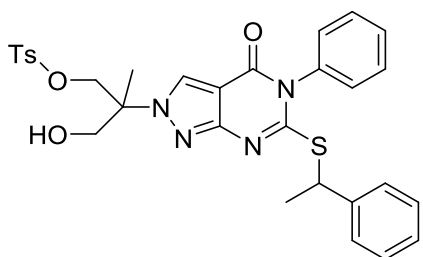
To a solution of **S4.8a** (1g, 4.09 mmol) and K_2CO_3 (1.414 g, 10.23 mmol) in 25mL DMF under N_2 was added (1-bromoethyl)benzene (0.557 ml, 4.09 mmol) by syringe. The mixture was stirred at RT for 1 h. Diethyl 2-bromo-2-methylmalonate (0.857 ml, 4.50 mmol) was added by syringe and the mixture was heated to 50°C overnight at which point the reaction was complete by HPLC. The mixture was diluted with water and extracted 3x with EtOAc. The combined organics were washed 3x with brine and dried over sodium sulfate. The crude oil was purified by flash (Gradient from 25-30% EtOAc in hexanes) to yield the titled compound as a clear colorless oil. (1.76 g, 3.38 mmol, 83 % yield) 1H NMR (400 MHz, $CDCl_3$) δ 8.41 (d, $J = 1.1$ Hz, 1H), 7.56 - 7.40 (m, 3H), 7.33 (d, $J = 7.3$ Hz, 2H), 7.30 - 7.14 (m, 6H), 5.21 (q, $J = 6.9$ Hz, 1H), 4.40 - 4.20 (m, 4H), 2.26 (d, $J = 1.1$ Hz, 3H), 1.78 - 1.69 (m, 3H), 1.45 - 1.05 (m, 6H).



2-(1,3-dihydroxy-2-methylpropan-2-yl)-5-phenyl-6-((1-phenylethyl)thio)-2H-pyrazolo[3,4-d]pyrimidin-4(5H)-one (S4.8c)

Note: REACTION PRODUCES POTENT THIOL SMELL. A dry flask under N_2 charged with $NaBH_4$ (0.481 g, 12.71 mmol) and 20mL anhydrous dimethoxyethane was cooled in an ice bath. Bromine (0.305 ml, 5.93 mmol) was dissolved in 2mL dimethoxyethane and added to the mixture dropwise by syringe. After complete addition, the reaction was removed from the cooling bath and stirred for 30 minutes at which point the solution was *colorless* with white

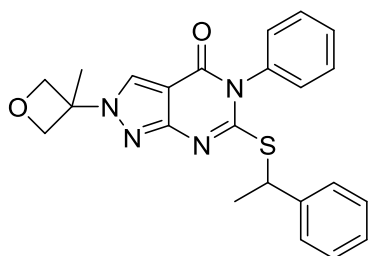
NaBr precipitate. The flask was cooled in an ice/brine bath and **S4.8b** (1.47g, 2.82 mmol) dissolved in 10mL dimethoxyethane was added by syringe. The mixture was kept in the bath for 1 h then allowed to warm to room temperature and stirred for 24 h. The reaction mixture was added dropwise to 200mL ACN then 5mL of water was added slowly followed by 5mL 1N HCl. The mixture was allowed to sit for 1 hour at which point ethyl acetate and 10mL water were added and two layers formed. Sodium sulfate was added to saturate the aqueous solution and the organic portion decanted off. The aqueous portion was extracted again with ethyl acetate. The combined organic portions were dried over sodium sulfate and concentrated. The residue was taken up in DCM and dried with additional sodium sulfate and then loaded onto silica and purified by flash (80% EtOAc in Hexanes) to afford the titled compound as a white solid (303mg, 0.694 mmol, 24.58 % yield). ¹H NMR (400 MHz, CDCl₃) δ 8.32 (d, J = 0.6 Hz, 1H), 7.56 - 7.42 (m, 2H), 7.35 (d, J = 7.3 Hz, 3H), 7.32 - 7.25 (m, 3H), 7.25 - 7.14 (m, 2H), 5.26 - 5.08 (m, 1H), 4.09 - 3.60 (m, 4H), 1.76 (d, J = 7.0 Hz, 3H), 1.60 (s, 3H).



3-hydroxy-2-methyl-2-(4-oxo-5-phenyl-6-((1-phenylethyl)thio)-4,5-dihydro-2H-pyrazolo[3,4-d]pyrimidin-2-yl)propyl 4-methylbenzenesulfonate (S4.8d)

A flask under N₂ charged with **S4.8c** (303 mg, 0.694 mmol) in 6mL THF was cooled to -78°C. nBuLi (278 µl, 0.694 mmol) 2.5M in hexanes was added and the mixture was stirred for 1 h. Ts-Cl (132 mg, 0.694 mmol) in 1mL THF was added and the reaction was stirred for 30 min at -

78°C and then allowed to warm to RT. The reaction was quenched with sat. aq. NH₄Cl, diluted with water and extracted 2x with EtOAc. The combined organics were washed with brine and dried over sodium sulfate and concentrated. The crude mixture was purified by flash (Eluting at 50% EtOAc in Hexanes) to afford the titled compound as a white foam (140mg, 0.237 mmol, 34.1 % yield). ¹H NMR (400 MHz, CDCl₃) δ 8.19 (d, J = 5.3 Hz, 1H), 7.68 (t, J = 8.6 Hz, 2H), 7.59 - 7.38 (m, 3H), 7.38 - 7.06 (m, 9H), 5.12 (qd, J = 7.0, 2.3 Hz, 1H), 4.51 (dd, J = 10.3, 4.4 Hz, 1H), 4.37 (dd, J = 10.2, 1.9 Hz, 1H), 3.95 (dd, J = 6.6, 2.9 Hz, 2H), 3.71 (t, J = 6.5 Hz, 1H), 2.41 (d, J = 17.6 Hz, 3H), 1.73 (t, J = 7.8 Hz, 3H), 1.64 (s, 3H).



2-(3-methyloxetan-3-yl)-5-phenyl-6-((1-phenylethyl)thio)-2H-pyrazolo[3,4-d]pyrimidin-4(5H)-one (264199)

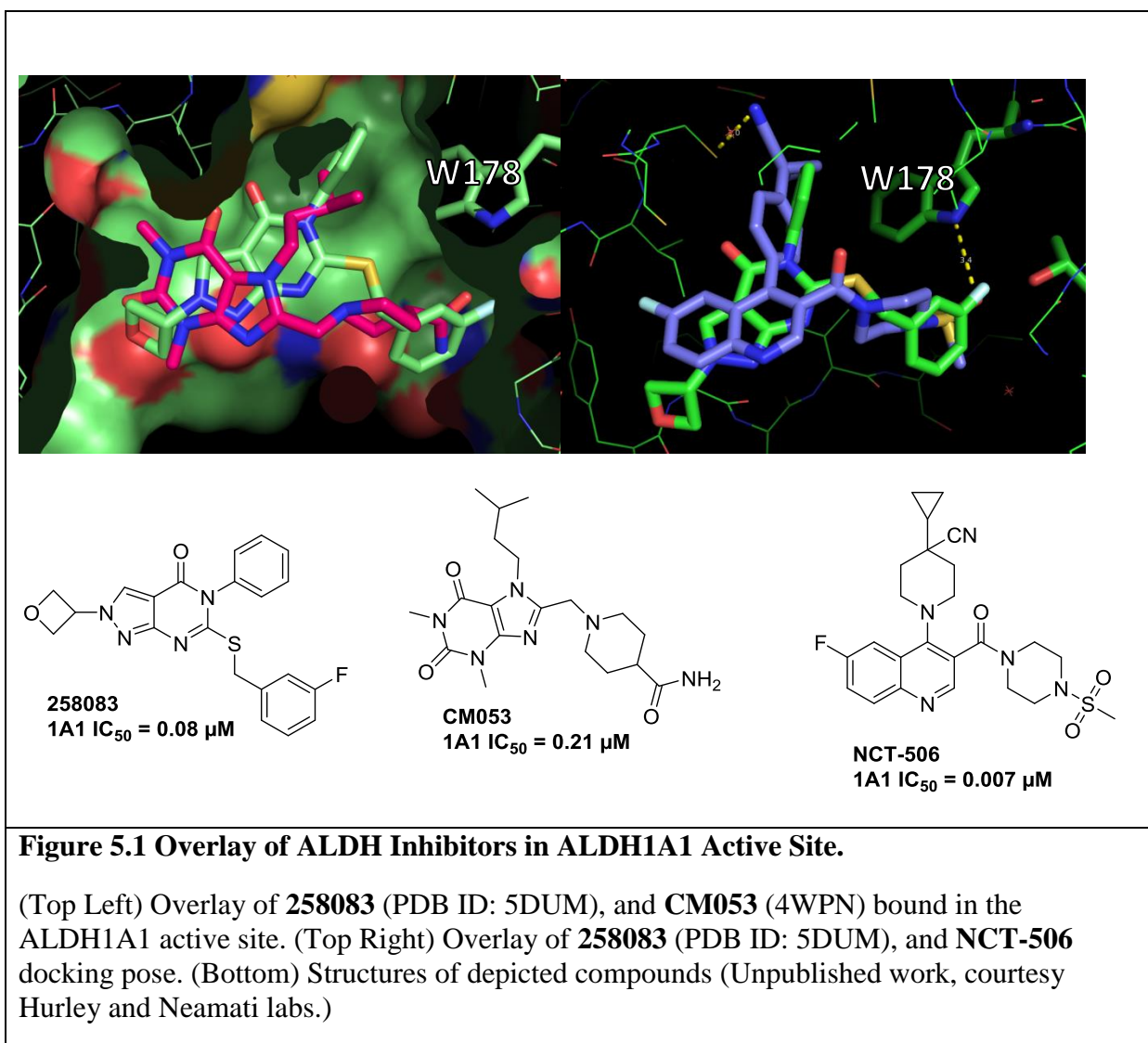
To a dry pressure tube charged with **S4.8d** (140 mg, 0.237 mmol) in 2mL at 0°C was added nBuLi (2.5M in Hexanes, 0.114 ml, 0.284 mmol) in THF. The mixture was stirred for 20 min then heated to 65°C overnight. The next morning the reaction was not complete by HPLC so the flask was cooled to 0°C and another portion of nBuLi (2.5M in Hexanes, .05 ml, 0.125 mmol) was added. The mixture was heated to 80°C for 4 hours at which point it was complete by HPLC and was quenched by adding a few drops of water then concentrated. The residue was taken up in water and ethyl acetate. The organic portion was washed with brine and dried over sodium sulfate and concentrated. The crude residue obtained was purified by flash (Eluting at 45% EtOAc in Hex). The white solid obtained was further recrystallized from hot ethanol to

yield the titled compound as white needles (40mg, 0.096 mmol, 40.3 % yield). MS (ESI): m/z 406.1340 $[M+H]^+$ 1H NMR (500 MHz, $CDCl_3$) δ 8.17 (s, 1H), 7.56 - 7.41 (m, 3H), 7.35 (d, J = 7.6 Hz, 2H), 7.31 - 7.25 (m, 3H), 7.25 - 7.15 (m, 2H), 5.29 (t, J = 5.9 Hz, 2H), 5.23 (q, J = 6.9 Hz, 1H), 4.72 (d, J = 6.5 Hz, 2H), 2.04 (s, 3H), 1.77 (d, J = 7.0 Hz, 3H). ^{13}C NMR (126 MHz, $CDCl_3$) δ 160.84, 158.77, 158.36, 141.44, 135.54, 129.84, 129.63, 129.60, 129.56, 129.52, 128.57, 127.70, 127.51, 126.17, 105.23, 81.35 (d, J = 5.0 Hz), 62.37, 46.51, 24.44, 22.18. NOE observed for oxetane and methyl protons at δ 5.29 and 2.04 respectively when irradiating pyrazole proton at δ 8.17. HPLC Purity 99%

Chapter 5 Future Directions and Conclusions

5.1. New and Proposed CM39 Analogs with Improved Property Forecast Index

As discussed in Chapter 4, there was an unfavorable trend of better in vivo exposure for compounds with high cLogP. According to the Property Forecast Index (PFI, $\text{ChromLogD}_{7.4} + \#$ aromatic rings), the high aromatic ring count combined with the lipophilicity of these compounds suggests a low probability of success in preclinical drug development. We do not currently have the capabilities to measure $\text{ChromLogD}_{7.4}$ to calculate the actual PFI. Assuming our cLogP results are predictive of this value, a PFI of (7-9) is typical for most analogs in the **CM39** series (3-5 is optimal). (Because all of the key compounds in this series are uncharged at pH 7.4, by definition $\text{cLogP} = \text{cLogD}_{7.4}$) Our series exhibits the difficulties with aqueous solubility and clearance associated with compounds with $\text{PFI} > 5$. Undesirable properties such as promiscuity, CYP450 inhibition, and high plasma protein binding are also associated with high PFI values, although these may be of less concern when developing proof-of-concept probes. Reducing the cLogP alone to reach the desired PFI of 4-5 would require reducing the $\text{ChromLogD}_{7.4}$ to < 1 , substantially reducing the probability of cell permeability. Therefore, reducing the number of aromatic rings and a more modest reduction in lipophilicity likely represents the best strategy to reach the desired PFI range.

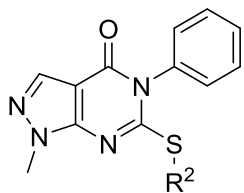


Examining the overlay of **258083** and **CM053** ALDH inhibitors in Figure 5.1 indicates the potential to replace the benzyl pendant with an appropriate non-aromatic hydrogen bond acceptor to engage W178. In **CM053** and **NCT-506** the amide and sulfonamide moieties overlay in the space occupied by the fluorobenzyl pendant.

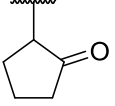
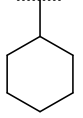
Before we had obtained crystal structures for the **CM39** series beyond the lead compound, I enumerated and docked a small virtual library looking for replacements of the benzyl pendant. This effort afforded amide **258476** (See Table 5.1). To expedite docking, these

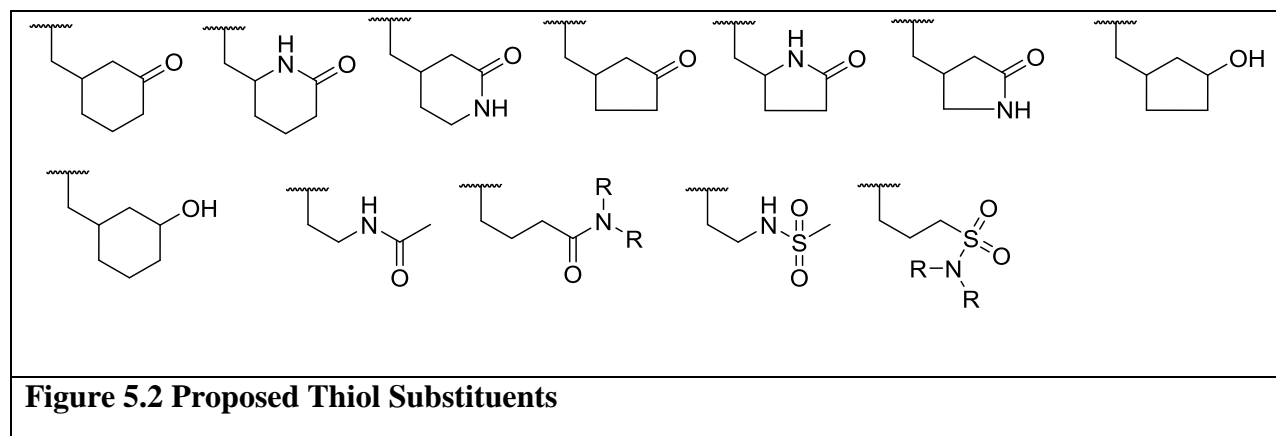
analogs were docked using the **CM39**-like binding mode as a template. Based on our SAR, the strong preference for lipophilic groups in the active site near the catalytic cysteine and hydrogen bond donors near W178 indicates it is more likely that the binding mode flipped to orient the amides toward W178. Although this compound was approximately 20-fold less potent than **259122**, the 2.6 unit decrease in cLogP drove the lipophilic ligand efficiency with respect to ALDH1A1 up by over 1 unit. The potent inhibition of 1A3 indicated the promise of similar compounds to potentially inhibit ALDH with much improved predicted ADME properties. Because of its 3 aromatic rings and cLogP = 1.9, **258476** attained a much more favorable PFI of 4.9 (assuming cLogP = ChromLogD_{7,4}). Consistent with this, aqueous solubility was 10-fold better than **259122**. Analogs designed around the structure of **258476** indicated that the selectivity profile was easily manipulated to afford our desired Pan-ALDH1A inhibition profile (**263056**). Assuming that these compounds adopt a similar binding mode to **258083**, the position of the carbonyl is not optimal. Based on the overlays in Figure 5.1, the carbonyl should be four atoms away from the thiol rather than two as it is in all the analogs in Table 5.1. In light of these promising preliminary findings, future work should focus on finding optimal new non-aromatic thiol substituents to achieve potent ALDH inhibition and reduce the PFI. Based on visual analysis of the active site, some proposed analogs are presented in Figure 5.2. Most should be accessible from alkyl halides in 1-2 steps. Virtual library enumeration and docking of commercially available alkyl halides would be prudent to discover additional, less obvious motifs.

Table 5.1 Characterization of Non-Aromatic Thiol Substituents



CMPD No.	R ²	ALDH ^a IC ₅₀ or ^b % Control at 20 μM			ADME Characterization		
		1A1	1A2	1A3	^c Aq. Sol	cLogP	^d LLE
259122		0.13 ±0.03	0.11 ±0.02	0.073 ±0.005	8	4.5	2.5
259009		21 ±3	3.5 ±0.4	0.9 ±0.2		1.4	3.3
258476		3.31 ±0.07	0.93 ±0.07	0.19 ±0.03	81	1.9	3.6
259008		1.8 ±0.1	4.9 ±0.2	0.25 ±0.02	75	2.4	3.3
263053		96%	73%	52%	60	2.0	
263054		65%	71%	47%		1.5	
263056		16%	25%	14%		3.4	

263055		23%	46%	64%		2.9	
262901		26%	34%	24%		4.1	
<p>Values are expressed as ^aMean \pm SEM (n=3), ^bMean (N=3) ^cThermodynamic solubility analysis was performed by Analiza Inc. using quantitative nitrogen detection. (www.analiza.com) ^dLLE = Lipophilic Ligand Efficiency (1A1 pIC₅₀ – cLogP). (Unpublished work, courtesy of Hurley lab)</p>							



5.2. Attempted Development of Proteolysis Targeting Chimeras (PROTACS) and Future Directions

Targeting proteins of interest for degradation by recruiting E3 ligases using chimeric ligands is a relatively new technology which allows for extremely potent cellular activity. By holding the protein target and an E3 ligase recruiting protein (e.g. Cereblon or pVHL) in close proximity, the chimeras promote ubiquitination and subsequent degradation of the protein. Once the protein has been ubiquitinated, the chimeric ligands are able to disassociate and bind to another protein molecule, theoretically enabling profound protein inhibition with sub-

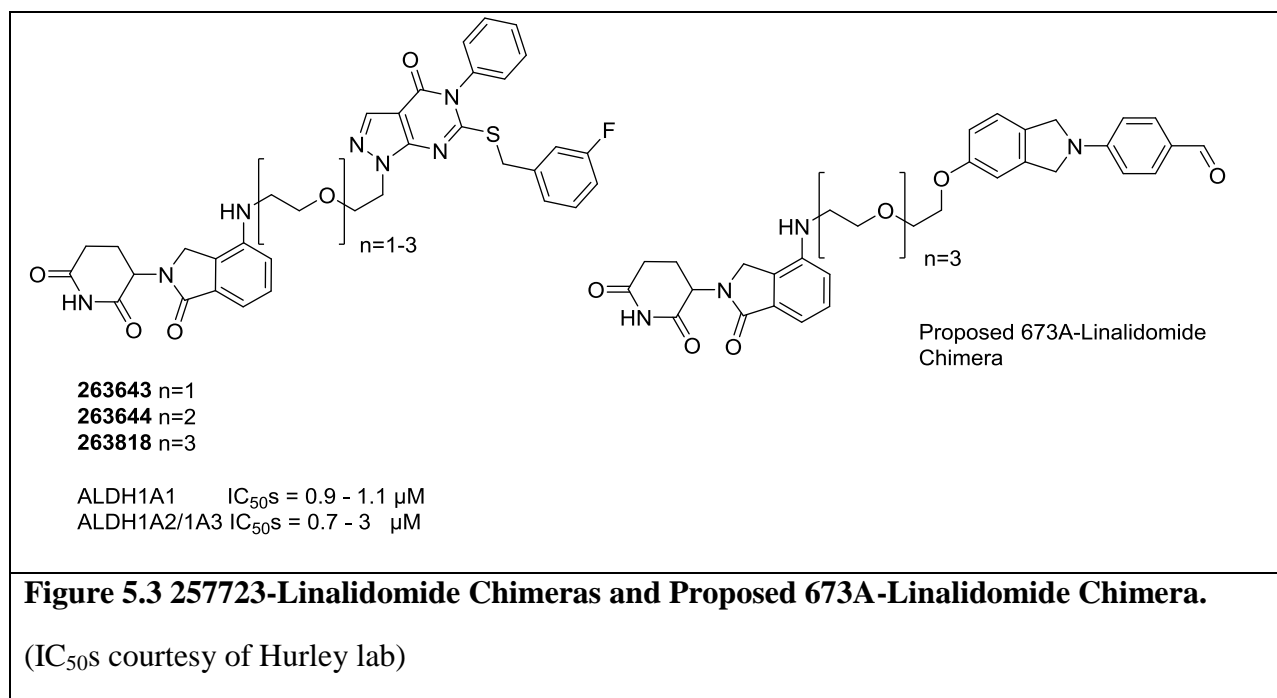
stoichiometric (fewer molecules of ligand than target protein) quantities of the ligand.¹⁵⁹⁻¹⁶⁰

Targeting the BET bromodomain proteins in this fashion has been particularly fruitful, affording degraders with cellular efficacy at 0.01 nM, and impressive in vivo antitumor activity at 1mg/kg.¹⁶¹

I attempted to create ALDH degraders by creating a chimera of the potent ALDH inhibitor **257723** and the Cereblon ligand linalidomide as shown in Figure 5.3 with variable length polyethylene glycol linkers. As linalidomide is commercially available and VHL ligands require multi-step syntheses, I chose to begin with linalidomide for synthetic ease. Due to the unstable chiral center in linalidomide, I chose not to use the alkyl-branched linker to avoid the final product containing an inseparable mixture of diastereomers. The crystal structures of **258085** and **262548** indicated that the linker should be projected into solvent as desired and not significantly impact affinity; however, regardless of the linker length, these compounds were 10-fold less potent inhibitors of ALDH in the enzyme assays. The Neamati lab performed western blots demonstrating that these compounds also did not show any degradation of ALDH1A1 or 1A3 proteins at 30 μ M. Although the exact parameters necessary to promote degradation are as-of-yet unknown and likely to be target dependent, most examples of successful degraders maintain < 100 nM IC₅₀ for their respective targets.¹⁵⁹⁻¹⁶¹ Presumably, a PROTACS ligand must be potent enough to achieve sufficient residence time on the target to effectively recruit the E3 ligase complex. It is also possible that some protein targets are not susceptible to ubiquitination by a particular E3 ligase complex.

The biotinylated probe **264441** (Chapter 2) maintained the ALDEFLUOR potency observed for **673A**, suggesting that the linker attachment point used in **264441** does not reduce ALDH potency and that the probe maintains good cell permeability. In light of these

observations, **673A**-based PROTACS (Figure 5.3) may have a better chance at effectively degrading ALDH. Additionally, considering its slow substrate/reversibly covalent mechanism, **673A** may be better suited to achieve the residence time necessary to promote degradation. In fact, the first proof-of-concept studies in the development of PROTACS used a covalent system; Halo-tagged pVHL ligand was used to promote degradation of a Halo-Tag fusion protein.¹⁶² If the rate determining step in the turnover of **673A** is the hydrolysis of the thioester, then **673A** can only dissociate as the acid. For this reason, it is unlikely that sub-stoichiometric quantities of the chimera could eradicate ALDH; however, reduction of the fairly high efficacious concentration of **673A** is still possible. If ALDH inhibition is diminished for this probe, appending a methoxy meta to the aldehyde (see **223960** in Chapter 2) might provide additional potency at the expense of ALDH2 selectivity.



5.3. Selective Inhibitors Based on ALDH1A2 Crystal Structure 6B5H

Recently the first high-quality crystal structure of ALDH1A2 was published.⁹⁸ As shown in Figure 5.4, one notable difference between the ALDH1A active sites is that the lipophilic Ile304 sidechain in 1A1 corresponds to a polar Threonine in 1A2/1A3. This residue is situated 4 Å from the 3-position of the pyrazole in the **262548** crystal structure. To explore the impact of this discrepancy on isoform selectivity, I synthesized C-3 substituted **CM39** analogs as shown in Table 5.2. The C-3 methyl **263865** did indeed promote 1A1 selectivity as we predicted based on the lipophilic isoleucine present in 1A1. If the methyl was binding close enough with the Ile/Thr site to impart this selectivity, then we did not predict that the ethyl (**264621**) would be tolerated. Ethyl analog **264621** was essentially equipotent, but slightly more selective against 1A3. An alternative explanation for the 1A3 selectivity of these analogs is that the C-3 substituents are causing a reversion to the **CM39**-like binding mode which may be disfavored by 1A2/1A3. The C-3 substituents would project into solvent in this binding mode, consistent with the flat SAR we observed. To date, we have no crystal structures of pan-inhibitors which are bound in the **CM39**-like binding mode. The amine substituted analog **264622**, designed to be 1A2/1A3 selective by engaging the threonine as mentioned above, was a modestly potent 1A1/1A3 selective inhibitor, which also might indicate a change in binding mode. Future crystallography studies with these inhibitors could provide useful information in how to exploit C-3 substituents to alter isoform selectivity.

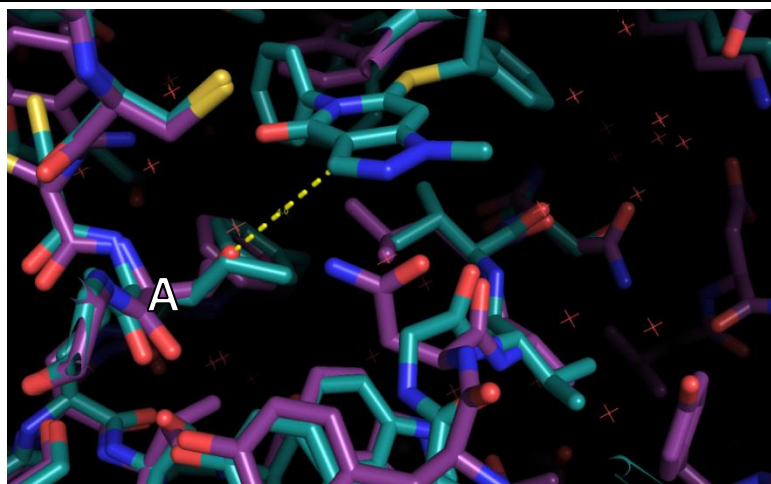
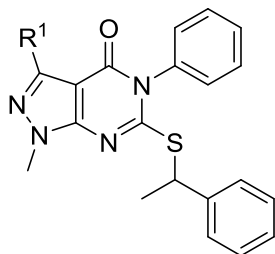


Figure 5.4 Overlay of 1A1 and 1A2 Crystal Structure

Unpublished 1A1-**262548** (teal) structure overlaid with 1A2 structure (PDB ID: 6B5H, purple). (A) Ile 304 4Å from 3-position of the pyrazole corresponds to Threonine in 1A2. (Unpublished work, courtesy Hurley lab)

Table 5.2 C-3 Substituted Pyrazole Analogs

CMPD No.	R ¹	ALDH ^a IC ₅₀ or ^b % Control at 5 μM		
		1A1	1A2	1A3
259122	-H	0.13 ±0.03	0.11 ±0.02	0.073 ±0.005
263865	-Methyl	0.22 ±0.05	71%	2.4 ±0.4
264621	-Ethyl	0.27 ±0.05	>5	>5
264622	-NH ₂	0.62 ±0.05	48%	0.93 ±0.08
Values are expressed as ^a Mean ± SEM (n=3), ^b Mean (N=3) (Unpublished work, courtesy of Hurley lab)				

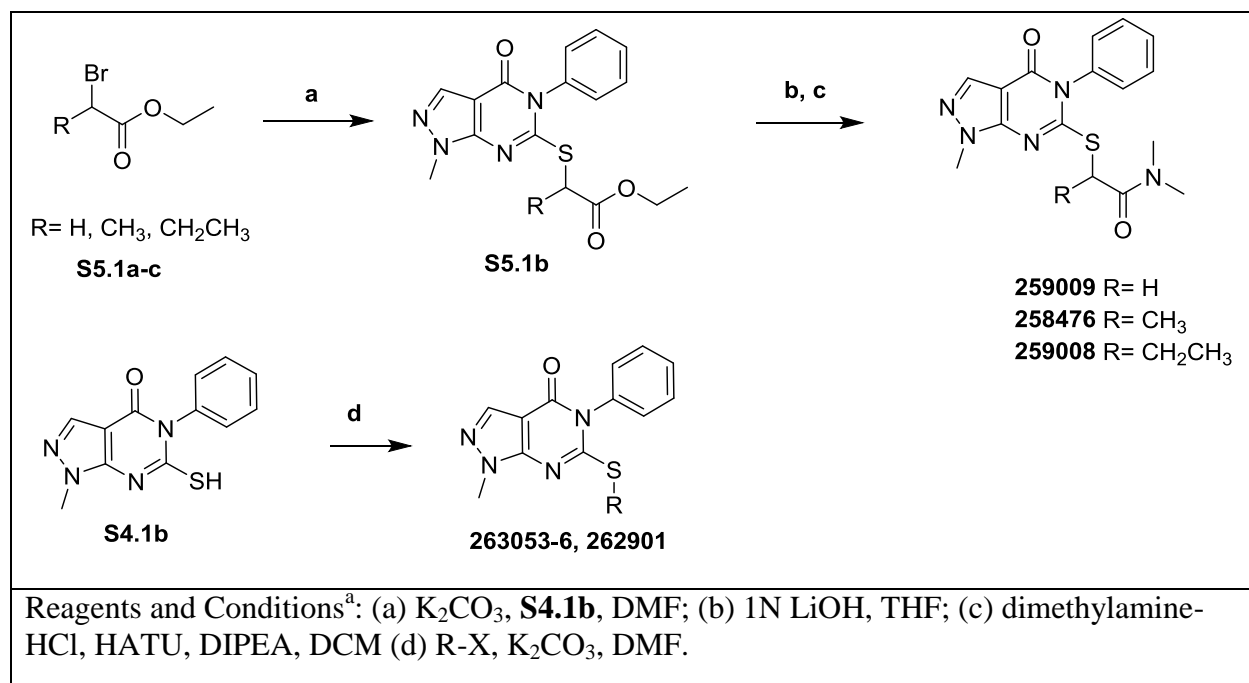
5.4. Future Evaluation of Analogs and Project Conclusion

One of our key hypotheses throughout the project has been the necessity of pan-ALDH1A inhibitors to provide broad spectrum efficacy in a multitude of cell lines with variable ALDH isoform expression. Currently, the Buckanovich lab is evaluating a panel of pan-inhibitors, and single isoform 1A1 and 1A3 selective inhibitors in two 1A3 high lines (OVCAR5 and PEO1) and one 1A1 high line (OV90). Activity in ALDEFLUOR, CD133⁺ and cisplatin synergy assays is being determined. We hope to demonstrate that: 1) pan inhibitors are effective in the 3 assays in all cell lines, 2) that selective inhibitors for a particular isoform are effective in a cell line primarily expressing that isoform, and 3) that the selective inhibitors are ineffective in

cell lines primarily expressing a different isoform. This ideal outcome would validate the mechanistic link between chemosensitization and CD133⁺ depletion and ALDH inhibition for this compound series. Additionally it would demonstrate the utility of our selective probes as an alternative to siRNA knockdown for assessing the role of a particular ALDH isoform in a biological system. The Buckanovich lab also plans to assess more compounds in spheroid assays given the more stem-like phenotype and elevated ALDH expression exhibited by many cell lines under these conditions, as discussed in Chapter 3. Compounds with adequate in vivo exposure and efficacy in pending chemosensitization assays will be advanced to xenograft studies.

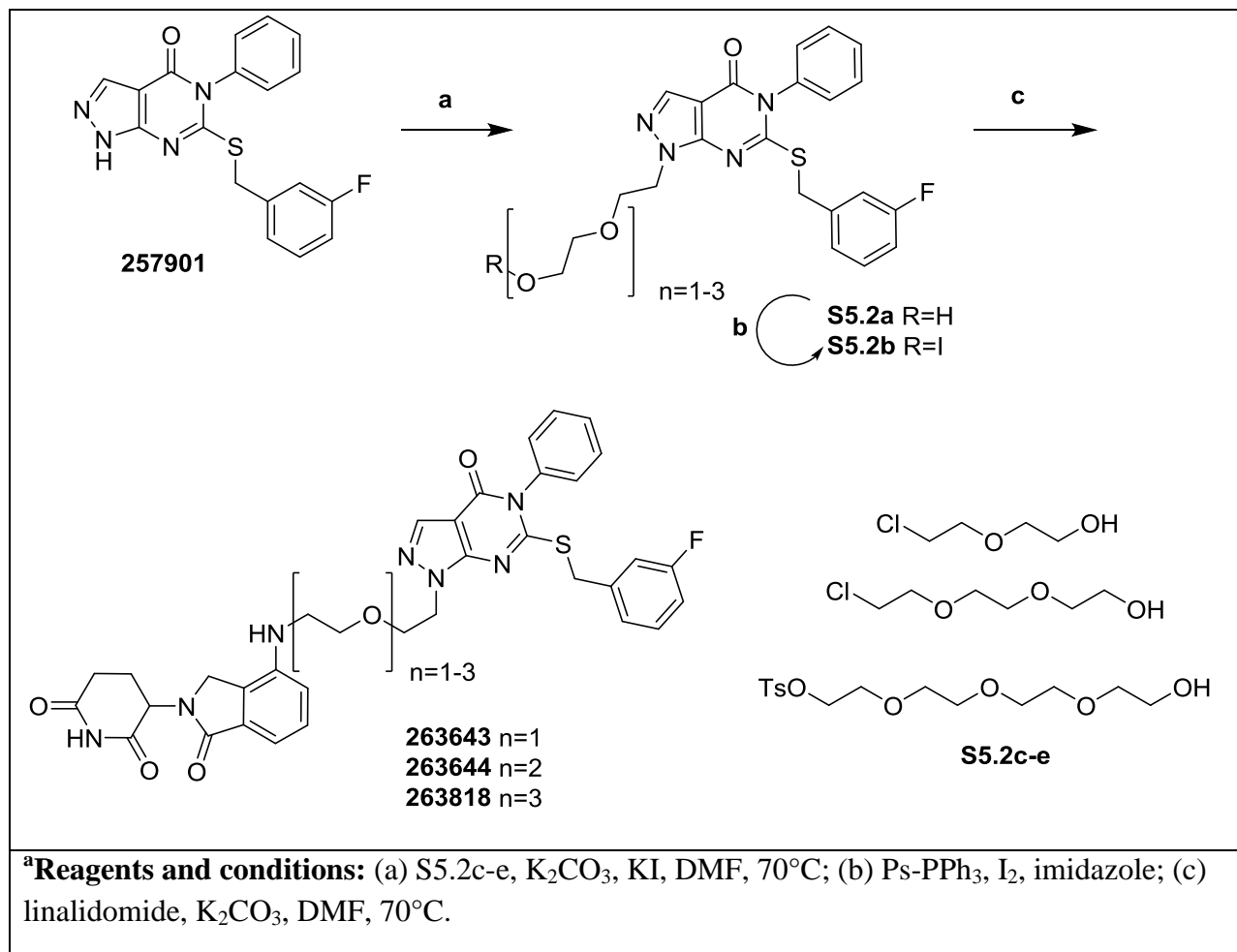
5.5. Chemistry

Scheme 5.1 Synthesis of Non-Aromatic Thiol Substituents^a



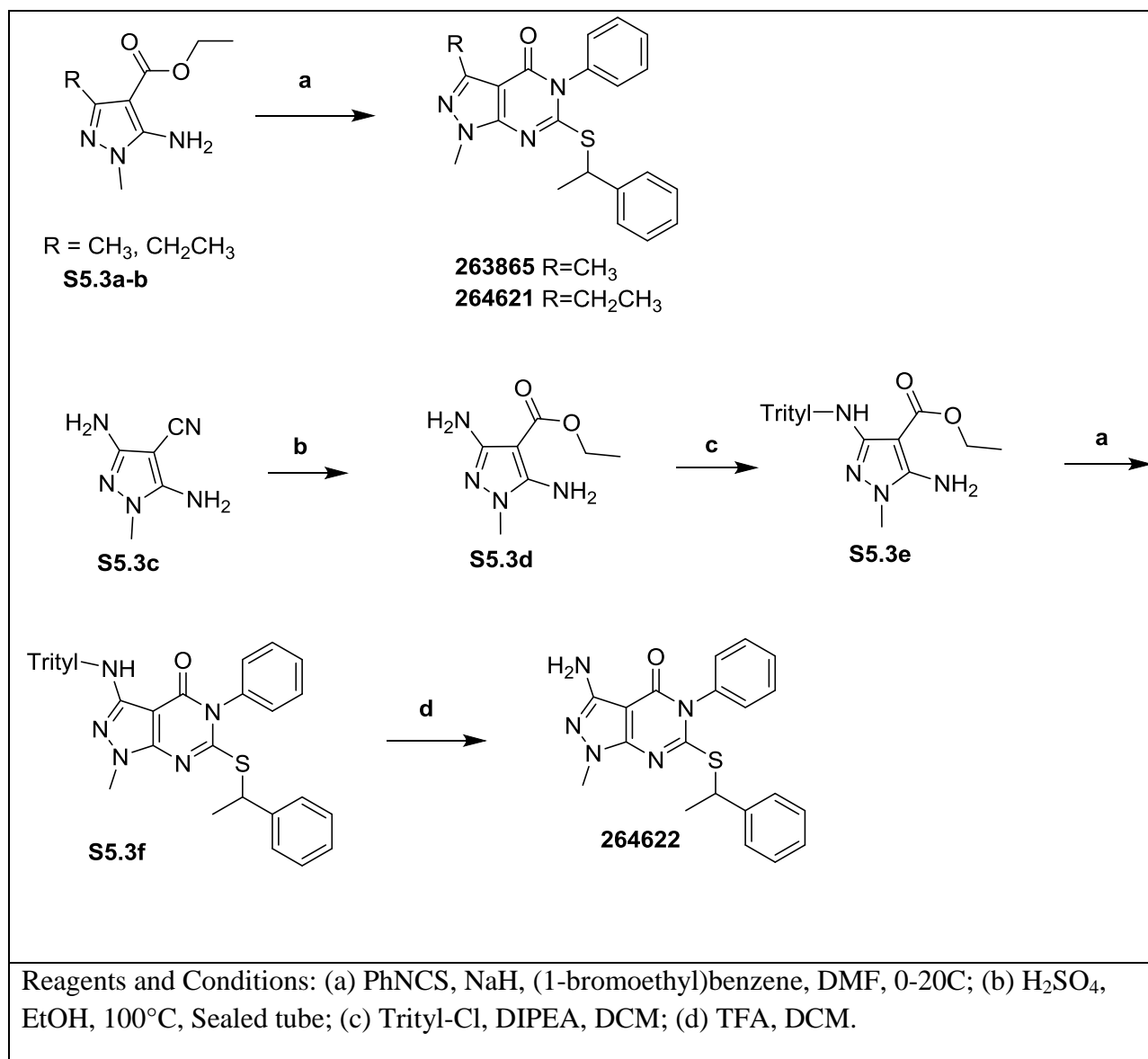
Amides **259008-9** and **258476** were synthesized from commercially available esters followed by hydrolysis and HATU coupling as depicted in Scheme 5.1. Other S-substituents were synthesized in one step from **S4.1b** and commercially available alkyl halides.

Scheme 5.2 Synthesis of 257723-Linalidomide Degraders^a



As shown in Scheme 5.2 synthesis of the **257723**-linalidomide degraders began by alkylation of **257901** with the appropriately functionalized ethoxy-ethanols **S5.2c-e**. Subsequent Appel iodination and displacement by linalidomide afforded the chimeric ligands **263643**, **263644**, and **263818**.

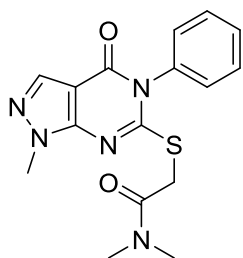
Scheme 5.3 Synthesis of C-3 Substituted Analogs^a



As shown in Scheme 5.3 synthesis of C-3 alkyl substituted analogs began with aminopyrazoles **S5.3a-b** prepared as previously described.¹⁶³ NaH mediated the addition of the amine into phenyl isothiocyanate, at which point the resulting thiourea cyclized spontaneously. Adding (1-bromoethyl)benzene to the reaction mixture at this point afforded the C-3 methyl and ethyl analogs. Synthesis of **264622** began with the pyrazole **S5.3c** prepared as previously

described.¹⁶⁴ Solvolysis of the nitrile under acidic conditions in ethanol afforded ester **S5.3d**. Exploiting the steric bulk of the trityl protecting group, regioselective protection of the C-3 amine was accomplished, affording **S5.3e** which afforded pyrazolopyrimidinone **S5.3f** upon treatment with phenyl isothiocyanate, NaH, and (1-bromoethyl)benzene. Finally TFA mediated removal of the trityl afforded **264622**.

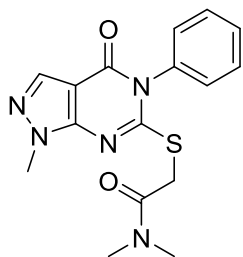
5.6. Experimental Procedures



N,N-dimethyl-2-((1-methyl-4-oxo-5-phenyl-4,5-dihydro-1H-pyrazolo[3,4-d]pyrimidin-6-yl)thio)acetamide (259009)

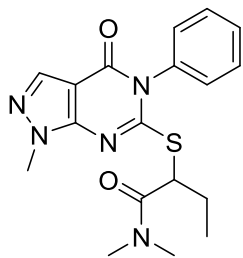
6-mercapto-1-methyl-5-phenyl-1H-pyrazolo[3,4-d]pyrimidin-4(5H)-one (200mg, 0.774 mmol), ethyl 2-bromoacetate (0.094 ml, 0.852 mmol), and K₂CO₃ (161 mg, 1.161 mmol) in 1mL DMF were stirred for 1 h. The ester was precipitated with water and redissolved in 10mL 3:3:1 THF/1N LiOH/EtOH and stirred for 1 h. The volatiles were removed and the residue taken up in water and washed 1x with EtOAc which was discarded. The aqueous layer was acidified with 1N HCl then extracted 3x with EtOAc. The combined organics were washed with brine and dried yielding a white solid. This white solid (170mg) and HATU (225 mg, 0.591 mmol) were added to a flask and dissolved in 3mL DMF and cooled to 0°C before adding DIPEA (282 µl, 1.612 mmol). 10 min later dimethylamine HCl (46.0 mg, 0.564 mmol) was added. The flask was

left in cooling bath to gradually warm to RT over several hours. The next day, the mixture was diluted with brine and extracted into EtOAc. The organic portion was dried and solvent removed. Purified by Flash (Elutes around 90% EA), the recrystallized from EtOAc, then Purified by flash again affording the titled compound as a white solid (20mg, 0.058 mmol, 10.84 % yield). MS (ESI): m/z 344.1175 $[M+H]^+$ 1H NMR (500 MHz, $CDCl_3$) δ 8.01 (s, 1H), 7.63 - 7.50 (m, 3H), 7.35 - 7.29 (m, 2H), 4.06 (s, 2H), 3.95 (s, 3H), 3.16 (s, 3H), 2.99 (s, 3H). ^{13}C NMR (126 MHz, $CDCl_3$) δ 166.60, 161.51, 157.58, 150.75, 135.32, 135.29, 130.14, 129.77, 129.30, 102.80, 37.58, 36.23, 35.94, 33.85.



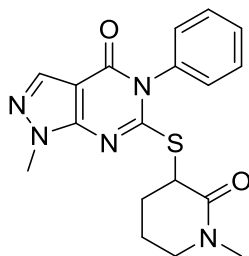
N,N-dimethyl-2-((1-methyl-4-oxo-5-phenyl-4,5-dihydro-1H-pyrazolo[3,4-d]pyrimidin-6-yl)thio)propanamide (258476)

Prepared in a similar manner to **259009**. White solid. (29mg, 0.081 mmol, 26.2 % yield) (ESI): m/z 359.1327 $[M+H]^+$ 1H NMR (500 MHz, $CDCl_3$) δ 8.02 (s, 1H), 7.48 - 7.59 (m, 3H), 7.20 - 7.33 (m, 2H), 4.89 (q, $J = 7.34$ Hz, 1H), 3.96 (s, 3H), 3.21 (s, 3H), 3.00 (s, 3H), 1.54 (d, $J = 6.85$ Hz, 3H) ^{13}C NMR (126 MHz, $CDCl_3$) δ 170.7, 161.6, 157.6, 150.9, 135.5, 135.3, 130.2, 129.9, 129.7, 129.4, 129.2, 103.0, 43.2, 37.5, 36.2, 33.9, 17.4.



N,N-dimethyl-2-((1-methyl-4-oxo-5-phenyl-4,5-dihydro-1H-pyrazolo[3,4-d]pyrimidin-6-yl)thio)butanamide (259008)

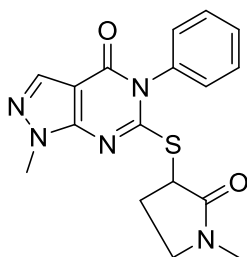
Prepared in a similar manner as **259009**. White solid. (29mg, 0.078 mmol, 25.2 % yield) (ESI): m/z 372.1485 $[M+H]^+$ 1H NMR (500 MHz, $CDCl_3$) δ 8.01 (s, 1H), 7.62 - 7.43 (m, 3H), 7.40 - 7.14 (m, 2H), 4.87 (t, $J = 7.1$ Hz, 1H), 3.96 (s, 3H), 3.22 (s, 3H), 3.00 (s, 3H), 2.09 - 1.96 (m, 1H), 1.93 - 1.78 (m, 1H), 1.01 (t, $J = 7.4$ Hz, 3H). ^{13}C NMR (126 MHz, $CDCl_3$) δ 170.21, 161.84, 157.62, 150.83, 135.46, 135.32, 130.14, 129.88, 129.77, 129.38, 129.22, 102.96, 48.85, 37.65, 36.13, 33.95, 25.88, 11.95.



1-methyl-6-((1-methyl-2-oxopiperidin-3-yl)thio)-5-phenyl-1H-pyrazolo[3,4-d]pyrimidin-4(5H)-one (263053)

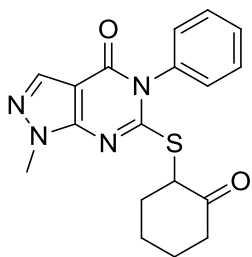
3-bromo-1-methylpiperidin-2-one (37.2 mg, 0.194 mmol), 6-mercapto-1-methyl-5-phenyl-1H-pyrazolo[3,4-d]pyrimidin-4(5H)-one (50mg, 0.194 mmol), and K_2CO_3 (26.8 mg, 0.194 mmol) were stirred overnight in 1mL DMF. The product was precipitated by addition of water and filtered. The precipitate was taken up in hot ethanol and the titled compound crystallized as a

white solid. (16mg, 0.043 mmol, 22.37 % yield) (ESI): m/z 370.1333 $[M+H]^+$ 1H NMR (500 MHz, $CDCl_3$) δ 8.01 (s, 1H), 7.60 - 7.41 (m, 3H), 7.37 - 7.29 (m, 1H), 7.25 (d, $J = 6.4$ Hz, 1H), 4.61 (t, $J = 6.5$ Hz, 1H), 3.94 (s, 3H), 3.41 - 3.27 (m, 2H), 2.95 (s, 3H), 2.42 - 2.28 (m, 1H), 2.25 - 2.13 (m, 1H), 2.08 - 1.96 (m, 1H), 1.96 - 1.77 (m, 1H). ^{13}C NMR (126 MHz, $CDCl_3$) δ 166.33, 161.04, 157.73, 150.84, 135.45, 130.05, 129.87, 129.68, 129.59, 129.29, 102.93, 50.00, 47.85, 35.46, 33.95, 28.64, 21.52.



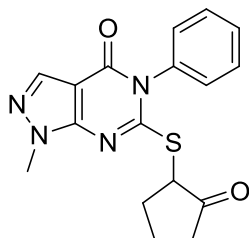
1-methyl-6-((1-methyl-2-oxopyrrolidin-3-yl)thio)-5-phenyl-1H-pyrazolo[3,4-d]pyrimidin-4(5H)-one

Prepared in a similar manner to **263053**. (27mg, 0.076 mmol, 39.2 % yield). (ESI): m/z 356.1177 $[M+H]^+$ 1H NMR (500 MHz, $CDCl_3$) δ 8.02 (s, 1H), 7.59 - 7.46 (m, 3H), 7.36 - 7.29 (m, 1H), 7.28 - 7.21 (m, 1H), 4.55 (t, $J = 8.4$ Hz, 1H), 3.95 (s, 3H), 3.51 - 3.36 (m, 2H), 2.89 (s, 3H), 2.83 - 2.71 (m, 1H), 2.24 (dq, $J = 15.3, 7.8$ Hz, 1H) ^{13}C NMR (126 MHz, $CDCl_3$) δ 170.14, 160.91, 157.61, 150.80, 135.48, 135.33, 130.18, 129.94, 129.64, 129.62, 129.24, 103.02, 47.37, 46.90, 33.96, 30.43, 26.84.



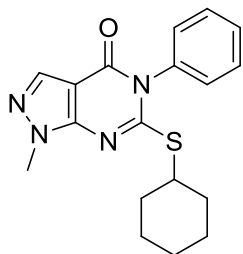
1-methyl-6-((2-oxocyclohexyl)thio)-5-phenyl-1H-pyrazolo[3,4-d]pyrimidin-4(5H)-one
263056

Prepared in a similar manner to **263053**. White Solid (34mg, 0.096 mmol, 49.6 % yield) MS (ESI): m/z 355.1223 $[M+H]^+$ 1H NMR (500 MHz, $CDCl_3$) δ 7.98 (s, 1H), 7.56 - 7.48 (m, 3H), 7.35 - 7.30 (m, 1H), 7.23 (dt, $J = 5.8, 2.8$ Hz, 1H), 4.61 (dd, $J = 11.5, 5.3$ Hz, 1H), 3.91 (s, 3H), 2.61 (dt, $J = 13.4, 4.5$ Hz, 1H), 2.53 - 2.42 (m, 2H), 2.11 (ddt, $J = 12.8, 6.3, 2.9$ Hz, 1H), 1.95 (dt, $J = 12.4, 3.8$ Hz, 1H), 1.89 - 1.67 (m, 3H). ^{13}C NMR (126 MHz, $CDCl_3$) δ 204.81, 160.89, 157.67, 150.76, 135.60, 135.34, 130.10, 129.90, 129.68, 129.47, 129.24, 102.89, 56.78, 41.66, 33.99, 33.86, 27.70, 25.36.



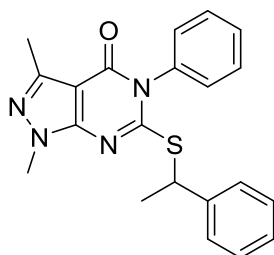
1-methyl-6-((2-oxocyclopentyl)thio)-5-phenyl-1H-pyrazolo[3,4-d]pyrimidin-4(5H)-one
(263055)

Prepared in a similar manner to **263053**. Off white solid (37mg, 0.109 mmol, 56.2 % yield) MS (ESI): m/z 341.1068 $[M+H]^+$ 1H NMR (500 MHz, $CDCl_3$) δ 8.02 (s, 1H), 7.57 - 7.50 (m, 3H), 7.35 - 7.26 (m, 2H), 4.15 (t, $J = 9.5$ Hz, 1H), 3.95 (s, 3H), 2.68 - 2.56 (m, 1H), 2.47 (dd, $J = 18.9, 8.7$ Hz, 1H), 2.34 (dt, $J = 18.9, 9.4$ Hz, 1H), 2.24 - 2.08 (m, 2H), 1.98 (p, $J = 9.7, 9.2$ Hz, 1H). ^{13}C NMR (126 MHz, $CDCl_3$) δ 212.37, 160.45, 157.59, 150.69, 135.49, 130.19, 129.85, 129.72, 129.48, 129.34, 103.11, 51.85, 37.02, 34.21, 30.08, 20.75.



6-(cyclohexylthio)-1-methyl-5-phenyl-1H-pyrazolo[3,4-d]pyrimidin-4(5H)-one (262901)

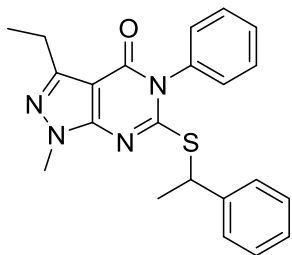
Prepared in a similar manner to **263053**. White solid. (42mg, 0.123 mmol, 45.5 % yield) MS (ESI): m/z 341.1432 $[M+H]^+$ 1H NMR (500 MHz, $CDCl_3$) δ 8.02 (s, 1H), 7.56 - 7.47 (m, 3H), 7.29 - 7.20 (m, 2H), 3.97 (s, 3H), 3.88 - 3.76 (m, 1H), 2.18 - 2.01 (m, 2H), 1.83 - 1.70 (m, 2H), 1.69 - 1.60 (m, 1H), 1.53 - 1.35 (m, 4H), 1.33 - 1.25 (m, 1H). ^{13}C NMR (126 MHz, $CDCl_3$) δ 162.12, 157.98, 151.16, 135.93, 135.37, 129.80, 129.61, 129.39, 102.76, 46.42, 33.78, 32.51, 26.12, 25.59.



1,3-dimethyl-5-phenyl-6-((1-phenylethyl)thio)-1H-pyrazolo[3,4-d]pyrimidin-4(5H)-one (263865)

To a solution of ethyl 5-amino-1,3-dimethyl-1H-pyrazole-4-carboxylate¹⁶³ (250mg, 1.365 mmol) in 2.5mL DMF at 0°C was added NaH (82 mg, 3.41 mmol). The mixture was stirred for 10 minutes under N_2 at which point isothiocyanatobenzene (0.163 ml, 1.365 mmol) was added by syringe. The mixture was stirred for an additional 20 min at which point it was allowed to warm to room temperature and stir for 1 h. The mixture was cooled to 0°C again and (1-bromoethyl)benzene (0.186 ml, 1.365 mmol) was added by syringe and the mixture was allowed to gradually warm to RT overnight. Some of the cyclized thiophenol intermediate

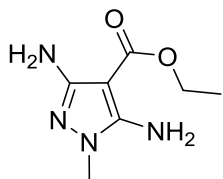
remained so (1-bromoethyl)benzene (0.186 ml, 1.365 mmol) was added to the solution at 0°C and then the mixture was stirred for another hour at RT. The mixture was diluted with ethyl acetate and washed 1x with water and 3x with brine. The organic portion was dried over sodium sulfate and concentrated yielding a yellow solid. The crude solid was taken up in hot ethanol and the pure product crystallized as a white solid upon cooling. (190mg, 0.505 mmol, 37.0 % yield)
MS (ESI): m/z 377.1427 [M+H]⁺ ¹H NMR (500 MHz, CDCl₃) δ 7.56 - 7.45 (m, 3H), 7.41 - 7.35 (m, 2H), 7.33 - 7.21 (m, 4H), 7.20 - 7.16 (m, 1H), 5.01 (q, J = 7.2 Hz, 1H), 3.92 (s, 3H), 2.52 (s, 3H), 1.70 (d, J = 7.1 Hz, 3H). ¹³C NMR (126 MHz, CDCl₃) δ 161.24, 158.58, 151.50, 146.24, 142.16, 135.63, 129.80, 129.62, 129.55, 129.44, 129.41, 128.49, 127.51, 100.97, 46.76, 33.59, 21.95, 13.36.



3-ethyl-1-methyl-5-phenyl-6-((1-phenylethyl)thio)-1H-pyrazolo[3,4-d]pyrimidin-4(5H)-one (264621)

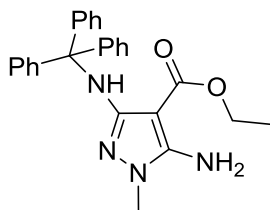
Prepared in a similar manner to **263865** to yield a white solid. (37mg, 0.095 mmol, 6.23 % yield)
MS (ESI): m/z 391.1588 [M+H]⁺ ¹H NMR (500 MHz, CDCl₃) δ 7.55 - 7.44 (m, 3H), 7.40 - 7.35 (m, 2H), 7.33 - 7.21 (m, 4H), 7.21 - 7.16 (m, 1H), 5.01 (q, J = 7.2 Hz, 1H), 3.93 (s, 3H), 2.90 (q, J = 7.6 Hz, 2H), 1.70 (d, J = 7.2 Hz, 3H), 1.31 (t, J = 7.5 Hz, 3H). ¹³C NMR (126 MHz, CDCl₃) δ 161.16, 158.28, 151.92, 151.63, 142.21, 135.71, 129.76, 129.62, 129.55, 129.46, 129.43, 128.49,

127.51, 100.26, 46.75, 33.59, 21.95, 21.62, 13.17



Ethyl 3,5-diamino-1-methyl-1H-pyrazole-4-carboxylate (S5.3d)

3,5-diamino-1-methyl-1H-pyrazole-4-carbonitrile¹⁶⁴(S5.3c) (200mg, 1.458 mmol), H₂SO₄ (.2 ml, 3.75 mmol), and 1mL ethanol were heated overnight in a sealed tube at 100C. The next day 0.5mL water was added and the tube was heated to 100°C for 30 minutes at which point it was added to saturated sodium carbonate and extracted 3x with ethyl acetate. The combined organics were washed with brine, dried over sodium sulfate, and concentrated. The crude was purified by flash (2.5% MeOH in DCM) yielding the product as a white solid. (100mg, 0.543 mmol, 37.2 % yield) ¹H NMR (400 MHz, DMSO-d₆) δ 5.98 (s, 2H), 4.95 (s, 2H), 4.12 (q, J = 7.1 Hz, 2H), 1.22 (t, J = 7.1 Hz, 3H).



Ethyl 5-amino-1-methyl-3-(tritylamino)-1H-pyrazole-4-carboxylate

Ethyl 3,5-diamino-1-methyl-1H-pyrazole-4-carboxylate (95mg, 0.516 mmol), Trityl-Cl (144 mg, 0.516 mmol), and DIPEA (0.108 ml, 0.619 mmol) were stirred for 2 days at RT in DCM. When

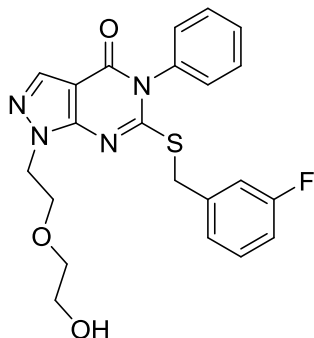
complete by TLC, the volatiles were removed and the reaction was purified by flash (0-50% EA in Hex) affording the titled compound as a white foam. (138mg, 0.324 mmol, 62.7 % yield) ^1H NMR (500 MHz, DMSO- d_6) δ 7.33 - 7.06 (m, 15H), 4.12 (q, J = 6.8, 6.4 Hz, 2H), 1.23 - 1.09 (m, 3H).

1-methyl-5-phenyl-6-((1-phenylethyl)thio)-3-(tritylamino)-1H-pyrazolo[3,4-d]pyrimidin-4(5H)-one (S5.3f)

Prepared in a similar manner to 263865 to afford the titled compound as a yellow oil (70mg, 0.113 mmol, 64.2 % yield). ^1H NMR (500 MHz, CDCl_3) δ 7.77 - 7.04 (m, 27H), 6.42 (s, 1H), 5.00 (q, J = 7.1 Hz, 1H), 3.56 (s, 3H), 1.72 (d, J = 7.2 Hz, 3H).

3-amino-1-methyl-5-phenyl-6-((1-phenylethyl)thio)-1H-pyrazolo[3,4-d]pyrimidin-4(5H)-one

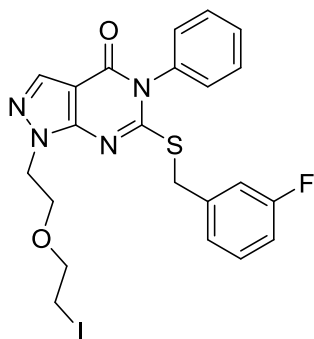
Stirred at RT in 1mL TFA and 1mL DCM for 3 h. The solvent was removed and the residue was taken up in sat. NaHCO_3 and extracted 3x with DCM. The combined organics were washed with brine and dried over sodium sulfate. Crude residue was purified by flash (Eluting at 60% EtOAc in Hex) affording the titled compound as a white solid. (11mg, 0.029 mmol, 60.2 % yield) MS (ESI): m/z 378.1384 $[\text{M}+\text{H}]^+$ ^1H NMR (499 MHz, CDCl_3) δ 7.55 - 7.45 (m, 3H), 7.40 - 7.35 (m, 2H), 7.32 - 7.21 (m, 4H), 7.20 - 7.16 (m, 1H), 4.99 (q, J = 7.1 Hz, 1H), 4.47 (s, 2H), 3.78 (s, 3H), 1.69 (d, J = 7.2 Hz, 3H). ^{13}C NMR (126 MHz, CDCl_3) δ 161.64, 158.48, 150.65, 150.40, 142.12, 135.37, 129.83, 129.61, 129.54, 129.50, 129.47, 128.49, 127.50, 90.78, 46.77, 33.11, 21.93.



6-((3-fluorobenzyl)thio)-1-(2-(2-hydroxyethoxy)ethyl)-5-phenyl-1H-pyrazolo[3,4-d]pyrimidin-4(5H)-one (S5.2a n=1)

Prepared according to (Chapter 3, Method B). Yellow Oil. (140mg, 0.318 mmol, 44.8 % yield)

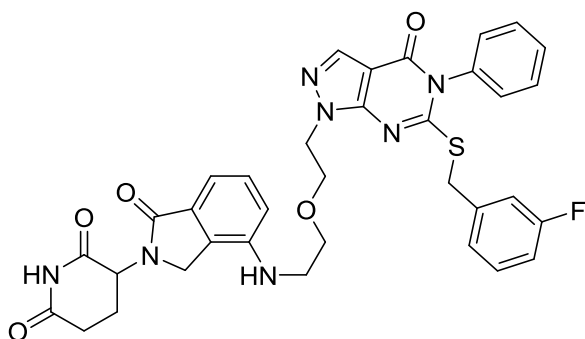
^1H NMR (500 MHz, CDCl_3) δ 8.03 (d, $J = 1.4$ Hz, 1H), 7.55 - 7.47 (m, 3H), 7.31 - 7.20 (m, 3H), 7.11 (d, $J = 7.7$ Hz, 1H), 7.06 (d, $J = 9.6$ Hz, 1H), 6.92 (d, $J = 7.9$ Hz, 1H), 4.52 (t, $J = 5.5$ Hz, 2H), 4.30 (s, 2H), 3.95 (t, $J = 5.6$ Hz, 2H), 3.67 (t, $J = 4.5$ Hz, 2H), 3.61 - 3.53 (m, 2H), 3.01 (s, 1H). No NOE when irradiating peak at 8.03



6-((3-fluorobenzyl)thio)-1-(2-(2-iodoethoxy)ethyl)-5-phenyl-1H-pyrazolo[3,4-d]pyrimidin-4(5H)-one (S5.2b n=1)

I_2 (113 mg, 0.445 mmol), and PS- PPh_3 (ALDRICH 3mmol/g, 160mg) were added to a vial along with 2mL THF and stirred via orbital shaker for 15 minutes. Imidazole (32.5 mg, 0.477 mmol) was added followed by (S5.2a n=1) (140mg, 0.318 mmol) dissolved in 2mL THF. The mixture was stirred by orbital shaker overnight. The next day an equal portion of PPh_3 , I_2 and Imidazole were added and the mixture stirred for an additional 3 days. The mixture was filtered

and diluted with ethyl acetate before washing with sat. sodium thiosulfate and brine and drying over sodium sulfate and concentrating. The yellow oil obtained was used without further purification (100mg, 0.182 mmol, 57.2 % yield)



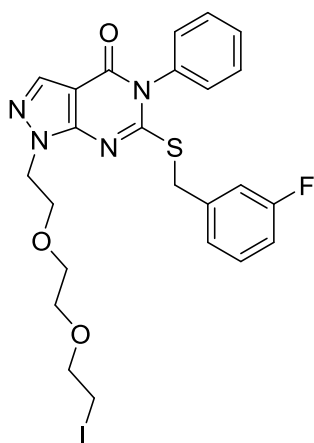
3-(4-((2-(2-(6-((3-fluorobenzyl)thio)-4-oxo-5-phenyl-4,5-dihydro-1H-pyrazolo[3,4-d]pyrimidin-1-yl)ethoxy)ethyl)amino)-1-oxoisindolin-2-yl)piperidine-2,6-dione (263643)

3-(4-amino-1-oxoisindolin-2-yl)piperidine-2,6-dione (188 mg, 0.727 mmol), K_2CO_3 (50.2 mg, 0.363 mmol), and 6-((3-fluorobenzyl)thio)-1-(2-(2-iodoethoxy)ethyl)-5-phenyl-1H-pyrazolo[3,4-d]pyrimidin-4(5H)-one (100mg, 0.182 mmol) were added to a pressure vial and stirred at 70C for 24hr. The mixture was diluted with water and extracted 2x with ethyl acetate. The organic portion was washed with brine and dried over sodium sulfate. The concentrated crude residue was purified by 2 successive flash columns (80-100% EA/Hex). (20mg, 0.029 mmol, 16.15 % yield) colorless oily solid. (ESI): m/z 704.2066 $[M+H]^+$ 1H NMR (500 MHz, $CDCl_3$) δ 8.06 (s, 1H), 7.55 - 7.46 (m, 2H), 7.46 - 7.39 (m, 1H), 7.36 - 7.19 (m, 5H), 7.13 (d, $J = 7.7$ Hz, 1H), 7.10 (dt, $J = 9.6, 2.1$ Hz, 1H), 6.95 (td, $J = 8.5, 2.5$ Hz, 1H), 6.81 (dd, $J = 7.4, 1.4$ Hz, 1H), 5.15 (dd, $J = 13.1, 5.4$ Hz, 1H), 4.60 - 4.41 (m, 2H), 4.34 (s, 2H), 4.23 (d, $J = 15.6$ Hz, 1H), 4.12 (d, $J = 15.6$ Hz, 1H), 4.05 - 3.81 (m, 4H), 3.58 - 3.51 (m, 1H), 3.51 - 3.43 (m, 1H), 2.90 (ddd, $J = 17.6, 4.6, 2.7$ Hz, 1H), 2.78 (ddd, $J = 18.0, 13.1, 5.6$ Hz, 1H), 2.27 - 2.15 (m, 1H), 2.15 - 2.07 (m, 1H). ^{13}C

NMR (126 MHz, CDCl₃) δ 171.12, 170.14, 169.89, 162.81 (d, J = 246.3 Hz), 161.88, 157.97, 151.44, 141.65, 138.67 (d, J = 7.8 Hz), 135.67, 135.57, 132.40, 130.26, 130.20, 129.83 (d, J = 2.4 Hz), 129.51, 129.45, 129.37, 126.47, 124.89 (d, J = 2.9 Hz), 118.15, 116.20 (d, J = 21.9 Hz), 114.70 (d, J = 21.2 Hz), 114.25, 103.17, 68.53, 67.66, 52.55, 47.49, 45.22, 39.22, 37.01, 32.11, 22.80.

6-((3-fluorobenzyl)thio)-1-(2-(2-(2-hydroxyethoxy)ethoxy)ethyl)-5-phenyl-1H-pyrazolo[3,4-d]pyrimidin-4(5H)-one (S5.2a n=2)

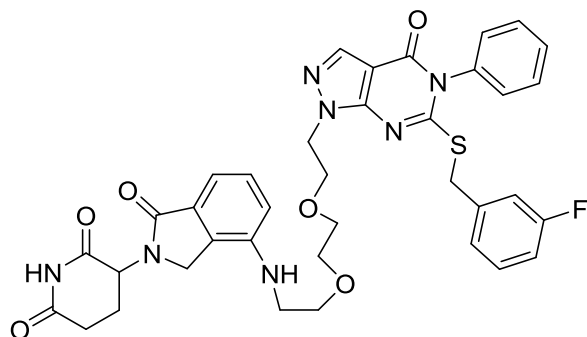
Prepared in a similar manner to(S5.2a n=1). Yellow oil. (110mg, 0.227 mmol, 32.0 % yield)
1H NMR (500 MHz, Chloroform-d) δ 8.03 (s, 1H), 7.54 - 7.43 (m, 3H), 7.30 - 7.19 (m, 3H), 7.11 (d, J = 7.7 Hz, 1H), 7.06 (dt, J = 9.7, 2.1 Hz, 1H), 6.92 (td, J = 8.4, 2.5 Hz, 1H), 4.52 (t, J = 5.9 Hz, 2H), 4.31 (s, 2H), 3.97 (t, J = 5.9 Hz, 2H), 3.66 (t, J = 4.5 Hz, 2H), 3.63 (dd, J = 6.3, 3.0 Hz, 2H), 3.60 (dd, J = 5.7, 2.7 Hz, 2H), 3.52 (t, J = 4.5 Hz, 2H), 2.42 (s, 1H).



6-((3-fluorobenzyl)thio)-1-(2-(2-(2-iodoethoxy)ethoxy)ethyl)-5-phenyl-1H-pyrazolo[3,4-d]pyrimidin-4(5H)-one (S5.2b n=2)

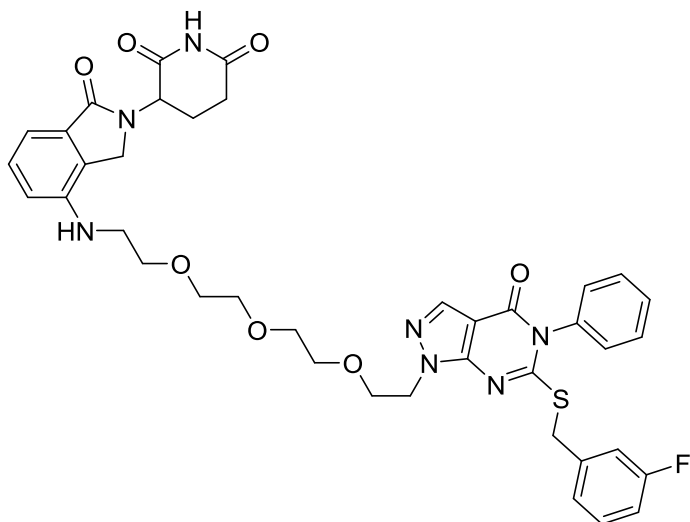
Prepared in a similar manner as(S5.2b n=2). Yellow oil.(135mg, 0.227 mmol, 100 % yield).

Taken forward without further purification.



3-(4-((2-(2-(2-(6-((3-fluorobenzyl)thio)-4-oxo-5-phenyl-4,5-dihydro-1H-pyrazolo[3,4-d]pyrimidin-1-yl)ethoxy)ethoxy)ethyl)amino)-1-oxoisindolin-2-yl)piperidine-2,6-dione
(263643)

Prepared in a manner similar to **263644**. (48mg, 0.066 mmol, 30.2 % yield) (ESI): m/z 748.2328
[M+H]⁺ ¹H NMR (500 MHz, CDCl₃) δ 7.99 (s, 1H), 7.51 - 7.39 (m, 3H), 7.29 - 7.16 (m, 5H),
7.11 - 7.06 (m, 1H), 7.03 (dt, J = 9.6, 2.1 Hz, 1H), 6.90 (td, J = 9.0, 1.8 Hz, 1H), 6.76 (dd, J = 7.4,
1.4 Hz, 1H), 5.14 (dd, J = 13.4, 5.1 Hz, 1H), 4.48 (t, J = 5.8 Hz, 2H), 4.27 (s, 2H), 4.19 (d, J =
15.7 Hz, 1H), 4.09 (d, J = 15.7 Hz, 1H), 4.03 - 3.85 (m, 4H), 3.60 - 3.46 (m, 6H), 2.88 (ddd, J =
17.6, 4.9, 2.6 Hz, 1H), 2.77 (ddd, J = 17.9, 13.3, 5.3 Hz, 1H), 2.20 (qd, J = 13.1, 4.7 Hz, 1H),
2.12 - 2.02 (m, 1H). ¹³C NMR (126 MHz, CDCl₃) δ 171.18, 170.05, 169.88, 162.63 (d, J = 246.2
Hz), 161.55, 157.79, 151.19, 141.61, 141.60, 138.50 (d, J = 7.5 Hz), 135.56, 135.44, 132.23,
130.13, 130.07, 129.70 (d, J = 1.7 Hz), 129.34, 129.31, 126.26, 117.90, 115.99 (d, J = 21.7 Hz),
114.54 (d, J = 21.0 Hz), 113.86, 102.93, 70.45, 69.76, 68.80, 67.51, 52.43, 46.91, 45.09, 39.04,
36.80 (d, J = 1.9 Hz), 31.97, 22.64.



3-(4-(((2-(2-(2-(2-(6-((3-fluorobenzyl)thio)-4-oxo-5-phenyl-4,5-dihydro-1H-pyrazolo[3,4-d]pyrimidin-1-yl)ethoxy)ethoxy)ethoxy)ethyl)amino)-1-oxoisindolin-2-yl)piperidine-2,6-dione (263818)

Prepared in a similar manner as **263643**. Yellow Foam. (34mg, 0.044 mmol, 33.9 % yield) (ESI): m/z 770.2758 $[M+H]^+$ 1H NMR (500 MHz, Chloroform- d) δ 8.02 (s, 1H), 7.54 - 7.46 (m, 3H), 7.31 - 7.20 (m, 5H), 7.11 (d, $J = 7.6$ Hz, 1H), 7.07 (dt, $J = 9.6, 2.1$ Hz, 1H), 6.93 (td, $J = 8.4, 2.6$ Hz, 1H), 6.80 (dd, $J = 7.4, 1.3$ Hz, 1H), 5.18 (dd, $J = 13.3, 5.1$ Hz, 1H), 4.51 (t, $J = 5.9$ Hz, 2H), 4.31 (s, 2H), 4.23 (d, $J = 15.6$ Hz, 1H), 4.12 (d, $J = 15.5$ Hz, 1H), 4.00 (t, $J = 6.0$ Hz, 2H), 3.95 (t, $J = 5.9$ Hz, 2H), 3.90 (br. s, 2H), 3.67 - 3.48 (m, 10H), 2.92 (ddd, $J = 17.6, 4.6, 2.6$ Hz, 1H), 2.80 (ddd, $J = 17.9, 13.4, 5.4$ Hz, 1H), 2.25 (qd, $J = 13.2, 4.5$ Hz, 1H), 2.14 - 2.07 (m, 1H). ^{13}C NMR (126 MHz, Chloroform- d) δ 171.10, 170.02, 169.78, 162.67 (d, $J = 246.4$ Hz), 161.46, 157.70, 151.11, 141.52, 138.50 (d, $J = 7.6$ Hz), 135.59, 135.48, 132.30, 130.16, 130.09, 129.75 (d, $J = 3.6$ Hz), 129.36, 129.33, 126.28, 124.78 (d, $J = 2.9$ Hz), 117.88, 116.02 (d, $J = 21.9$ Hz), 114.57

(d, $J = 21.0$ Hz), 113.98, 102.98, 70.55, 70.50, 70.32, 69.78, 68.92, 67.53, 52.41, 46.94, 44.98,
39.06, 36.85, 32.01, 22.70.

Bibliography

1. Society, A. C. Cancer Facts and Figures. **2018**.
2. Ozols, R. F.; Bundy, B. N.; Greer, B. E.; Fowler, J. M.; Clarke-Pearson, D.; Burger, R. A.; Mannel, R. S.; DeGeest, K.; Hartenbach, E. M.; Baergen, R. Phase III Trial of Carboplatin and Paclitaxel Compared With Cisplatin and Paclitaxel in Patients With Optimally Resected Stage III Ovarian Cancer: A Gynecologic Oncology Group Study. *Journal of Clinical Oncology* **2003**, *21* (17), 3194-3200.
3. Thigpen, T.; duBois, A.; McAlpine, J.; DiSaia, P.; Fujiwara, K.; Hoskins, W.; Kristensen, G.; Mannel, R.; Markman, M.; Pfisterer, J.; Quinn, M.; Reed, N.; Swart, A. M.; Berek, J.; Colombo, N.; Freyer, G.; Gallardo, D.; Plante, M.; Poveda, A.; Rubinstein, L.; Bacon, M.; Kitchener, H.; Stuart, G. C. First-line Therapy in Ovarian Cancer Trials. *Int J Gynecol Cancer* **2011**, *21* (4), 756-762.
4. Cannistra, S. A. Cancer of the Ovary. *New England Journal of Medicine* **2004**, *351* (24), 2519-2529.
5. Mylavarapu, S.; Das, A.; Roy, M. Role of BRCA Mutations in the Modulation of Response to Platinum Therapy. *Frontiers in Oncology* **2018**, *8*, 16.
6. Rossi, L.; Verrico, M.; Zaccarelli, E.; Papa, A.; Colonna, M.; Strudel, M.; Vici, P.; Bianco, V.; Tomao, F. Bevacizumab in ovarian cancer: A critical review of phase III studies. *Oncotarget* **2017**, *8* (7), 12389-12405.
7. McLachlan, J.; George, A.; Banerjee, S. The current status of PARP inhibitors in ovarian cancer. *Tumori* **2016**, *102* (5), 433-440.
8. Bitler, B. G.; Watson, Z. L.; Wheeler, L. J.; Behbakht, K. PARP inhibitors: Clinical utility and possibilities of overcoming resistance. *Gynecol Oncol* **2017**, *147* (3), 695-704.
9. Sharma, N. J. C. A., *PARP Inhibitors for Cancer Therapy*. Humana Press, Cham: 2015.

10. Reya, T.; Morrison, S. J.; Clarke, M. F.; Weissman, I. L. Stem cells, cancer, and cancer stem cells. *Nature* **2001**, *414* (6859), 105-111.
11. Wicha, M. S.; Liu, S.; Dontu, G. Cancer Stem Cells: An Old Idea—A Paradigm Shift. *Cancer Research* **2006**, *66* (4), 1883.
12. Prasetyanti, P. R.; Medema, J. P. Intra-tumor heterogeneity from a cancer stem cell perspective. *Molecular Cancer* **2017**, *16* (1), 41.
13. Yoshida, G. J.; Saya, H. Therapeutic Strategies Targeting Cancer Stem Cells. *Cancer Sci* **2016**, *107* (1), 5-11.
14. Burgos-Ojeda, D.; Rueda, B. R.; Buckanovich, R. J. Ovarian cancer stem cell markers: prognostic and therapeutic implications. *Cancer Lett* **2012**, *322* (1), 1-7.
15. Garson, K.; Vanderhyden, B. C. Epithelial ovarian cancer stem cells: underlying complexity of a simple paradigm. *Reproduction* **2015**, *149* (2), R59-R70.
16. Clevers, H. The cancer stem cell: premises, promises and challenges. *Nature Medicine* **2011**, *17*, 313.
17. Walsh, N.; Kenney, L.; Jangalwe, S.; Aryee, K.-E.; Greiner, D. L.; Brehm, M. A.; Shultz, L. D. Humanized mouse models of clinical disease. *Annual review of pathology* **2017**, *12*, 187-215.
18. Silva, I. A.; Bai, S.; McLean, K.; Yang, K.; Griffith, K.; Thomas, D.; Ginestier, C.; Johnston, C.; Kueck, A.; Reynolds, R. K.; Wicha, M. S.; Buckanovich, R. J. Aldehyde Dehydrogenase in Combination with CD133 Defines Angiogenic Ovarian Cancer Stem Cells that Portend Poor Patient Survival. *Cancer Res* **2011**, *71* (11), 3991-4001.
19. Ma, S.; Chan, K. W.; Lee, T. K.; Tang, K. H.; Wo, J. Y.; Zheng, B. J.; Guan, X. Y. Aldehyde dehydrogenase discriminates the CD133 liver cancer stem cell populations. *Molecular cancer research : MCR* **2008**, *6* (7), 1146-1153.
20. Kryczek, I.; Liu, S.; Roh, M.; Vatan, L.; Szeliga, W.; Wei, S.; Banerjee, M.; Mao, Y.; Kotarski, J.; Wicha, M. S.; Liu, R.; Zou, W. Expression of aldehyde dehydrogenase and CD133 defines ovarian cancer stem cells. *Int J Cancer* **2012**, *130* (1), 29-39.

21. Choi, Y.-J.; Ingram, P. N.; Yang, K.; Coffman, L.; Iyengar, M.; Bai, S.; Thomas, D. G.; Yoon, E.; Buckanovich, R. J. Identifying an Ovarian Cancer Cell Hierarchy Regulated by Bone Morphogenetic Protein 2. *Proceedings of the National Academy of Sciences* **2015**, *112* (50), E6882-E6888.
22. Jang, J.-W.; Song, Y.; Kim, S.-H.; Kim, J.; Seo, H. R. Potential mechanisms of CD133 in cancer stem cells. *Life Sciences* **2017**, *184*, 25-29.
23. Li, Z. CD133: a stem cell biomarker and beyond. *Experimental Hematology & Oncology* **2013**, *2*, 17-17.
24. Liu, C.; Li, Y.; Xing, Y.; Cao, B.; Yang, F.; Yang, T.; Ai, Z.; Wei, Y.; Jiang, J. The Interaction between Cancer Stem Cell Marker CD133 and Src Protein Promotes Focal Adhesion Kinase (FAK) Phosphorylation and Cell Migration. *Journal of Biological Chemistry* **2016**, *291* (30), 15540-15550.
25. Weng, C.-C.; Kuo, K.-K.; Su, H.-T.; Hsiao, P.-J.; Chen, Y.-W.; Wu, D.-C.; Hung, W.-C.; Cheng, K.-H. Pancreatic Tumor Progression Associated With CD133 Overexpression: Involvement of Increased TERT Expression and Epidermal Growth Factor Receptor-Dependent Akt Activation. *Pancreas* **2016**, *45* (3), 443-457.
26. Chen, H.; Luo, Z.; Dong, L.; Tan, Y.; Yang, J.; Feng, G.; Wu, M.; Li, Z.; Wang, H. CD133/Prominin-1-Mediated Autophagy and Glucose Uptake Beneficial for Hepatoma Cell Survival. *PLOS ONE* **2013**, *8* (2), e56878.
27. Song, Y.; Jang, J.; Shin, T. H.; Bae, S. M.; Kim, J. S.; Kim, K. M.; Myung, S. J.; Choi, E. K.; Seo, H. R. Sulfasalazine attenuates evading anticancer response of CD133-positive hepatocellular carcinoma cells. *Journal of experimental & clinical cancer research : CR* **2017**, *36* (1), 38.
28. Koppaka, V.; Thompson, D. C.; Chen, Y.; Ellermann, M.; Nicolaou, K. C.; Juvonen, R. O.; Petersen, D.; Deitrich, R. A.; Hurley, T. D.; Vasiliou, V. Aldehyde Dehydrogenase Inhibitors: a Comprehensive Review of the Pharmacology, Mechanism of Action, Substrate Specificity, and Clinical Application. *Pharmacological Reviews* **2012**, *64* (3), 520-539.
29. Tomita, H.; Tanaka, K.; Tanaka, T.; Hara, A. Aldehyde dehydrogenase 1A1 in stem cells and cancer. *Oncotarget* **2016**, *7* (10), 11018-11032.
30. Jiang-Jie, D.; Jiao, C.; Yu-Feng, G.; Xiu-Wu, B.; Shi-Cang, Y. ALDH1A3, a metabolic target for cancer diagnosis and therapy. *International Journal of Cancer* **2016**, *139* (5), 965-975.

31. Landen, C. N., Jr.; Goodman, B.; Katre, A. A.; Steg, A. D.; Nick, A. M.; Stone, R. L.; Miller, L. D.; Mejia, P. V.; Jennings, N. B.; Gershenson, D. M.; Bast, R. C., Jr.; Coleman, R. L.; Lopez-Berestein, G.; Sood, A. K. Targeting Aldehyde Dehydrogenase Cancer Stem Cells in Ovarian Cancer. *Mol Cancer Ther* **2010**, *9* (12), 3186-3199.
32. Moreb, J. S.; Baker, H. V.; Chang, L. J.; Amaya, M.; Lopez, M. C.; Ostmark, B.; Chou, W. ALDH Isozymes Downregulation Affects Cell Growth, Cell Motility and Gene Expression in Lung Cancer Cells. *Mol Cancer* **2008**, *7*, 87.
33. Luo, Y.; Dallaglio, K.; Chen, Y.; Robinson, W. A.; Robinson, S. E.; McCarter, M. D.; Wang, J.; Gonzalez, R.; Thompson, D. C.; Norris, D. A.; Roop, D. R.; Vasiliou, V.; Fujita, M. ALDH1A Isozymes are Markers of Human Melanoma Stem Cells and Potential Therapeutic Targets. *Stem Cells* **2012**, *30* (10), 2100-2113.
34. Li, Z.; Xiang, Y.; Xiang, L.; Xiao, Y.; Li, F.; Hao, P. ALDH Maintains the Stemness of Lung Adenoma Stem Cells by Suppressing the Notch/CDK2/CCNE Pathway. *PLoS One* **2014**, *9* (3), e92669.
35. Duong, H. Q.; Hwang, J. S.; Kim, H. J.; Kang, H. J.; Seong, Y. S.; Bae, I. Aldehyde Dehydrogenase 1A1 Confers Intrinsic and Acquired Resistance to Gemcitabine in Human Pancreatic Adenocarcinoma MIA PaCa-2 Cells. *Int J Oncol* **2012**, *41* (3), 855-861.
36. Condello, S.; Morgan, C. A.; Nagdas, S.; Cao, L.; Turek, J.; Hurley, T. D.; Matei, D. Beta-Catenin-Regulated ALDH1A1 is a Target in Ovarian Cancer Spheroids. *Oncogene* **2015**, *34* (18), 2297-2308.
37. Yokoyama, Y.; Zhu, H.; Lee, J. H.; Kossenkov, A. V.; Wu, S. Y.; Wickramasinghe, J. M.; Yin, X.; Palozola, K. C.; Gardini, A.; Showe, L. C.; Zaret, K. S.; Liu, Q.; Speicher, D.; Conejo-Garcia, J. R.; Bradner, J. E.; Zhang, Z.; Sood, A. K.; Ordog, T.; Bitler, B. G.; Zhang, R. BET Inhibitors Suppress ALDH Activity by Targeting ALDH1A1 Super-Enhancer in Ovarian Cancer. *Cancer Res* **2016**, *76* (21), 6320-6330.
38. Chen, M. H.; Weng, J. J.; Cheng, C. T.; Wu, R. C.; Huang, S. C.; Wu, C. E.; Chung, Y. H.; Liu, C. Y.; Chang, M. H.; Chiang, K. C.; Yeh, T. S.; Su, Y.; Yeh, C. N. ALDH1A3, the Major Aldehyde Dehydrogenase Isoform in Human Cholangiocarcinoma Cells, Affects Prognosis and Gemcitabine Resistance in Cholangiocarcinoma Patients. *Clin Cancer Res* **2016**, *22* (16), 4225-4235.

39. Cortes-Dericks, L.; Froment, L.; Boesch, R.; Schmid, R. A.; Karoubi, G. Cisplatin-Resistant Cells in Malignant Pleural Mesothelioma Cell Lines Show ALDH(high)CD44(+) Phenotype and Sphere-Forming Capacity. *BMC cancer* **2014**, *14*, 304.
40. Parajuli, B.; Fishel, M. L.; Hurley, T. D. Selective ALDH3A1 inhibition by benzimidazole analogues increase mafosfamide sensitivity in cancer cells. *J Med Chem* **2014**, *57* (2), 449-461.
41. Morgan, C. A.; Parajuli, B.; Buchman, C. D.; Dria, K.; Hurley, T. D. N,N-Diethylaminobenzaldehyde (DEAB) as a Substrate and Mechanism-Based Inhibitor for Human ALDH Isoenzymes. *Chemico-Biological Interactions* **2015**, *234* (0), 18-28.
42. Barrera, G. Oxidative Stress and Lipid Peroxidation Products in Cancer Progression and Therapy. *ISRN Oncology* **2012**, *2012*, 137289.
43. Xu, X.; Chai, S.; Wang, P.; Zhang, C.; Yang, Y.; Wang, K. Aldehyde Dehydrogenases and Cancer Stem Cells. *Cancer Lett* **2015**, *369* (1), 50-57.
44. Schenk, T.; Stengel, S.; Zelent, A. Unlocking the potential of retinoic acid in anticancer therapy. *British Journal of Cancer* **2014**, *111* (11), 2039-2045.
45. Schug, T. T.; Berry, D. C.; Shaw, N. S.; Travis, S. N.; Noy, N. Opposing Effects of Retinoic Acid on Cell Growth Result from Alternate Activation of Two Different Nuclear Receptors. *Cell* **2007**, *129* (4), 723-733.
46. Chang, L.; Graham, P. H.; Hao, J.; Ni, J.; Bucci, J.; Cozzi, P. J.; Kearsley, J. H.; Li, Y. Acquisition of epithelial–mesenchymal transition and cancer stem cell phenotypes is associated with activation of the PI3K/Akt/mTOR pathway in prostate cancer radioresistance. *Cell Death & Disease* **2013**, *4*, e875.
47. Roberts, C. M.; Tran, M. A.; Pitruzzello, M. C.; Wen, W.; Loeza, J.; Dellinger, T. H.; Mor, G.; Glackin, C. A. TWIST1 drives cisplatin resistance and cell survival in an ovarian cancer model, via upregulation of GAS6, L1CAM, and Akt signalling. *Scientific Reports* **2016**, *6*, 37652.
48. Haslehurst, A. M.; Koti, M.; Dharsee, M.; Nuin, P.; Evans, K.; Geraci, J.; Childs, T.; Chen, J.; Li, J.; Weberpals, J.; Davey, S.; Squire, J.; Park, P. C.; Feilotter, H. EMT transcription factors snail and slug directly contribute to cisplatin resistance in ovarian cancer. *BMC cancer* **2012**, *12* (1), 91.

49. Kang, J. H.; Lee, S. H.; Hong, D.; Lee, J. S.; Ahn, H. S.; Ahn, J. H.; Seong, T. W.; Lee, C. H.; Jang, H.; Hong, K. M.; Lee, C.; Lee, J. H.; Kim, S. Y. Aldehyde dehydrogenase is used by cancer cells for energy metabolism. *Experimental & molecular medicine* **2016**, *48* (11), e272.
50. Bach, D.-H.; Park, H. J.; Lee, S. K. The Dual Role of Bone Morphogenetic Proteins in Cancer. *Molecular Therapy Oncolytics* **2018**, *8*, 1-13.
51. Rahman, M. S.; Akhtar, N.; Jamil, H. M.; Banik, R. S.; Asaduzzaman, S. M. TGF-beta/BMP signaling and other molecular events: regulation of osteoblastogenesis and bone formation. *Bone research* **2015**, *3*, 15005.
52. Zhang, Y. E. Non-Smad pathways in TGF- β signaling. *Cell research* **2009**, *19* (1), 128-139.
53. Dolle, L.; Boulter, L.; Leclercq, I. A.; van Grunsven, L. A. Next generation of ALDH substrates and their potential to study maturational lineage biology in stem and progenitor cells. *American journal of physiology. Gastrointestinal and liver physiology* **2015**, *308* (7), G573-578.
54. Feng, H.; Liu, Y.; Bian, X.; Zhou, F.; Liu, Y. ALDH1A3 affects colon cancer in vitro proliferation and invasion depending on CXCR4 status. *British Journal Of Cancer* **2017**, *118*, 224.
55. Wang, M.-F.; Han, C.-L.; Yin, S.-J. Substrate specificity of human and yeast aldehyde dehydrogenases. *Chemico-Biological Interactions* **2009**, *178* (1), 36-39.
56. Minn, I.; Wang, H.; Mease, R. C.; Byun, Y.; Yang, X.; Wang, J.; Leach, S. D.; Pomper, M. G. A red-shifted fluorescent substrate for aldehyde dehydrogenase. *Nature communications* **2014**, *5*, 3662-3662.
57. Malcolm, R.; Olive, M. F.; Lechner, W. The safety of disulfiram for the treatment of alcohol and cocaine dependence in randomized clinical trials: guidance for clinical practice. *Expert opinion on drug safety* **2008**, *7* (4), 459-472.
58. Kwon, H. J.; Won, Y. S.; Park, O.; Chang, B.; Duryee, M. J.; Thiele, G. E.; Matsumoto, A.; Singh, S.; Abdelmegeed, M. A.; Song, B. J.; Kawamoto, T.; Vasiliou, V.; Thiele, G. M.; Gao, B. Aldehyde dehydrogenase 2 deficiency ameliorates alcoholic fatty liver but worsens liver inflammation and fibrosis in mice. *Hepatology (Baltimore, Md.)* **2014**, *60* (1), 146-157.

59. Lang, B. S.; Gorren, A. C. F.; Oberdorfer, G.; Wenzl, M. V.; Furdui, C. M.; Poole, L. B.; Mayer, B.; Gruber, K. Vascular Bioactivation of Nitroglycerin by Aldehyde Dehydrogenase-2: REACTION INTERMEDIATES REVEALED BY CRYSTALLOGRAPHY AND MASS SPECTROMETRY. *The Journal of Biological Chemistry* **2012**, *287* (45), 38124-38134.
60. Chen, C. H.; Budas, G. R.; Churchill, E. N.; Disatnik, M. H.; Hurley, T. D.; Mochly-Rosen, D. Activation of aldehyde dehydrogenase-2 reduces ischemic damage to the heart. *Science* **2008**, *321* (5895), 1493-1495.
61. Eriksson, C. J. The role of acetaldehyde in the actions of alcohol (update 2000). *Alcoholism, clinical and experimental research* **2001**, *25* (5 Suppl ISBRA), 15s-32s.
62. Lee, H.; Kim, S. S.; You, K. S.; Park, W.; Yang, J. H.; Kim, M.; Hayman, L. L. Asian Flushing: Genetic and Sociocultural Factors of Alcoholism Among East Asians. *Gastroenterology Nursing* **2014**, *37* (5), 327-336.
63. Dufour, P.; Lang, J.-M.; Giron, C.; Duclos, B.; Haehnel, P.; Jaeck, D.; Jung, J.-M.; Oberling, F. Sodium ditiocarb as adjuvant immunotherapy for high risk breast cancer: A randomized study. *Biotherapy* **1993**, *6* (1), 9-12.
64. Skrott, Z.; Mistrik, M.; Andersen, K. K.; Friis, S.; Majera, D.; Gursky, J.; Ozdian, T.; Bartkova, J.; Turi, Z.; Moudry, P.; Kraus, M.; Michalova, M.; Vaclavkova, J.; Dzubak, P.; Vrobel, I.; Pouckova, P.; Sedlacek, J.; Miklovcova, A.; Kutt, A.; Li, J.; Mattova, J.; Driessen, C.; Dou, Q. P.; Olsen, J.; Hajduch, M.; Cvek, B.; Deshaies, R. J.; Bartek, J. Alcohol-abuse drug disulfiram targets cancer via p97 segregase adaptor NPL4. *Nature* **2017**, *552*, 194.
65. Croker, A. K.; Allan, A. L. Inhibition of Aldehyde Dehydrogenase (ALDH) Activity Reduces Chemotherapy and Radiation Resistance of Stem-Like ALDHhiCD44+ Human Breast Cancer Cells. *Breast Cancer Research and Treatment* **2012**, *133* (1), 75-87.
66. Morgan, C. A.; Hurley, T. D. Development of a High-Throughput In Vitro Assay to Identify Selective Inhibitors for Human ALDH1A1. *Chemico-Biological Interactions* **2015**, *234* (0), 29-37.
67. Morgan, C. A.; Hurley, T. D. Characterization of Two Distinct Structural Classes of Selective Aldehyde Dehydrogenase 1A1 Inhibitors. *J Med Chem* **2015**, *58* (4), 1964-1975.
68. Yang, S. M.; Yasgar, A.; Miller, B.; Lal-Nag, M.; Brimacombe, K.; Hu, X.; Sun, H.; Wang, A.; Xu, X.; Nguyen, K.; Oppermann, U.; Ferrer, M.; Vasiliou, V.; Simeonov, A.; Jadhav,

A.; Maloney, D. J. Discovery of NCT-501, a Potent and Selective Theophylline-Based Inhibitor of Aldehyde Dehydrogenase 1A1 (ALDH1A1). *J Med Chem* **2015**, *58* (15), 5967-5978.

69. Yang, S. M.; Martinez, N. J.; Yasgar, A.; Danchik, C.; Johansson, C.; Wang, Y.; Baljinnyam, B.; Wang, A. Q.; Xu, X.; Shah, P.; Cheff, D.; Wang, X. S.; Roth, J.; Lal-Nag, M.; Dunford, J. E.; Oppermann, U.; Vasiliou, V.; Simeonov, A.; Jadhav, A.; Maloney, D. J. Discovery of Orally Bioavailable, Quinoline-Based Aldehyde Dehydrogenase 1A1 (ALDH1A1) Inhibitors with Potent Cellular Activity. *J Med Chem* **2018**, *61* (11), 4883-4903.

70. He, G. W.; Gunther, C.; Thonn, V.; Yu, Y. Q.; Martini, E.; Buchen, B.; Neurath, M. F.; Sturzl, M.; Becker, C. Regression of apoptosis-resistant colorectal tumors by induction of necroptosis in mice. *The Journal of experimental medicine* **2017**, *214* (6), 1655-1662.

71. Calculated in Cambridge Soft Chem3D Pro 12.0 using default parameters.

72. Hansch, C.; Leo, A.; Taft, R. W. A survey of Hammett substituent constants and resonance and field parameters. *Chemical Reviews* **1991**, *91* (2), 165-195.

73. Ehmke, V.; Quinsaat, J. E.; Rivera-Fuentes, P.; Heindl, C.; Freymond, C.; Rottmann, M.; Brun, R.; Schirmeister, T.; Diederich, F. Tuning and predicting biological affinity: aryl nitriles as cysteine protease inhibitors. *Organic & biomolecular chemistry* **2012**, *10* (30), 5764-5768.

74. Kumar, A.; Zhang, K. Y. J. Advances in the development of SUMO specific protease (SENP) inhibitors. *Computational and Structural Biotechnology Journal* **2015**, *13*, 204-211.

75. Zhu, H.; Zhu, X.; Zheng, L.; Hu, X.; Sun, L.; Zhu, X. The role of the androgen receptor in ovarian cancer carcinogenesis and its clinical implications. *Oncotarget* **2017**, *8* (17), 29395-29405.

76. Wilson, A. J.; Fadare, O.; Beeghly-Fadiel, A.; Son, D. S.; Liu, Q.; Zhao, S.; Saskowski, J.; Uddin, M. J.; Daniel, C.; Crews, B.; Lehmann, B. D.; Pietenpol, J. A.; Crispens, M. A.; Marnett, L. J.; Khabele, D. Aberrant over-expression of COX-1 intersects multiple pro-tumorigenic pathways in high-grade serous ovarian cancer. *Oncotarget* **2015**, *6* (25), 21353-21368.

77. Sun, H.; Zhang, X.; Sun, D.; Jia, X.; Xu, L.; Qiao, Y.; Jin, Y. COX-2 expression in ovarian cancer: an updated meta-analysis. *Oncotarget* **2017**, *8* (50), 88152-88162.

78. Lin, Y.-C.; Chang, Y.-T.; Campbell, M.; Lin, T.-P.; Pan, C.-C.; Lee, H.-C.; Shih, J. C.; Chang, P.-C. MAOA-a novel decision maker of apoptosis and autophagy in hormone refractory neuroendocrine prostate cancer cells. *Scientific Reports* **2017**, *7*, 46338.
79. The Human Protein Atlas. <https://www.proteinatlas.org/ENSG00000189221-MAOA/tissue> (accessed 07/18/2018).
80. Chau, W. K.; Ip, C. K.; Mak, A. S.; Lai, H. C.; Wong, A. S. c-Kit mediates chemoresistance and tumor-initiating capacity of ovarian cancer cells through activation of Wnt/beta-catenin-ATP-binding cassette G2 signaling. *Oncogene* **2013**, *32* (22), 2767-2781.
81. Tonary, A. M.; Macdonald, E. A.; Faught, W.; Senterman, M. K.; Vanderhyden, B. C. Lack of expression of c-KIT in ovarian cancers is associated with poor prognosis. *Int J Cancer* **2000**, *89* (3), 242-250.
82. Yi, C.; Li, L. I.; Chen, K.; Lin, S.; Liu, X. Expression of c-Kit and PDGFR α in epithelial ovarian tumors and tumor stroma. *Oncology Letters* **2012**, *3* (2), 369-372.
83. Dungal, D. A.; Maginn, E. N.; Stronach, E. A. Preventing Damage Limitation: Targeting DNA-PKcs and DNA Double-Strand Break Repair Pathways for Ovarian Cancer Therapy. *Frontiers in Oncology* **2015**, *5*, 240.
84. Nomura, D. K.; Dix, M. M.; Cravatt, B. F. Activity-based protein profiling for biochemical pathway discovery in cancer. *Nature reviews. Cancer* **2010**, *10* (9), 630-638.
85. Phizicky, E. M.; Fields, S. Protein-protein interactions: methods for detection and analysis. *Microbiological Reviews* **1995**, *59* (1), 94-123.
86. Zhao, D.; Mo, Y.; Li, M.-T.; Zou, S.-W.; Cheng, Z.-L.; Sun, Y.-P.; Xiong, Y.; Guan, K.-L.; Lei, Q.-Y. NOTCH-induced aldehyde dehydrogenase 1A1 deacetylation promotes breast cancer stem cells. *The Journal of Clinical Investigation* **2014**, *124* (12), 5453-5465.
87. Daniels, D. L.; Méndez, J.; Benink, H.; Niles, A.; Murphy, N.; Ford, M.; Jones, R.; Amunugama, R.; Allen, D.; Urh, M. Discovering Protein Interactions and Characterizing Protein Function Using HaloTag Technology. *Journal of Visualized Experiments : JoVE* **2014**, (89), 51553.

88. Shinji, C.; Nakamura, T.; Maeda, S.; Yoshida, M.; Hashimoto, Y.; Miyachi, H. Design and synthesis of phthalimide-type histone deacetylase inhibitors. *Bioorganic & Medicinal Chemistry Letters* **2005**, *15* (20), 4427-4431.
89. Sinhababu, A. K.; Kawase, M.; Borchardt, R. T. Desilylation of tert-Butyldimethylsilyl Ethers of Phenols. *Synthesis* **1988**, 1988 (09), 710-712.
90. Ju, Y.; Varma, R. S. Aqueous N-Heterocyclization of Primary Amines and Hydrazines with Dihalides: Microwave-Assisted Syntheses of N-Azacycloalkanes, Isoindole, Pyrazole, Pyrazolidine, and Phthalazine Derivatives. *The Journal of Organic Chemistry* **2006**, *71* (1), 135-141.
91. Valois-Escamilla, I.; Alvarez-Hernandez, A.; Rangel-Ramos, L. F.; Suárez-Castillo, O. R.; Ayala-Mata, F.; Zepeda-Vallejo, G. Synthesis of 6-bromo-2-arylindoles using 2-iodobenzoic acid as precursor. *Tetrahedron Letters* **2011**, *52* (29), 3726-3728.
92. Nieman, J. A.; Ennis, M. D. Synthesis of 3-Methoxycarbonylmethyl Derivatives of Dihydroquinolone and Dihydrochromenone. *The Journal of Organic Chemistry* **2001**, *66* (6), 2175-2177.
93. Salvagnini, C.; Gharbi, S.; Boxus, T.; Marchand-Brynaert, J. Synthesis and evaluation of a small library of graftable thrombin inhibitors derived from (L)-arginine. *Eur J Med Chem* **2007**, *42* (1), 37-53.
94. Zhou, C.; Abdel-Rahman, M. A.; Li, W.; Liu, K.; Zhang, A. Thermoresponsive dendronized copolymers for protein recognitions based on biotin-avidin interaction. *Chinese Chemical Letters* **2017**, *28* (4), 832-838.
95. Kinzler, K.; Nilbert, M.; Su, L.; Vogelstein, B.; Bryan, T.; Levy, D.; Smith, K.; Preisinger, A.; Hedge, P.; McKechnie, D. Identification of FAP Locus Genes from Chromosome 5q21. *Science* **1991**, *253* (5020), 661-665.
96. Yasgar, A.; Titus, S. A.; Wang, Y.; Danchik, C.; Yang, S.-M.; Vasiliou, V.; Jadhav, A.; Maloney, D. J.; Simeonov, A.; Martinez, N. J. Correction: A High-Content Assay Enables the Automated Screening and Identification of Small Molecules with Specific ALDH1A1-Inhibitory Activity. *PLOS ONE* **2018**, *13* (5), e0197292.
97. *MarvinSketch Calculator Plugins were used for ADME predictions, Marvin 15.6.15, 2015, ChemAxon <http://www.chemaxon.com> (accessed: 06/05/2018).*

98. Chen, Y.; Zhu, J. Y.; Hong, K. H.; Mikles, D. C.; Georg, G. I.; Goldstein, A. S.; Amory, J. K.; Schonbrunn, E. Structural Basis of ALDH1A2 Inhibition by Irreversible and Reversible Small Molecule Inhibitors. *ACS chemical biology* **2018**, *13* (3), 582-590.
99. Beaufort, C. M.; Helmijr, J. C. A.; Piskorz, A. M.; Hoogstraat, M.; Ruigrok-Ritstier, K.; Besselink, N.; Murtaza, M.; van Ijcken, W. F. J.; Heine, A. A. J.; Smid, M.; Koudijs, M. J.; Brenton, J. D.; Berns, E. M. J. J.; Helleman, J. Ovarian Cancer Cell Line Panel (OCCP): Clinical Importance of In Vitro Morphological Subtypes. *PLOS ONE* **2014**, *9* (9), e103988.
100. Blayney, J. K.; Davison, T.; McCabe, N.; Walker, S.; Keating, K.; Delaney, T.; Greenan, C.; Williams, A. R.; McCluggage, W. G.; Capes-Davis, A.; Harkin, D. P.; Gourley, C.; Kennedy, R. D. Prior Knowledge Transfer Across Transcriptional Data Sets and Technologies Using Compositional Statistics Yields New Mislabeled Ovarian Cell Line. *Nucleic Acids Res* **2016**, *44* (17), e137.
101. Zhou, Q.; Chen, A.; Song, H.; Tao, J.; Yang, H.; Zuo, M. Prognostic Value of Cancer Stem Cell Marker CD133 in Ovarian Cancer: a Meta-Analysis. *International Journal of Clinical and Experimental Medicine* **2015**, *8* (3), 3080-3088.
102. Okita, K.; Matsumura, Y.; Sato, Y.; Okada, A.; Morizane, A.; Okamoto, S.; Hong, H.; Nakagawa, M.; Tanabe, K.; Tezuka, K.; Shibata, T.; Kunisada, T.; Takahashi, M.; Takahashi, J.; Saji, H.; Yamanaka, S. A More Efficient Method to Generate Integration-Free Human iPS Cells. *Nature methods* **2011**, *8* (5), 409-412.
103. Bretz, N.; Noske, A.; Keller, S.; Erbe-Hofmann, N.; Schlange, T.; Salnikov, A. V.; Moldenhauer, G.; Kristiansen, G.; Altevogt, P. CD24 Promotes Tumor Cell Invasion by Suppressing Tissue Factor Pathway Inhibitor-2 (TFPI-2) in a c-Src-Dependent Fashion. *Clin Exp Metastasis* **2012**, *29* (1), 27-38.
104. Dylla, S. J.; Beviglia, L.; Park, I. K.; Chartier, C.; Raval, J.; Ngan, L.; Pickell, K.; Aguilar, J.; Lazetic, S.; Smith-Berdan, S.; Clarke, M. F.; Hoey, T.; Lewicki, J.; Gurney, A. L. Colorectal Cancer Stem Cells are Enriched in Xenogeneic Tumors Following Chemotherapy. *PLoS ONE* **2008**, *3* (6), e2428.
105. Wheeler, A. R.; Thronset, W. R.; Whelan, R. J.; Leach, A. M.; Zare, R. N.; Liao, Y. H.; Farrell, K.; Manger, I. D.; Daridon, A. Microfluidic Device for Single-Cell Analysis. *Analytical chemistry* **2003**, *75* (14), 3581-3586.

106. Canino, C.; Luo, Y.; Marcato, P.; Blandino, G.; Pass, H. I.; Cioce, M. A STAT3-NFkB/DDIT3/CEBP β Axis Modulates ALDH1A3 Expression in Chemoresistant Cell Subpopulations. *Oncotarget* **2015**, *6* (14), 12637-12653.
107. Golubovskaya, V.; O'Brien, S.; Ho, B.; Heffler, M.; Conroy, J.; Hu, Q.; Wang, D.; Liu, S.; Cance, W. G. Down-Regulation of ALDH1A3, CD44 or MDR1 Sensitizes Resistant Cancer Cells to FAK Autophosphorylation Inhibitor Y15. *Journal of cancer research and clinical oncology* **2015**, *141* (9), 1613-1631.
108. Raha, D.; Wilson, T. R.; Peng, J.; Peterson, D.; Yue, P.; Evangelista, M.; Wilson, C.; Merchant, M.; Settleman, J. The Cancer Stem Cell Marker Aldehyde Dehydrogenase is Required to Maintain a Drug-Tolerant Tumor Cell Subpopulation. *Cancer Res* **2014**, *74* (13), 3579-3590.
109. Chou, T. C.; Talalay, P. Quantitative Analysis of Dose-Effect Relationships: the Combined Effects of Multiple Drugs or Enzyme Inhibitors. *Adv Enzyme Regul* **1984**, *22*, 27-55.
110. Raghavan, S.; Ward, M. R.; Rowley, K. R.; Wold, R. M.; Takayama, S.; Buckanovich, R. J.; Mehta, G. Formation of Stable Small Cell Number Three-Dimensional Ovarian Cancer Spheroids Using Hanging Drop Arrays for Preclinical Drug Sensitivity Assays. *Gynecologic Oncology* **2015**, *138* (1), 181-189.
111. Shield, K.; Ackland, M. L.; Ahmed, N.; Rice, G. E. Multicellular Spheroids in Ovarian Cancer Metastases: Biology and Pathology. *Gynecologic Oncology* **2009**, *113* (1), 143-148.
112. Raghavan, S.; Mehta, P.; Ward, M. R.; Bregenzner, M. E.; Fleck, E. M. A.; Tan, L.; McLean, K.; Buckanovich, R. J.; Mehta, G. Personalized Medicine-Based Approach to Model Patterns of Chemoresistance and Tumor Recurrence Using Ovarian Cancer Stem Cell Spheroids. *Clin Cancer Res* **2017**, *23* (22), 6934-6945.
113. Hall, M. D.; Telma, K. A.; Chang, K. E.; Lee, T. D.; Madigan, J. P.; Lloyd, J. R.; Goldlust, I. S.; Hoeschele, J. D.; Gottesman, M. M. Say no to DMSO: dimethylsulfoxide inactivates cisplatin, carboplatin, and other platinum complexes. *Cancer Res* **2014**, *74* (14), 3913-3922.
114. Dasari, S.; Tchounwou, P. B. Cisplatin in cancer therapy: molecular mechanisms of action. *European journal of pharmacology* **2014**, *0*, 364-378.
115. Lempers, E. L. M.; Reedijk, J. Reversibility of binding of cisplatin-methionine in proteins by diethyldithiocarbamate or thiourea: a study with model adducts. *Inorganic Chemistry* **1990**, *29* (2), 217-222.

116. Liu, J.; Mao, L.; Wang, X.; Xu, X.; Zhao, L. Pyrazolopyrimidine Derivatives and Uses as Anticancer Agents. WO2012097196A1, 2012.
117. Guccione, S.; Russo, F.; Raffaelli, A.; Barretta, G. U.; Pucci, S.; Scolaro, L. M. Potential of Alkyl Orthoformates as Alkylating Agents of Non-Electron Rich Nitrogen Heterocycles. *Journal of Heterocyclic Chemistry* **1995**, 32 (4), 1149-1158.
118. Nath, J.; Ghosh, H.; Yella, R.; Patel, B. K. Molecular Iodine Mediated Preparation of Isothiocyanates from Dithiocarbamic Acid Salts. *European Journal of Organic Chemistry* **2009**, 2009 (12), 1849-1851.
119. Otwinowski, Z.; Minor, W. Processing of X-ray Diffraction Data Collected in Oscillation Mode. *Methods Enzymol* **1997**, 276, 307-326.
120. The CCP4 Suite: Programs for Protein Crystallography. *Acta Crystallogr D Biol Crystallogr* **1994**, 50 (Pt 5), 760-763.
121. Emsley, P.; Cowtan, K. Coot: Model-Building Tools for Molecular Graphics. *Acta Crystallogr D Biol Crystallogr* **2004**, 60 (Pt 12 Pt 1), 2126-2132.
122. Painter, J.; Merritt, E. A. Optimal Description of a Protein Structure in Terms of Multiple Groups Undergoing TLS Motion. *Acta Crystallogr D Biol Crystallogr* **2006**, 62 (Pt 4), 439-450.
123. Painter, J.; Merritt, E. A. A Molecular Viewer for the Analysis of TLS Rigid-Body Motion in Macromolecules. *Acta Crystallogr D Biol Crystallogr* **2005**, 61 (Pt 4), 465-471.
124. Hammen, P. K.; Allali-Hassani, A.; Hallenga, K.; Hurley, T. D.; Weiner, H. Multiple Conformations of NAD and NADH when Bound to Human Cytosolic and Mitochondrial Aldehyde Dehydrogenase. *Biochemistry* **2002**, 41 (22), 7156-7168.
125. Parajuli, B.; Kimble-Hill, A. C.; Khanna, M.; Ivanova, Y.; Meroueh, S.; Hurley, T. D. Discovery of Novel Regulators of Aldehyde Dehydrogenase Isoenzymes. *Chem Biol Interact* **2011**, 191 (1-3), 153-158.
126. Parajuli, B.; Georgiadis, T. M.; Fishel, M. L.; Hurley, T. D. Development of Selective Inhibitors for Human Aldehyde Dehydrogenase 3A1 (ALDH3A1) for the Enhancement of Cyclophosphamide Cytotoxicity. *Chembiochem* **2014**, 15 (5), 701-712.

127. Buchman, C. D.; Hurley, T. D. Inhibition of the Aldehyde Dehydrogenase 1/2 Family by Psoralen and Coumarin Derivatives. *J Med Chem* **2017**, *60* (6), 2439-2455.
128. Raghavan, S.; Mehta, P.; Horst, E. N.; Ward, M. R.; Rowley, K. R.; Mehta, G.; Raghavan, S.; Mehta, P.; Horst, E. N.; Ward, M. R.; Rowley, K. R.; Mehta, G. Comparative Analysis of Tumor Spheroid Generation Techniques for Differential In Vitro Drug Toxicity. *Oncotarget* **2016**, *7* (13), 16948-16961.
129. Biasini, M.; Bienert, S.; Waterhouse, A.; Arnold, K.; Studer, G.; Schmidt, T.; Kiefer, F.; Gallo Cassarino, T.; Bertoni, M.; Bordoli, L.; Schwede, T. SWISS-MODEL: Modelling Protein Tertiary and Quaternary Structure Using Evolutionary Information. *Nucleic Acids Res* **2014**, *42* (Web Server issue), W252-258.
130. Arnold, K.; Bordoli, L.; Kopp, J.; Schwede, T. The SWISS-MODEL Workspace: a Web-Based Environment for Protein Structure Homology Modelling. *Bioinformatics* **2006**, *22* (2), 195-201.
131. Benkert, P.; Biasini, M.; Schwede, T. Toward the Estimation of the Absolute Quality of Individual Protein Structure Models. *Bioinformatics* **2011**, *27* (3), 343-350.
132. Walther, C.; Guenet, J. L.; Simon, D.; Deutsch, U.; Jostes, B.; Goulding, M. D.; Plachov, D.; Balling, R.; Gruss, P. Pax: a Murine Multigene Family of Paired Box-Containing Genes. *Genomics* **1991**, *11* (2), 424-434.
133. Laskowski, R. A.; MacArthur, M. W.; Moss, D. S.; Thornton, J. M. PROCHECK - a Program to Check the Stereochemical Quality of Protein Structures. *J. App. Cryst.* **1993**, *26*, 283-291.
134. McGann, M. FRED and HYBRID Docking Performance on Standardized Datasets. *J Comput Aided Mol Des* **2012**, *26* (8), 897-906.
135. Hawkins, P. C.; Skillman, A. G.; Warren, G. L.; Ellingson, B. A.; Stahl, M. T. Conformer Generation with OMEGA: Algorithm and Validation Using High Quality Structures from the Protein Databank and Cambridge Structural Database. *J Chem Inf Model* **2010**, *50* (4), 572-584.
136. Kehler, J.; Rasmussen, L. K.; Jessing, M. Triazolopyrazinones as PDE1 Inhibitors. Patent: WO2016055618 A1. 2016.

137. Evans, G. B.; Furneaux, R. H.; Greatrex, B.; Murkin, A. S.; Schramm, V. L.; Tyler, P. C. Azetidine Based Transition State Analogue Inhibitors of N-Ribosyl Hydrolases and Phosphorylases. *Journal of Medicinal Chemistry* **2008**, *51* (4), 948-956.
138. Patani, G. A.; LaVoie, E. J. Bioisosterism: A Rational Approach in Drug Design. *Chemical Reviews* **1996**, *96* (8), 3147-3176.
139. Barrows, R. D.; Blacklock, K. M.; Rablen, P. R.; Khare, S. D.; Knapp, S. Computational assessment of thioether isosteres. *Journal of Molecular Graphics and Modelling* **2018**, *80*, 282-292.
140. Fang, Z.; Song, Y.; Zhan, P.; Zhang, Q.; Liu, X. Conformational restriction: an effective tactic in 'follow-on'-based drug discovery. *Future medicinal chemistry* **2014**, *6* (8), 885-901.
141. Toselli, F.; Fredenwall, M.; Svensson, P.; Li, X.-Q.; Johansson, A.; Weidolf, L.; Hayes, M. A. Oxetane Substrates of Human Microsomal Epoxide Hydrolase. *Drug Metabolism and Disposition* **2017**, *45* (8), 966.
142. Li, X.-Q.; Hayes, M. A.; Grönberg, G.; Berggren, K.; Castagnoli, N.; Weidolf, L. Discovery of a Novel Microsomal Epoxide Hydrolase-Catalyzed Hydration of a Spiro Oxetane. *Drug Metabolism and Disposition* **2016**, *44* (8), 1341.
143. Rioux, N.; Duncan, K. W.; Lantz, R. J.; Miao, X.; Chan-Penebre, E.; Moyer, M. P.; Munchhof, M. J.; Copeland, R. A.; Chesworth, R.; Waters, N. J. Species differences in metabolism of EPZ015666, an oxetane-containing protein arginine methyltransferase-5 (PRMT5) inhibitor. *Xenobiotica* **2016**, *46* (3), 268-277.
144. Ikawa, M.; Impraim, C. C.; Wang, G.; Yoshida, A. Isolation and characterization of aldehyde dehydrogenase isozymes from usual and atypical human livers. *J Biol Chem* **1983**, *258* (10), 6282-6287.
145. Di, L.; Keefer, C.; Scott, D. O.; Strelevitz, T. J.; Chang, G.; Bi, Y. A.; Lai, Y.; Duckworth, J.; Fenner, K.; Troutman, M. D.; Obach, R. S. Mechanistic insights from comparing intrinsic clearance values between human liver microsomes and hepatocytes to guide drug design. *Eur J Med Chem* **2012**, *57*, 441-448.
146. Ritchie, T. J.; Macdonald, S. J.; Young, R. J.; Pickett, S. D. The impact of aromatic ring count on compound developability: further insights by examining carbo- and hetero-aromatic and -aliphatic ring types. *Drug Discov Today* **2011**, *16* (3-4), 164-171.

147. Yoshikazu, K.; Nobuya, K.; Teruaki, M. A Convenient Method for the Preparation of Alkyl Aryl Sulfides from Alcohols and (Chloromethylene)dimethylammonium Chloride. *Chemistry Letters* **2005**, *34* (12), 1612-1613.
148. Alkynyl Alcohols And Methods Of Use. WO2015025026 (2015).
149. Inhibitors Of PI3 Kinase. WO2011089400 (2011).
150. Wilkinson, M. C. "Greener" Friedel–Crafts Acylations: A Metal- and Halogen-Free Methodology. *Organic Letters* **2011**, *13* (9), 2232-2235.
151. Yasuda, M.; Onishi, Y.; Ueba, M.; Miyai, T.; Baba, A. Direct Reduction of Alcohols: Highly Chemoselective Reducing System for Secondary or Tertiary Alcohols Using Chlorodiphenylsilane with a Catalytic Amount of Indium Trichloride. *The Journal of Organic Chemistry* **2001**, *66* (23), 7741-7744.
152. Piscitelli, F.; Ligresti, A.; La Regina, G.; Coluccia, A.; Morera, L.; Allarà, M.; Novellino, E.; Di Marzo, V.; Silvestri, R. Indole-2-carboxamides as Allosteric Modulators of the Cannabinoid CB1 Receptor. *Journal of Medicinal Chemistry* **2012**, *55* (11), 5627-5631.
153. Tudge, M.; Mashima, H.; Savarin, C.; Humphrey, G.; Davies, I. Facile reduction of malonate derivatives using NaBH₄/Br₂: an efficient route to 1,3-diols. *Tetrahedron Letters* **2008**, *49* (6), 1041-1044.
154. SMITHKLINE BEECHAM CORPORATION. BENZIMIDAZOLE THIOPHENE COMPOUNDS - WO2007/143456. 2007.
155. Olah, G. A.; Gupta, B. G. B.; Malhotra, R.; Narang, S. C. Chlorotrimethylsilane/lithium bromide and hexamethyldisilane/pyridinium bromide perbromide: effective and selective reagents for the conversion of alkyl (cycloalkyl and aralkyl) alcohols into bromides. *The Journal of Organic Chemistry* **1980**, *45* (9), 1638-1639.
156. Heim-Riether, A.; Healy, J. A Novel Method for the Synthesis of Imidazo[5,1-f][1,2,4]triazin-4(3H)-ones. *The Journal of Organic Chemistry* **2005**, *70* (18), 7331-7337.
157. Mapelli, C.; Natarajan, S. I.; Meyer, J.-P.; Bastos, M. M.; Bernatowicz, M. S.; Lee, V. G.; Pluscec, J.; Riexinger, D. J.; Sieber-McMaster, E. S.; Constantine, K. L.; Smith-Monroy, C. A.; Golla, R.; Ma, Z.; Longhi, D. A.; Shi, D.; Xin, L.; Taylor, J. R.; Koplowitz, B.; Chi, C. L.;

- Khanna, A.; Robinson, G. W.; Seethala, R.; Antal-Zimanyi, I. A.; Stoffel, R. H.; Han, S.; Whaley, J. M.; Huang, C. S.; Krupinski, J.; Ewing, W. R. Eleven Amino Acid Glucagon-like Peptide-1 Receptor Agonists with Antidiabetic Activity. *Journal of Medicinal Chemistry* **2009**, *52* (23), 7788-7799.
158. Khenkin, A. M.; Weiner, L.; Wang, Y.; Neumann, R. Electron and Oxygen Transfer in Polyoxometalate, H₅PV₂Mo₁₀O₄₀, Catalyzed Oxidation of Aromatic and Alkyl Aromatic Compounds: Evidence for Aerobic Mars-van Krevelen-Type Reactions in the Liquid Homogeneous Phase. *Journal of the American Chemical Society* **2001**, *123* (35), 8531-8542.
159. Churcher, I. Protac-Induced Protein Degradation in Drug Discovery: Breaking the Rules or Just Making New Ones? *J Med Chem* **2018**, *61* (2), 444-452.
160. Toure, M.; Crews, C. M. Small-Molecule PROTACS: New Approaches to Protein Degradation. *Angewandte Chemie (International ed. in English)* **2016**, *55* (6), 1966-1973.
161. Qin, C.; Hu, Y.; Zhou, B.; Fernandez-Salas, E.; Yang, C.-Y.; Liu, L.; McEachern, D.; Przybranowski, S.; Wang, M.; Stuckey, J.; Meagher, J.; Bai, L.; Chen, Z.; Lin, M.; Yang, J.; Ziazadeh, D. N.; Xu, F.; Hu, J.; Xiang, W.; Huang, L.; Li, S.; Wen, B.; Sun, D.; Wang, S. Discovery of QCA570 as an Exceptionally Potent and Efficacious Proteolysis Targeting Chimera (PROTAC) Degradation of the Bromodomain and Extra-Terminal (BET) Proteins Capable of Inducing Complete and Durable Tumor Regression. *Journal of Medicinal Chemistry* **2018**.
162. Buckley, D. L.; Raina, K.; Darricarrere, N.; Hines, J.; Gustafson, J. L.; Smith, I. E.; Miah, A. H.; Harling, J. D.; Crews, C. M. HaloPROTACS: Use of Small Molecule PROTACs to Induce Degradation of HaloTag Fusion Proteins. *ACS chemical biology* **2015**, *10* (8), 1831-1837.
163. Fandrick, D. R.; Sanyal, S.; Kaloko, J.; Mulder, J. A.; Wang, Y.; Wu, L.; Lee, H.; Roschangar, F.; Hoffmann, M.; Senanayake, C. H. A Michael Equilibration Model To Control Site Selectivity in the Condensation toward Aminopyrazoles. *Organic Letters* **2015**, *17* (12), 2964-2967.
164. Bobko, M. A.; Kaura, A. C.; Evans, K. A.; Su, D.-S. Novel Synthesis of 5-Amino-3-bromo-1-(tert-butyl)-1H-pyrazole-4-carbonitrile: A Versatile Intermediate for the Preparation of 5-Amino-3-aryl-1-(tert-butyl)-1H-pyrazole-4-carboxamides. *Organic Letters* **2012**, *14* (15), 3906-3908.